UNIVERSITÉ DU QUÉBEC À MONTRÉAL

CONTRASTE SAISONNIER ET VARIABILITÉ CLIMATIQUE MILLÉNAIRE EN EUROPE DU SUD AU COURS DE LA DERNIÈRE PÉRIODE GLACIAIRE À PARTIR DE SÉQUENCES POLLINIQUES

THÈSE

PRÉSENTÉE

COMME EXIGENCE PARTIELLE

DU DOCTORAT EN SCIENCES DE LA TERRE ET DE L'ATMOSPHÈRE

PAR

JENA ZUMAQUE

JANVIER 2024

REMERCIEMENTS

Voici la dernière partie qu'il me reste à écrire, pas nécessairement la plus simple. Elle traite de tout le reste, de ce qui n'est pas scientifique, elle traite des interactions humaines, des personnes qui ont fait que j'ai commencé et que je termine cette thèse aujourd'hui, celles qui m'ont soutenue, celles qui m'ont poussée dans mes retranchements. Toutes m'ont faite grandir.

Je tiens avant tout à remercier ma directrice, Anne de Vernal. Merci de m'avoir donné cette nouvelle chance après que je me suis égarée, d'avoir cru en moi, de m'avoir fait confiance. Mais surtout merci de ton soutien et de ta bienveillance, particulièrement cette dernière année… Malgré les obstacles, tu as fait en sorte que je ne perde jamais confiance, que je garde toujours espoir. Merci.

Je tiens également à exprimer toute ma gratitude à Bianca Fréchette pour son aide, son temps et sa patience dans mon apprentissage des pollens. Cette dernière année aurait été très difficile sans toi! Merci à Joël Guiot, Maria Sanchez-Goni, Chéima Barhoumi, Odile Peyron, Matthew Peros, Basil Davis, Shawn Marshall, et tous ceux que j'oublie, pour leur temps, leur travail, ou simplement leurs précieux conseils. Merci à Ariane Burke de m'avoir intégré au groupe HDRG et de m'avoir offert la possibilité de participer à l'INQUA à Rome l'été dernier. Une expérience fabuleuse!

Merci à toute la gang du Geotop, et plus particulièrement à Marie-Michèle, Jade, Natasha, Sandrine, Anna, Tiphany, Xiner, Tengfei et là aussi j'en oublie… même si je n'arpente pas souvent les couloirs, je suis toujours heureuse de vous retrouver. Merci également d'avoir contribué, avec le groupe Arctrain (Camille, Antoine, Damien, Charles et les autres), à rendre ces congrès inoubliables! Merci également à Arctrain de m'avoir permis d'embarquer sur le Polarstern, une expérience à jamais gravée dans ma mémoire!

Un grand merci également à mes amis, la famille qu'on se choisit. Merci d'avoir été là dans les bons, comme les mauvais moments. J'ai une pensée toute particulière pour mon Triton (merci d'être dans ma vie) et pour mes petits Peio et Raspi. À vous trois, vous me rappelez sans cesse que cela vaut la peine de se battre pour vivre de ses passions, et si je franchis la ligne d'arrivée aujourd'hui, c'est aussi grâce à vous.

Y ahora lo mas importante.

A mi familia querida, los Zumaques, los Briosos y los demas. Os quiero.

À mes parents, Thérèse et Alfred, sans qui je n'en serais pas là aujourd'hui. Merci pour votre soutien, votre confiance, votre amour. Merci pour tous les encouragements mais aussi les sacrifices. Et surtout merci de m'avoir répété toute mon enfance « Travaille fort à l'école, fais des études ». Bravo! Résultats des courses, à 35 ans, j'y suis encore! Je ne suis pas certaine que ce soit ce que vous aviez en tête haha!

Enfin, je voudrais remercier ma petite famille à moi, mes deux amours, mon équipe. Cette thèse est aussi la leur. Marine, merci d'avoir compris à quel point cette thèse était importante pour moi, merci d'en avoir fait, toi aussi, un objectif de vie. Merci pour tous ces sacrifices, pour ton soutien indéfectible, ton optimisme sans faille, même dans les moments les plus difficiles. À ma petite Manoé, mon rayon de soleil, je sais que cela aura été difficile pour toi que Ama ne soit pas toujours disponible. On sera toutes ensemble maintenant.

TABLE DES MATIÈRES

REMERCIEMENTS ii

LISTE DES FIGURES vii

LISTE DES TABLEAUX xvii

RÉSUMÉ xix

ABSTRACT xxi

INTRODUCTION 1

0.1 Mise en contexte 1

0.2 Objectif principal et hypothèse 6

0.3 Méthodes 7

0.4 Structure de la thèse 8

CHAPITRE 1 METHODOLOGY 10

1.1 Introduction 11

1.2 Study sites 13

1.2.1 Data compilation and selection criteria 13

1.2.2 Chronologies 13

1.3 Methodology 14

1.3.1 Raw pollen counts 14

1.3.2 Vegetation reconstruction: Plant Functional Types (PFTs) 14

1.3.3 Pollen-based climate reconstruction 15

1.3.3.1 Significance of pollen assemblages in terms of climate 16

1.3.3.1.1 The atmospheric CO_2 effect 17

1.3.3.2 Modern Analogue Technique (MAT): Theory, limitations and relevance 18

1.3.3.3 Modern pollen database 20

1.3.3.4 Climate reconstruction in marine cores 22

1.3.3.4.1 Tests based on results from marine core MD95-2042 24

1.3.4 Comparison to modern values 27

1.3.5 Multivariate analyses 27

1.4 Conclusion 28

1.5 References 29

CHAPITRE 2 DECOUPLED WINTER AND SUMMER CLIMATE CHANGES IN SOUTHERN EUROPE DURING DANSGAARD-OESCHGER CYCLES 52

2.1 Introduction 53

2.2 Material 55

2.2.1 Data compilation and selection criteria 55
2.2.2 Chronologies 55
2.3 Pollen data and related vegetation and climate signal 57
2.3.1 Raw pollen counts 57
2.3.2 Vegetation reconstruction: Plant Functional Types (PFTs) 57
2.3.3 Climate reconstructions 58
2.3.3.1 Modern pollen database 59
2.3.3.2 Climatic reconstruction from marine core pollen data 60
2.3.3.3 The atmospheric CO_2 effect 62
2.3.3.4 Comparison to modern values 63
2.3.3.5 Multivariate analyses 63
2.4 Results and Discussion 64
2.4.1 Millennial-scale alternation of arboreal and non-arboreal PFTs 64
2.4.2 Winter forcing of millennial-scale vegetation shifts 65
2.4.3 Warm summer climate stability despite large amplitude winter variations in southern Europe throughout MIS 3 67
2.4.4 Possible linkage with North Atlantic Oscillation-like atmospheric phenomenon and Subpolar Gyre (SPG) dynamics 68
2.4.5 The key role of warm summer temperatures throughout MIS 3 70
2.5 Conclusion 71
2.6 Acknowledgments 72
2.7 References 72
2.8 SUPPLEMENTARY INFORMATION 87
2.8.1 Modern Analogue Technique (MAT): Theory, limitations and relevance 87
2.8.2 Significance of pollen assemblages in terms of climate 90
2.8.3 Climate reconstruction in marine cores 91
2.8.3.1 Tests based on results from marine core MD95-2042 93
2.8.4 References 117
CHAPITRE 3 HIGH WINTER PRECIPITATION INFERRED FROM POLLEN SEQUENCES IN SOUTHERN EUROPE DURING THE LAST GLACIAL MAXIMUM 122
3.1 Introduction 124
3.2 Environmental setting 125
3.2.1 Climate and Vegetation 125
3.2.2 Oceanography and sedimental processes at marine core locations 126
3.3 Material and Methods 127
3.3.1 Pollen data and chronologies 127
3.3.2 Vegetation: Plant Functional Types (PFTs) 128
3.3.3 Pollen-based climate reconstruction 128
3.3.4 Redundancy analysis (RDA) 130
3.3.5 Paleohydrographic reconstructions at site SU81-18 131
3.4 Results 131

3.4.1 Primary patterns of PFT variations 131
3.4.2 Vegetation and climate during the glacial episode 132
3.4.2.1 Southwestern Iberian margin 132
3.4.2.2 Alboran Sea and Southeastern Spain....133
3.4.2.3 Southern Italy....135
3.4.2.4 Greece....136
3.5 Discussion....137
3.5.1 Regionally coherent winter-annual precipitation pattern from 28 to 10 ka 137
3.5.1.1 Regional increase of winter-annual precipitation during the LGM 138
3.5.2 Vegetation dynamics in southern Europe during the LGM and West-East gradient of winter temperatures 140
3.5.3 Highly variable climate conditions in southwestern Europe during the LGM 141
3.6 Conclusion 143
3.7 References....145
3.8 SUPPLEMENTARY DATA 169
3.8.1 References 173
CONCLUSION 174
ANNEXE A A ready-to-use version of the Eurasian Modern Pollen Database 2 (EMPD 2; Davis et al., 2020) for paleoclimatic reconstructions 183
RÉFÉRENCES 216

LISTE DES FIGURES

Figure 0.1 Enregistrement isotopique de l'oxygène NGRIP (North Greenland Ice Core Project members, 2004). Les interstadiaires (GIs) et stadiaires (GSs) sont délimités selon Rasmussen et al. (2014), les stades isotopiques marins (MIS – Marine Isotope Stage) selon Lisiecki et Raymo (2005) et le LGM selon Mix et al. (2001). 3

Figure 1.1 Location of the fossil pollen records (red dots) studied in this work and NGRIP (black dot); North Greenland Ice Core Project (NGRIP, 2004)). The main European biomes are defined from Olson et al. (2001). EGC: East Greenland Current; IC: Irminger Current; NAD: North Atlantic Drift. 46

Figure 1.2 Biomes and locations of the modern pollen samples included in the final version of the EMPD2 used in this work (modified from Davis et al. (2020)). 47

Figure 1.3 Modern pollen samples defined by their biomes in the climatic space (modified from Davis et al. (2020)). 48

Figure 1.4 Cross - validation results of the observed against estimated climatic parameters. The blue and red open circles correspond to the calibration and verification data sets, respectively. The Root Mean Square Error of Prediction (RMSEP) and the coefficient of correlation (R^2) indicate the degree of accuracy of estimates. MTCO: mean-temperature of the coldest month; MTWA: mean-temperature of the warmest month; Seasonality = MTWA – MTCO; Pann: annual precipitation; Pdjf: winter precipitation; Pjja: summer precipitation. 49

Figure 1.5 Comparison between NGRIP oxygen isotopic record (North Greenland Ice Core Project members, 2004) and records related to sea-surface conditions, vegetation and climate (reconstructions with (A) and (B) without *Pinus*) at site 3 (core MD95-2042), off southern Portugal (Figure 1.1; Table 1.1 and references therein): (from left to right) $\delta^{18}O$ of *Globigerina bulloides* (Gb) (Shackleton et al., 2000) used as a proxy of sea-surface temperature (Malevich et al., 2019), the warm sea-surface phases are indicated by red bars; RDA axis-1 scores (with number of samples (n) for each side; MTCO (blue line) and MTWA (red line); seasonality (difference between MTWA and MTCO); summer (red line), winter (blue line) and annual precipitation (black line); SCD of the 1st (green circles) and 5th (red circles) analogues for each sample and SCD threshold (red line) and half of this threshold (black dotted line). 50

Figure 1.6 CCA ordination diagram of pollen taxa (green (trees+shrubs) and orange (herbs) dots) (see Table 1.3 for codes) vs. environmental variables (blue arrows). Analyses were performed on logarithmic (ln) values of the relative frequency of pollen taxa (%) using the CANOCO software of (Smilauer and Leps, 2014). MTCO: mean-temperature of the coldest month; MTWA: mean-temperature of the warmest month; Seasonality = MTWA – MTCO; Pann: annual precipitation; Pdjf: winter precipitation; Pjja: summer precipitation. 51

Figure 2.1 Map showing the location of the pollen data sites (numbered purple stars) used in this study (Table 2.1 and references therein) and of other sites referred to in the text (black dot). The main modern European biomes are defined by Olson et al. (2001). White areas represent the ice limits at the end of MIS 3 (around 30 ka) following Batchelor et al. (2019), except for the Alps and Pyrenees for which, in the absence of precise data for 30 ka, ice limits of the LGM are represented (Ehlers and

Gibbard, 2004) (paleocoastlines not represented). The main modern surface currents and gyres are indicated as follows: Irminger Current (IC), North Atlantic Drift (NAD), East Greenland Current (EGC), Subpolar Gyre (SPG), Subtropical Gyre (STG). 82

Figure 2.2 Results of the redundancy analysis (RDA) performed with MIS 3 data from a) marine core MD95-2042 (site 2 in Fig. 2.1), off Portugal (Sanchez-Goñi et al., 2000, 2002, 2008, 2009; Sanchez-Goñi, 2006) and b) terrestrial core Megali Limni (site 12 in Fig. 2.1), in Greece (Margari et al., 2009). Green and yellow arrows represent the arboreal and non-arboreal PFTs respectively (see Table 2.2 for further details on PFTs). Grey dashed arrows represent the climatic parameter discussed in this paper. Arrows pointing in the same/opposite direction indicate that they are positively/negatively correlated. The percentages along the axes indicate how much of the total variance they explain. Climatic parameters: Mean-temperature of the warmest (MTWA) and the coldest (MTCO) months; Summer (Pjja), Winter (Pdjf) Annual (Pann) precipitation; Seasonality (Season) = MTWA-MTCO.... 83

Figure 2.3 a) Time series encompassing MIS 3 showing the NGRIP oxygen isotopic data (NGRIP, 2004) and climate-related records from core MD2042 (site 2 in Fig. 2.1) : (from left to right) $\delta^{18}O$ of *Globigerina bulloides* (Gb) from Shackleton et al. (2000); MTCO (blue line) and MTWA (orange line); seasonality (difference between MTWA and MTCO); summer (orange line), winter (blue line) and annual precipitation (black line); square-chord distances of the 1st and 5th best analogues and analogue thresholds (see Material and Methods). Horizontal pink bars indicate the warm sea-surface phases defined after the $\delta^{18}O$ (Gb) record. b) Time series encompassing MIS 3 showing the NGRIP oxygen isotopic data (NGRIP, 2004) and climate-related records from Megali Limni (site 12 in Fig. 2.1): (from left to right) RDA axis-1 scores (with number of samples (n) for each side; MTCO (blue line) and MTWA (orange line); seasonality (difference between MTWA and MTCO); summer (orange line), winter (blue line) and annual precipitation (black line); square-chord distances of the 1st and 5th best analogues and analogue thresholds (see Chapter 2.3.3). Dashed vertical color lines in represent the mean 1901-2022 climate values (see Chapter 2.3.3.4). Horizontal green bars indicate the phases of arboreal increase defined after the RDA axis-1 scores. 84

Figure 2.4 Difference between mean climatic values associated with arboreal (GIs) and non-arboreal (GSs) sides of the axis-1 scores for each marine (light blue) and terrestrial (light green) site (Figs. 2.1-2.3; Figs. 2.S1-2.S12). When the bars are full, GI values (upper limit of the bar) > GS values (lower limit of the bar). When the bars are empty, GS values (upper limit of the bar) > GI values (lower limit of the bar). 85

Figure 2.5 Conceptual scheme of seasonal climate and vegetation during GSs and GIs. Conifer-like tree symbols illustrate a majority of conifers or pioneers in the arboreal vegetation (whether it be from boreal forests or eurythermic conifer forests). The presence of deciduous (oak-like symbols) indicates a high proportion of temperate trees in the arboreal vegetation. Herb-like symbols indicate the presence of non-arboreal vegetation (green symbols for grass and yellow symbols for steppe forb/desert forb/shrub). NAD: North Atlantic Drift; NAO: North Atlantic Oscillation; SPG: Subpolar Gyre; SSTs: Sea-Surface Temperatures. White areas: ice limits at the end of MIS 3 (around 30 ka) following Batchelor et al. (2019), except for the Alps and Pyrenees for which, in the absence of precise data for 30 ka, ice limits of the LGM are represented (Elhers and Gibbard, 2004) (paleocoastlines not represented). Red solid arrow: the NAD flows at the surface; Red dashed arrow: the NAD flows under the freshwater lid (eastward extended SPG). The extent of the sea-ice cover is not illustrated, hence the question marks. 86

Figure 2.S1 (a) Age model of core MD95-2039 (site 1), off southern Portugal (Fig. 2.1; Table 2.1 and references therein), obtained by using CLAM (Blaauw, 2010) (see Chapter 2.2.2.Chronologies, Table 2.1 and related files in Sanchez et al. (2017) for further details and data). The black line corresponds to the weighted average. Gray areas show the confidence intervals of the age-depth models calculated by defaults at 95% (2 sigma). The dates are indicated in blue and the correlated tie points are indicated in green. (b) RDA graph for site 1. Yellow arrows represent the non-arboreal PFTs while the green arrows represent the arboreal PFTs (see Table 2.2 for more details). Grey arrows represent the climatic parameters reconstructed. The percentages next to each axis indicate how much of the total constrained variance of PFTs they explain. (c) Comparison between NGRIP oxygen isotopic record (NGRIP, 2004) and records related to sea-surface conditions, vegetation and climate at site 1: (from bottom to top) $\delta^{18}O$ of *Globigerina bulloides* (Gb) (Eynaud et al., 2009) used as a proxy of sea-surface temperature (Malevich et al., 2019), the warm sea-surface phases are indicated by red bars; RDA axis-1 scores (with number of samples (n) for each side; MTCO (blue line) and MTWA (orange line); seasonality (difference between MTWA and MTCO); summer (orange line), winter (blue line) and annual precipitation (black line); square-chord distances of the 1st and 5th best analogues and analogue thresholds (see Material and Methods). 102

Figure 2.S2 (a) Age model of core MD95-2042 (site 2), off southern Portugal (Fig. 2.1; Table 2.1 and references therein), obtained by using CLAM (Blaauw, 2010) (see Chapter 2.2.2.Chronologies, Table 2.1 and related files in Sanchez et al. (2017) for further details and data). The black line corresponds to the weighted average. Gray areas show the confidence intervals of the age-depth models calculated by defaults at 95% (2 sigma). The dates are indicated in blue and the correlated tie points are indicated in green. (b) RDA graph for site 2. Yellow arrows represent the non-arboreal PFTs while the green arrows represent the arboreal PFTs (see Table 2.2 for more details). Grey arrows represent the climatic parameters reconstructed. The percentages next to each axis indicate how much of the total constrained variance of PFTs they explain. (c) Comparison between NGRIP oxygen isotopic record (NGRIP, 2004) and records related to sea-surface conditions, vegetation and climate at site 2: (from bottom to top) $\delta^{18}O$ of *Globigerina bulloides* (Gb) (Shackleton et al., 2000) used as a proxy of sea-surface temperature (Malevich et al., 2019), the warm sea-surface phases are indicated by red bars; RDA axis-1 scores (with number of samples (n) for each side; MTCO (blue line) and MTWA (orange line); seasonality (difference between MTWA and MTCO); summer (orange line), winter (blue line) and annual precipitation (black line); square-chord distances of the 1st and 5th best analogues and analogue thresholds (see Material and Methods). 103

Figure 2.S3 (a) Age model of core ODP 976 (site 3), in the Alboran Sea (Fig. 2.1; Table 2.1 and references therein), obtained by using CLAM (Blaauw, 2010) (see Chapter 2.2.2.Chronologies, Table 2.1 and related files in Sanchez et al. (2017) for further details and data). The black line corresponds to the weighted average. Gray areas show the confidence intervals of the age-depth models calculated by defaults at 95% (2 sigma). The dates are indicated in blue and the correlated tie points are indicated in green. (b) RDA graph for site 3. Yellow arrows represent the non-arboreal PFTs while the green arrows represent the arboreal PFTs (see Table 2.2 for more details). Grey arrows represent the climatic parameters reconstructed. The percentages next to each axis indicate how much of the total constrained variance of PFTs they explain. (c) Comparison between NGRIP oxygen isotopic record (NGRIP, 2004) and records related to vegetation and climate at site 3: (from bottom to top) RDA axis-1 scores (with number of samples (n) for each side; MTCO (blue line) and MTWA (orange line); seasonality (difference between MTWA and MTCO); summer (orange line), winter (blue line) and annual precipitation (black line); square-chord distances of the 1st and 5th best analogues and

analogue thresholds (see Material and Methods). Green bars indicate the phases of arboreal increase defined after the RDA axis-1 scores. 104

Figure 2.S4 (a) Age model of core MD95-2043 (site 4), in the Alboran Sea (Fig. 2.1; Table 2.1 and references therein), obtained by using CLAM (Blaauw, 2010) (see Chapter 2.2.2.Chronologies, Table 2.1 and related files in Sanchez et al. (2017) for further details and data). The black line corresponds to the weighted average. Gray areas show the confidence intervals of the age-depth models calculated by defaults at 95% (2 sigma). The dates are indicated in blue and the correlated tie points are indicated in green. (b) RDA graph for site 4. Yellow arrows represent the non-arboreal PFTs while the green arrows represent the arboreal PFTs (see Table 2.2 for more details). Grey arrows represent the climatic parameters reconstructed. The percentages next to each axis indicate how much of the total constrained variance of PFTs they explain. (c) Comparison between NGRIP oxygen isotopic record (NGRIP, 2004) and records related to sea-surface conditions, vegetation and climate at site 4: (from bottom to top) benthic $\delta^{18}O$ record based on *C. pachydermus* (Cp) (Cacho et al., 2006) which is indicative of global temperature, warm phases are indicated by red bars; RDA axis-1 scores (with number of samples (n) for each side; MTCO (blue line) and MTWA (orange line); seasonality (difference between MTWA and MTCO); summer (orange line), winter (blue line) and annual precipitation (black line); square-chord distances of the 1st and 5th best analogues and analogue thresholds (see Material and Methods). 105

Figure 2.S5 (a) Age model of the Lac du Bouchet sequence (site 5), France (Fig. 2.1; Table 2.1 and references therein), obtained by using CLAM (Blaauw, 2010) (see Chapter 2.2.2.Chronologies, Table 2.1 and related files in Sanchez et al. (2017) for further details and data). The black line corresponds to the weighted average. Gray areas show the confidence intervals of the age-depth models calculated by defaults at 95% (2 sigma). The dates are indicated in blue and the correlated tie points are indicated in green. (a) RDA graph for site 5. Yellow arrows represent the non-arboreal PFTs while the green arrows represent the arboreal PFTs (see Table 2.2 for more details). Grey arrows represent the climatic parameters reconstructed. The percentages next to each axis indicate how much of the total constrained variance of PFTs they explain. (b) Comparison between NGRIP oxygen isotopic record (NGRIP, 2004) and records related to vegetation and climate at site 5: (from bottom to top) RDA axis-1 scores (with number of samples (n) for each side; MTCO (blue line) and MTWA (orange line); seasonality (difference between MTWA and MTCO); summer (orange line), winter (blue line) and annual precipitation (black line); square-chord distances of the 1st and 5th best analogues and analogue thresholds (see Material and Methods). Dashed colour lines represent the mean 1901-2022 climate values (see Material and Methods). Green bars indicate the phases of arboreal increase defined after the RDA axis-1 scores. 106

Figure 2.S6 (a) Age model of the Lagaccione sequence (site 6), Italy (Fig. 2.1; Table 2.1 and references therein), obtained by using CLAM (Blaauw, 2010) (see Chapter 2.2.2.Chronologies, Table 2.1 and related files in Sanchez et al. (2017) for further details and data). The black line corresponds to the weighted average. Gray areas show the confidence intervals of the age-depth models calculated by defaults at 95% (2 sigma). The dates are indicated in blue and the correlated tie points are indicated in green. (b) RDA graph for site 6. Yellow arrows represent the non-arboreal PFTs while the green arrows represent the arboreal PFTs (see Table 2.2 for more details). Grey arrows represent the climatic parameters reconstructed. The percentages next to each axis indicate how much of the total constrained variance of PFTs they explain. (c) Comparison between NGRIP oxygen isotopic record (NGRIP, 2004) and records related to vegetation and climate at site 6: (from bottom to top) RDA axis-1 scores (with number of samples (n) for each side; MTCO (blue line) and MTWA (orange line);

seasonality (difference between MTWA and MTCO); summer (orange line), winter (blue line) and annual precipitation (black line); square-chord distances of the 1st and 5th best analogues and analogue thresholds (see Material and Methods). Dashed colour lines represent the mean 1901-2022 climate values (see Material and Methods). Green bars indicate the phases of arboreal increase defined after the RDA axis-1 scores. 107

Figure 2.S7 (a) Age model of the Stracciacappa sequence (site 7), Italy (Fig. 2.1; Table 2.1 and references therein), obtained by using CLAM (Blaauw, 2010) (see Chapter 2.2.2.Chronologies, Table 2.1 and related files in Sanchez et al. (2017) for further details and data). The black line corresponds to the weighted average. Gray areas show the confidence intervals of the age-depth models calculated by defaults at 95% (2 sigma). The dates are indicated in blue and the correlated tie points are indicated in green. (b) RDA graph for site 7. Yellow arrows represent the non-arboreal PFTs while the green arrows represent the arboreal PFTs (see Table 2.2 for more details). Grey arrows represent the climatic parameters reconstructed. The percentages next to each axis indicate how much of the total constrained variance of PFTs they explain. (c) Comparison between NGRIP oxygen isotopic record (NGRIP, 2004) and records related to vegetation and climate at site 7: (from bottom to top) RDA axis-1 scores (with number of samples (n) for each side; MTCO (blue line) and MTWA (orange line); seasonality (difference between MTWA and MTCO); summer (orange line), winter (blue line) and annual precipitation (black line); square-chord distances of the 1st and 5th best analogues and analogue thresholds (see Material and Methods). Dashed colour lines represent the mean 1901-2022 climate values (see Material and Methods). Green bars indicate the phases of arboreal increase defined after the RDA axis-1 scores. 108

Figure 2.S8 (a) Age model of the Valle di Castiglione sequence (site 8), Italy (Fig. 2.1; Table 2.1 and references therein), obtained by using CLAM (Blaauw, 2010) (see Chapter 2.2.2.Chronologies, Table 2.1 and related files in Sanchez et al. (2017) for further details and data). The black line corresponds to the weighted average. Gray areas show the confidence intervals of the age-depth models calculated by defaults at 95% (2 sigma). The dates are indicated in blue and the correlated tie points and tephra layer are indicated in green and orange respectively. (b) RDA graph for site 8. Yellow arrows represent the non-arboreal PFTs while the green arrows represent the arboreal PFTs (see Table 2.2 for more details). Grey arrows represent the climatic parameters reconstructed. The percentages next to each axis indicate how much of the total constrained variance of PFTs they explain. (c) Comparison between NGRIP oxygen isotopic record (NGRIP, 2004) and records related to vegetation and climate at site: (from bottom to top) RDA axis-1 scores (with number of samples (n) for each side; MTCO (blue line) and MTWA (orange line); seasonality (difference between MTWA and MTCO); summer (orange line), winter (blue line) and annual precipitation (black line); square-chord distances of the 1st and 5th best analogues and analogue thresholds (see Material and Methods). Dashed colour lines represent the mean 1901-2022 climate values (see Material and Methods). Green bars indicate the phases of arboreal increase defined after the RDA axis-1 scores. 109

Figure 2.S9 (b) RDA graph for site 9 (Lago Grandi di Monticchio), Italy (Fig. 2.1; Table 2.1 and references therein). Yellow arrows represent the non-arboreal PFTs while the green arrows represent the arboreal PFTs (see Table 2.2 for more details). Grey arrows represent the climatic parameters reconstructed. The percentages next to each axis indicate how much of the total constrained variance of PFTs they explain. (c) Comparison between NGRIP oxygen isotopic record (NGRIP, 2004) and records related to vegetation and climate at site 9: (from bottom to top) RDA axis-1 scores (with number of samples (n) for each side; MTCO (blue line) and MTWA (orange line); seasonality (difference between MTWA and MTCO); summer (orange line), winter (blue line) and annual

precipitation (black line); square-chord distances of the 1st and 5th best analogues and analogue thresholds (see Material and Methods). Dashed colour lines represent the mean 1901-2022 climate values (see Material and Methods). Green bars indicate the phases of arboreal increase defined after the RDA axis-1 scores. As mentioned in the main core of the paper, we used the initial chronology based on annual lamination ("varve") counts and sedimentological features in the non-varved intervals (Zolitschka and Negendank, 1996), hence the absence of an a) age model. 110

Figure 2.S10 (a) Age model of the Ioannina sequence (site 10), Greece (Fig. 2.1; Table 2.1 and references therein), obtained by using CLAM (Blaauw, 2010) (see Chapter 2.2.2.Chronologies, Table 2.1 and related files in Sanchez et al. (2017) for further details and data). The black line corresponds to the weighted average. Gray areas show the confidence intervals of the age-depth models calculated by defaults at 95% (2 sigma). The dates are indicated in blue and the correlated tie points are indicated in green. (b) RDA graph for site 10. Yellow arrows represent the non-arboreal PFTs while the green arrows represent the arboreal PFTs (see Table 2.2 for more details). Grey arrows represent the climatic parameters reconstructed. The percentages next to each axis indicate how much of the total constrained variance of PFTs they explain. (c) Comparison between NGRIP oxygen isotopic record (NGRIP, 2004) and records related to vegetation and climate at site 10: (from bottom to top) RDA axis-1 scores (with number of samples (n) for each side; MTCO (blue line) and MTWA (orange line); seasonality (difference between MTWA and MTCO); summer (orange line), winter (blue line) and annual precipitation (black line); square-chord distances of the 1st and 5th best analogues and analogue thresholds (see Material and Methods). Dashed colour lines represent the mean 1901-2022 climate values (see Material and Methods). Green bars indicate the phases of arboreal increase defined after the RDA axis-1 scores. 111

Figure 2.S11 (a) Age model of the Xinias sequence (site 11), Greece (Fig. 2.1; Table 2.1 and references therein), obtained by using CLAM (Blaauw, 2010) (see Chapter 2.2.2.Chronologies, Table 2.1 and related files in Sanchez et al. (2017) for further details and data). The black line corresponds to the weighted average. Gray areas show the confidence intervals of the age-depth models calculated by defaults at 95% (2 sigma). The dates are indicated in blue and the correlated tie points are indicated in green. (b) RDA graph for site 11. Yellow arrows represent the non-arboreal PFTs while the green arrows represent the arboreal PFTs (see Table 2.2 for more details). Grey arrows represent the climatic parameters reconstructed. The percentages next to each axis indicate how much of the total constrained variance of PFTs they explain. (c) Comparison between NGRIP oxygen isotopic record (NGRIP, 2004) and records related to vegetation and climate at site 11: (from bottom to top) RDA axis-1 scores (with number of samples (n) for each side; MTCO (blue line) and MTWA (orange line); seasonality (difference between MTWA and MTCO); summer (orange line), winter (blue line) and annual precipitation (black line); square-chord distances of the 1st and 5th best analogues and analogue thresholds (see Material and Methods). Dashed colour lines represent the mean 1901-2022 climate values (see Material and Methods). Green bars indicate the phases of arboreal increase defined after the RDA axis-1 scores. 112

Figure 2.S12 (a) Age model of the Megali limni sequence (site 12), Greece (Fig. 2.1; Table 2.1 and references therein), obtained by using CLAM (Blaauw, 2010) (see Chapter 2.2.2.Chronologies, Table 2.1 and related files in Sanchez et al. (2017) for further details and data). The black line corresponds to the weighted average. Gray areas show the confidence intervals of the age-depth models calculated by defaults at 95% (2 sigma). The dates are indicated in blue and the correlated tie points and tephra layer are indicated in green and orange respectively. (b) RDA graph for site 12. Yellow arrows represent the non-arboreal PFTs while the green arrows represent the arboreal PFTs (see Table 2.2

for more details). Grey arrows represent the climatic parameters reconstructed. The percentages next to each axis indicate how much of the total constrained variance of PFTs they explain. (c) Comparison between NGRIP oxygen isotopic record (NGRIP, 2004) and records related to vegetation and climate at site 12: (from bottom to top) RDA axis-1 scores (with number of samples (n) for each side; MTCO (blue line) and MTWA (orange line); seasonality (difference between MTWA and MTCO); summer (orange line), winter (blue line) and annual precipitation (black line); square-chord distances of the 1st and 5th best analogues and analogue thresholds (see Material and Methods). Dashed colour lines represent the mean 1901-2022 climate values (see Material and Methods). Green bars indicate the phases of arboreal increase defined after the RDA axis-1 scores. 113

Figure 2.S13 Cross-validation results of the observed against estimated climatic parameters. The blue and red open circles correspond to the calibration and verification data sets, respectively. The Root Mean Square Error of Prediction (RMSEP) and the coefficient of correlation (R^2) indicate the degree of accuracy of estimates. MTCO: mean-temperature of the coldest month; MTWA: mean-temperature of the warmest month; Seasonality = MTWA – MTCO; Pann: annual precipitation; Pdjf: winter precipitation; Pjja: summer precipitation. 114

Figure 2.S14 Comparison between NGRIP oxygen isotopic record (NGRIP, 2004) and records related to sea-surface conditions and climate reconstructions with (A) and without *Pinus* (B) at site 2 (core MD95-2042), off southern Portugal (Fig. 2.1; Table 2.1 and references therein): (from left to right) $\delta^{18}O$ of *Globigerina bulloides* (Gb) (Shackleton et al., 2000) used as a proxy of sea-surface temperature (Malevich et al., 2019), the warm sea-surface phases are indicated by red bars; MTCO (blue line) and MTWA (red line); seasonality (difference between MTWA and MTCO); summer (red line), winter (blue line) and annual precipitation (black line); SCD of the 1st (green circles) and 5th (red circles) analogues for each sample and SCD threshold (red line) and half of this threshold (black dotted line). 115

Figure 2.S15 CCA ordination diagram of pollen taxa (green (trees+shrubs) and orange (herbs) dots) (see Table 2.2 for codes) vs. environmental variables (blue arrows) of the European modern database. Analyses were performed on square root values of the relative frequency of pollen taxa (%) using the CANOCO software of (Šmilauer and Lepš, 2014). 116

Figure 3.1 Map showing the location of the five pollen sequences (yellow stars) used in this study (Table 3.1 and references therein). Black dots show the location of records that are mentioned in the text: NGRIP (NGRIP, 2004), BS79-38 and BS79-33 (Cacho et al., 2001). The main surface currents and gyres are indicated as follows: Irminger Current (IC), North Atlantic Drift (NAD), East Greenland Current (EGC), Subpolar Gyre (SPG), Subtropical Gyre (STG). White areas represent LGM ice sheets. The transparent blue line defines the jet stream and notably the Rossby wave breaking west of the Alps as illustrated in Luetscher et al. (2015) and the schematic ice limits at LGM are defined after Ehlers et al. (2004). 159

Figure 3.2 Results of the redundancy analysis (RDA) in the 4 study sequences. a) SU81-18 off South Portugal (Turon et al., 2003); b) ODP Site 976 in Alboran Sea (Combourieu-Nebout et al., 2009); c) Padul in Southeastern Spain (Camuera et al., 2018, 2019); d) Monticchio in Southern Italy (Allen et al., 2000) and e) Xinias in Greece (Bottema, 1979). Green and yellow arrows represent the arboreal and non-arboreal PFTs respectively (Table 3.2). Grey dashed arrows represent the climatic parameter discussed in this paper. Climatic parameters as in Table 3.3. 160

Figure 3.3 Records related to vegetation, sea-surface conditions, and pollen-based climate reconstructions at site SU81-18 (Figure 3.1; Table 3.1). a) NGRIP reference oxygen isotope record (NGRIP, 2004), b) RDA axis-1 scores (see Figure 3.2a) and foraminifera-based sea-ice cover duration reconstructions (this study, see Chapter 3.3.5.), c) foraminifera – based Sea-Surface Temperatures (SSTs) (this study, see Chapter 3.3.5.), d) Mean temperature of the coldest (MTCO) and the warmest months (MTWA), e) *Neogloboquadina pachyderma* (Nps) percentages in planktic foraminifer assemblages (Eynaud et al., 2009) and IRD (Bard et al., 2000), f) Seasonality (MTWA-MTCO), g) annual and seasonal precipitation, h) square-chord distances of the 1st and 5th best analogues and analogue thresholds (see text). Light curves: MAT values; Bold curves: 3-point running mean. The blue zones correspond to the Heinrich Stadials (HS) as defined in Sánchez-Goñi and Harrison (2010) and the Younger Dryas (YD) as defined in Rasmussen et al. (2014). 161

Figure 3.4 Records related to vegetation, sea-surface conditions, and pollen-based climatic reconstructions at ODP Site 976 (Figure 3.1; Table 3.1). a) reference NGRIP oxygen isotope record (NGRIP, 2004), b) RDA axis-1 scores (see Figure 3.2b), c) Mean temperature of the coldest (MTCO) and the warmest months (MTWA), d) Alkenone-based mean annual Sea-Surface Temperatures (SSTs) (Martrat et al., 2014), e) Seasonality (MTWA-MTCO), f) annual and seasonal precipitation and g) square-chord distances of the 1st and 5th best analogues and analogue threshold values (see text). Light curves: MAT values; Bold curves: 3-points running mean). The blue zones correspond to the Heinrich Stadials (HS) as defined in Sánchez-Goñi and Harrison (2010) and the Younger Dryas (YD) as defined in Rasmussen et al. (2014)..... 162

Figure 3.5 Records related to vegetation and pollen-based climatic reconstructions at Padul (Figure 3.1; Table 3.1). a) reference NGRIP oxygen isotope record (NGRIP, 2004), b) RDA axis-1 scores (see Figure 3.2c), c) Mean temperature of the coldest (MTCO) and the warmest months (MTWA), d) Seasonality (MTWA-MTCO), e) annual and seasonal precipitation and f) square-chord distances of the 1st and 5th best analogues and analogue threshold values (see text). Dashed color lines in c and e represent the mean 1901-2022 climate values (see Material and Methods). The blue zones correspond to the Heinrich Stadials (HS) as defined in Sánchez-Goñi and Harrison (2010) and the Younger Dryas (YD) as defined in Rasmussen et al. (2014). Dashed red lines indicate an alternative chronology. 163

Figure 3.6 Records related to vegetation, and pollen-based climatic reconstructions at Monticchio (Figure 3.1; Table 3.1) and sea-surface conditions from proximal marine cores. a) reference NGRIP oxygen isotope record (GRIP, 2004), b) RDA axis-1 scores (see Figure 3.2d), c) Alkenone-based mean annual Sea-Surface Temperatures (SSTs) from cores BS79-33 and BS79-38 located in Tyrrhenian Sea (Cacho et al., 2001), d) Mean temperature of the coldest (MTCO) and the warmest months (MTWA) (MAT), e) Seasonality (MTWA-MTCO) (MAT), f) annual and seasonal precipitation (MAT) and g) square-chord distances of the 1st and 5th best analogues and threshold values for significant analogue (see text). 164

Figure 3.7 Records related to vegetation and pollen-based climatic reconstructions at Xinias (Figure 3.1; Table 3.1). a) reference NGRIP oxygen isotope record (NGRIP, 2004), b) RDA axis-2 scores (see Figure 3.2e), c) Mean temperature of the coldest (MTCO) and the warmest months (MTWA), d) Seasonality (MTWA-MTCO), e) annual and seasonal precipitation and f) square-chord distances of the 1st and 5th best analogues and analogue threshold values (see text). Dashed color lines in c and e represent the mean 1901-2022 climate values (see Material and Methods). The blue zones correspond to the Heinrich Stadials (HS) as defined in Sánchez-Goñi and Harrison (2010) and the Younger Dryas (YD) as defined in Rasmussen et al. (2014). Dashed red lines indicate an alternative chronology. 165

Figure 3.8 Pollen-based winter (Pdjf) and annual precipitation (Pann) estimates from the 5 studied sequences. Light curves: MAT values; Bold curves: 3-points running mean. The blue zones correspond to the Heinrich Stadials (HS) as defined in Sánchez-Goñi and Harrison (2010) and the Younger Dryas (YD) as defined in Rasmussen et al. (2014). Dashed blue and black lines represent the mean 1901-2022 climate values for winter and annual precipitation respectively (see Material and Methods). Dashed red lines indicate alternative chronologies for the Padul, Monticchio and Xinias sequences. 166

Figure 3.9 NGRIP oxygen isotope record (NGRIP, 2004) and RDA axis-1 scores (axis-2 scores for Xinias, see also Figure 3.2 and text) of the record from the five studied pollen sequences (Figure 3.1; Table 3.1). Dashed red lines indicate alternative chronologies for the Padul, Monticchio and Xinias sequences. 167

Figure 3.10 Pollen-based mean temperature of the coldest month (MTCO) estimates from the 5 studied sequences. Light curves: MAT values; Bold curves: 3-points running mean. The blue zones correspond to the Heinrich Stadials (HS) as defined in Sánchez-Goñi and Harrison (2010) and the Younger Dryas (YD) as defined in Rasmussen et al. (2014). Dashed blue lines represent the mean 1901-2022 climate values (see Material and Methods). Dashed red lines indicate alternative chronologies for the Padul, Monticchio and Xinias sequences. 168

Figure 3.S1 Age model of core SU81-18, off southern Portugal (Figure 3.1; Table 3.1 and references therein), obtained by using CLAM (Blaauw, 2010) (see Material and Methods and related files in Sanchez et al. (2017) for further details and data). The black line corresponds to the weighted average. Gray areas show the confidence intervals of the age-depth models calculated by defaults at 95% (2 sigma). The dates are indicated in blue. 169

Figure 3.S2 Age model of core ODP Site 976, located in the Alboran Sea (Figure 3.1; Table 3.1 and references therein), obtained by using CLAM (Blaauw, 2010) (see Material and Methods and related files in Sanchez et al. (2017) for further details and data). The black line corresponds to the weighted average. Gray areas show the confidence intervals of the age-depth models calculated by defaults at 95% (2 sigma). The dates are indicated in blue and the correlated tie points are indicated in green. 170

Figure 3.S3 Age model of the Xinias sequence, located in Greece (Figure 3.1; Table 3.1 and references therein), obtained by using CLAM (Blaauw, 2010) (see Material and Methods and related files in Sanchez et al. (2017) for further details and data). The black line corresponds to the weighted average. Gray areas show the confidence intervals of the age-depth models calculated by defaults at 95% (2 sigma). The dates are indicated in blue. 171

Figure 3.S4 Records related to vegetation and pollen-based climatic reconstructions at Xinias (Figure 3.1; Table 3.1) as it is presented in Figure 3.7. a) reference NGRIP oxygen isotope record (NGRIP, 2004), b) RDA axis-2 scores (see Figure 3.2e), c) Mean temperature of the coldest (MTCO) and the warmest months (MTWA), d) Seasonality (MTWA-MTCO), e) annual and seasonal precipitation and f) square-chord distances of the 1st and 5th best analogues and analogue threshold values (see text). Dashed color lines in c and e represent the mean 1901-2022 climate values (see Material and Methods). The blue zones correspond to the Heinrich Stadials (HS) as defined in Sánchez-Goñi and Harrison (2010) and the Younger Dryas (YD) as defined in Rasmussen et al. (2014). Dashed red lines indicate an alternative chronology. 172

Figure 4.1 Enregistrements de signaux climatiques extra-régionaux et des variations de la végétation et de paramètres climatiques à partir des assemblages polliniques de Lago Grandi di Monticchio (Figure 3.1). De bas en haut : courbe de la composition isotopique de l'oxygène de carottes de glace du Groenland (North Greenland Ice Core Project members, 2004), évolution de la végétation à Monticchio telle que définie par une analyse multivariée des PFTs, , niveau marin (Spratt et Lisiecki, 2016), températures moyennes du mois le plus froid (MTCO - *Mean temperature of the coldest month*), précipitations annuelles et saisonnières et distances des premiers et cinquièmes meilleurs analogues, les distances inférieures au seuil/2 correspondant à de bons analogues, alors que celles comprises entre le seuil et le seuil/2 indiquent des analogues acceptables (de Vernal et al., 2005). 177

Figure 4.2 Enregistrements de signaux climatiques extra-régionaux et des variations de la végétation et de paramètres climatiques à partir des assemblages polliniques des carottes MD95-2042 et SU81-18 (Figure 1.1). De bas en haut : courbe de la composition isotopique de l'oxygène de carottes de glace du Groenland (North Greenland Ice Core Project members, 2004), évolution de la végétation telle que définie par une analyse multivariée des PFTs , courbes d'insolations estivale à 65°N et hivernale à 38°N (Laskar et al., 2004), températures moyennes du mois le plus froid (MTCO - *Mean temperature of the coldest month*) (lissage selon une fenêtre de 3 points en gras), précipitations annuelles (lissage selon une fenêtre de 9 valeurs en gras) et hivernales (lissage selon une fenêtre de 3 valeurs en gras), et distances des premiers et cinquièmes meilleurs analogues , les distances inférieures au seuil/2 correspondant à de bon analogues, alors que celles comprises entre le seuil et le seuil/2 indiquent des analogues acceptables (de Vernal et al., 2005). 179

Figure 4.3 Enregistrements de signaux climatiques extra-régionaux et des variations de la végétation et de paramètres climatiques à partir des assemblages polliniques de la carotte ODP Site 976 (Figure 1.1). De bas en haut : courbe de la composition isotopique de l'oxygène de carottes de glace du Groenland (North Greenland Ice Core Project members, 2004), évolution de la végétation telle que définie par une analyse multivariée des PFTs , courbes d'insolations estivale à 65°N et hivernale à 38°N (Laskar et al., 2004), températures moyennes du mois le plus froid (MTCO - Mean temperature of the coldest month), précipitations annuelles (lissage selon une fenêtre de 9 valeurs en gras) et hivernales (lissage selon une fenêtre de 3 valeurs en gras), et distances des premiers et cinquièmes meilleurs analogues, les distances inférieures au seuil/2 correspondant à de bon analogues, alors que celles comprises entre le seuil et le seuil/2 indiquent des analogues acceptables (de Vernal et al., 2005). 181

LISTE DES TABLEAUX

Table 1.1 Marine and terrestrial pollen records used for this study. 38

Table 1.2 Assignments used for the PFTs. Codes in green represent arboreal PFTs while those in brown represent non-arboreal PFTs. 39

Table 1.3 (also next page). List of the 88 pollen taxa retained for this work in the EMPD2 including 7634 sites. The taxa highlighted in grey were the ones removed for the 77 taxa version of the EMPD2 tested (see Chapter 1.3.3.3). 40

Table 1.4 Accuracy of reconstructions (RMSEP and R^2) for the 88 and 77 taxa databases (5 analogues). The best results are highlighted in grey. Climatic variables: MTCO (mean-temperature of the coldest month), MTWA (mean-temperature of the warmest month), Pdjf (winter precipitation), Pjja (summer precipitation), Pann (annual precipitation), Seasonality (MTWA – MTCO). 42

Table 1.5 Accuracy of reconstructions (root mean square error of prediction (RMSEP) and coefficient of correlation (R^2)) for different numbers of analogues (from 5 to 10) with the 88 taxa database. Best results are highlighted in grey. Climatic variables: MTCO (mean-temperature of the coldest month), MTWA (mean-temperature of the warmest month), Pdjf (winter precipitation), Pjja (summer precipitation), Pann (annual precipitation), Seasonality (MTWA – MTCO). 43

Table 1.6 Taxonomical diversity of most fossil records included in this study. N: number. *Most sequences cover partly or entirely MIS 3, but some of them also cover the previous and/or subsequent isotope stage (MIS 2 and 4). [1] only covers MIS 2. 44

Table 1.7 Accuracy of reconstructions as indicated from the root mean square error of prediction (RMSEP) and the coefficient of correlation (R^2) for the 88 and 87 (Pinus excluded) taxa databases (5 analogues). Climatic variables: MTCO (mean-temperature of the coldest month), MTWA (mean-temperature of the warmest month), Pdjf (winter precipitation), Pjja (summer precipitation), Pann (annual precipitation), Seasonality (MTWA – MTCO). 45

Table 2.1 Terrestrial and marine pollen records used in this study *(Sánchez Goñi et al., 2017) 80

Table 2.2 Assignments used for the PFTs. Codes in green represent arboreal PFTs while those in brown represent non-arboreal PFTs. 81

Table 2.S1 Mean temporal resolution of the pollen records included in this study (Fig. 2.1; Table 2.1). .. 96

Table 2.S2 (also next page). List of the 88 pollen taxa retained in the data set with 7634 sites. 97

Table 2.S3 Accuracy of reconstructions (root mean square error of prediction (RMSEP) and coefficient of correlation (R^2)) for different numbers of analogues (from 5 to 10) with the 88 taxa database. The best results are highlighted in grey. Climatic variables: MTCO (mean-temperature of the coldest month), MTWA (mean-temperature of the warmest month), Pdjf (winter precipitation), Pjja (summer precipitation), Pann (annual precipitation), Seasonality (MTWA – MTCO). 99

Table 2.S4 Taxonomical diversity of the fossil records included in this study (Fig. 2.1; Table 2.1). *N*: number. *All sequences cover partly or entirely MIS 3, but some of them also cover the previous and/or subsequent isotope stage (MIS 2 and 4). Marine and terrestrial sites are indicated in blue and green respectively. 100

Table 2.S5 Accuracy of reconstructions as indicated from the root mean square error of prediction (RMSEP) and the coefficient of correlation (R^2) for the 88 and 87 (*Pinus* excluded) taxa databases (5 analogues). Climatic variables: MTCO (mean-temperature of the coldest month), MTWA (mean-temperature of the warmest month), Pdjf (winter precipitation), Pjja (summer precipitation), Pann (annual precipitation), Seasonality (MTWA – MTCO). 101

Table 3.1 Marine and terrestrial pollen records used in this study. 156

Table 3.2 Assignments used for the PFTs. Codes in green represent arboreal PFTs while those in brown represent non-arboreal PFTs. 157

Table 3.3 Accuracy of MAT reconstructions estimated from the root mean square error of prediction (RMSEP) and the coefficient of correlation (R^2) for the 88 and 87 (*Pinus* excluded) taxa databases. MTCO: mean-temperature of the coldest month in °C; MTWA: mean-temperature of the warmest month in °C; Pdjf: winter precipitation in mm; Pjja: summer precipitation in mm; Pann: annual precipitation in mm; Seasonality: MTWA – MTCO in °C. 158

RÉSUMÉ

La dernière période glaciaire (115 à 11,7 ka) a été le théâtre de grands oscillations climatiques de fréquence millénaire connues sous le nom de cycles de Dansgaard-Oeschger (DO). Détectée pour la première fois dans les enregistrements isotopiques de l'oxygène de la glace du Groenland, cette alternance de phases chaudes, dites interstadiaires (GIs – *Greenland Interstadials*), et froides dites stadiaires (GSs – *Greenland Stadials*), a depuis été enregistrée partout à travers le globe, mais apparait particulièrement prononcée dans la région Atlantique Nord. Cependant, les forçages et mécanismes qui régissent cette variabilité climatique millénaire ne sont pas entièrement élucidés et demeurent un sujet de débats.

Le rôle de la saisonnalité pourrait avoir été sous-estimé car la plupart des traceurs ou proxies permettent de reconstituer les conditions moyennes annuelles ou estivales. Pourtant, quelques études ont démontré une variabilité plus grande du climat de la saison hivernale, certaines études allant même jusqu'à suggérer que les DOs pourraient représenter principalement un signal hivernal et que des températures estivales élevées pourraient avoir caractérisé la dernière période glaciaire. Cette hypothèse n'a malheureusement jamais pu être traitée en l'absence de reconstitutions quantitatives du contraste climatique saisonnier entre l'hiver et l'été, en général, et sur les continents en particulier.

Les données polliniques, qui renseignent sur le couvert végétal, sont l'un des rares traceurs biogéniques permettant d'obtenir des reconstitutions quantitatives saisonnières du climat en raison de la relation étroite qui existe entre le climat, actuel et passé, et la dynamique de la végétation. Or, la végétation du sud/sud-ouest de l'Europe s'est révélée avoir été particulièrement sensible à la variabilité climatique millénaire de la dernière période glaciaire. Nous avons donc sélectionné 14 séquences polliniques déjà publiées (5 issues de carottes marines, 9 de séquences terrestres), provenant du sud et sud-ouest de l'Europe et couvrant de 60 à 10 ka pour reconstituer les paramètres climatiques des saisons estivales et hivernales à partir de la méthode des analogues modernes (MAT – *Modern Analogue Technique*) et en utilisant la dernière version de la base de données polliniques modernes eurasienne (EMPD2).

Les reconstitutions de végétation, par l'examen des types de plantes fonctionnelles (PFT), ont permis de mettre en lumière d'importantes variations d'ordre millénaire au cours de la dernière période glaciaire, avec une alternance de phases plus arborées et de phases plus steppiques, qui, grâce à l'utilisation d'enregistrements de carottes marines, ont pu être corrélées aux GIs et GSs respectivement. Des analyses multivariées menées sur la végétation et les paramètres climatiques saisonniers indiquent une prédominance de l'influence hivernale sur la dynamique de la végétation, avec des hivers doux et humides au cours des phases arborées (GIs) et des hivers froids et secs durant les phases steppiques (GSs). Nos résultats révèlent également un comportement différent de l'été par rapport à l'hiver, avec des températures estivales élevées relativement stables tout au long de la période glaciaire, validant ainsi la principale hypothèse défendue dans cette thèse mettant en exergue l'importance de la saisonnalité.

De nos jours, la végétation du sud de l'Europe dépend de la quantité de pluie reçue en hiver, laquelle est déterminée par les modes de variations de l'Oscillation Nord Atlantique (NAO – *North Atlantic Oscillation*), qui correspondent aux mouvements latitudinaux de la trajectoire des tempêtes au-dessus du continent Européen selon la force des vents d'ouest. Bien que la NAO varie selon des échelles de temps interannuelles à décennales, nous suggérons que les DOs dans le sud/sud-ouest de l'Europe pourraient

être le fruit de variations millénaires de ce phénomène atmosphérique hivernal : des vents d'ouest renforcés au cours des GSs (NAO positive actuelle), génèreraient un déplacement des tempêtes vers le nord du continent, induisant des hivers froids et secs dans le sud de l'Europe. À l'inverse, de plus faibles vents d'ouest au cours des GIs (NAO négative actuelle) provoqueraient un déplacement des tempêtes vers le sud, générant un climat doux et humide, propice au développement de la végétation. Nous émettons également l'hypothèse que les températures estivales élevées relativement stables tout au long du dernier glaciaire auraient joué un rôle clé, en générant quantité d'eaux de fonte en provenance des calottes canadiennes et groenlandaises, mais que l'impact de ces eaux de fonte sur l'étendue du couvert de glace de mer en Atlantique Nord, la circulation thermohaline et le climat européen en général aurait été modulé par les variations millénaires de la circulation atmosphérique hivernale mentionnées précédemment.

Nos résultats démontrent également de fortes précipitations hivernales et annuelles en Europe du Sud au cours du dernier maximum glaciaire (LGM – *Last Glacial Maximum*). Une augmentation des précipitations pourrait être le résultat d'une réorganisation atmosphérique et une position plus méridionale des oscillations latitudinales des tempêtes due à l'extension maximale des calottes glaciaires. Des variations de températures et précipitations hivernales plus prononcées sur la marge ouest ibérique que dans le bassin méditerranéen suggèrent également la présence d'un front atmosphérique et/ou hydrologique entre les deux régions.

Mots clés : variabilité climatique millénaire, Europe du Sud, saisonnalité, séquences polliniques, technique des analogues modernes, circulation atmosphérique hivernale, vents d'ouest

ABSTRACT

The last glacial period (115 - 11,7 ka) underwent significant millennial-scale climatic oscillations, known as the Dansgaard-Oeschger (DO) cycles. First detected in the oxygen isotopic records of Greenland ice cores, this alternance of warm (GIs - Greenland Interstadials) and cold phases (GSs – Greenland Stadials) has since been recorded worldwide but appears particularly pronounced in the North Atlantic region. However, the forcings and mechanisms behind this millennial-scale climatic variability remain elusive and are still a matter of debate.

The role of seasonality may have been underestimated as most proxies reconstruct mean annual or summer conditions. Still, few studies have demonstrated a greater variability of the winter season, some suggesting that DO might mainly represent a winter signal but that warm summer temperatures might have prevailed during the whole last glacial period. This hypothesis has never been fully explored nor confirmed as very few studies propose quantitative reconstructions of the seasonal contrast between winter and summer in general, especially for the continents.

Pollen assemblages, which inform on vegetation cover, are one of the rare biogenic proxies enabling seasonal quantitative reconstructions of climate, due to strong linkages between climate and vegetation dynamics. Since vegetation in southern Europe has been revealed to be particularly sensitive to DO, we selected 14 published pollen records from Southern and Southwestern Europe (5 from marine cores and 9 from terrestrial sequences), covering partly or entirely the period from 60 to 10 ka, and we applied the Modern Analogue Technique (MAT) to reconstruct seasonal climatic parameters, using the last version of the Eurasian modern pollen database (EMP2).

Vegetation reconstructions through Plant Functional Types (PFT) highlighted important millennial-scale variations during the last glacial period, with alternating arboreal and steppe phases, which have been correlated with GIs and GSs, respectively, using the marine records. Multivariate analyses on PFT and seasonal climatic reconstructions indicate a predominant influence of winter on vegetation dynamics, with mild and humid winters during GIs, while cold and dry winters characterize GSs. Our results also evidence a different behaviour of summer compared to winter, with warm and relatively stable summer temperatures throughout the last glacial period, confirming the main hypothesis of this work.

Today, the vegetation of Southern Europe depends on the amount of winter precipitation, determined by the variation modes of the North Atlantic Oscillation (NAO), which correspond to the latitudinal movements of the storm track over the European continent induced by the strength variations of the westerlies. Although the current NAO varies on interannual to decadal timescales, we suggest that the DO in Southern Europe might be the expression of millennial-scale variations of winter atmospheric phenomenon: strong westerlies during GSs, resembling the current NAO positive mode, forcing a displacement of the storm-track over Northern Europe, generating cold and dry winters in Southern Europe. Conversely, weaker westerlies during GIs (NAO negative mode) induce a southward displacement of the storm track, thus mild and humid winters over Southern Europe, favouring forested vegetation. We also hypothesize that warm and stable summer temperatures throughout the last glacial may have played a key role in the millennial-scale climatic variability, providing continuous meltwater supply from Greenland and Canadian ice sheets into the North Atlantic basin, but that the impact of these meltwaters on the extent of winter sea-ice cover in the North Atlantic, thermohaline circulation and European climate,

in general, was mainly modulated by the millennial variations of the winter atmospheric circulation previously mentioned.

Our results demonstrate significant amounts of winter and annual precipitation in southern Europe during the Last Glacial Maximum. The precipitation increase may be the result of an atmospheric reorganization, and a more southern position of the storm track due to the maximum extension of ice sheets. Larger variations of winter temperatures and precipitation on the western Iberian margin than in the Mediterranean basin area also suggest the presence of an atmospheric and/or hydrological front between both regions.

Keywords : millennial climatic variability, Southern Europe, seasonality, pollen sequences, modern analogue technique, winter atmospheric circulation, westerlies

INTRODUCTION

0.1 Mise en contexte

La dernière période glaciaire (115 à 11,7 ka) a été marquée par d'importantes oscillations climatiques et environnementales de fréquence millénaire. Cette variabilité millénaire a pour la première fois été identifiée dans les enregistrements isotopiques de l'oxygène de la glace du Groenland (Figure 0.1) (Dansgaard et al., 1982, 1993) et s'avère particulièrement prononcée au cours du stade isotopique marin (MIS – *Marine Isotope Stage*) 3 (~ 60 – 28 ka), bien que quelques variations caractérisent aussi le début du MIS 1 (~ 14,5 – 11,7 ka cal. BP) et ainsi que le MIS 2 (~ 28 – 14,5 ka cal. BP; Lisiecki et Raymo, 2005), ce dernier incluant notamment le dernier maximum glaciaire (LGM – *Last Glacial Maximum*) pendant lequel le volume des glaces continentales a atteint un maximum (Mix et al., 2001). La variabilité millénaire se traduit par des variations rapides des températures au-dessus du Groenland, avec des amplitudes de 5 à 16,5 °C (Kindler et al., 2014), définissant ainsi une alternance de phases chaudes, dites interstadiaires (GIs – *Greenland Interstadials*), et froides, dites stadiaires (GSs – *Greenland Stadials*), aussi connue sous le nom de cycles de Dansgaard-Oeschger (DO). Un cycle « typique » de DO dans les carottes de glace groenlandaises présente un profil en dent de scie, avec un réchauffement important pendant quelques décennies, suivi d'un refroidissement plus lent et progressif sur plusieurs siècles, avant un retour abrupt à des conditions glaciaires jusqu'au réchauffement suivant qui marque le début d'un nouveau cycle (Figure 0.1).

Bien qu'une certaine variabilité du climat de fréquence millénaire ait été enregistrée à l'échelle du globe pendant la dernière période glaciaire (e.g., Schmittner et al., 2007), elle semble avoir été particulièrement prononcée dans l'Atlantique Nord, ses mers subpolaires et les terres adjacentes. La région nord-atlantique a ainsi reçue une attention particulière de la part des paléoclimatologues. Par ailleurs, le transfert de chaleur vers le pôle Nord via la dérive nord atlantique (NAD – *North Atlantic Drift*), est une composante majeure de la circulation thermohaline globale à laquelle on se réfère en évoquant l'*Atlantic Meridional Overturning Circulation* (AMOC) (cf. Carton and Hakkinen, 2011). Ainsi, de nombreux

travaux de paléocéanographie réalisés à partir de carottes de sédiment ont permis de retracer des variations millénaires de paramètres hydrographiques de surface et de subsurface (e.g., Bond et al., 1993; Bond et Lotti, 1995; Elliot et al., 1998; Rasmussen et al., 2003; Rasmussen et Thomsen, 2004; Schmidt et al., 2004; Hall et al., 2011; Penaud et al., 2011; Zumaque et al., 2012; Datema et al., 2019), notamment dans l'Atlantique Nord et dans les mers nordiques (e.g., Rasmussen et al., 1996; Eynaud et al., 2002; Wary et al., 2015, 2016, 2017) ainsi qu'en mer Méditerranée (e.g., Sierro et al., 2005; Penaud et al., 2011). Des variations du taux de formation des eaux profondes de l'Atlantique Nord (NADW – *North Atlantic Deep Water*) (cf. Rasmussen et al., 1999, 2003; Kissel et al., 1999; Elliot et al., 2001, 2002; Gottschalk et al., 2015) et de celles formées en Méditerranée (cf. Toucanne et al., 2007; Penaud et al., 2011; Bahr et al., 2015) ont également été retracées à partir d'indicateurs géochimiques. Les sédiments marins de l'Atlantique Nord et des mers nordiques enregistrent par ailleurs des variations des apports de particules silico-clastiques grossières issues du délestage par des radeaux de glace (IRD- *Ice-Rafted Debris*). Ceux-ci proviennent de la calotte Laurentidienne (LIS – *Laurentide Ice Sheet*), ainsi que des calottes entourant les mers nordiques, soit la calotte groenlandaise (GIS – *Greenland Ice Sheet*), la calotte islandaise (IIS – *Iceland Ice Sheet*), la calotte fennoscandinave (FIS – *Fennoscandian Ice Sheet*) et la calotte britannique qui comprend la calotte irlandaise (BIIS – *British-Irish Ice Sheet*) (e.g. Bond et Lotti, 1995; Rasmussen et al., 1996; Elliot et al., 1998; Peters et al., 2008; Hall et al., 2011). Enfin, sur la moitié sud du continent Européen, le nord étant englacé, des alternances rapides de périodes chaudes et froides, marquées par des sécheresses et de fortes précipitations ont été retracées à partir de différents traceurs micropaléontologiques et géochimiques (e.g. Leuschner et Sirocko, 2000; Leduc et al., 2007; Strikis et al., 2018), notamment en Europe de l'Ouest (Genty et al., 2010; Bahr et al., 2015; Kaboth et al., 2018; Budsky et al., 2019).

Bien que la fréquence millénaire des variations attribuées aux DOs soit reconnue, le mode de variabilité, l'amplitude, ainsi que la chronologie des variations climatiques et environnementales peuvent différer d'un enregistrement à un autre (e.g., Wary et al., 2016; Rasmussen et al., 2016; Bauska et al., 2021; Denton et al., 2022), mettant en lumière la complexité des interactions et délais de réponse liant l'océan, l'atmosphère et la cryosphère. Ainsi, malgré plus de trois décennies de recherche sur le sujet, les forçages et mécanismes qui régissent la variabilité climatique millénaire restent un sujet de débat.

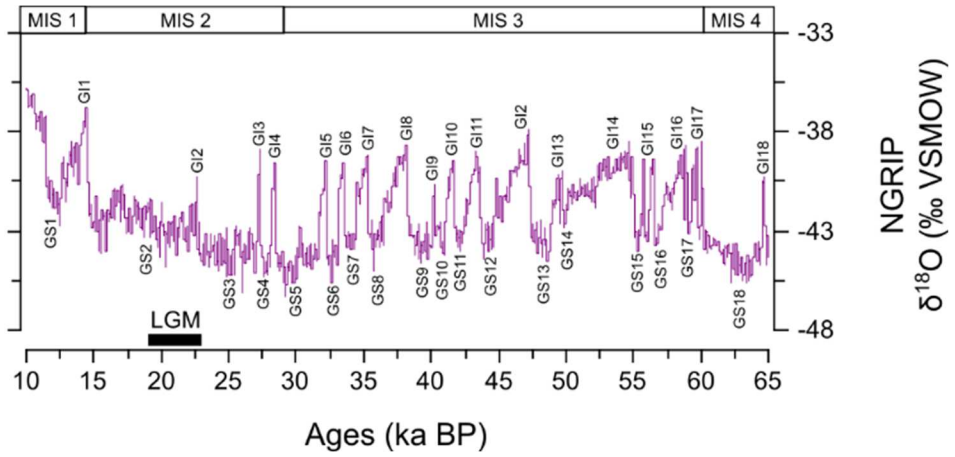

Figure 0.1 Enregistrement isotopique de l'oxygène NGRIP (*North Greenland Ice Core Project members*, 2004). Les interstadiaires (GIs) et stadiaires (GSs) sont délimités selon Rasmussen et al. (2014), les stades isotopiques marins (MIS – Marine Isotope Stage) selon Lisiecki et Raymo (2005) et le LGM selon Mix et al. (2001).

Un paramètre dont l'importance dans le signal climatique des DOs a longtemps été sous-estimée est la saisonnalité (Denton et al., 2005; Carré et Cheddadi, 2017), car la plupart des traceurs ou proxies sont utilisés pour reconstituer les conditions moyennes annuelles ou estivales. Sánchez-Goñi et al. (2000) furent parmi les premiers à mettre en évidence un refroidissement plus prononcé pendant l'hiver que pendant l'été au cours des GSs en Europe. Par la suite, des incohérences entre les variations des températures annuelles moyennes calculées à partir de la signature isotopique des glaces du Groenland et les variations d'avancée/recul des glaciers dans l'est du Groenland ont été soulignées par Denton et al. (2005) qui ont proposé que les DOs représentent avant tout un signal hivernal alors que des températures estivales relativement clémentes auraient pu caractériser la dernière période glaciaire, notamment les GSs. Quelques années plus tard, Denton et al. (2022) avancent que les températures estivales pourraient jouer un rôle clé dans la variabilité climatique millénaire, via la modulation de la fonte des glaces, et donc l'apport d'eaux de fonte vers l'Atlantique Nord, avec des conséquences sur l'AMOC et l'étendue du couvert de glace de mer hivernal. Le caractère hivernal plus prononcé des DOs a depuis été illustré par plusieurs études de la région Nord Atlantique (e.g., Fluckiger et al., 2008; Datema et al., 2019), et a notamment été associé à des variations du couvert de glace de mer aux hautes latitudes (Denton et al., 2005, 2022; Fluckiger et al., 2008). Des reconstitutions quantitatives des variations climatiques hivernales sont toutefois peu nombreuses pour le milieu continental (e.g., Sanchez-Goni et al., 2002, 2021), et sont plus souvent établies à partir de reconstitutions des températures de surface de l'océan (e.g., Zumaque et al.,

2012; Datema et al., 2016). Ainsi, très peu d'études proposent des reconstitutions quantitatives du contraste climatique saisonnier entre hiver et été en général, et sur les continents en particulier. En outre, l'hypothèse de températures de l'air relativement élevées en été tout au long de la dernière période glaciaire, et notamment au cours des GSs, n'a pas encore été quantitativement démontrée sur le continent. Pour pallier l'absence d'évidence, Denton et al. (2022) ont suggéré que la signature climatique estivale devait être masquée dans de nombreux enregistrements paléoclimatiques par un signal hivernal dominant. Quoi qu'il en soit, différencier le comportement de l'hiver par rapport à celui de l'été est essentiel pour la compréhension des DOs et de leur dynamique.

Beaucoup de traceurs biogéniques permettent des reconstitutions de la température de l'eau ou de l'air, mais peu portent véritablement l'empreinte des saisons estivales et hivernales, et rares sont ceux calibrés pour retracer de façon quantitative les contrastes saisonniers. En milieu marin des données sur les températures estivales et hivernales sont fournies par quelques traceurs biogéniques, tels les dinokystes, dont la distribution dépend de la longueur de la saison de croissance en plus des optima saisonniers (e.g., Rochon et al., 1999; de Vernal et al., 2020; Datema et al., 2019). En milieu continental, les données polliniques, qui renseignent sur le couvert végétal, sont l'un des rares traceurs pouvant être utilisés pour retracer les conditions saisonnières de température ou de pluviométrie, en raison de la relation étroite qui existe entre le climat, actuel et passé, et la dynamique de la végétation (e.g., Sánchez-Goñi et al., 2000, 2021).

La végétation des régions sud/sud-ouest de l'Europe a démontré une grande sensibilité à la variabilité climatique millénaire et aux changements climatiques de la dernière période glaciaire en général (e.g., Sánchez-Goñi et al., 2000, 2002, 2008, 2009, 2021; Turon et al., 2003; Roucoux et al., 2005; Combourieu-Nebout et al., 2002, 2009; Rodrigo-Gamiz et al., 2022). En effet, les carottes marines, qui enregistrent aussi bien l'information continentale (végétation) que les conditions paléohydrographiques de surface, ont permis de faire une corrélation directe entre les deux signaux, tout en s'affranchissant des incertitudes chronologiques, démontrant ainsi que la végétation régionale variait de façon concomitante aux changements de conditions de surface dans l'Atlantique Nord et dans l'ouest de la Méditerranée (e.g., Sánchez-Goñi et al., 2000, 2002, 2008, 2009, 2021; Turon et al., 2003; Roucoux et al., 2005; Combourieu-Nebout et al., 2002, 2009). C'est ainsi que des corrélations avec les DOs du Groenland ont pu être proposées (Austin et Hibbert, 2012). Les données polliniques du sud/sud-ouest européen paraissent donc particulièrement pertinentes pour tenter de caractériser les variations climatiques, hivernales et estivales,

au cours de la dernière période glaciaire. Le lien étroit entre végétation et climat au sud-ouest de l'Europe a par ailleurs été utilisé à de nombreuses reprises pour quantifier les variations climatiques passées à l'aide de différentes méthodes numériques (e.g., Guiot, 1990; Peyron et al., 1998; Sánchez-Goñi et al., 2021). Toutefois, aucune de ces études ne propose une reconstitution quantitative du contraste climatique saisonnier hiver/été. Même les plus récentes études se concentrent sur le comportement hivernal (Sánchez-Goñi et al., 2021), les moyennes annuelles de températures (Rodrigo-Gamiz et al., 2022), ou le contraste saisonnier entre précipitations hivernales et estivales mais à une résolution insuffisante pour attester de leur comportement lors des DOs (Camuera et al., 2022).

De nos jours, le climat du sud/sud-ouest européen est principalement fonction des modes de variations de l'Oscillation Nord Atlantique (NAO – *North Atlantic Oscillation*), surtout en hiver. La NAO est un mode de circulation atmosphérique défini comme la différence de pression atmosphérique entre la dépression Islandaise et l'anticyclone des Açores et dont l'indice est calculé entre novembre et avril (Hurrell, 1995). Un indice positif de la NAO correspond à de forts gradients de pression et résulte en un déplacement des vents d'ouest et donc de la trajectoire des tempêtes vers le nord du continent Européen, générant des hivers froids et secs sur la partie méridionale. À l'inverse, un indice négatif correspond à un déplacement vers le sud de la trajectoire des tempêtes, générant des hivers froids et secs au nord et humides et doux au sud. En été, l'influence des vents d'ouest faiblit au profit de cellules anticycloniques renforcées au-dessus du bassin est subtropical de l'Atlantique Nord, ce qui confère à la région les étés secs caractéristiques du climat Méditerranéen (Rodwell et Hoskins, 2001).

Or, des études ont démontré que la végétation actuelle du sud/sud-ouest de l'Europe varie en fonction de la quantité de pluie reçue en hiver, laquelle dépend des modes de variations de la NAO (Gouveia et al., 2008). Des reconstitutions des précipitations hivernales au cours des DOs et de la dernière période glaciaire en général aideraient ainsi à caractériser cette oscillation climatique, qui varie aujourd'hui selon une fréquence interannuelle à décennale, et dont le mode dominant pourrait avoir changé de concert avec les DOs du Groenland.

Au cours de la période glaciaire, le dernier maximum glaciaire (LGM – *Last glacial maximum*), qui s'étend d'environ 23 à 19 ka (Mix et al., 2001; MARGO, 2009) (Figure 0.1), est défini comme la période la plus récente de volume maximum de glace. Néanmoins, bien qu'il s'agisse d'un des épisodes les plus documentés du Quaternaire, les informations fournies par les séquences polliniques et celles issues des

modèles climatiques et autres traceurs tels que les niveaux de lacs (cf., Jost et al., 2005; Beghin et al., 2016; Davis et al., 2022), illustrent de nombreuses incohérences pour l'Europe notamment en ce qui a trait à l'humidité régionale. De nombreuses simulations numériques du climat au LGM indiquent en effet une augmentation importante des précipitations hivernales au-dessus de la Péninsule Ibérique (e.g., Lainé et al., 2009; Löfverström et al., 2014; Beghin et al., 2016; Löfverström et Lora, 2017; D'Agostino et Lionello, 2020; Kageyama et al., 2021), avec des valeurs supérieures à celles de la période préindustrielle dans plusieurs cas (Beghin et al., 2016), alors que les séquences polliniques situées pour la plupart autour des Pyrénées indiquent plutôt une végétation steppique et donc un climat aride (e.g., Andrieu et al., 1993; Reille et Andrieu, 1995; Valero-Garces et al., 2004; Gonzalez-Sampériz et al., 2006). Alors que les reconstitutions paléoclimatiques basées sur les données polliniques sont rares pour le LGM, de nouvelles reconstitutions paléoclimatiques saisonnières, à partir de carottes provenant du sud de la Péninsule Ibérique, permettraient peut-être de vérifier ou combler l'écart entre les résultats de modèles et ceux des enregistrements polliniques.

0.2 Objectif principal et hypothèse

L'objectif principal de cette thèse est ainsi de caractériser le contraste saisonnier entre l'hiver et l'été au cours de la dernière période glaciaire. Plus précisément, le premier objectif est de produire, à partir des enregistrements polliniques, des série temporelles de haute résolution de la température et des précipitations hivernales et estivales en Europe du sud/sud-ouest. Sur de telles bases, il sera ensuite possible d'établir des relations entre la végétation et les paramètres du climat lors des DOs tels que définit au Groenland grâce aux corrélations directes avec les indicateurs de conditions océaniques de surface (Austin et Hibbert, 2012) dans les carottes pour lesquelles on dispose de séries polliniques. L'hypothèse principale défendue ici est que la variabilité climatique millénaire qui caractérise la dernière période glaciaire pourrait se résumer dans la région de l'Atlantique Nord à un signal hivernal et que des températures estivales élevées pourraient avoir prévalu tout au long de la période glaciaire, tel que suggéré par Denton et al. (2005, 2022).

Le second objectif est de fournir des enregistrements haute résolution de températures et précipitations hivernales et estivales pour la période du LGM en Europe du sud/sud-ouest. En outre, les reconstitutions réalisées à partir de séquences polliniques du sud de la Péninsule Ibérique et de l'Italie, permettent des comparaisons avec les résultats de simulations numériques du climat qui décrivent tous

une augmentation prononcée des précipitations hivernales lors du LGM (e.g., Beghin et al., 2016) alors que les données polliniques à la limite nord de la Péninsule Ibérique indiquent une forte aridité. Enfin, alors que le climat hivernal de la région dépend aujourd'hui des mouvements latitudinaux des vents d'ouest et donc de la trajectoire des tempêtes au-dessus du continent Européen (NAO; Hurrell, 1995), des variations de précipitations hivernales cohérentes à échelle régionale permettraient de retracer les variations de circulation atmosphérique au-dessus de l'Atlantique Nord-est et du continent Européen.

0.3 Méthodes

De nombreuses approches méthodologiques exploitant les assemblages polliniques (cf., Chevalier et al., 2020) s'appuient sur les affinités écologiques actuelles des espèces végétales pour reconstituer les paramètres climatiques passés. Elles se fondent sur le principe de l'uniformitarisme, ou actualisme, selon lequel les affinités écologiques des espèces ne changent pas au cours du temps (Jackson et Overpeck, 2000). C'est le cas notamment de la technique des analogues modernes (MAT - *Modern Analogue Technique*; Guiot, 1990), qui utilise la similarité entre des échantillons anciens et ceux de sédiments modernes, sur la base de l'analyse statistique de la composition des assemblages polliniques, pour reconstituer le climat. Elle nécessite donc des bases de données contenant les assemblages polliniques d'échantillons de sédiments modernes ainsi que les paramètres climatiques mesurés ou calculés à l'endroit de la collecte de ces échantillons. Comme cette approche repose sur des analogies, il est important que les bases de données modernes couvrent vaste gamme d'environnements, de biomes et de situations climatiques possibles. Or, l'une des limites soulevées de nombreuses fois pour ce qui concerne les reconstitutions climatiques, en général, et plus particulièrement pour la dernière période glaciaire, est le peu d'analogues modernes (e.g., Davis et al., 2003).

Au cours des dernières années, Davis et al. (2013, 2020) ont réalisé un travail remarquable pour élargir la base de données moderne européenne à l'Eurasie, en développant la *Eurasian Modern Pollen Database* (EMPD; Davis et al., 2013) dont la deuxième version (EMPD2; Davis et al., 2020) inclut quelques milliers de sites additionnels, dont la majorité se situe en Russie/Sibérie, offrant ainsi davantage d'analogues potentiels pour les climats et environnements de la dernière période glaciaire (Magyari et al., 2014; Davis et al., 2022). Dans le cadre de ma thèse, j'ai rendu accessible la base de données EMPD2 pour son utilisation par la communauté scientifique en procédant à l'harmonisation des taxons (https://doi.pangaea.de/10.1594/PANGAEA.909130; Zumaque et al., soumis à *Data in Brief*). La base de

données comprend un grand nombre d'échantillons modernes (> 8000 échantillons dans la région Paléarctique et un total de neuf biomes différents; cf. Davis et al., 2020) et une grande diversité taxonomique (plus de 840 taxons de plantes). Il était donc nécessaire de faire un important travail de groupements et d'harmonisation des taxons avant de pouvoir l'utiliser.

La technique des analogues modernes (Guiot, 1990) a été utilisée pour des reconstitutions à partir d'enregistrements polliniques d'Europe du sud et sud-ouest déjà publiés, en utilisant la version la plus récente de la base de données moderne eurasienne (EMPD2; Davis et al., 2020) que nous avons mise en forme. Les enregistrements polliniques choisis ont été sélectionnés pour respecter un certain nombre de critères. En particulier, ils doivent être continus et avoir une résolution temporelle suffisamment élevée pour enregistrer des variations environnementales millénaires. Les variations de végétation seront également reconstituées, et, pour s'affranchir de l'immense diversité taxonomique qui peut exister entre les différents enregistrements polliniques, les taxons ont été regroupés par type fonctionnel de plantes (PFTs – *Plant Functional Types*), qui sont des groupes de plantes définis par plusieurs critères, dont la stature, la phénologie ou encore les seuils climatiques (Prentice et al., 1992, 1996; Peyron et al., 1998). Le groupement en 23 PFTs permet de gérer moins de variables environnementales et facilite la comparaison entre sites. Les deux jeux de données (PFTs et climat) ont ensuite fait l'objet d'analyses multivariées afin de visualiser quel(s) paramètre(s) climatique(s) influence(nt) le plus les variations de végétation.

0.4 Structure de la thèse

Cette thèse se présente sous la forme de trois chapitres rédigés en anglais.

Le chapitre 1 est un chapitre méthodologique dans lequel sont présentés les enregistrements polliniques à l'étude, la méthode de regroupements des taxons polliniques (PFTs; Peyron et al., 1998), la technique des analogues modernes (MAT; Guiot, 1990) et les analyses multivariées utilisées pour comparer les deux jeux de données obtenus à chaque site (PFTs vs. MAT). Le chapitre s'attarde également à présenter les détails de la mise en forme de la base de données polliniques modernes eurasienne (EMPD2; Davis et al., 2020), dont la version finale est téléchargeable sur PANGAEA (https://doi.pangaea.de/10.1594/PANGAEA.973997; Zumaque et al., soumis à *Data in Brief*). Enfin, les avantages et limites de MAT, notamment concernant les problèmes d'autocorrélation spatiale (e.g., Telford and Birks, 2005, 2009, 2011; Guiot and de Vernal, 2011a, 2011b; Birks et al., 2010; Chevalier et al.,

2020), des problèmes liés aux variations passées du CO_2 atmosphérique (e.g., Cleator et al., 2020; Prentice et al., 2022) ou encore de son utilisation sur des séquences polliniques marines (cf. Sánchez-Goñi et al., 2018; Chevalier et al., 2020; Davis et al., 2022) sont discutées en détail. La plus grande partie de ce chapitre sera publiée comme supplément méthodologique pour les articles qui sont issus des deux chapitres suivants. La version « prête-à-l 'emploi » de la base de données polliniques modernes eurasienne (EMPD2; Davis et al., 2020) est disponible sur PANGAEA (https://doi.pangaea.de/10.1594/PANGAEA.973997). Les détails sur celle-ci paraitront dans la revue *Data in Brief* et sont présentés en ANNEXE A de cette thèse.

Le chapitre 2 examine la principale hypothèse défendue dans cette thèse, soit le signal climatique des DOs comme essentiellement hivernal, des températures estivales élevées ayant prévalu durant tout le stade 3 (~ 60 – 28 ka) au cours duquel les DOs sont les plus prononcés (Figure 0.1). Nous reconstituons ainsi les températures et précipitations hivernales et estivales pour une douzaine d'enregistrements polliniques du sud/sud-ouest de l'Europe (4 marins, 8 terrestres) et portons une attention particulière à la dynamique de la végétation par rapport aux paramètres saisonniers du climat. Ce chapitre est accepté sous réserve de révisions dans la revue *Quaternary Science Reviews*.

Enfin, le chapitre 3 porte sur les paramètres climatiques saisonniers dans 5 carottes sédimentaires dont 3 étudiées au chapitre précédent, mais au cours du stade isotopique marin (MIS) 2 (~ 28 – 14,5 ka) ainsi qu'au début du MIS 1. Nous examinons notamment si les reconstitutions paléoclimatiques saisonnières faites à partir de la nouvelle version de la EMPD2 (Davis et al., 2020) dans des carottes du Sud de la Péninsule Ibérique, du Sud de l'Italie et de la Grèce permettent de retracer ou pas une augmentation des précipitations hivernales, telle que simulée par certains modèles climatiques (e.g., Beghin et al., 2016). Ce chapitre sera soumis à la revue *Quaternary Science Reviews*.

CHAPITRE 1

METHODOLOGY

Résumé en français

Le rôle de la saisonnalité pourrait avoir été sous-estimé dans les études portant sur les cycles de Dansgaard-Oeschger (DO). Grâce au lien étroit qui existe entre les variations de végétation et les variations climatiques passées, les pollens, qui renseignent sur le couvert végétal, sont l'un des rares traceurs permettant de reconstituer la saisonnalité. Ici, nous présentons les séquences polliniques utilisées dans ce travail ainsi que les informations chronologiques qui leur sont associées. Ces séquences proviennent du sud de l'Europe, une région qui s'est révélée particulièrement sensible aux DO. Nous adressons les incertitudes inhérentes aux modèles de reconstitutions climatiques basés sur les pollens, telles que les différences entre les représentations polliniques des taxons dans une végétation source et les différents facteurs influents. Pour contourner ces incertitudes difficilement quantifiables, nous encourageons les comparaisons avec des reconstitutions paléoclimatiques basées sur d'autres traceurs que les pollens. Nous adressons également le problème des variations de concentrations en CO_2 atmosphériques au cours du temps, lesquelles, si elles ne sont pas prises en compte, peuvent entrainer une légère sous-estimation des précipitations pour les reconstitutions faites pour des périodes de faibles concentrations en CO_2 atmosphériques, telles que la dernière période glaciaire. Enfin, nous présentons les avantages et inconvénients spécifiques à la technique des analogues modernes (MAT - *Modern Analogue Technique*) choisie ici pour faire nos reconstitutions climatiques à partir des données polliniques, et notamment la principale préoccupation mentionnée dans la littérature, à savoir l'autocorrélation spatiale. Nous soutenons qu'il s'agit là d'une propriété intrinsèque de la plupart des données écologiques sur lesquelles les modèles de reconstitutions paléoclimatiques sont fondés, et que cela ne constitue pas un problème en autant que les utilisateurs de MAT demeurent vigilants quant à la qualité des analogues. Nous adressons également le problème de l'utilisation de séquences sédimentaires marines pour reconstituer des paramètres paléoclimatiques continentaux et la pertinence de supprimer *Pinus* des assemblages fossiles et modernes pour les reconstitutions paléoclimatiques en raison de la surreprésentation de ce taxon dans les assemblages polliniques marins. La littérature ainsi que des tests de reconstitutions paléoclimatiques avec et sans *Pinus* effectués sur la séquence sédimentaire marine MD95-2042 nous ont mené à conclure que l'utilisation de séquences marines est pertinente et qu'en dépit de bons résultats statistiques sur les tests effectués en conservant *Pinus*, supprimer le taxon des assemblages permet de mieux capturer les changements climatiques régionaux.

Abstract

The role of seasonality may have been overlooked in the Dansgaard-Oeschger (DO) cycle studies. Because of the close link existing between vegetation and climatic variations of the past, pollen, which informs on the vegetation cover, is one of the few proxies that allow for seasonality reconstructions. Here we present the pollen sequences and associated chronological information used for this work. They come from southern Europe, a region where vegetation has proven to be highly sensitive to DO cycles. We address

the uncertainties inherent to pollen-based models of climate reconstructions, such as the differences between the pollen representation of taxa in the source vegetation and the different factors that affect it. To overcome these uncertainties hardly measurable, we encourage comparison with non-pollen-based climatic reconstructions. We also address the problem of atmospheric CO_2 concentration variations through time which, when not taken into account, can lead to slight underestimation of precipitation for reconstructions during periods of low CO_2 concentration values such as the last glacial. Finally, we present the advantages and limitations specific to the Modern Analogue Technique (MAT) chosen here to infer paleoclimates based on pollen data, and notably the main limitation raised in the literature which is spatial autocorrelation. We argue that it is an intrinsic property of most ecological data on which climate reconstruction models are built and that it is not an issue as long as MAT users remain careful with the quality of the analogues. We also address the issue of using marine sedimentary sequences for inferring continental paleoclimate parameters and the relevance of removing *Pinus* from the fossil and modern assemblages for climatic reconstructions since this taxon is overrepresented in marine pollen assemblages. The literature along with paleoclimatic reconstruction tests with and without *Pinus* conducted on marine core MD95-2042 led us to conclude that the use of marine sequences is relevant and that despite statistically good MAT results with *Pinus*, removing *Pinus* from the dataset permits to better capture the regional climate changes.

1.1 Introduction

The role of seasonality might have been underestimated in the climatic signal of Dansgaard-Oeschger cycles (DO) (Denton et al., 2005, 2022; Carré and Cheddadi, 2017). Pollen, which relates to vegetation cover, is one of the rare proxies that allow for seasonality reconstructions over the continents as many studies have demonstrated close linkages between vegetation and climatic variations of the past (Sánchez-Goñi et al., 2000, 2021). A region where vegetation has been proved highly sensitive to DO is southwestern and southern Europe, where cold phases of DO are characterized by increased steppe vegetation (e.g., Sánchez-Goñi et al., 2000, 2002, 2008, 2009, 2021; Turon et al., 2003; Roucoux et al., 2005; Combourieu-Nebout et al., 2002, 2009; Rodrigo-Gamiz et al., 2022). Pollen-based paleoclimatic approaches should thus permit inferring seasonality during DO cycles of the last glacial period to investigate the link between the vegetation dynamics and the seasonal climatic parameters reconstructed.

Many methods have been developed to infer paleoclimatic parameters from pollen data (cf. Chevalier et al., 2020). The Modern Analogue Technique (MAT, Overpeck et al., 1985; Guiot, 1990) is among the most efficient and the most frequently used methods for paleoclimate reconstructions (Guiot and de Vernal, 2011a; Chevalier et al., 2020). It is based on the principle that the ecological affinities of plants have not changed through time (Jackson and Overpeck, 2000), and it compares a fossil pollen assemblage to all modern pollen assemblages within a given geographic area. MAT thus needs a modern pollen database that encompasses a large variety of vegetation types and related climatic conditions, especially for paleoclimatic reconstructions of the last glacial period. The recent update of the Eurasian

Modern Pollen Database (EMPD2; Davis et al., 2020), with many additional samples from cold environments such as Siberia, provides potential analogues for the last glacial period (Magyari et al., 2014; Davis et al., 2022). The EMPD2 comprises around 8000 modern samples from the Palearctic region, for a total of 9 biomes (cf. Davis et al., 2020) and presents a great taxonomic diversity (more than 840 plant taxa). An important work of taxa grouping, and harmonization is thus necessary before being able to use it, which was one of the first steps of this work.

However, like many other pollen-based paleoclimatic reconstructive methods, MAT has its limitations (cf. Birks et al., 2010; Chevalier et al., 2020). Many authors have for example raised concerns about spatial autocorrelation (Telford and Birks, 2005, 2009, 2011; Guiot and de Vernal, 2011a, 2011b; Birks et al., 2010; Chevalier et al., 2020), which relates to the fact that sites geographically close to each other tend to be more similar than randomly selected sites. They argue that it biases the evaluation of MAT performance (Telford and Birks, 2005, 2009, 2011), resulting in overoptimistic estimates of the errors. Concern has also been raised regarding the fact that past CO_2 variations are not taken into account by MAT and that low CO_2 concentrations prevailing during the last glacial period might have affected the relationships between vegetation and climate by lowering the plant water-use efficiency (Harrison and Prentice, 2003; Prentice et al., 2017), resulting in pollen-based climatic estimates possibly biased toward drier values (e.g., Cleator et al., 2020; Prentice et al., 2022). Finally, modern samples in the modern databases are all terrestrial (cf. Davis et al., 2020), and paleoclimatologists have been reluctant to use MAT on marine pollen sequences, arguing that the vegetation information integrated into marine and terrestrial cores comes from very different areas (cf. Birks et al., 2010; Chevalier et al., 2020).

Here, we present the MAT approach we have used and discuss its advantages and limitations, notably the problem of spatial autocorrelation. We also discuss and test its applicability to marine pollen sequences. More broadly, we discuss of the significance of pollen assemblages in terms of climate and since we aim at reconstructing paleoclimate for glacial times, we briefly address the fact that MAT, as many other pollen-based climate reconstruction methods, does not account for variations in CO_2 concentrations. Finally, we also describe the Plant Functional Type (PFT) approach (Peyron et al., 1998) we used to better visualize the vegetation dynamics.

1.2 Study sites

1.2.1 Data compilation and selection criteria

The present compilation includes 5 marine and 9 terrestrial pollen records from Southern Europe (Table 1.1; Fig. 1.1) that encompass partly or entirely MIS 3 and/or MIS 2 and have sufficient temporal resolution to record centennial to millennial-scale variations. These pollen records are sourced from the ACER (Abrupt Climate Changes and Environmental Responses) database (Sánchez-Goñi et al., 2017) (Table 1.1), with the exception of the pollen data from the Padul site (Fig. 1.1) which were shared by the authors (Camuera et al., 2018, 2019).

1.2.2 Chronologies

A good chronology was at first a prerequisite for the inclusion of pollen records in the compilation. Marine cores from open ocean settings are usually well-dated and permit direct land-sea correlations by comparing pollen and proxy indicators of the ocean environment in single cores (Sánchez-Goñi et al., 2002, 2008, 2009; Roucoux et al., 2005). Furthermore, if they have sufficiently high resolution, marine cores from the North Atlantic sector can be correlated to the reference Greenland GI and GS succession (Kissel et al., 1999; Austin and Hibbert, 2012). Conversely, for most continental sites, the chronology is not robust enough to allow for an age-based identification of GIs/GSs. Nevertheless, these data provide information on the linkages between vegetation and climate. Hence, we included some not-so-well-dated but long and continuous terrestrial records in this work, in addition to some well-dated records (especially those from marine sites), to investigate the land-sea linkages.

For each site from the ACER database (Sanchez-Goni et al., 2017; Table 1.1), we used the updated chronologies proposed in the ACER database (for more details, see Sánchez-Goñi et al., 2017) with exception of Lago Grande di Monticchio (Watts et al., 1996, 2000; Allen et al., 2000; Brauer et al., 2007; Allen and Huntley, 2018) because no alternative chronology was proposed by the authors of the ACER database (Sánchez-Goñi et al., 2017). At this site, we thus kept the initial chronology based on annual lamination ("varves") counts and sedimentological features in the non-varved intervals (Zolitschka and Negendank, 1996). However, although the chronology of the entire Monticchio sequence was overall corroborated by many dated tephra layers with a mean deviation of ~ 5% (Wulf et al., 2004), some sections appear problematic as demonstrated by (Genty et al., 2010). Hence, we must remain cautious regarding the interpretation of the timing of vegetation and climatic shifts from this sequence. The dates are available on the file "dating_info" of the ACER database.

As mentioned earlier, marine cores from the North Atlantic sector contain pollen grains that can be linked directly to the millennial-scale variability recorded in sea-subsurface temperatures, which vary concomitantly with the oxygen isotope data of the Greenland Ice cores (Austin and Hibbert, 2012). Hence, to compare the marine and continental signals from the marine cores, we applied the exact same age model to all these records and thus recalculated the age for each marine core using CLAM (Blaauw, 2010), implemented in R (R version 3.3.1) (R Development Core Team, 2016) based on the dates that were kept after harmonization of the chronologies of the ACER database (Sánchez-Goñi et al., 2017). To stay consistent with the harmonized chronological work of Sanchez-Goñi et al. (2017), we used the Marine13 calibration curves (Reimer et al., 2013).

The chronology used for the Padul sequence is the original chronology presented in Camuera et al. (2018).

All age-models, with the exception of those of Padul and Lago Grande di Monticchio, are presented in the Supplementary material of chapters 2 and 3.

1.3 Methodology

1.3.1 Raw pollen counts

Raw counts, and pollen percentages in the case of the Lac du Bouchet and Megali Limni sequences (Sanchez-Goñi et al., 2017), were kept as such except for the aquatic taxa that were removed from the total pollen counts (relative abundances were recalculated after aquatic taxa removal).

1.3.2 Vegetation reconstruction: Plant Functional Types (PFTs)

To visualize past vegetation changes through time, we grouped the pollen taxa into Plant Functional Types (PFTs) based on the concept developed by Prentice et al. (1992). PFTs are broad classes of plants defined by certain vegetation criteria (e.g., stature, leaf form and phenology) and climatic thresholds. Grouping the taxa into those categories allows us to reduce the variable number and facilitate the comparison between sites and periods, especially since all the data derived from different projects and investigators, and because the taxonomic can thus vary from one site to another.

The fossil records were consequently harmonized in 94 taxa to characterize 15 arboreal and 8 shrub/herbaceous PFTs (Table 1.2) with each taxon being assigned to a PFT according to the known biology

of the species it includes (Prentice et al., 1996; Peyron et al., 1998). Here we followed the concept developed by Peyron et al. (1998) which allows each pollen taxon to belong to only one PFT. Virtual PFTs (ECPI, TSAA, TSBS; Table 1.2), which are a combination of the potential PFTs that a taxon could possibly belong to, were created to handle ambiguous taxa and were initially reassigned afterwards depending on the biome identified for the pollen sample (Peyron et al., 1998). In this work, there was no reassignment and the virtual PFTs were kept as such since we did not intend to make interpretation in terms of biomes. After several trials, we found that reassignments generated biases when applying a redundancy analysis (RDA) to the PFT and climatic data since they created clusters (one for each biome identified) in the RDA graph, thus generating jumps from one mode to another in Axis-1 scores instead of showing the progressive nature of vegetation variations. For each pollen sample, we simply calculated the abundance of each pollen taxon relative to the sum of all the 94 pollen taxa included in this work (Table 1.2) and took the square-root to amplify the importance of the rare versus the more abundant taxa. We then summed the relative abundances of the taxon combinations associated with each PFT (Table 1.2) and calculated percentages from the scores obtained for each PFT. Unlike Prentice et al. (1996) and Peyron et al. (1998), we did not remove taxa with low abundances (< 0.5%).

1.3.3 Pollen-based climate reconstruction

Various methods have been developed over time to reconstruct paleoclimates from pollen data (Birks et al., 2010; Chevalier et al., 2020). They include the Weighted Averaging Partial Least Squares regression (WAPLS, Ter Braak and Juggins, 1993; Ter Braak et al., 1993), the Modern Analogue Technique (MAT, Overpeck et al., 1985; Guiot, 1990), the Artificial Neural Networks (ANN, Peyron et al., 1998), the Bayesian Hierarchical Models (BHM, Ohlwein and Wahl, 2012), the Probability Density Functions (PDF, Chevalier et al., 2014), and the Boosted Regression Trees (BRT, Salonen et al., 2014). They all have their own advantages and limitations (cf. Birks et al., 2010; Chevalier et al., 2020). In this work, we do not intend to compare the methods but choose to use the Modern Analogue Technique (MAT) (Overpeck et al., 1985; Guiot, 1990) because it is among the most efficient methods for reconstructing high climate variability. Since MAT does not require an explicit model to define the pollen-climate relationship, it allows a much larger climatic and environmental range of the modern dataset compared to other methods and thus provides a wide range of different analogues for high variable climate such as the one expected during MIS 3 (cf. Chevalier et al., 2020).

1.3.3.1 Significance of pollen assemblages in terms of climate

MAT as any other models of climate reconstruction relies on the assumptions that the fossil assemblage is related to climate and that the ecological affinities of the taxa have remained unchanged through time, according to the uniformitarian principle (Juggins, 2013; Chevalier et al., 2020).

Pollen assemblages do not straightforwardly reflect the associations in the surrounding vegetation. The differences between the pollen representation of taxa in the source vegetation can be due to several factors. They include pollen productivity rates that differ from one taxon to another, the mechanisms of pollen transports (wind, rivers, animals) and the potential of wind transport depending upon the height of the inflorescence and pollen morphology, and differential pollen grain preservation, in addition to the depositional environment and related-processes, not to mention microclimates and anthropogenic activities (cf. Fréchette et al., 2018; Chevalier et al., 2020; Robles et al., 2022 and references therein). Among these factors, some bring more uncertainties than others.

Some studies about the variation in pollen productivity (e.g., Brostrom et al., 2008; Theuerkauf et al., 2015) concluded that a taxon like *Poaceae* can have pollen productivity differences depending upon the species. But a specific species can also present different pollen productivity depending on whether it is located in the middle (optimum climatic conditions) or at the edge of its geographical distribution (Brostrom et al., 2008). Actually, very little is known about the link between pollen productivity of given species and climate. For example, lower concentrations of atmospheric CO_2 during glacial times impacted vegetation distribution and net primary production (Martin Calvo and Prentice, 2015) but did it also affect productivity rates of pollen species? Unfortunately, such information is not currently available.

Pollen preservation is also a source of uncertainties. Studies by Havinga (1967) and Li et al. (2005) have shown that differences in sporopollenin content or thickness and ornaments of the pollen walls play an important role in the potential of pollen preservation. The pH of soils, oxidation and degradation are also important and depend upon the nature of soils as well as climate. This is why a high proportion of pollen grains is lost from surface sediments to deeper buried levels (Li et al., 2005). Because the potential of pollen preservation is different from one species to another, we can question the representativeness of ancient pollen assemblages and that is why comparison with non-pollen-based climatic reconstructions must always be encouraged.

Because human activities (e.g., deforestation, agriculture) have altered the natural vegetation distribution (Theuerkauf et al., 2015; Marchant et al., 2018; Robles et al., 2022) since long time over Europe (e.g., Giesecke et al., 2019), concerns have been raised about the relationship between climate and recent pollen assemblages (St-Jacques et al., 2015) and thus on the capability of pollen-based models to accurately reconstruct climate. Nevertheless, comparisons of pollen-based climatic reconstructions with other sources of climate information support the reliability of pollen-based models (e.g., Mauri et al., 2015). Here again, multi-technique or multi-proxy climatic reconstructions to cope with the inherent uncertainties of pollen-based models appear highly relevant.

1.3.3.1.1 The atmospheric CO_2 effect

The atmospheric CO_2 concentration is another parameter that may affect the vegetation since it controls plant water-use efficiency (Prentice et al., 2017). Hence, it has been argued that accounting for CO_2 changes when reconstructing climatic parameters from vegetation proxies such as pollen assemblages is important, especially for periods with low CO_2 concentrations such as the last glacial (Bauska et al., 2021), during which climate estimates from pollen were possibly biased toward drier values (e.g., Prentice et al., 2022).

MAT, like most other paleoclimate proxies or reconstruction techniques, does not account for the atmospheric CO_2 effect, which may be a limitation. In a recent study, Davis et al. (2022) tried to assess the bias that might result from atmospheric CO_2 variations by reconstructing the paleoclimate of the LGM in Europe, North Africa and the Middle East using MAT and Inverse Modelling (see Guiot et al., 2000). The results show good agreement between the two methods, strengthening the reliability of MAT for climatic reconstructions of glacial times and suggesting that low CO_2 concentrations during the LGM had little impact on the pollen-based reconstructions of climate (Davis et al., 2022). Although the results of this last study (Davis et al., 2022) were encouraging, we cannot exclude a slight underestimation of the precipitation values, especially toward the end of MIS 3 and during MIS 2, since CO_2 concentrations were lower than today's (Bauska et al., 2021).

However, it has been demonstrated that vegetation during MIS 3 in Europe covaries with the climate signal in the Greenland Ice cores (Sanchez-Goñi et al., 2000). Additionally, atmospheric CO_2 concentration during the last glacial period shows variations in phase with the Antarctic temperature record rather than with the Greenland temperature record (Bauska et al., 2021; Denton et al., 2022). Since

both Antarctic and Greenland temperature records are “apparently” out of phase, the changes in vegetation or the inferred climatic reconstructions in western Europe likely reflect regional climate dynamics, rather than variations in atmospheric CO_2. However, as previously mentioned, we cannot exclude an underestimation of the precipitation values reconstructed at times of low atmospheric CO_2 concentrations.

1.3.3.2 Modern Analogue Technique (MAT): Theory, limitations and relevance

Climate parameters were reconstructed from pollen data using the Modern Analogue Technique (MAT) (Overpeck et al., 1985; Guiot, 1990). MAT is based on the principle that the ecological affinities of the different species have not changed through time (Jackson and Overpeck, 2000), which is also named niche conservatism (Wiens et al., 2010) or uniformitarian principle (Chevalier et al., 2020). MAT principally compares a fossil pollen assemblage to all modern pollen assemblages within a given geographic area. This similarity assessment between fossil (i) and modern (j) pollen assemblages is based on the squared chord distance (SCD) (d^2) dissimilarity metric (Overpeck et al., 1985) which can be computed using the following formula:

$$d_{ij}^{2} = \sum_{k=1}^{m} (\sqrt{P_{ik}} - \sqrt{P_{jk}})^2 \qquad (1)$$

Where m is the number of taxa and P the relative abundances (percentage values) for each taxon (k = 1−m). The square-root transformation reduces the weight of ubiquitous taxa that are usually very abundant and increases the weight of underrepresented taxa. The equation (1) also shows the dependence between SCD and the number of pollen taxa (Sawada et al., 2004).

The SCD values vary between 0 and 2. Low values indicate high degree of similarity between two samples, whereas high values indicate large dissimilarity. The modern samples presenting the lowest SCD are thus selected as the best analogues, and past climatic conditions are calculated from their average associated climatic parameters, weighted inversely to their distance. The number of analogues retained for interpolation of climate data is set usually from 5 to 10 depending on the studies and the software/script used (e.g., Sawada et al., 2004; Fréchette et al., 2008; Dugerdil et al., 2021). There are situations, however, characterized by poor or no modern analogues (e.g., Ortu et al., 2006). Such situations

can be due, for example, to anthropogenic disturbance of the ecosystems, different climatic configurations (low atmospheric CO_2 concentrations, unique combination of seasonal irradiance, unprecedented speed of climate changes, lack of modern samples from some ecosystems, etc). To assess the "quality" of the analogues, an SCD threshold beyond which any analogue is rejected is calculated with a Monte-Carlo approach. Distance vectors are calculated between one modern spectrum randomly selected and each of the remaining modern spectra. The operation is repeated 1000 times and the final threshold is defined as the first quartile for these 1000 values (Guiot and de Vernal., 2007). In this work, we followed de Vernal et al. (2005) who defined a reliability index with three categories: 1) Poor or no analogue situation when the SCD of the closest analogue is higher than the SCD threshold, 2) Acceptable analogue situation when the SCD is between half of the threshold value and the threshold, and 3) Good analogue situation when the SCD is between 0 and half of the threshold value.

Model performances are assessed mostly based on two indicators that are calculated from different cross-validation tests, with a subset of the modern dataset used for calibration and another for prediction (see Chevalier et al., 2020 for more details). One indicator is the coefficient of correlation (R^2) between estimated and observed climatic values. The other indicator is the root mean square error of prediction (RMSEP), which also corresponds to the deviation standard of the difference between observed and reconstructed values (Guiot and de Vernal, 2007). With MAT, a measure of the uncertainty can also be given from the climatic dispersion of the selected closest modern analogues for a target sample (Guiot, 1990).

A remaining issue debated in the community is spatial autocorrelation (Telford and Birks, 2005, 2009, 2011; Guiot and de Vernal, 2011a, 2011b; Birks et al., 2010; Chevalier et al., 2020), which relates to the fact that sites geographically close to each other tend to be more similar than randomly selected sites. Many authors, notably Telford and colleagues (Telford and Birks, 2005, 2009, 2011), argue that spatial autocorrelation biases the evaluation of MAT performance, making it look better than it is. They consider MAT to be oversensitive to spatial autocorrelation and to select analogues geographically close to the target sample, resulting in over-optimistic estimates of the errors. They also show that MAT performance decreases significantly when prevented from selecting geographically close analogues (Telford and Birks, 2011). Regardless of the issue of spatial autocorrelation, the important question is the ability of the approach to make sensible reconstructions. In other words, is MAT working or not? As mentioned before, MAT like most models leading to climate reconstruction uses reference ecological data sets and is based

on the principle that ecological affinities of species have not changed through time (Jackson and Overpeck, 2000). It also means that they do not change through space either providing the ecological properties are the same. Since climate is a large-scale phenomenon and vegetation intimately depends upon climate, one might expect that geographically close modern pollen samples, under very similar climatic conditions, present similar assemblages. The high values of R2 for many climatic parameters that are often calculated on large modern pollen database (e.g., Fréchette et al., 2008; Dugerdil et al., 2021; Davis et al., 2022) illustrate the spatial consistency of climate (Guiot and de Vernal, 2011a). Positive spatial autocorrelation is thus a property of most ecological data (Legendre, 1993) and a basis on which climate reconstruction models are built. However, it indeed can impact performance indicators. For example, in validation runs, if we have X analogues with a high distance to the target samples but with a small distance to each other, the "error" (RMSE or RMSEP) will be small (little spread between the analogues), but the results won't be accurate (Chevalier et al., 2020). On the other hand, if X analogues spatially close to the target sample are selected and the SCDs indicate good or acceptable analogue situations (cf. de Vernal et al., 2005), the estimate is correct, and the approach performs at its best. Preventing selection of spatially close modern analogue would thus necessarily deteriorates the performances. This highlights the necessity of a modern database that covers the widest possible range of ecological configurations, hence the recent works to grow the reference modern pollen databases that should highly improve MAT results (e.g., Davis et al., 2020). But most importantly, it emphasizes the importance of always taking into account the SCDs of the selected analogues whenever a MAT reconstruction is made.

As approach for paleoclimate reconstruction, MAT remains one of the most robust methods regarding paleoclimate reconstructions, as long as the following conditions are met: 1) a modern pollen database covering the widest possible range of ecological configurations, 2) high R^2(P) and low RMSEP, 3) good analogue situations with low SCD, 4) strong relationships between pollen assemblages and climatic parameters to estimate. Lastly, although MAT is reliable for climatic reconstructions, confrontation with other paleoclimatic proxy records is always relevant (cf. Chevalier et al., 2020 and references therein).

1.3.3.3 Modern pollen database

The paleoclimate reconstructions were made with the "bioindic" package (ftp://ftp.cerege.fr/R/Package_bioindic/), built on the R-platform (http://cran.r-project.org/), using a modern calibration dataset taken from the latest Eurasian Modern Pollen Database (version 2) (EMPD2) (Davis et al., 2020). The EMPD2 comprises more than 8000 modern pollen samples from the Paleartic

realm, which includes Europe and Asia, from the Atlantic to Pacific margins (Fig. 1.2) and represents a significant improvement compared to the 4826 samples of the EMPD1 (Davis et al., 2013). Most of the additional modern samples in EMPD2 come from Russia (+ 2274 samples), Italy, Norway and Spain, and also from Japan, Cyprus and Kyrgyzstan that were not represented in EMPD1 (Davis et al., 2020). This wide data set covers a total of nine biomes (cf. Olson et al., 2001) (Fig. 1.2), and thus comprises a large number of potential modern analogues for many different climates and vegetation types, which is particularly critical when considering the objective of climatic reconstructions for glacial times (Magyari et al., 2014; Davis et al., 2022). Figure 1.3 shows how the modern samples, and their associated biomes, are distributed in climate space.

The climatic data for each modern sample were assigned according to the nearest grid point of the WorldClim2 grid (within ~1 km^2) and reflect the period between 1970 and 2000 (Fick and Hijmans, 2017). They include mean monthly, seasonal and annual temperatures and precipitation (Davis et al., 2020). We added the mean-temperature of the warmest (MTWA) and the coldest months (MTCO), and the seasonality defined as the difference between MTWA and MTCO. At 77% of the sites, MTWA corresponds to July temperatures, while at 83% of the sites, MTCO represents January temperatures. MTWA, MTCO, seasonality, winter (Pdjf) and summer (Pjja) precipitation along with annual precipitation (Pann) were the climatic variables we retained for this work.

The pollen analyses of modern samples were done in various laboratories, by different analysts, and with different taxonomic level (e.g., family, genus, species). Hence, the whole database includes a very high number of pollen taxa (840). We grouped these 840 different pollen taxa into 184 taxa after downgrading of taxa to genera or family levels in order to homogenize the database (Supplementary Material of the paper presented as Appendix A), and further reduce this number to the most common terrestrial taxon types based mainly on the number of occurrence (>100). Exceptions were made for three taxa with occurrence below 100 that are often identified in European pollen fossil records (Anacardiaceae (mostly *Rhus*), *Ceratonia*, *Celtis*). We retained two versions of the database: one with 88 taxa and another one with 77 taxa (Table 1.3). Cross-validation tests (cf. Guiot and de Vernal, 2007; Chevalier et al., 2020) were conducted with both to evaluate which one results in the most accurate reconstructions (Table 1.4). Differences are very small, but the 88 taxa database seems to provide the most accurate reconstructions. We thus used the 88 taxa database for this work (Table 1.4).

In the database with 88 taxa (Table 1.3), we kept samples with a pollen sum (excluding *Pinus*) equal or superior to 100 grains, for a total of 7634 remaining modern pollen samples from the EMPD2. The same criterion was applied to the fossil records for which any sample with a pollen sum (excluding *Pinus*) inferior to 100 was removed. A list of the occurrence and relative abundance of the 88 taxa in the database is shown in Table 1.3.

To assess the number of analogues to use for the most accurate reconstructions, cross-validation tests were run with 5 to 10 analogues (Table 1.5), which are usually the numbers of analogues retained by MAT users (e.g., Sawada et al., 2004; Fréchette et al., 2008; Dugerdil et al., 2021). Differences are small but the best results were obtained with 5 to 7 analogues (Table 1.5), "5 analogues" showing the highest R^2. With more than 7 analogues, the RMSEP slightly increases, especially for precipitation. Since we aimed at paleoclimatic reconstructions for glacial times, which are often feared as poor analogue situations, we decided to keep 5 analogues.

The results of the cross-validation test performed with 5 analogues on the EMPD2 subset (Davis et al., 2020) containing 7634 sites and 88 pollen taxa are plotted in Figure 1.4. The linearity of the relationship between reconstructed and observed values, with a slope close to one and high coefficients of correlation (R2), highlights the reliability of the method, especially for temperature reconstructions. The highest R^2 value is recorded for MTCO (0.91), which also shows higher RMSEP (3.41°C) than MTWA (1.95°C), reflecting the larger range of winter temperatures in the dataset compared to summer temperatures. The high spatial variability of precipitation in the geographical extent of the database explains the weaker R^2 values for precipitation, especially winter and annual precipitation. The RMSEP for annual, winter and summer precipitation are 199.8, 68.8 and 46.3 mm respectively.

1.3.3.4 Climate reconstruction in marine cores

Deposition environment and processes are important parameters in the redistribution of pollen (Chevalier et al., 2020). Modern pollen samples in our final version of the EMPD2 are all terrestrial since we removed the marine ones, which could not have climatic assignment (see Davis et al., 2020). Terrestrial modern samples are retrieved from various environments such as mosses and peatlands, lake sediment, soil, etc. Small lakes or small peatlands usually record a more local signal while larger lakes integrate local and regional vegetation. Marine sediments record regional vegetation of the adjacent continent since no pollen is locally produced (Turon, 1984; Naughton et al., 2007; Sánchez-Goñi et al., 2018). Pollen in marine

sediment principally results from long distance transport by wind and rivers, the contribution from oceanic currents being negligible (Koreneva, 1966). However, we may question to what extent marine pollen assemblages can represent the adjacent continental vegetation.

We previously mentioned that pollen grains are transported through different mechanisms, and that preservation may vary from one taxon to another. In marine cores collected more than 300 km offshore, it has been shown that pollen transport is mainly aeolian and input from rivers is weak (e.g., Hooghiemstra et al., 2006), thus leading to potential biases due to differential source of wind transport of pollen taxa. However, the marine cores used in this study are all located less than 150 km offshore (Fig. 1.1; Table 1.1 and references therein). Some cores are situated on the Western Iberian margin where well-developed hydrographic system results in large pollen inputs from fluvial transport (Naughton et al., 2007). The others are located off the Southeastern Iberian Margin, in the Alboran Sea, where there is no major river system. Nevertheless, local torrential rains may generate large riverine inputs to the Alboran Sea, whereas aeolian lithogenic particles only represent 12% of the total particle supply (Fabrés et al., 2002). It thus implies that the main pollen contribution to these sites likely comes from the adjacent riverine system (Sánchez-Goñi et al., 2002). Furthermore, even if pollen of nearshore marine settings essentially comes from fluvial and/or riverine transport, pollen input related to wind contribution is not negligible. Hence selective pollen transport by wind results in the overrepresentation of some pollen taxa, notably *Pinus* (Connor et al., 2004), which can be transported over very long distance and is produced in large quantities (Li et al., 2005). *Pinus* can dominate pollen assemblages even when not present in the local environment (Campbell et al., 1999). This is especially the case in marine cores, in which *Pinus* is largely overrepresented (Heusser and Balsam, 1977; Turon, 1984). Finally, there are also concerns about the diversity of species, which is supposedly very low in marine sediment compared to terrestrial samples. Despite the impact of distal transport and overrepresentation of *Pinus*, several studies conducted in Western Europe and in the Mediterranean region led to demonstrate that pollen assemblages in nearshore marine settings reflect the regional vegetation allowing comparisons with terrestrial pollen assemblages of the adjacent continent (Sánchez-Goñi et al., 2018 and references therein). However, the interpretation of pollen assemblages from marine sediment in terms of paleoclimate needs caution.

The use of marine sedimentary sequences for inferring continental paleoclimate parameters is still highly debated (e.g., Sánchez-Goñi et al., 2018; Chevalier et al., 2020; Davis et al., 2022). Detractors (e.g., Birks et al., 2010) stated that fossil and modern pollen samples should originate from comparable

sedimentary environment for assuming identical linkages between pollen and climate. Others on the other side have addressed this issue and demonstrated a strong concordance between marine and terrestrial pollen spectra of the adjacent landmasses (Sánchez-Goñi et al., 2018 and references therein), acknowledging however an overrepresentation of *Pinus*.

To cope with the issue of *Pinus* overrepresentation, some authors (e.g., Sánchez-Goñi et al., 2002; Combourieu-Nebout et al., 2009) have excluded *Pinus* from the fossil spectra and from the modern pollen database to apply MAT for quantitative reconstruction. However, it was argued that this removal might generate significant biases (e.g., Davis et al., 2022) because *Pinus* was the most abundant tree taxon in Southwestern Europe during the last glacial with important climatic significance (García-Amorena et al., 2007). Moreover, by removing *Pinus*, pollen sums lower than 100 are problematic in numbers of samples, which do not meet quality criteria and are often removed from the datasets (see chapter 2.3.2). Therefore, there are arguments in favor and against removing *Pinus* from the pollen sum.

1.3.3.4.1 Tests based on results from marine core MD95-2042

In this study, we feel confident with the representativeness of the pollen assemblages from the nearshore marine cores we are using. The counts are high enough (> 100 (excluding *Pinus*)), and the diversity of species, which is generally very low in marine sediment, is comparable with that of terrestrial sequences (Table 1.6). For reconstructions, we decided to test the MAT approach with and without *Pinus* using the data from the marine core MD95-2042 (Sánchez-Goñi et al., 2000, 2008, 2009), located near the southwestern margin of the Iberian Peninsula (Fig. 1.1; Table 1.1). The reconstructions are compared to sea-surface temperature estimates from the same core (Shackleton et al., 2000). Marine cores indeed provide the opportunity to make direct land-sea correlation (Sánchez-Goñi et al., 2002, 2008, 2009; Roucoux et al., 2005), and to develop a chronology based on stable oxygen isotope records in foraminifera, which can be correlated with the Greenland Ice core stratigraphy (Kissel et al., 1999; Austin and Hibbert, 2012). The MIS 3 section in core MD95-2042 shows very high percentages of *Pinus* up to 94.7%, with a mean of 82.6 ± 7.1%. As mentioned above, the application of MAT after exclusion of *Pinus* requires removing *Pinus* from the modern pollen database and recalculating percentages. Since modern samples with a pollen sum excluding *Pinus* <100 grains were already removed from the database, this version of the database with 87 taxa comprises the same number of modern samples (i.e., 7634 sites). Validation tests with and without *Pinus* (87 or 88 taxa) yield comparable results, with slightly higher RMSEP for the without *Pinus* version (see Table 1.7).

Figure 1.5 shows the MAT reconstructions from core MD95-2042, with and without *Pinus*, compared to the $\delta^{18}O$ of G. bulloides (Shackleton et al., 2000), which is interpreted as a proxy of sea-surface temperature (Malevich et al., 2019). The MAT curves are different, with much larger variations without *Pinus*. In both cases, however, winter temperatures depict larger variations than summer temperatures, with the cold winter phases corresponding to Greenland Stadials (GSs) identified from the $\delta^{18}O$ record (Austin and Hibbert, 2012). The cooling pulses are clear for every GSs in the reconstructions without *Pinus* and appear more subtle in the reconstructions with *Pinus*. Summer temperatures remained relatively unchanged throughout MIS 3 regardless of the approach and do not necessarily follow winter temperature variation. This is particularly visible for Heinrich Event 5 (HE5) (between GI 13 and GI 12; Fig. 1.5) characterized by an important cooling of more than 10°C in winter temperatures whereas summer temperatures do not depict any change. As a consequence of summer temperature stability and high winter variability, seasonality shows more variability in the reconstruction without *Pinus*, with high values recorded during all GSs.

The largest differences in the reconstructions with and without *Pinus* are seen in the precipitation (Figs. 1.5A and 1.5B). In both cases, summer precipitation remains low with little changes throughout the record, in contrary to the annual and winter precipitation. However, estimates without *Pinus* (Fig. 1.5B) are characterized by much larger winter and annual precipitation with high values during all Greenland Interstadial phases (GIs) and significant drops during all GSs. In comparison, winter and annual precipitation reconstructed with *Pinus* (Fig. 1.5A) depicts low amplitude variations of winter precipitation during most MIS 3.

To decipher which is the most correct reconstruction is an important question. The cross-validation test showed similar performance with both datasets (with and without *Pinus*), with slightly lower RMSEP with *Pinus* (Table 1.7). The SCD values may, however, help us to discriminate which reference data to use (see chapter 2.3.1) as the quality of analogues is much better with *Pinus* (Figs. 1.5A and 1.5B). Based on this criterion, we should opt for keeping *Pinus* in our MAT reconstructions from marine cores.

There are, however, some counterarguments. Given the very high percentages of *Pinus* in core MD95-2042, and thus low percentages of other taxa, low SCD values are expected as long as analogues have a very close percentage of *Pinus*. Taken into considerations the 88 fossil pollen samples of the MIS 3 section in core MD95-2042 and that 5 analogues are retained for each fossil sample, there is a maximum

possibility of 440 analogues to be selected among the 7634 modern samples in the database. A total of 30 modern samples, belonging to three different biomes (temperate broadleaf and mixed forests; Mediterranean forests, woodlands and scrubs; Boreal forests / Taiga), were selected. These samples have high percentages of *Pinus* as well, comparable to those in core MD95-2042, which explains the low SCDs. It is worth noting that without *Pinus*, over 440 analogues possible, 88 modern analogues were retained, which is almost the triple of the number of analogues retained when we keep *Pinus*. These 88 modern analogues belong to seven biomes, out of the 9 included in the EMPD2. This explains the larger dispersal of reconstructions when excluding *Pinus*.

Should we favor an approach that focuses on the relative abundance of dominant and cosmopolitan taxon or an approach that excludes this overrepresented taxon to focus on the relative abundances of the rest of the assemblage, which might be more sensitive to climate? How to distinguish which part of these fossil pollen spectra bears the most representative climate signature? A closer look at our MAT reconstructions and the literature might help us disentangle these issues. First, the comparison of MAT reconstructions (Fig. 1.5) with the $\delta^{18}O$ record of *G. bulloides* (Shackelton et al., 2000) shows variations similar to winter temperatures and precipitation reconstructed without *Pinus*. Second, when *Pinus* is included (Fig. 1.5A), annual precipitation remains high throughout MIS 3, with very few low values below 600 mm. Even HE4 (between GI9 and GI8), which is supposedly one of the most extreme events of MIS 3 in the North Atlantic and European continent (e.g., Hemming, 2004; Sepulchre et al., 2007; Lopez-Garcia et al., 2013), is only marked by slight decreases in annual precipitation and winter temperatures (Fig. 1.5A). Such high precipitation values could not explain the ecological stress (cf. Tzedakis et al., 2004) necessary for the major changes recorded in the regional vegetation based on terrestrial pollen sequences (e.g., Guiot et al., 1993; Carrion and van Geel, 1999; Camuera et al., 2019), especially without important drops of temperatures (Fig. 1.5A). High precipitation values do not echo either the pronounced episodes of dryness inferred from speleothems of Southwestern France (Genty et al., 2003, 2010). Conversely, significant decrease in winter and annual precipitation during GSs in reconstructions without *Pinus* (Fig. 1.5B), along with more pronounced winter cooling (Fig. 1.5B) could have triggered the climate deteriorations recorded regionally (e.g., Guiot et al., 1993; Carrion and Van geel, 1999; Camuera et al., 2019; Budsky et al., 2019).

We conclude that despite statistical better MAT results with *Pinus*, deeper examination of the reconstructions and comparison with regional data suggest that removing *Pinus* in the dataset permits to

better capture the climate changes. However, because of weak analogue situation, results should be handled with caution.

1.3.4 Comparison to modern values

Paleoclimatic reconstructions were then compared to modern values for all terrestrial sites using the mean climatic values calculated from 1901 to 2022 with Climate Explorer (https://climexp.knmi.nl/start.cgi). The grid for the climatic compilation is 0.5° x 0.5°. Because pollen in marine cores may be advected from wider areas, we did not assess the modern climatic values at marine sites.

1.3.5 Multivariate analyses

Canonical Correspondence analyses (CCA) were performed on the modern database using the Canoco 5 software (Šmilauer and Lepš, 2014) to evaluate the relationship between pollen taxa and the environmental variables (Fig. 1.6). Square root transformation was applied to pollen assemblages to increase the weight of taxa occurring in low abundance. Figure 1.6 shows the CCA ordination diagram of pollen taxa vs. environmental variables. The first axis explains 60.15% of the constrained variance and is negatively correlated with MTWA and, to a lesser extent with MTCO. Axis 2 explains 21,48% of the constrained variance and is positively correlated with Pann and Pdjf, and, to a lesser extent, positively and negatively correlated with Pjja and Seasonality, respectively. Overall, the first two CCA axes show different scores for the climatic parameters and a relatively large scatter of the 88 taxa, which confirms that the modern database can be used to reconstruct the climatic parameters selected (Fig. 1.6). Many taxa, including thermophilous taxa such as *Olea*, *Pistacia* or *Phillyrea* are grouped along with MTWA while we observe many taxa from temperate forests along the Pdjf and MTCO arrows, which illustrates their strong relationship with these climatic parameters (Fig. 1.6).

For each site, redundancy analysis (RDA) was performed with Canoco 5 (Šmilauer and Lepš, 2014) using the PFT and paleoclimatic estimates with two objectives: 1) to examine the primary variation patterns of the vegetation as illustrated from PFTs; 2) to identify which climatic parameter(s) influence(s) the primary variation patterns in the vegetation. Since square root transformations were applied to the initial pollen percentages for the PFT grouping, no additional transformation was made before running the RDAs.

1.4 Conclusion

In this chapter about the methods used in this work, we presented the pollen data and associated chronological information from the ACER database (Sánchez-Goñi et al., 2017) and the Padul sequence (Camuera et al., 2018, 2019). Plant Functional Types (PFTs), which are classes of plants defined by certain vegetation criteria (e.g., stature, leaf form and phenology), and climatic thresholds (e.g., Peyron et al., 1998) enabled the handling of a limited number of variables ($n < 23$) facilitating comparison between sites and investigation of the linkages between the vegetation dynamics and the seasonal climatic parameters reconstructed via multivariate analyses. This chapter also presents the uncertainties inherent to pollen-based models of climate reconstruction, notably the differences between the pollen representation of taxa in the source vegetation, which can be due to several factors and can bias the significance of pollen assemblages in terms of climate. Since these uncertainties are hard to assess, we encourage comparison with non-pollen-based climatic reconstructions. We also address the fact that atmospheric CO_2 concentration variations through time are not taken into account by most pollen-based models of climate reconstructions, such as the Modern Analogue Technique (MAT) we choose here, despite the fact that it affects the relationships between pollen assemblages and climate, especially since we aim at reconstructing climate for times of low atmospheric CO_2 values such as MIS 2 and the end of MIS 3. Although we cannot exclude a slight underestimation of precipitation reconstructions, literature indicates that low CO_2 concentrations during MIS 2 had little impact on pollen-based climate reconstructions with MAT. This chapter also addresses the advantages and limitations specific to the Modern Analogue Technique (MAT) chosen here to infer paleoclimates based on pollen data (cf. Birks et al., 2010; Chevalier et al., 2020).

The main limitation of MAT raised in the literature is spatial autocorrelation (Telford and Birks, 2005, 2009, 2011; Birks et al., 2010; Chevalier et al., 2020). Here, we rather argue that it is an intrinsic property of most ecological data (Legendre, 1993) on which climate reconstruction models are built. Since climate is a large-scale phenomenon and vegetation intimately depends upon climate, it is normal that geographically close modern pollen samples present similar assemblages. We also addressed the debate about the use of marine sedimentary sequences for inferring continental paleoclimate parameters (cf. Birks et al., 2010; Sánchez-Goñi et al., 2017; Chevalier et al., 2020), and the relevance of removing *Pinus* from the fossil and modern assemblages for climatic reconstructions. A strong concordance between marine and terrestrial pollen spectra of the adjacent landmasses (Sánchez-Goñi et al., 2018 and references therein), especially for marine pollen sequences located less than 300 km offshore as in this study, let us

to argue for the use of pollen data from marine cores. Acknowledging the overrepresentation of *Pinus* in marine sediments, we performed tests with and without *Pinus* in marine core MD95-2042 (site 3). The comparison with proxies of surface ocean conditions led to highlighting that despite statistically good MAT results with *Pinus*, removing *Pinus* from the dataset permits us to better capture the regional climate changes.

1.5 References

Allen, J. R., Watts, W. A., & Huntley, B. (2000). Weichselian palynostratigraphy, palaeovegetation and palaeoenvironment; the record from Lago Grande di Monticchio, southern Italy. *Quaternary International*, *73*, 91-110.

Allen, J. R., & Huntley, B. (2018). Effects of tephra falls on vegetation: A Late-Quaternary record from southern Italy. *Journal of Ecology*, *106*(6), 2456-2472.

Austin, W. E., & Hibbert, F. D. (2012). Tracing time in the ocean: a brief review of chronological constraints (60–8 kyr) on North Atlantic marine event-based stratigraphies. *Quaternary Science Reviews*, *36*, 28-37.

Bauska, T. K., Marcott, S. A., & Brook, E. J. (2021). Abrupt changes in the global carbon cycle during the last glacial period. *Nature Geoscience*, *14*(2), 91-96.

Birks, H. J. B., Heiri, O., Seppä, H., & Bjune, A. E. (2010). Strengths and weaknesses of quantitative climate reconstructions based on Late-Quaternary. *The Open Ecology Journal*, *3*(1).

Blaauw, M. (2010). Methods and code for 'classical'age-modelling of radiocarbon sequences. *Quaternary geochronology*, *5*(5), 512-518.

Bottema, S. (1979). Pollen analytical investigations in Thessaly (Greece). *Palaeohistoria*, 19-40.

Brauer, A., Allen, J. R., Mingram, J., Dulski, P., Wulf, S., & Huntley, B. (2007). Evidence for last interglacial chronology and environmental change from Southern Europe. *Proceedings of the National Academy of Sciences*, *104*(2), 450-455.

Broström, A., Nielsen, A. B., Gaillard, M. J., Hjelle, K., Mazier, F., Binney, H., ... & Sugita, S. (2008). Pollen productivity estimates of key European plant taxa for quantitative reconstruction of past vegetation: a review. *Vegetation history and archaeobotany*, *17*, 461-478.

Budsky, A., Wassenburg, J. A., Mertz-Kraus, R., Spötl, C., Jochum, K. P., Gibert, L., & Scholz, D. (2019). Western Mediterranean climate response to Dansgaard/Oeschger events: New insights from speleothem records. *Geophysical Research Letters*, *46*(15), 9042-9053.

Campbell, I. D., McDonald, K., Flannigan, M. D., & Kringayark, J. (1999). Long-distance transport of pollen into the Arctic. *Nature*, *399*(6731), 29-30.

Camuera, J., Jiménez-Moreno, G., Ramos-Román, M. J., García-Alix, A., Toney, J. L., Anderson, R. S., ... & Martínez-Ruiz, F. (2018). Orbital-scale environmental and climatic changes recorded in a new~ 200,000-year-long multiproxy sedimentary record from Padul, southern Iberian Peninsula. *Quaternary Science Reviews*, *198*, 91-114.

Camuera, J., Jiménez-Moreno, G., Ramos-Román, M. J., García-Alix, A., Toney, J. L., Anderson, R. S., ... & Carrión, J. S. (2019). Vegetation and climate changes during the last two glacial-interglacial cycles in the western Mediterranean: a new long pollen record from Padul (southern Iberian Peninsula). *Quaternary Science Reviews*, *205*, 86-105.

Carré, M., & Cheddadi, R. (2017). Seasonality in long-term climate change. *Quaternaire. Revue de l'Association française pour l'étude du Quaternaire*, *28*(2), 173-177.

Carrión, J. S., & Van Geel, B. (1999). Fine-resolution Upper Weichselian and Holocene palynological record from Navarrés (Valencia, Spain) and a discussion about factors of Mediterranean forest succession. *Review of Palaeobotany and Palynology*, *106*(3-4), 209-236.

Chevalier, M., Cheddadi, R., & Chase, B. M. (2014). CREST (Climate REconstruction SofTware): a probability density function (PDF)-based quantitative climate reconstruction method. *Climate of the Past*, *10*(6), 2081-2098.

Chevalier, M., Davis, B. A., Heiri, O., Seppä, H., Chase, B. M., Gajewski, K., ... & Kupriyanov, D. (2020). Pollen-based climate reconstruction techniques for late Quaternary studies. *Earth-Science Reviews*, *210*, 103384.

Cleator, S. F., Harrison, S. P., Nichols, N. K., Prentice, I. C., & Roulstone, I. (2020). A new multivariable benchmark for Last Glacial Maximum climate simulations. *Climate of the Past*, *16*(2), 699-712.

Combourieu Nebout, N., Turon, J. L., Zahn, R., Capotondi, L., Londeix, L., & Pahnke, K. (2002). Enhanced aridity and atmospheric high-pressure stability over the western Mediterranean during the North Atlantic cold events of the past 50 ky. *Geology*, *30*(10), 863-866.

Combourieu Nebout, N., Peyron, O., Dormoy, I., Desprat, S., Beaudouin, C., Kotthoff, U., & Marret, F. (2009). Rapid climatic variability in the west Mediterranean during the last 25 000 years from high resolution pollen data. *Climate of the Past*, *5*(3), 503-521.

Connor, S. E., Thomas, I., Kvavadze, E. V., Arabuli, G. J., Avakov, G. S., & Sagona, A. (2004). A survey of modern pollen and vegetation along an altitudinal transect in southern Georgia, Caucasus region. *Review of Palaeobotany and Palynology*, *129*(4), 229-250.

Davis, B. A., Zanon, M., Collins, P., Mauri, A., Bakker, J., Barboni, D., ... & Kaplan, J. O. (2013). The European modern pollen database (EMPD) project. *Vegetation history and archaeobotany*, *22*(6), 521-530.

Davis, B. A., Chevalier, M., Sommer, P., Carter, V. A., Finsinger, W., Mauri, A., ... & Zimny, M. (2020). The Eurasian Modern Pollen Database (EMPD), version 2. *Earth System Science Data Discussions*, *2020*, 1-41.

Davis, B. A. S., Fasel, M., Kaplan, J. O., Russo, E., & Burke, A. (2022). The climate and vegetation of Europe, North Africa and the Middle East during the Last Glacial Maximum (21,000 years BP) based on pollen data. *Climate of the Past Discussions*, 1-66.

de Vernal, A. D., Eynaud, F., Henry, M., Hillaire-Marcel, C., Londeix, L., Mangin, S., ... & Turon, J. L. (2005). Reconstruction of sea-surface conditions at middle to high latitudes of the Northern Hemisphere during the Last Glacial Maximum (LGM) based on dinoflagellate cyst assemblages. *Quaternary Science Reviews*, *24*(7-9), 897-924.

Denton, G. H., Alley, R. B., Comer, G. C., & Broecker, W. S. (2005). The role of seasonality in abrupt climate change. *Quaternary Science Reviews*, *24*(10-11), 1159-1182.

Denton, G. H., Toucanne, S., Putnam, A. E., Barrell, D. J., & Russell, J. L. (2022). Heinrich summers. *Quaternary Science Reviews*, *295*, 107750.

Dugerdil, L., Ménot, G., Peyron, O., Jouffroy-Bapicot, I., Ansanay-Alex, S., Antheaume, I., ... & Joannin, S. (2021). Late Holocene Mongolian climate and environment reconstructions from brGDGTs, NPPs and pollen transfer functions for Lake Ayrag: Paleoclimate implications for Arid Central Asia. *Quaternary Science Reviews*, *273*, 107235.

Fabres, J., Calafat, A., Sanchez-Vidal, A., Canals, M., & Heussner, S. (2002). Composition and spatio-temporal variability of particle fluxes in the Western Alboran Gyre, Mediterranean Sea. *Journal of Marine Systems*, *33*, 431-456.

Fick, S. E., & Hijmans, R. J. (2017). WorldClim 2: new 1-km spatial resolution climate surfaces for global land areas. *International journal of climatology*, *37*(12), 4302-4315.

Follieri, M. (1988). 250, 000-year pollen record from Valle di Castiglione. *Pollen et spores*, (3), 329-356.

Follieri, M., Magri, D., & Sadori, L. (1989). Pollen stratigraphical synthesis from Valle di Castiglione (Roma). *Quaternary International*, *3*, 81-84.

Follieri, M., Giardini, M., Magri, D., & Sadori, L. (1998). Palynostratigraphy of the last glacial period in the volcanic region of central Italy. *Quaternary International*, *47*, 3-20.

Frechette, B., De Vernal, A., Guiot, J., Wolfe, A. P., Miller, G. H., Fredskild, B., ... & Richard, P. J. (2008). Methodological basis for quantitative reconstruction of air temperature and sunshine from pollen assemblages in Arctic Canada and Greenland. *Quaternary Science Reviews*, *27*(11-12), 1197-1216.

Fréchette, B., Richard, P. J., Grondin, P., Lavoie, M., & Larouche, A. C. (2018). *Histoire postglaciaire de la végétation et du climat des pessières et des sapinières de l'ouest du Québec*. Gouvernement du Québec, ministère des Forêts, de la Faune et des Parcs.

García-Amorena, I., Manzaneque, F. G., Rubiales, J. M., Granja, H. M., de Carvalho, G. S., & Morla, C. (2007). The Late Quaternary coastal forests of western Iberia: A study of their macroremains. *Palaeogeography, Palaeoclimatology, Palaeoecology*, *254*(3-4), 448-461.

Genty, D., Blamart, D., Ouahdi, R., Gilmour, M., Baker, A., Jouzel, J., & Van-Exter, S. (2003). Precise dating of Dansgaard–Oeschger climate oscillations in western Europe from stalagmite data. *Nature*, *421*(6925), 833-837.

Genty, D., Combourieu-Nebout, N., Peyron, O., Blamart, D., Wainer, K., Mansuri, F., ... & Brauer, A. (2010). Isotopic characterization of rapid climatic events during OIS3 and OIS4 in Villars Cave stalagmites (SW-France) and correlation with Atlantic and Mediterranean pollen records. *Quaternary Science Reviews*, *29*(19-20), 2799-2820.

Giardini, M. (2007). Late quaternary vegetation history at Stracciacappa (Rome, central Italy). *Vegetation History and Archaeobotany*, *16*(4), 301-316.

Giesecke, T., Wolters, S., van Leeuwen, J. F., van Der Knaap, P. W., Leydet, M., & Brewer, S. (2019). Postglacial change of the floristic diversity gradient in Europe. *Nature communications*, *10*(1), 5422.

Guiot, J. (1990). Methodology of the last climatic cycle reconstruction in France from pollen data. *Palaeogeography, Palaeoclimatology, Palaeoecology*, *80*(1), 49-69.

Guiot, J., De Beaulieu, J. L., Cheddadi, R., David, F., Ponel, P., & Reille, M. (1993). The climate in Western Europe during the last Glacial/Interglacial cycle derived from pollen and insect remains. *Palaeogeography, Palaeoclimatology, Palaeoecology*, *103*(1-2), 73-93.

Guiot, J., Torre, F., Jolly, D., Peyron, O., Boreux, J. J., & Cheddadi, R. (2000). Inverse vegetation modeling by Monte Carlo sampling to reconstruct palaeoclimates under changed precipitation seasonality and CO2 conditions: application to glacial climate in Mediterranean region. *Ecological modelling*, *127*(2-3), 119-140.

Guiot, J., & de Vernal, A. (2007). Chapter thirteen transfer functions: methods for quantitative paleoceanography based on microfossils. *Developments in marine geology*, *1*, 523-563.

Guiot, J., & De Vernal, A. (2011a). Is spatial autocorrelation introducing biases in the apparent accuracy of paleoclimatic reconstructions?. *Quaternary Science Reviews*, *30*(15-16), 1965-1972.

Guiot, J., & De Vernal, A. (2011b). QSR Correspondence “Is spatial autocorrelation introducing biases in the apparent accuracy of palaeoclimatic reconstructions?” Reply to Telford and Birks. *Quaternary Science Reviews*, *21*(30), 3214-3216.

Harrison, S. P., & Prentice, C. I. (2003). Climate and CO2 controls on global vegetation distribution at the last glacial maximum: analysis based on palaeovegetation data, biome modelling and palaeoclimate simulations. *Global Change Biology*, *9*(7), 983-1004.

Havinga, A. J. (1967). Palynology and pollen preservation. *Review of Palaeobotany and Palynology*, *2*(1-4), 81-98.

Hemming, S. R. (2004). Heinrich events: Massive late Pleistocene detritus layers of the North Atlantic and their global climate imprint. *Reviews of Geophysics*, *42*(1).

Heusser, L., & Balsam, W. L. (1977). Pollen distribution in the northeast Pacific Ocean. *Quaternary Research*, *7*(1), 45-62.

Hooghiemstra, H., Lézine, A. M., Leroy, S. A., Dupont, L., & Marret, F. (2006). Late Quaternary palynology in marine sediments: a synthesis of the understanding of pollen distribution patterns in the NW African setting. *Quaternary International*, *148*(1), 29-44.

Jackson, S. T., & Overpeck, J. T. (2000). Responses of plant populations and communities to environmental changes of the late Quaternary. *Paleobiology*, *26*(S4), 194-220.

Juggins, S. (2013). Quantitative reconstructions in palaeolimnology: new paradigm or sick science?. *Quaternary Science Reviews*, *64*, 20-32.

Kissel, C., Laj, C., Labeyrie, L., Dokken, T., Voelker, A., & Blamart, D. (1999). Rapid climatic variations during marine isotopic stage 3: magnetic analysis of sediments from Nordic Seas and North Atlantic. *Earth and Planetary Science Letters*, *171*(3), 489-502.

Koreneva, E. V. (1966). Marine palynological researches in the USSR. *Marine Geology*, *4*(6), 565-574.

Legendre, P. (1993). Spatial autocorrelation: trouble or new paradigm?. *Ecology*, *74*(6), 1659-1673.

Li, Y. C., Xu, Q. H., Yang, X. L., Chen, H., & Lu, X. M. (2005). Pollen-vegetation relationship and pollen preservation on the Northeastern Qinghai-Tibetan Plateau. *Grana*, *44*(3), 160-171.

López-García, J. M., Blain, H. A., Bennàsar, M., Sanz, M., & Daura, J. (2013). Heinrich event 4 characterized by terrestrial proxies in southwestern Europe. *Climate of the Past*, *9*(3), 1053-1064.

Magri, D. (1999). Late Quaternary vegetation history at Lagaccione near Lago di Bolsena (central Italy). *Review of Palaeobotany and Palynology*, *106*(3-4), 171-208.

Magri, D., & Tzedakis, P. C. (2000). Orbital signatures and long-term vegetation patterns in the Mediterranean. *Quaternary International*, *73*, 69-78.

Magyari, E. K., Kuneš, P., Jakab, G., Sümegi, P., Pelánková, B., Schäbitz, F., ... & Chytrý, M. (2014). Late Pleniglacial vegetation in eastern-central Europe: are there modern analogues in Siberia?. *Quaternary Science Reviews*, *95*, 60-79.

Malevich, S. B., Vetter, L., & Tierney, J. E. (2019). Global core top calibration of δ 18O in planktic foraminifera to sea surface temperature. *Paleoceanography and Paleoclimatology*, *34*(8), 1292-1315.

Marchant, R., Richer, S., Boles, O., Capitani, C., Courtney-Mustaphi, C. J., Lane, P., ... & Wright, D. (2018). Drivers and trajectories of land cover change in East Africa: Human and environmental interactions from 6000 years ago to present. *Earth-Science Reviews*, *178*, 322-378.

Margari, V., Gibbard, P. L., Bryant, C. L., & Tzedakis, P. C. (2009). Character of vegetational and environmental changes in southern Europe during the last glacial period; evidence from Lesvos Island, Greece. *Quaternary Science Reviews*, *28*(13-14), 1317-1339.

Martin Calvo, M., & Prentice, I. C. (2015). Effects of fire and CO 2 on biogeography and primary production in glacial and modern climates. *New Phytologist*, *208*(3), 987-994.

Mauri, A., Davis, B. A., Collins, P. M., & Kaplan, J. O. (2015). The climate of Europe during the Holocene: a gridded pollen-based reconstruction and its multi-proxy evaluation. *Quaternary Science Reviews*, *112*, 109-127.

Naughton, F., Goñi, M. S., Desprat, S., Turon, J. L., Duprat, J., Malaizé, B., ... & Freitas, M. C. (2007). Present-day and past (last 25 000 years) marine pollen signal off western Iberia. *Marine Micropaleontology*, *62*(2), 91-114.

North, G. R. I. P. (2004). Ice Core Project members. High-resolution record of northern hemisphere climate extending into the last interglacial period. *Nature*, *431*, 147-151.

Ohlwein, C., & Wahl, E. R. (2012). Review of probabilistic pollen-climate transfer methods. *Quaternary Science Reviews*, *31*, 17-29.

Olson, D. M., Dinerstein, E., Wikramanayake, E. D., Burgess, N. D., Powell, G. V., Underwood, E. C., ... & Kassem, K. R. (2001). Terrestrial Ecoregions of the World: A New Map of Life on Earth: A new global map of terrestrial ecoregions provides an innovative tool for conserving biodiversity. *BioScience*, *51*(11), 933-938.

Ortu, E., Brewer, S., & Peyron, O. (2006). Pollen-inferred palaeoclimate reconstructions in mountain areas: problems and perspectives. *Journal of Quaternary Science: Published for the Quaternary Research Association*, *21*(6), 615-627.

Overpeck, J. T., Webb, T. I. I. I., & Prentice, I. C. (1985). Quantitative interpretation of fossil pollen spectra: dissimilarity coefficients and the method of modern analogs. *Quaternary Research*, *23*(1), 87-108.

Peyron, O., Guiot, J., Cheddadi, R., Tarasov, P., Reille, M., de Beaulieu, J. L., ... & Andrieu, V. (1998). Climatic reconstruction in Europe for 18,000 yr BP from pollen data. *Quaternary research*, *49*(2), 183-196.

Prentice, I. C., Cramer, W., Harrison, S. P., Leemans, R., Monserud, R. A., & Solomon, A. M. (1992). Special paper: a global biome model based on plant physiology and dominance, soil properties and climate. *Journal of biogeography*, 117-134.

Prentice, C., Guiot, J., Huntley, B., Jolly, D., & Cheddadi, R. (1996). Reconstructing biomes from palaeoecological data: a general method and its application to European pollen data at 0 and 6 ka. *Climate Dynamics*, *12*, 185-194.

Prentice, I. C., Cleator, S. F., Huang, Y. H., Harrison, S. P., & Roulstone, I. (2017). Reconstructing ice-age palaeoclimates: Quantifying low-CO2 effects on plants. *Global and Planetary Change*, *149*, 166-176.

Prentice, I. C., Villegas-Diaz, R., & Harrison, S. P. (2022). Accounting for atmospheric carbon dioxide variations in pollen-based reconstruction of past hydroclimates. *Global and Planetary Change*, *211*, 103790.

Robles, M., Peyron, O., Brugiapaglia, E., Ménot, G., Dugerdil, L., Ollivier, V., ... & Joannin, S. (2022). Impact of climate changes on vegetation and human societies during the Holocene in the South Caucasus (Vanevan, Armenia): A multiproxy approach including pollen, NPPs and brGDGTs. *Quaternary Science Reviews*, *277*, 107297.

Rodrigo-Gámiz, M., García-Alix, A., Jiménez-Moreno, G., Ramos-Román, M. J., Camuera, J., Toney, J. L., ... & Damsté, J. S. S. (2022). Paleoclimate reconstruction of the last 36 kyr based on branched glycerol dialkyl glycerol tetraethers in the Padul palaeolake record (Sierra Nevada, southern Iberian Peninsula). *Quaternary Science Reviews*, *281*, 107434.

Roucoux, K. H., Shackleton, N. J., de Abreu, L., Schönfeld, J., & Tzedakis, P. C. (2001). Combined marine proxy and pollen analyses reveal rapid Iberian vegetation response to North Atlantic millennial-scale climate oscillations. *Quaternary Research*, *56*(1), 128-132.

Roucoux, K. H., De Abreu, L., Shackleton, N. J., & Tzedakis, P. C. (2005). The response of NW Iberian vegetation to North Atlantic climate oscillations during the last 65 kyr. *Quaternary Science Reviews*, *24*(14-15), 1637-1653.

Salonen, J. S., Luoto, M., Alenius, T., Heikkilä, M., Seppä, H., Telford, R. J., & Birks, H. J. B. (2014). Reconstructing palaeoclimatic variables from fossil pollen using boosted regression trees: comparison and synthesis with other quantitative reconstruction methods. *Quaternary Science Reviews*, *88*, 69-81.

Sánchez Goñi, M. F., Turon, J. L., Eynaud, F., & Gendreau, S. (2000). European climatic response to millennial-scale changes in the atmosphere–ocean system during the Last Glacial period. *Quaternary Research*, *54*(3), 394-403.

Sánchez Goñi, M. F., Cacho, I., Turon, J. L., Guiot, J., Sierro, F. J., Peypouquet, J. P., ... & Shackleton, N. J. (2002). Synchroneity between marine and terrestrial responses to millennial scale climatic variability during the last glacial period in the Mediterranean region. *Climate dynamics*, *19*, 95-105.

Sánchez Goñi, M. F., (2006). Interactions végétation-climat au cours des derniers 425.000 ans en Europe occidentale. Le message du pollen des archives marines. *Quaternaire. Revue de l'Association française pour l'étude du Quaternaire*, *17*(1), 3-25.

Sánchez Goñi, M. F., Landais, A., Fletcher, W. J., Naughton, F., Desprat, S., & Duprat, J. (2008). Contrasting impacts of Dansgaard–Oeschger events over a western European latitudinal transect modulated by orbital parameters. *Quaternary Science Reviews*, *27*(11-12), 1136-1151.

Sánchez Goñi, M. F., Landais, A., Cacho, I., Duprat, J., & Rossignol, L. (2009). Contrasting intrainterstadial climatic evolution between high and middle North Atlantic latitudes: a close-up of Greenland Interstadials 8 and 12. *Geochemistry, Geophysics, Geosystems*, *10*(4).

Sánchez Goñi, M. F., Desprat, S., Daniau, A. L., Bassinot, F. C., Polanco-Martínez, J. M., Harrison, S. P., ... & Yamamoto, M. (2017). The ACER pollen and charcoal database: a global resource to document

vegetation and fire response to abrupt climate changes during the last glacial period. *Earth System Science Data Discussions*, *2017*, 1-33.

Sánchez Goñi, M. F., Desprat, S., Fletcher, W. J., Morales-Molino, C., Naughton, F., Oliveira, D., ... & Zorzi, C. (2018). Pollen from the deep-sea: A breakthrough in the mystery of the Ice Ages. *Frontiers in Plant Science*, *9*, 38.

Sánchez Goñi, M. F., Fourcade, T., Salonen, S., Lesven, J., Frigola, J., Swingedouw, D., & Sierro, F. J. (2021). Muted cooling and drying of NW Mediterranean in response to the strongest last glacial North American ice surges. *Bulletin*, *133*(3-4), 451-460.

Sawada, M., Viau, A. E., Vettoretti, G., Peltier, W. R., & Gajewski, K. (2004). Comparison of North-American pollen-based temperature and global lake-status with CCCma AGCM2 output at 6 ka. *Quaternary Science Reviews*, *23*(3-4), 225-244.

Sepulchre, P., Ramstein, G., Kageyama, M., Vanhaeren, M., Krinner, G., Sánchez-Goñi, M. F., & d'Errico, F. (2007). H4 abrupt event and late Neanderthal presence in Iberia. *Earth and Planetary Science Letters*, *258*(1-2), 283-292.

Shackleton, N. J., Hall, M. A., & Vincent, E. (2000). Phase relationships between millennial-scale events 64,000–24,000 years ago. *Paleoceanography*, *15*(6), 565-569.

Šmilauer, P., & Lepš, J. (2014). *Multivariate analysis of ecological data using CANOCO 5*. Cambridge university press.

St. Jacques, J. M., Cumming, B. F., Sauchyn, D. J., & Smol, J. P. (2015). The bias and signal attenuation present in conventional pollen-based climate reconstructions as assessed by early climate data from Minnesota, USA. *PloSone*, *10*(1), e0113806.

Telford, R. J., & Birks, H. J. B. (2005). The secret assumption of transfer functions: problems with spatial autocorrelation in evaluating model performance. *Quaternary Science Reviews*, *24*(20-21), 2173-2179.

Telford, R. J., & Birks, H. J. B. (2009). Evaluation of transfer functions in spatially structured environments. *Quaternary Science Reviews*, *28*(13-14), 1309-1316.

Telford, R. J., & Birks, H. J. B. (2011). QSR Correspondence" Is spatial autocorrelation introducing biases in the apparent accuracy of palaeoclimatic reconstructions?". *Quaternary Science Reviews*, *30*(21), 3210-3213.

ter Braak, C. J., & Juggins, S. (1993). Weighted averaging partial least squares regression (WA-PLS): an improved method for reconstructing environmental variables from species assemblages. In *Twelfth international diatom symposium: Proceedings of the twelfth international diatom symposium, Renesse, The Netherlands, 30 August–5 September 1992* (pp. 485-502). Springer Netherlands.

Ter Braak, C. J. F., Juggins, S., Birks, H. J. B., & Van der Voet, H. (1993). Weighted averaging partial least squares regression (WA-PLS): definition and comparison with other methods for species-environment calibration. In *Multivariate environmental statistics* (No. 6, pp. 525-560). Elsevier.

Theuerkauf, M., Dräger, N., Kienel, U., Kuparinen, A., & Brauer, A. (2015). Effects of changes in land management practices on pollen productivity of open vegetation during the last century derived from varved lake sediments. *The Holocene*, *25*(5), 733-744.

Turon, J. L. (1984). Direct land/sea correlations in the last interglacial complex. *Nature*, *309*(5970), 673-676.

Tzedakis, P. C., Lawson, I. T., Frogley, M. R., Hewitt, G. M., & Preece, R. C. (2002). Buffered tree population changes in a Quaternary refugium: evolutionary implications. *science*, *297*(5589), 2044-2047.

Tzedakis, P. C., Frogley, M. R., Lawson, I. T., Preece, R. C., Cacho, I., & De Abreu, L. (2004). Ecological thresholds and patterns of millennial-scale climate variability: the response of vegetation in Greece during the last glacial period. *Geology*, *32*(2), 109-112.

WAIS Divide Project Members. Precise interpolar phasing of abrupt climate change during the last ice age. *Nature*, 2015, vol. 520, no 7549, p. 661-665.

Watts, W. A., Allen, J. R. M., & Huntley, B. (1996). Vegetation history and palaeoclimate of the last glacial period at Lago Grande di Monticchio, southern Italy. *Quaternary Science Reviews*, *15*(2-3), 133-153.

Watts, W. A., Allen, J. R. M., & Huntley, B. (2000). Palaeoecology of three interstadial events during oxygen-isotope Stages 3 and 4: a lacustrine record from Lago Grande di Monticchio, southern Italy. *Palaeogeography, Palaeoclimatology, Palaeoecology*, *155*(1-2), 83-93.

Wiens, J. J., Ackerly, D. D., Allen, A. P., Anacker, B. L., Buckley, L. B., Cornell, H. V., ... & Stephens, P. R. (2010). Niche conservatism as an emerging principle in ecology and conservation biology. *Ecology letters*, *13*(10), 1310-1324.

Wulf, S., Kraml, M., Brauer, A., Keller, J., & Negendank, J. F. (2004). Tephrochronology of the 100 ka lacustrine sediment record of Lago Grande di Monticchio (southern Italy). *Quaternary International*, *122*(1), 7-30.

Table 1.1 Marine and terrestrial pollen records used for this study.

Site name	Code	Site type	Latitude (°N)	Longitude (°E)	Elevation (m)	References	Sources	Chronologies	MIS 3	MIS 2
MD95-2039	1	Marine	40.58	-10.35	-3381	Sánchez-Goñi et al. (2000); Roucoux et al. (2001. 2005)	ACER database[1]	ACER (file "dating_info_ACER)[1] (recalculated)	Yes	–
SU81-18	2	Marine	37.77	-10.18	-3135	Lézine and Denèfle (1997); Turon et al. (2003)	ACER database[1]	ACER (file "dating_info_ACER)[1] (recalculated)	–	Yes
MD95-2042	3	Marine	37.8	-10.17	-3148	Sánchez-Goñi et al. (2000. 2002. 2008. 2009); Sánchez-Goñi (2006)	ACER database[1]	ACER (file "dating_info_ACER)[1] (recalculated)	Yes	–
ODP Site 976	4	Marine	36.2	-4.3	-1108	Combourieu-Nebout et al. (2002. 2009)	ACER database[1]	ACER (file "dating_info_ACER)[1]	Yes	Yes
MD95-2043	5	Marine	36.14	-2.62	-1841	Sánchez-Goñi et al. (2002. 2009); Sánchez-Goñi (2006)	ACER database[1]	ACER (file "dating_info_ACER)[1] (recalculated)	Yes	–
Lac du Bouchet	6	Terrestrial	44.83	3.82	1200	Guiot et al. (1993)	ACER database[1]	ACER (file "dating_info_ACER)[1]	Yes	–
Lagaccione	7	Terrestrial	42.57	11.8	355	Magri (1999)	ACER database[1]	ACER (file "dating_info_ACER)[1]	Yes	–
Stracciacappa	8	Terrestrial	42.13	12.32	220	Follieri et al. (1998); Giardini (2007)	ACER database[1]	ACER (file "dating_info_ACER)[1]	Yes	–
Valle di Castiglione	9	Terrestrial	41.9	12.76	44	Follieri (1988); Follieri et al. (1989); Magri and Tzedakis (2000)	ACER database[1]	ACER (file "dating_info_ACER)[1]	Yes	–
Lago Grande di Monticchio	10	Terrestrial	40.94	15.61	656	Watts et al. (1996. 2000); Allen et al. (2000); Brauer et al. (2007) ; Allen and Huntley (2018)	ACER database[1]	See references associated (file "dating_info"[1])	Yes	Yes
Ioannina	11	Terrestrial	39.75	20.85	470	Tzedakis et al. (2002. 2004)	ACER database[1]	ACER (file "dating_info_ACER)[1]	Yes	–
Lake Xinias	12	Terrestrial	39.05	22.27	500	Bottema (1979)	ACER database[1]	ACER (file "dating_info_ACER)[1]	Yes	Yes
Megali Limni	13	Terrestrial	39.1	26.32	323	Margari et al. (2009)	ACER database[1]	ACER (file "dating_info_ACER)[1]	Yes	–
Padul	14	Terrestrial	37.01	-3,6	726	Camuera et al. (2018, 2019, 2022)	Shared by authors	See Camuera et al. (2018)	-	Yes

Table 1.2 Assignments used for the PFTs. Codes in green represent arboreal PFTs while those in brown represent non-arboreal PFTs.

Codes	PFTs	Taxa included in PFTs
EC	Eurythermic conifer	*Pinus, Pinus* subgen. *Diploxylon*
ECPI	Eurythermic conifer/Pioneer	*Juniperus*
BS	Boreal summergreen	*Larix*
PI	Pioneer	*Betula*
BEC	Boreal evergreen conifer	*Picea, Pinus* subgen. *Haploxylon*
BCTC	Boreal evergreen/cool-temperate conifer	*Abies*
CTC1	Intermediate temperate conifer	*Cedrus, Taxus*
TSAA	Temperate/boreal summergreen/arctic-alpine	*Alnus, Salix*
TSBS	Temperate/boreal summergreen	*Populus*
TS	Temperate summergreen	*Acer, Fraxinus, Fraxinus excelsior, Quercus (*deciduous*)*
TS1	Cool-temperate summergreen	*Carpinus, Corylus, Fagus, Frangula, Tilia, Ulmus*
TS2	Warm-temperate summergreen	*Castanea, Fraxinus ornus, Juglans, Ostrya, Platanus,* Rhamnaceae*, Vitis*
WTE	Warm-temperate broad-leaved evergreen	*Quercus (*evergreen*)*
WTE1	Cool-temperate broad-leaved evergreen	*Buxus, Hedera, Ilex*
WTE2	Warm-temperate sclerophyll trees/shrub	*Acacia, Arbutus, Cistus, Mercuria,* Myrtaceae*, Olea, Phillyrea, Pistacia, Rhus*
AA	Arctic-alpine dwarf shrub	*Alnus fructicosa, Betula nana, Dryas, Empetrum, Rhododendron, Saxifraga, Vaccinium*
COGS	Cold grass shrub	*Hippophaë, Polygonum*
H	Heath	*Calluna,* Ericaceae
GR	Grass	Poaceae
WAGS	Warm grass shrub	Brassicaceae*, Ceratonia,* Crassulaceae*, Echium, Ephedra fragilis,* Fabaceae*, Galium,* Scrophulariaceae*, Zizyphus*
SF	Steppe forb/shrub	Apiaceae, *Armeria*, *Artemisia*, *Carduus*, Campanulaceae, Caryophyllaceae, *Centaurea*, Cyperaceae, Dipsacaceae, *Filipendula*, *Helianthemum*, *Plantago*, Plumbaginaceae, *Ranunculus*, Rosaceae, *Rosmarinus*, Rubiaceae, *Rumex*, *Sanguisorba*, *Thalictrum*, Urticaceae, *Viburnum*
SFDF	Steppe/desert forb/shrub	Boraginaceae*,* Compositae*,* Compositae *tubuliflore,* Compositae *liguliflore,* Zygophyllaceae
DF	Desert forb/shrub	Chenopodiaceae*, Ephedra, Ephedra distachya*

Table 1.3 (also next page). List of the 88 pollen taxa retained for this work in the EMPD2 including 7634 sites. The taxa highlighted in grey were the ones removed for the 77 taxa version of the EMPD2 tested (see Chapter 1.3.3.3).

Taxa	Code	N (sites)	Range of %	Mean % ± SD	Median %
Trees+shrubs					
Acer	AACER	1064	0,02 - 30,58	0,80 ± 2,29	0,26
Anacardiaceae	ANACA	69	0,02 - 9,77	0,75 ± 1,72	0,22
Pistacia	APISTA	668	0,03 - 51,82	1,78 ± 4,14	0,45
Hedera	AHEDE	342	0,02 - 22,07	0,74 ± 1,81	0,30
Ilex	AILEX	231	0,01 - 51,13	2,57 ± 7,17	0,34
Alnus	BALBU	6362	0,02 - 96,44	6,62 ± 9,98	2,79
Betula	BBETU	5951	0,03 - 93,96	17,01 ± 17,44	10,54
Carpinus/Ostrya	BCARP	2661	0,03 - 70,36	2,99 ± 6,40	0,85
Corylus	BCORY	4159	0,03 - 69,71	2,08 ± 3,50	1,06
Buxus	BBUXU	243	0,03 - 20,45	0,63 ± 1,94	0,26
Caprifoliaceae	CAPRI	997	0,04 - 54,34	0,73 ± 2,37	0,29
Cistus	CCIST	621	0,03 - 40,56	2,00 ± 3,97	0,68
Helianthemum	CHELI	627	0,03 - 13,04	0,60 ± 0,93	0,33
Cornus	CCORN	146	0,02 - 3,31	0,35 ± 0,51	0,21
Cupressaceae	CUPRE	3166	0,01 - 98,12	2,79 ± 6,19	0,91
Hippophae	EHIPP	122	0,00 - 5,77	0,53 ± 0,85	0,29
Ephedra	EEPHE	623	0,01 - 70,90	1,17 ± 5,23	0,27
Ericaceae	ERICA	3991	0,01 - 74,29	3,58 ± 7,56	0,87
Calluna	ECALL	1623	0,01 - 73,27	4,10 ± 9,36	0,63
Ceratonia	FCERA	38	0,08 - 23,94	1,93 ± 4,87	0,35
Quercus deciduous	FQDEC	5057	0,02 - 92,24	7,07 ± 11,83	2,62
Quercus evergreen	FQEVE	1690	0,06 - 97,70	10,90 ± 17,81	3,03
Castanea	FCAST	1857	0,03 - 90,29	2,52 ± 8,07	0,63
Fagus	FFAGU	2777	0,03 - 77,55	5,19 ± 8,85	1,90
Juglans	JJUGL	1812	0,01 - 82,23	0,98 ± 4,28	0,30
Myricaceae	MYRIC	318	0,06 - 62,12	3,25 ± 7,77	0,73
Myrtaceae	MYRTA	258	0,02 - 40,84	1,22 ± 4,27	0,31
Oleaceae	OLEAC	406	0,01 - 68,18	0,77 ± 3,50	0,32
Olea	OOLEA	1986	0,03 - 83,88	4,72 ± 9,59	1,29
Phillyrea	OPHIL	636	0,05 - 62,62	1,59 ± 3,96	0,56
Fraxinus	OFRAX	2920	0,03 - 66,39	1,31 ± 3,25	0,49
Abies	PABIE	2599	0,00 - 74,17	2,51 ± 6,06	0,61
Picea	PPICE	4461	0,01 - 84,22	7,85 ± 11,77	2,81
Cedrus	PCEDR	358	0,04 - 89,40	11,95 ± 23,63	0,81
Larix	PLARI	1604	0,04 - 44,00	2,31 ± 4,08	0,92
Pinus	PPINU	7265	0,04 - 93,24	23,77 ± 20,37	18,25
Platanus	PPLAT	487	0,03 - 55,79	1,63 ± 4,99	0,33
Rhamnaceae	RHAMN	561	0,01 - 85,07	0,76 ± 3,88	0,23
Populus	SPOPU	845	0,02 - 19,44	0,66 ± 1,43	0,28
Salix	SSALI	4714	0,01 - 66,67	1,75 ± 4,46	0,57
Tamarix	TTAMA	100	0,06 - 39,18	2,47 ± 5,70	0,64
Taxus	TTAXU	184	0,00 - 95,34	3,88 ± 14,41	0,29
Daphne	TDAPH	173	0,03 - 11,85	0,92 ± 1,72	0,36
Tilia	TTILI	1731	0,02 - 47,97	0,74 ± 2,31	0,28
Celtis	UCELT	36	0,01 - 16,14	0,68 ± 2,62	0,18
Ulmus	UULMU	2539	0,01 - 54,19	0,79 ± 2,25	0,33
Vitis	VVITI	515	0,01 - 37,59	0,69 ± 2,97	0,24

Taxa	Code	N (sites)	Range of %	Mean % ± SD	Median %
Herbs					
Amaranthaceae	AMARA	5216	0,02 - 91,78	3,29 ± 9,51	0,62
Apiaceae	APIACE	3853	0,02 - 52,79	1,13 ± 2,69	0,42
Liguliflore	ALIGU	3890	0,02 - 61,01	2,34 ± 4,89	0,65
Tubuliflore	ATUBU	5604	0,03 - 63,93	1,97 ± 4,16	0,71
Artemisia	AARTE	5508	0,02 - 99,83	3,33 ± 8,31	0,81
Centaurea	ACENTA	1131	0,01 - 17,21	0,64 ± 1,24	0,29
Boraginaceae	BORAG	778	0,00 - 24,53	0,88 ± 1,87	0,36
Brassicaceae	BRASS	3619	0,03 - 56,25	1,04 ± 2,09	0,51
Campanulaceae	CAMPA	772	0,00 - 16,17	0,53 ± 1,23	0,26
Caryophyllaceae	CARYO	3559	0,01 - 43,28	0,92 ± 2,11	0,41
Convolvulaceae	CONVO	239	0,01 - 30,17	0,58 ± 2,23	0,24
Crassulaceae	CRASS	414	0,03 - 13,33	0,63 ± 1,32	0,30
Cyperaceae	CYPER	5801	0,01 - 82,38	5,12 ± 9,26	1,45
Dipsacaceae	DIPSA	469	0,01 - 13,64	0,46 ± 0,82	0,26
Euphorbiaceae	EUPHO	634	0,00 - 78,38	0,87 ± 3,58	0,28
Fabaceae	FABAC	3147	0,01 - 62,82	1,28 ± 3,13	0,47
Gentianaceae	GENTI	322	0,01 - 4,48	0,44 ± 0,57	0,26
Geraniaceae	GERAN	488	0,03 - 18,67	0,49 ± 1,31	0,24
Lamiaceae	LAMIA	1830	0,01 - 40,82	0,94 ± 2,00	0,37
Liliaceae	LILIA	1046	0,00 - 19,10	0,63 ± 1,20	0,34
Asphodelus	LASPH	228	0,03 - 15,48	0,88 ± 1,41	0,47
Onagraceae	ONAGR	444	0,00 - 75,77	0,87 ± 4,13	0,26
Papaveraceae	PAPAV	383	0,00 - 17,67	0,91 ± 1,72	0,29
Plantaginaceae	PLANT	4498	0,03 - 66,69	1,88 ± 3,98	0,80
Plumbaginaceae	PLUMB	226	0,03 - 11,89	0,92 ± 1,47	0,35
Poaceae	POACE	7347	0,04 - 92,86	12,74 ± 13,39	8,04
Polemoniaceae	POLEM	160	0,06 - 75,98	5,76 ± 12,03	0,67
Rumex/Oxyria	PRUME	4331	0,01 - 63,01	1,50 ± 3,77	0,67
Polygonum	PPOLY	1230	0,01 - 43,41	0,79 ± 2,19	0,30
Primulaceae	PRIMU	573	0,01 - 41,02	0,59 ± 1,85	0,25
Ranunculaceae	RANUN	4147	0,02 - 56,81	1,20 ± 2,57	0,55
Thalictrum	RTHAL	1224	0,01 - 21,88	0,70 ± 1,69	0,29
Rosaceae	ROSAC	4767	0,01 - 35,67	1,31 ± 2,43	0,60
Sanguisorba	RSANG	809	0,02 - 46,02	1,03 ± 3,71	0,29
Rubiaceae	RUBIA	2089	0,00 - 36,07	0,80 ± 2,13	0,29
Saxifragaceae	SAXIF	823	0,02 - 21,58	0,71 ± 1,56	0,32
Scrophulariaceae	SCROP	2284	0,01 - 13,93	0,67 ± 1,06	0,34
Solanaceae	SOLAN	243	0,01 - 33,04	0,62 ± 2,22	0,25
Cannabaceae/Urticace	CANURT	2795	0,02 - 88,91	1,29 ± 3,97	0,55
Valerianaceae	VALER	468	0,02 - 18,09	0,74 ± 1,52	0,30
Viola	VVIOL	168	0,03 - 9,45	0,49 ± 0,89	0,26

Table 1.4 Accuracy of reconstructions (RMSEP and R^2) for the 88 and 77 taxa databases (5 analogues). The best results are highlighted in grey. Climatic variables: MTCO (mean-temperature of the coldest month), MTWA (mean-temperature of the warmest month), Pdjf (winter precipitation), Pjja (summer precipitation), Pann (annual precipitation), Seasonality (MTWA – MTCO).

Climatic parameters	RMSEP		R^2	
	88 taxa	77 taxa	88 taxa	77 taxa
MTCO	3,41	3,38	0,91	0,90
MTWA	1,95	2,10	0,83	0,83
Seasonality	3,44	3,37	0,88	0,87
Pdjf	68,76	69,85	0,76	0,76
Pjja	46,34	53,16	0,79	0,79
Pann	199,79	205,90	0,76	0,76

Table 1.5 Accuracy of reconstructions (root mean square error of prediction (RMSEP) and coefficient of correlation (R^2)) for different numbers of analogues (from 5 to 10) with the 88 taxa database. Best results are highlighted in grey. Climatic variables: MTCO (mean-temperature of the coldest month), MTWA (mean-temperature of the warmest month), Pdjf (winter precipitation), Pjja (summer precipitation), Pann (annual precipitation), Seasonality (MTWA – MTCO).

	Number of analogues	Climatic parameters					
		MTCO (°C)	MTWA (°C)	Seasonality (°C)	Pdjf (mm)	Pjja (mm)	Pann (mm)
RMSEP	**5**	3.414497	1.953582	3.440109	68.757042	46.342813	199.787684
	6	3.425351	1.954279	3.455829	68.721954	46.270163	199.748578
	7	3.451749	1.949297	3.485838	68.469971	46.303684	199.329668
	8	3.494682	1.954600	3.529512	69.965425	46.837990	202.785832
	9	3.501833	1.971908	3.527256	70.824726	47.178894	204.838904
	10	3.506025	1.991342	3.537390	71.551070	47.082822	205.982384
		MTCO	MTWA	Seasonality	Pdjf	Pjja	Pann
R^2	**5**	0.9101497	0.8292628	0.8812178	0.7556163	0.7856114	0.7566075
	6	0.9097372	0.8285066	0.8807862	0.7521746	0.7833981	0.7545963
	7	0.9078079	0.8280451	0.8781339	0.7505066	0.7844397	0.7546756
	8	0.9063351	0.8278121	0.8760379	0.7466206	0.7823130	0.7523563
	9	0.9049654	0.8254401	0.8747762	0.7428946	0.7817327	0.7488131
	10	0.9032987	0.8221383	0.8726062	0.7400858	0.7774092	0.7452280

Table 1.6 Taxonomical diversity of most fossil records included in this study. N: number. *Most sequences cover partly or entirely MIS 3, but some of them also cover the previous and/or subsequent isotope stage (MIS 2 and 4). [1] only covers MIS 2.

Sites	Number of taxa initially identified*	Number of taxa kept for MAT		Number of taxa kept for PFT	
		N	**%**	***N***	**%**
MD95-2039	95	88	92,6	69	72,6
SU81-18[1]	57	53	93,0	50	87,7
MD95-2042	131	118	90,1	98	74,8
ODP 976	132	111	84,1	85	64,4
MD95-2043	96	90	93,8	77	80,2
Lac du Bouchet	63	62	98,4	56	88,9
Lagaccione	80	75	93,8	66	82,5
Stracciacappa	56	53	94,6	49	87,5
Valle du Castiglione	65	61	93,8	57	87,7
Lago Grande di Monticchio	138	126	91,3	100	72,5
Ioannina	92	85	92,4	71	77,2
Xinias	178	161	90,4	132	74,2
Megali Limni	75	70	93,3	56	74,7

Table 1.7 Accuracy of reconstructions as indicated from the root mean square error of prediction (RMSEP) and the coefficient of correlation (R^2) for the 88 and 87 (Pinus excluded) taxa databases (5 analogues). Climatic variables: MTCO (mean-temperature of the coldest month), MTWA (mean-temperature of the warmest month), Pdjf (winter precipitation), Pjja (summer precipitation), Pann (annual precipitation), Seasonality (MTWA – MTCO).

Climatic parameters	RMSEP		R^2	
	88 taxa	87 taxa (without *Pinus*)	88 taxa	87 taxa (without *Pinus*)
MTCO	3,41	3,52	0,91	0,91
MTWA	1,95	1,94	0,83	0,83
Seasonality	3,44	3,51	0,88	0,87
Pdjf	68,76	71,65	0,76	0,74
Pjja	46,34	47,34	0,79	0,79
Pann	199,79	204,84	0,76	0,75

Figure 1.1 Location of the fossil pollen records (red dots) studied in this work and NGRIP (black dot); North Greenland Ice Core Project (NGRIP, 2004)). The main European biomes are defined from Olson et al. (2001). EGC: East Greenland Current; IC: Irminger Current; NAD: North Atlantic Drift.

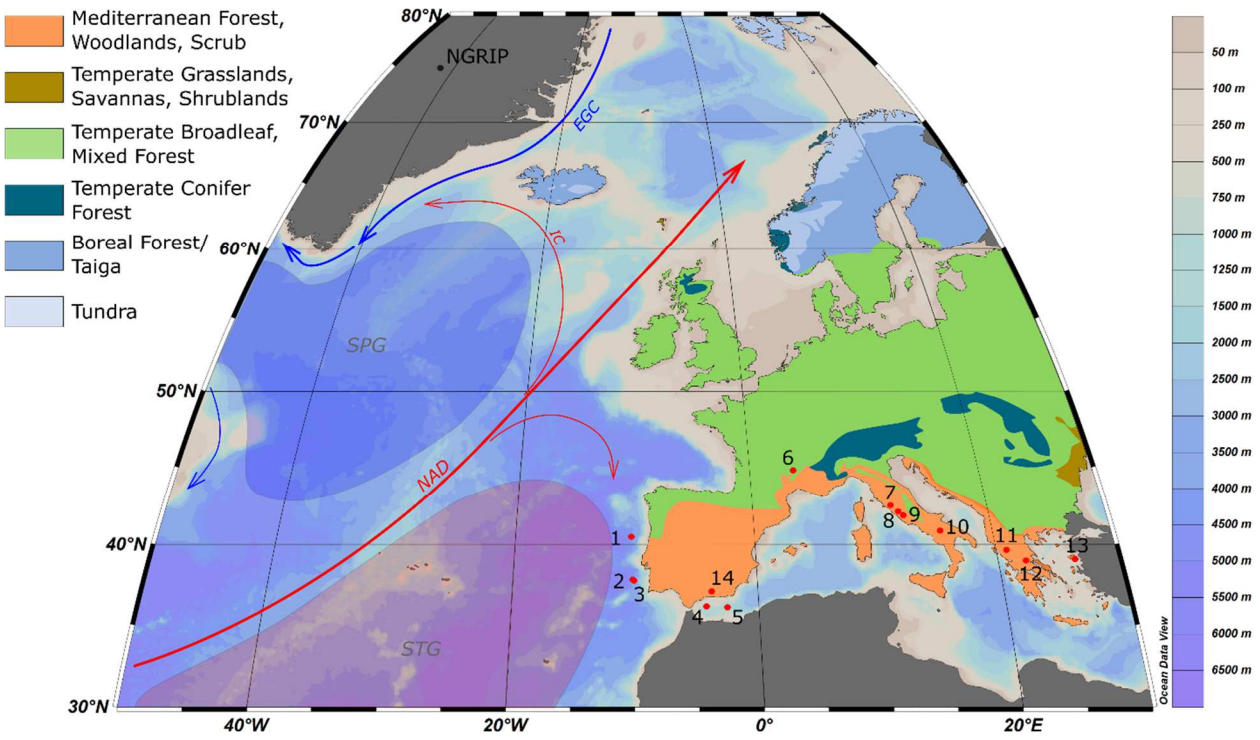

Figure 1.2 Biomes and locations of the modern pollen samples included in the final version of the EMPD2 used in this work (modified from Davis et al. (2020)).

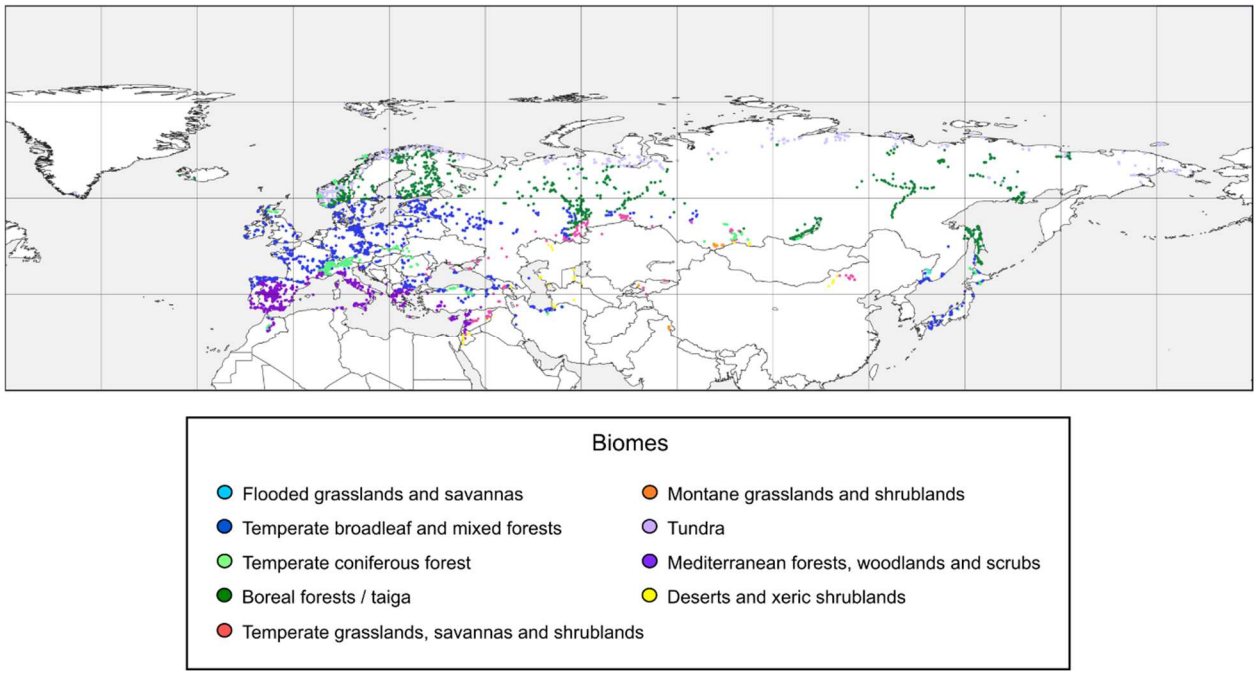

Figure 1.3 Modern pollen samples defined by their biomes in the climatic space (modified from Davis et al. (2020)).

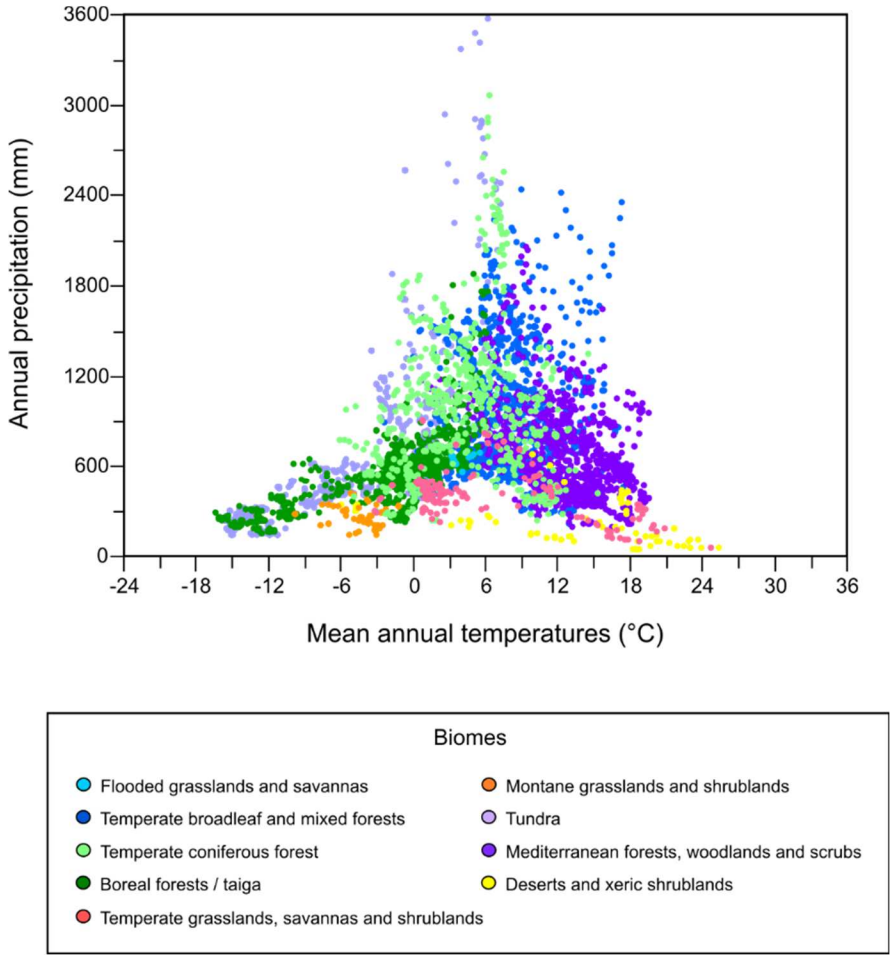

Figure 1.4 Cross - validation results of the observed against estimated climatic parameters. The blue and red open circles correspond to the calibration and verification data sets, respectively. The Root Mean Square Error of Prediction (RMSEP) and the coefficient of correlation (R^2) indicate the degree of accuracy of estimates. MTCO: mean-temperature of the coldest month; MTWA: mean-temperature of the warmest month; Seasonality = MTWA – MTCO; Pann: annual precipitation; Pdjf: winter precipitation; Pjja: summer precipitation.

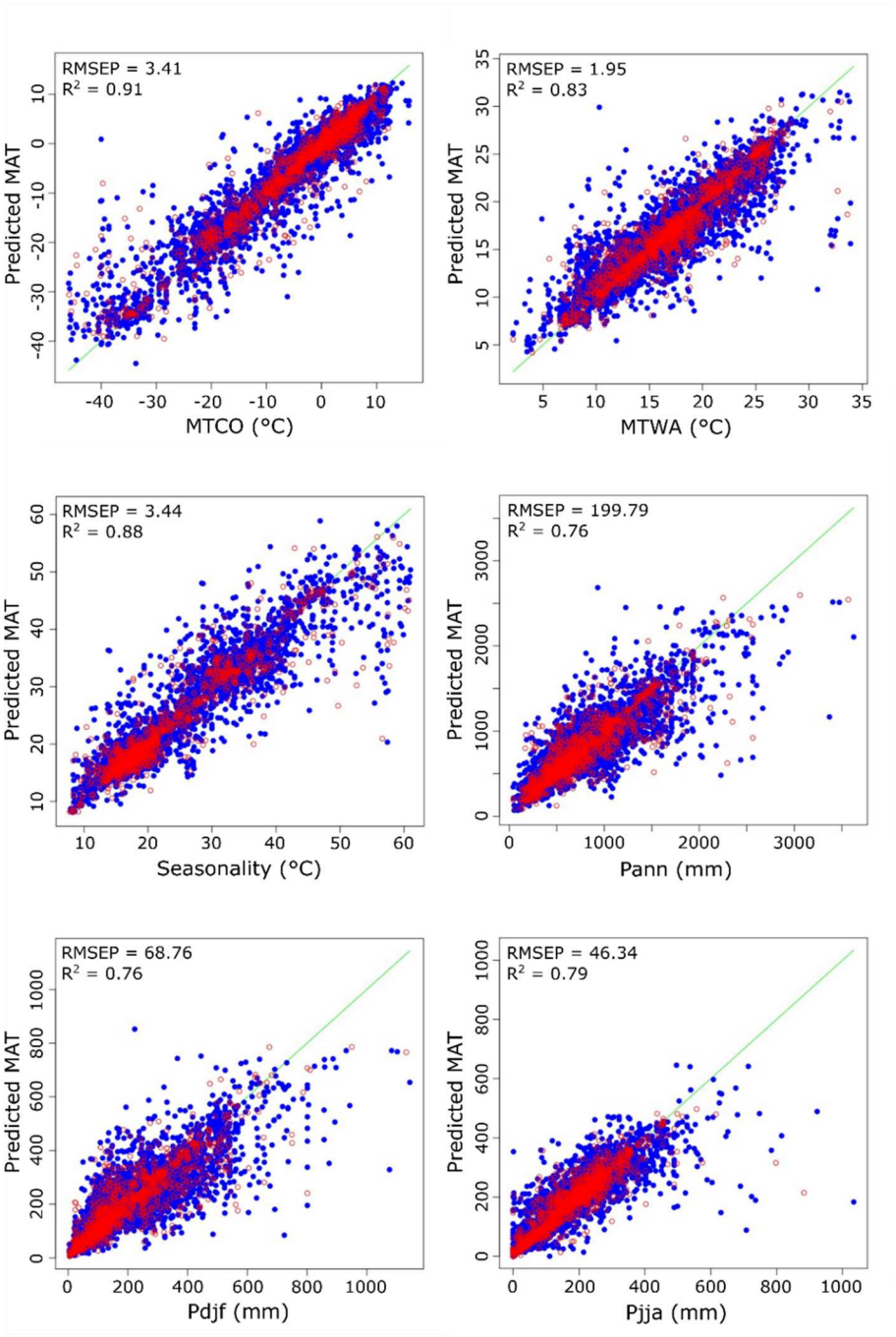

Figure 1.5 Comparison between NGRIP oxygen isotopic record (North Greenland Ice Core Project members, 2004) and records related to sea-surface conditions, vegetation and climate (reconstructions with (A) and (B) without *Pinus*) at site 3 (core MD95-2042), off southern Portugal (Figure 1.1; Table 1.1 and references therein): (from left to right) $\delta^{18}O$ of *Globigerina bulloides* (Gb) (Shackleton et al., 2000) used as a proxy of sea-surface temperature (Malevich et al., 2019), the warm sea-surface phases are indicated by red bars; RDA axis-1 scores (with number of samples (n) for each side; MTCO (blue line) and MTWA (red line); seasonality (difference between MTWA and MTCO); summer (red line), winter (blue line) and annual precipitation (black line); SCD of the 1st (green circles) and 5th (red circles) analogues for each sample and SCD threshold (red line) and half of this threshold (black dotted line).

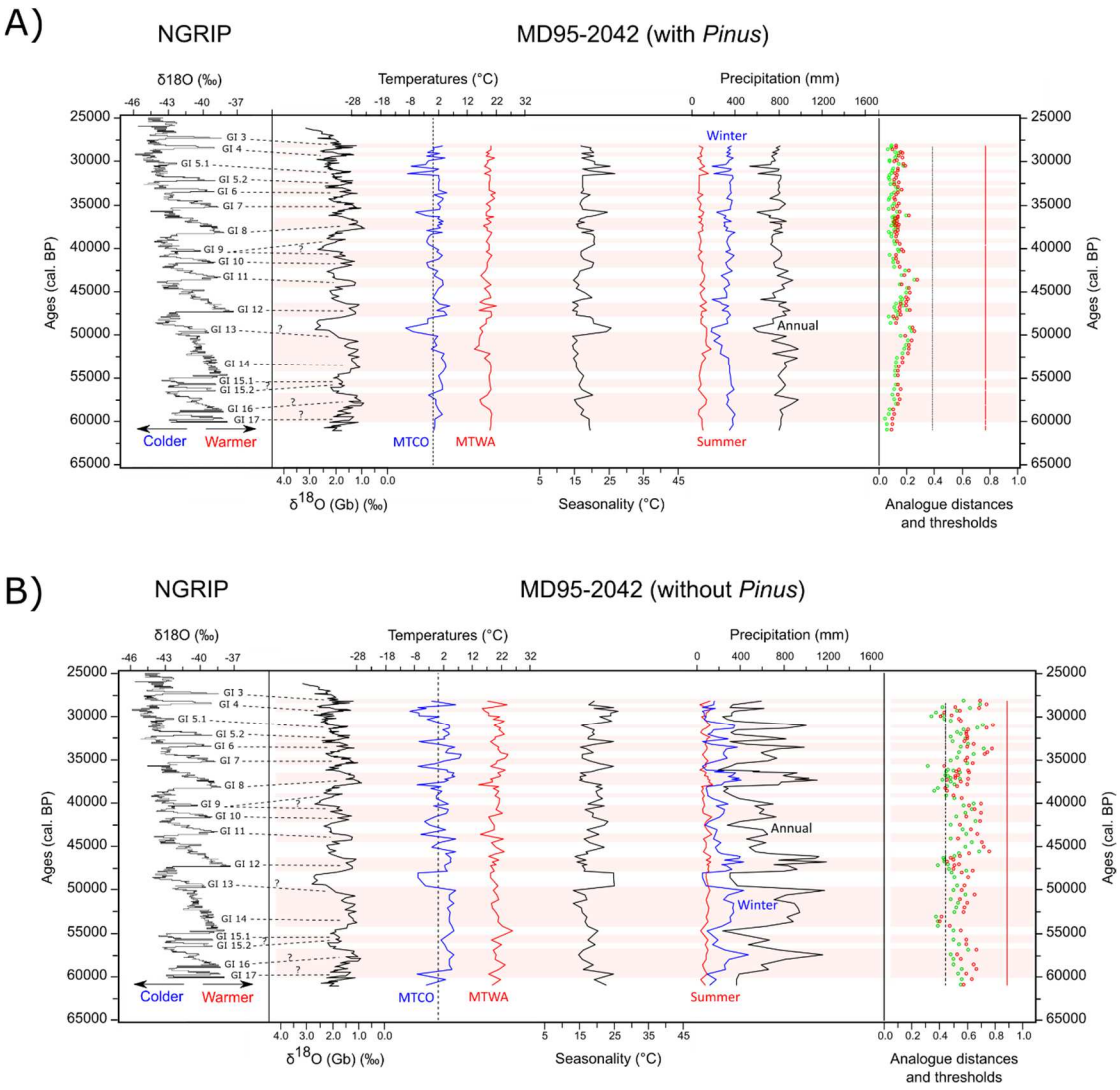

Figure 1.6 CCA ordination diagram of pollen taxa (green (trees+shrubs) and orange (herbs) dots) (see Table 1.3 for codes) vs. environmental variables (blue arrows). Analyses were performed on logarithmic (ln) values of the relative frequency of pollen taxa (%) using the CANOCO software of (Smilauer and Leps, 2014). MTCO: mean-temperature of the coldest month; MTWA: mean-temperature of the warmest month; Seasonality = MTWA – MTCO; Pann: annual precipitation; Pdjf: winter precipitation; Pja: summer precipitation.

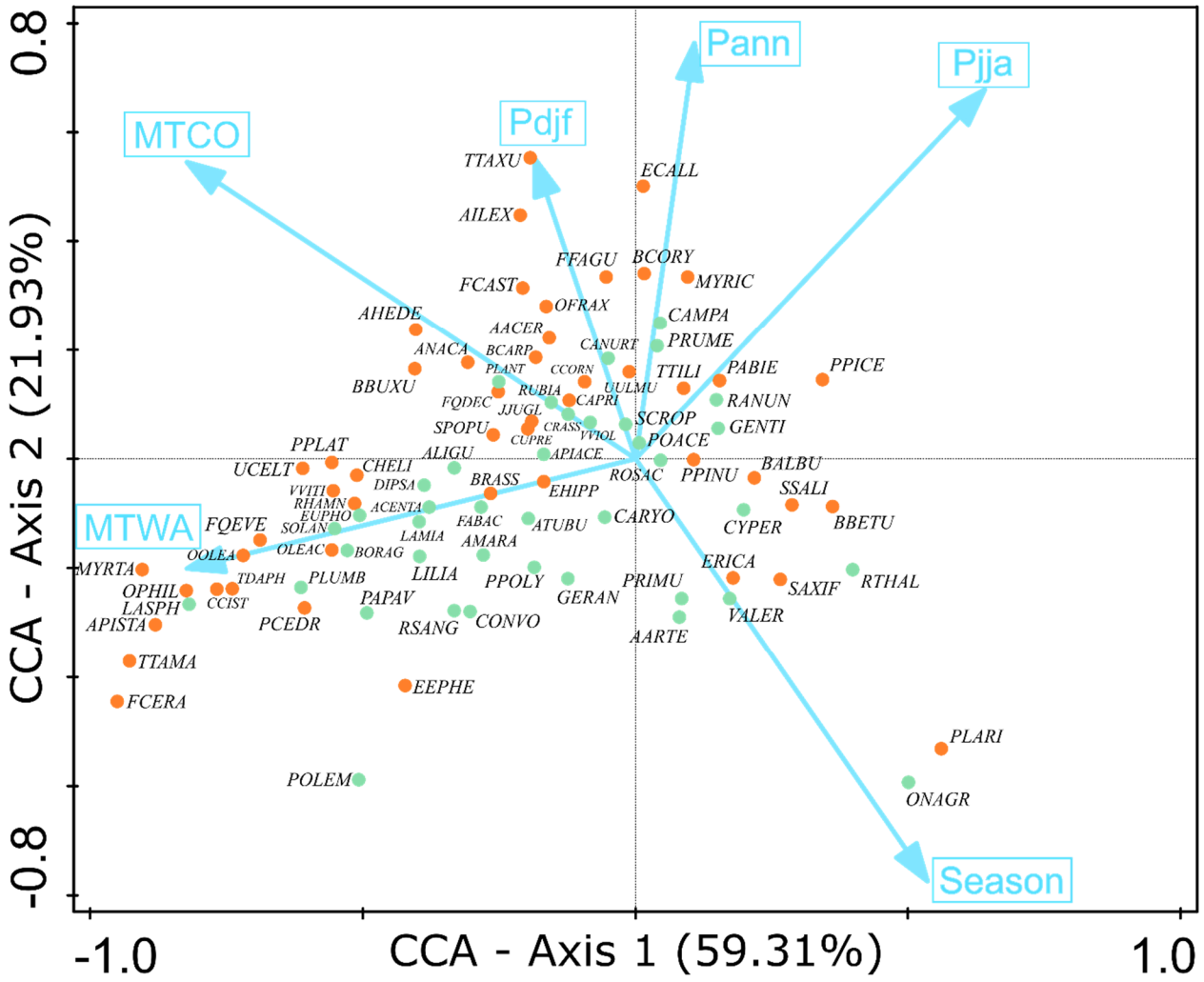

CHAPITRE 2

DECOUPLED WINTER AND SUMMER CLIMATE CHANGES IN SOUTHERN EUROPE DURING DANSGAARD-OESCHGER CYCLES

Jena Zumaque*[a], Anne de Vernal[a], Bianca Fréchette[a], Joël Guiot[b], Maria F. Sánchez-Goñi[c,d], Chéïma Barhoumi[e], Odile Peyron[e], Matthew Peros[f], Ariane Burke[g], Jon Camuera[h], Gonzalo Jiménez-Moreno[i], María J. Ramos-Román[j]

[a] *GEOTOP - Centre de recherche en géochimie et géodynamique, Université du Québec à Montréal, Canada*
[b] *Aix Marseille Univ, CNRS, IRD, INRA, CEREGE, Aix-en-Provence, France*
[c] *École Pratique des Hautes Etudes (EPHE, PSL University), France*
[d] *University of Bordeaux, Environnements et Paléoenvironnements Océaniques et Continentaux, France*
[e] *Institut des Sciences de l'Évolution de Montpellier, Université de Montpellier, France*
[f] *Department of Environmental and Geography, Bishop's University, Canada*
[g] *Département d'Anthropologie, Université de Montréal, Canada*
[h] *Unit of Botany, Faculty of Pharmacy, Complutense University of Madrid, Spain*
[i] *Department of Stratigraphy and Paleontology, University of Granada, Spain*
[j] *Faculty of Education, Mid-Atlantic University, Madrid, Spain*
*Correspondence: zumaquej@gmail.com

Article accepté sous réserve de modifications dans la revue *Quaternary Science Reviews*.

Résumé en français

Le stade isotopique marin 3 (MIS 3 – *Marine Isotope Stage* 3) (~60-30 ka) est caractérisé par des oscillations climatiques millénaires de large amplitude, aussi connues sous le nom de cycles de Dansgaard-Oeschger (DO), et qui sont marquées par l'alternance de phases chaudes ou interstadiaires (GIs – *Greenland interstadials*) et froides ou stadiaires (GSs – *Greenland stadials*). Ici, nous explorons la nature saisonnière du signal climatique des DO dans le sud de l'Europe à l'aide de 12 enregistrements polliniques qui nous permettent de reconstituer les types de végétations et des paramètres climatiques clés tels que les températures et précipitations saisonnières. Nos résultats montrent une réponse claire de végétation arborée au cours des GIs et de végétation non-arborée au cours des GSs. Les résultats indiquent également que les changements de végétation sont principalement liés à des variations de températures et précipitations hivernales et suggèrent que des conditions estivales relativement chaudes et stables ont caractérisé l'ensemble du MIS 3. De ce fait, nous suggérons que le signal des DO dans le sud de l'Europe représente principalement des anomalies de la saison hivernale. Nous émettons également l'hypothèse que des oscillations atmosphériques hivernales semblables aux modes de variabilité de l'actuelle Oscillation Nord Atlantique furent déterminants dans la modulation de la distribution des eaux de fonte dans l'océan Atlantique Nord au travers de l'extension/contraction de la Gyre Subpolaire, impactant ainsi le couvert de glace de mer hivernal, la température et l'humidité disponible au-dessus du sud de l'Europe.

Abstract

The marine isotope stage 3 (MIS 3) (~60-30 ka) exhibits large amplitude millennial climatic oscillations, also named Dansgaard-Oeschger (DO) cycles, which are marked by alternation of warm (GIs – Greenland interstadials) and cold phases (GSs – Greenland stadials). Here, we explore the seasonal nature of the DO cycle climate signal in southern Europe using 12 pollen records that allow us to reconstruct the vegetation types and key climatic parameters such as seasonal temperatures and precipitation. Our results show a clear response of arboreal vegetation during GIs and non-arboreal vegetation during GSs. The results also indicate that vegetation changes were mainly driven by winter precipitation and temperatures and suggest that relatively stable and warm summer conditions prevailed throughout MIS 3. On these bases, we suggest that the DO signal in southern Europe represents winter-season anomalies. We further hypothesize that winter atmospheric oscillations resembling the current North Atlantic Oscillation (NAO) modes of variability were instrumental in modulating the distribution of freshwaters in the North Atlantic Ocean through extension/contraction of the subpolar gyre (SPG), impacting the extent of winter sea-ice cover, temperature and moisture availability over southern Europe.

Keywords

Millennial-scale climate variability, Marine Isotope Stage 3, Seasonality, Modern Analogue Technique, Vegetation

2.1 Introduction

The marine isotope stage 3 (MIS 3) (~60-30 ka) was characterized by large amplitude centennial to millennial-scale climatic variability. These alternating warm (Greenland Interstadials – GIs) and cold (Greenland Stadials – GSs) phases, referred to as Dansgaard-Oeschger (DO) events, were first detected in the oxygen isotopic records of the Greenland Ice cores (Dansgaard et al., 1993) and have since been reported worldwide. They appear particularly pronounced in the North Atlantic region where they are evidenced in sea-surface temperature (SST; Wary et al., 2017; Datema et al., 2019) and deep-water production indicators (Gottschalk et al., 2015), but also in speleothems (Genty et al., 2010; Budsky et al., 2019) and other terrestrial records of the adjacent European continent (Moreno et al., 2014; Rodrigo-Gámiz et al., 2022). Some of the coldest GSs also coincide with the episodes of abrupt ice-sheet meltwater discharge events in the North Atlantic known as Heinrich events (Hemming, 2004) and designated as Heinrich Stadials (HS; Sanchez-Goñi and Harrison, 2010).

While millennial pacing is generally recognized as a common feature of these climatic variations, their pattern, amplitude, shape and timing (e.g., Rasmussen et al., 2016; Wary et al., 2017; Bauska et al., 2021; Denton et al., 2022) may differ from one site to another. The trigger(s) and mechanism(s) of these large-amplitude climate changes remain elusive despite three decades of research on the subject.

One parameter probably underestimated or overlooked in DO cycle studies is the seasonal contrast from winter to summer (Denton et al., 2005; Carré and Cheddadi, 2017), although some authors highlighted more pronounced winter than summer cooling during GSs (e.g., Sanchez-Goñi et al., 2000). Investigation of mismatches between mean annual temperature oscillations from Greenland ice cores and snowline changes in East Greenland have led some to conclude that DO cycles were mainly a winter phenomenon and that mild summer temperatures might have occurred even during GSs (see Denton et al., 2005). The pronounced winter signature of DO cycles has since been illustrated in several records from the North Atlantic region and adjacent lands (e.g., Flückiger et al., 2008; Datema et al., 2019) where it has been associated with variations in sea-ice cover extent in the northern North Atlantic (Denton et al., 2005, 2022; Flückiger et al., 2008). However, evidence of the hypothetical prevalence of relatively high summer atmospheric temperatures throughout MIS 3, including GSs (Denton et al., 2005, 2022), were lacking. Denton et al. (Denton et al., 2022) suggested that summer behaviour might have been muted in many paleoclimatic reconstructions by stronger winter signals during DO events, emphasizing the need to differentiate summer from winter effects for a better understanding of DO cycles. In a recent study, a continental record from Germany has shown temperatures of the warm seasons with conditions being close to the modern ones and varying very subtly from GSs to GIs (Zander et al., 2024). In comparison, mean annual temperatures inferred from the same sequence indicated larger drops of temperatures during GSs, suggesting that DO changes might have been primarily driven by varying winter conditions but that summer may have been more stable (Denton et al., 2022; Zander et al., 2024). Still, to the best of our knowledge, the seasonal contrast from winter to summer has not been fully addressed nor quantified by any continental records from around the North Atlantic Region.

Very few proxies allow for the reconstruction of seasonality, but pollen, which is related to vegetation is one of them. The close link between past climate and vegetation has been thoroughly demonstrated (Sanchez-Goñi et al., 2000, 2021), especially for the eastern North Atlantic sector and the European continent where vegetation appears highly sensitive to DO cycles (e.g., Sanchez-Goñi et al., 2000, 2008, 2009; Roucoux et al., 2005; Fletcher et al., 2010; Rodrigo-Gámiz et al., 2022). This link has been used

as a basis for the quantification of past climate variables using numerical methods (Guiot, 1990; Peyron et al., 1998; Sanchez-Goñi et al., 2021).

Here, we aim to address the issue of environmental variability and seasonality changes in climate over southern Europe during MIS 3 by analyzing vegetation types and seasonal climatic parameters reconstructed from pollen assemblages. We selected 12 published pollen records from the ACER **(Abrupt Climate Changes and Environmental Responses)** database (Sánchez Goñi et al., 2017) that encompass at least part of MIS 3 and have sufficient temporal resolution to resolve centennial to millennial-scale variations (Fig. 2.1; Table 2.1 and references therein). These records comprise data from both lake and marine core sediments. In terrestrial pollen records, uncertainty in the age model often prevents an independent age-based identification of GIs and GSs. Hence, the advantage of including marine core data in this compilation lies in the fact that they allow for direct comparisons between pollen records and proxy indicators of the ocean changes and stratigraphy (Sánchez Goñi et al., 2008, 2009) that can be directly correlated to Greenland GI and GS succession (Austin and Hibbert, 2012).

2.2 Material

2.2.1 Data compilation and selection criteria

The present compilation includes 4 marine and 8 terrestrial pollen records from Southern Europe (Table 2.1; Fig. 2.1) that encompass partly or entirely MIS 3 and have sufficient temporal resolution (Table 2.S1) to record centennial to millennial-scale variations. These pollen records are sourced from the ACER (Abrupt Climate Changes and Environmental Responses) database (Sánchez Goñi et al., 2017; Table 2.1).

2.2.2 Chronologies

A reliable chronology was a prerequisite for the inclusion of pollen records in the compilation. Marine cores from open ocean settings are usually well-dated and permit direct land-sea correlations by comparing pollen and proxy indicators of the ocean environment in single cores (Sanchez-Goñi et al., 2002, 2008, 2009; Roucoux et al., 2005). Furthermore, providing adequate temporal resolution, marine cores from the North Atlantic sector can be correlated to the reference Greenland GI and GS succession (Austin and Hibbert, 2012). Conversely, for most continental sites, the chronology is not robust enough to allow for an age-based identification of GIs/GSs. Indeed, age models for the terrestrial sequences presented here, except for Lago Grande di Monticchio (Site 9, Fig. 2.1; Table 2.1 and references therein), are mostly

based on radiocarbon dating of organic material (see Sanchez-Goñi et al., 2017 for more details). They thus present some inherent limitations, especially for dating of the MIS 3, such as no radiocarbon dates prior to 45 ka, large ^{14}C calibration uncertainties, potential contamination and scarcity of datable organic material (Fletcher et al., 2010). Nevertheless, these data provide precious information on the linkages between vegetation and climate. Hence, we included some poorly dated but long and continuous terrestrial records in this work, in addition to well-dated records (especially those from marine sites), to investigate land-sea linkages.

For every site except the Lago Grandi di Monticchio, we used the updated chronology proposed in the ACER database (Figs. 2.S1a-2.S12a; for more details, see Sanchez-Goñi et al., 2017). For Lago Grande di Monticchio (Fig. 2.1; Table 2.1 and reference therein), we used the initial chronology based on annual lamination ("varve") counts and sedimentological features in the non-varved intervals (Zolitschka and Negendank, 1996) as was done by the ACER group (Sanchez-Goñi et al., 2017). However, although the chronology of the entire Monticchio sequence was overall corroborated by many dated tephra layers with a mean deviation of ~ 5% (Wulf et al., 2004), some sections appear problematic as demonstrated by (Genty et al., 2010). Hence, we must remain cautious regarding the interpretation of the timing of vegetation and climatic shifts from this sequence.

Marine cores from the North Atlantic sector contain pollen grains that can be linked directly to the millennial-scale variability recorded in sea-subsurface temperatures, which vary concomitantly with the oxygen isotope data of the Greenland Ice cores (Austin and Hibbert, 2012). Hence, to compare the marine and continental signals from 3 of the marine cores (cf. Table 2.1), we applied the exact same age model to all these records and thus recalculated the age for each of these 3 marine cores using CLAM (Blaauw, 2010), implemented in R (R version 3.3.1) (R Development Core Team, 2016) based on the dates retained for the updated chronologies of the ACER database (Sanchez-Goñi et al., 2017). To stay consistent with the harmonized chronological work of Sanchez-Goñi et al. (2017), we used the Marine13 calibration curves (Reimer et al., 2013).

2.3 Pollen data and related vegetation and climate signal

2.3.1 Raw pollen counts

Raw counts, and pollen percentages in the case of the Lac du Bouchet and Megali Limni sequences (Sanchez-Goñi et al., 2017), were kept as such except for the aquatic taxa that were removed from the total pollen counts (relative abundances were recalculated after aquatic taxa removal).

2.3.2 Vegetation reconstruction: Plant Functional Types (PFTs)

To visualize past vegetation changes through time, we grouped the pollen taxa into Plant Functional Types (PFTs) based on the concept developed by Prentice et al. (1992). PFTs are broad classes of plants defined by certain vegetation criteria (e.g., stature, leaf form and phenology) and climatic thresholds. Grouping the taxa into those categories allows us to reduce the number of variables and facilitate the comparison between sites and periods, especially due to data derived from several different projects and investigators, and because the taxonomy can thus vary from one site to another.

The fossil records were harmonized in 94 taxa to characterize 15 arboreal and 8 shrub/herbaceous PFTs (Table 2.2) with each taxon being assigned to a PFT according to the known biology of the species it includes (Peyron et al., 1998; Prentice et al., 1996). Here, we followed the concept developed by Peyron et al. (1998) which allows each pollen taxon to belong to only one PFT. Virtual PFTs (ECPI, TSAA, TSBS; Table 2.2), which are a combination of the potential PFTs that a taxon could belong to, were created to handle ambiguous taxa and were initially reassigned afterwards depending on the biome identified for the pollen sample (Peyron et al., 1998). In this work, there was no reassignment and the virtual PFTs were kept as such since we did not intend to undertake interpretation in terms of biomes. After several trials, we found that reassignments generated biases when applying a redundancy analysis (RDA) to the PFT and climatic data since they created clusters (one for each biome identified) in the RDA graph, thus generating jumps from one mode to another in Axis-1 scores instead of showing the progressive nature of vegetation variations. For each pollen sample, we simply calculated the abundance of each pollen taxon relative to the sum of all the 94 pollen taxa included in this work (Table 2.2) and took the square root to amplify the importance of the rare versus the more abundant taxa. We then summed the relative abundances of the taxon combinations associated with each PFT (Table 2.2) and calculated percentages from the scores obtained for each PFT. Unlike what was done in refs. (Peyron et al., 1998; Prentice et al., 1996), we did not remove taxa with low abundances (< 0.5%).

2.3.3 Climate reconstructions

Various methods have been developed over time to reconstruct paleoclimates from pollen data (Chevalier et al., 2020). They all have advantages and limitations (cf. Birks et al., 2010; Chevalier et al., 2020). In this study, we do not intend to compare the methods but choose to use the Modern Analogue Technique (MAT) (Overpeck et al., 1985; Guiot, 1990) because it is among the most efficient methods for reconstructing high climate variability. Since MAT does not require an explicit model to define the pollen-climate relationship, it allows a much larger climatic and environmental range of the modern dataset compared to other methods and thus provides a wide range of different analogues for high variable climate such as the one expected during MIS 3 (cf. Chevalier et al., 2020).

MAT is based on the principle that the ecological affinities of the different species have not changed through time (Jackson and Overpeck, 2000). MAT principally compares a fossil pollen assemblage to all modern pollen assemblages within a given geographic area for which the climate is known. The similarity assessment between fossil (*i*) and modern (*j*) pollen assemblages is based on the squared chord distance (SCD) (d^2) dissimilarity metric (Overpeck et al., 1985) which can be computed using the following formula:

$$d_{ij}^{2} = \sum_{k=1}^{m} (\sqrt{P_{ik}} - \sqrt{P_{jk}})^2 \qquad (1)$$

Where *m* is the number of taxa and *P* is the relative abundances (percentage value) for each taxon (k = 1−m). The square-root transformation reduces the weight of ubiquitous taxa that are usually very abundant and increases the weight of underrepresented taxa. The equation (1) also shows the dependence between SCD and the number of pollen taxa.

The SCD values vary between 0 and 2. Low values indicate a high degree of similarity between two samples, whereas high values indicate large dissimilarity. The modern samples presenting the lowest SCD are thus selected as the best analogues, and past climatic conditions are calculated from their average associated climatic parameters, weighted inversely to their distance. An SCD threshold beyond which any analogue is rejected is calculated based on a Monte Carlo method. Distance vectors are calculated between one modern spectrum randomly selected and each of the remaining modern spectra. The operation is repeated 1000 times and the final threshold is defined as the first quartile for these 1000

values (Guiot and de Vernal., 2007). In this work, we followed de Vernal et al. (2005) who defined a reliability index with three categories: 1) Poor or no analogue situation when the SCD of the closest analogue is higher than the SCD threshold, 2) Acceptable analogue situation when the SCD is between half of the threshold value and the threshold, and 3) Good analogue situation when the SCD is between 0 and half of the threshold value. The MAT theory, its relevance and limitations, notably regarding spatial autocorrelation, are further discussed in Supplementary Information (Detailed methodology, Chapter 2.8.1).

2.3.3.1 Modern pollen database

The paleoclimate reconstructions were made with the "bioindic" package (ftp://ftp.cerege.fr/R/Package_bioindic/), built on the R-platform (http://cran.r-project.org/), using a modern calibration dataset taken from the latest Eurasian Modern Pollen Database (version 2) (EMPD2; Chevalier et al., 2019; Davis et al., 2020). The EMPD2 includes more than 8000 modern pollen samples from the Palearctic realm and covers a total of nine biomes (cf. Davis et al., 2020). It thus comprises a large number of potential modern analogues from many different climates and vegetation types, which is particularly critical when considering the objective of climatic reconstructions for glacial times (Magyari et al., 2014; Davis et al., 2022). The climatic data for each modern sample were assigned according to the nearest grid point of the WorldClim2 grid (within ~1 km^2) and reflect the period between 1970 and 2000 (Fick and Hijmans, 2017). They include mean monthly, seasonal, and annual temperatures and precipitation (Davis et al., 2020). We added the mean temperature of the warmest (MTWA) and the coldest (MTCO) months, and the seasonality defined as the difference between MTWA and MTCO. At 77% of the sites, MTWA corresponds to July temperature, while at 83% of the sites, MTCO represents January temperature. At other sites, MTCO is mostly February, and MTWA is mostly August. MTWA, MTCO, seasonality, winter (Pdjf) and summer (Pjja) precipitation, along with annual precipitation (Pann), were the climatic variables we retained for this work.

Since the pollen analyses of modern samples were done in different laboratories by different analysts using different taxonomic levels (e.g., family, genus, species), the whole database includes a very high number of pollen taxa (840). We downgraded the taxa to genera or family levels to homogenize the database and obtained a total of 184 taxa (not shown). We further reduced this number to the most common terrestrial taxon types based mostly on the number of occurrences (the taxon must be present in more than 100 modern assemblages). Some exceptions were made for three taxa with occurrences

below 100 that are often identified in European pollen fossil records (Table 2.S2). The final database contains 88 taxa (Table 2.S2). We then removed all the samples with a pollen sum (excluding *Pinus*) inferior to 100 grains, yielding a total of 7634 remaining modern pollen samples. The same criterion was applied to the fossil records for which any sample with a pollen sum (excluding *Pinus*) inferior to 100 was removed. A list of the occurrence and relative abundance of the 88 taxa in the database is shown in Table 2.S2.

Model performances are based mostly on two indicators that are calculated from different cross-validation tests, with a subset of the modern dataset used for calibration and another for prediction (see also Chevalier et al., 2020). One indicator is the coefficient of correlation (R^2) between estimated and observed climatic values. The other indicator is the root mean square error of prediction (RMSEP), which also corresponds to the standard deviation of the difference between observed and reconstructed values of a verification subset of data (Guiot and de Vernal., 2007).

To assess the number of analogues to use for the most accurate reconstructions, cross-validation tests were run with 5 to 10 analogues (Table 2.S3), which is usually the number of analogues retained by MAT users. The differences are very small regardless of the number of analogues (5-10), but the best results with the highest R^2 were obtained with 5 analogues, so we kept this number (Table 2.S3).

The results of the cross-validation test performed with 5 analogues on the EMPD2 subset (Chevalier et al., 2019; Davis et al., 2020) containing 7634 sites and 88 pollen taxa are plotted in Figure 2.S13. The linearity of the relationship between reconstructed and observed values, with a slope close to one and high R^2, highlights the reliability of the method, especially for temperature reconstructions. The highest R^2 value is recorded for MTCO (0.91), which, however, shows a larger RMSEP (3.4°C) than MTWA (2.0°C) due to the large range of winter temperatures in the dataset compared to summer temperatures. The high spatial variability of precipitation within the geographical extent of the database explains the weaker R^2 values for precipitation, especially winter and annual precipitation. The RMSEP for annual, winter and summer precipitation are 199.8, 68.8 and 46.3 mm respectively.

2.3.3.2 Climatic reconstruction from marine core pollen data

There is debate about the use of marine cores for pollen-based climatic reconstructions (e.g., Sánchez Goñi et al., 2018; Chevalier et al., 2020; Davis et al., 2022). There were some concerns raised about the diversity of species, which is supposedly very low in marine sediments compared to terrestrial samples. This point

is addressed in Table 2.S4 which shows comparable taxonomic diversity between terrestrial and marine pollen records in our compilation. It was also argued that depositional mechanisms are important parameters in the redistribution of pollen (See Supplementary information Section 2.8.2), and that marine records cannot be used for pollen-based climatic reconstructions as samples in the modern pollen databases are mainly terrestrial and do not integrate the same scale of pollen source areas (cf. Chevalier et al., 2020; See also Supplementary information Section 2.8.3), with distal transport to marine sites resulting in the overrepresentation of some pollen taxa such as *Pinus* (Turon, 1984). Still, many studies (Sánchez Goñi et al., 2018 and references therein) conducted in Western Europe and the Mediterranean region have addressed the selective transport issue and demonstrated that despite the impact of distal transport and overrepresentation of *Pinus*, pollen assemblages in nearshore marine settings reflect the regional vegetation, thus permitting comparisons with terrestrial pollen assemblages of the adjacent continent (Morales-Morino et al., 2020). In many of these studies, however, *Pinus* was removed from the pollen records (fossil and modern) for the climatic reconstructions. This removal is disputed by Davis et al. (2022) who argued that 1) *Pinus* is a strong component of the last glacial vegetation in Southwestern Europe, which thus bears an important climatic signature, and 2) the remaining terrestrial taxa might not constitute pollen sums high enough (<100 grains) to be representative of the vegetation (cf. see also Chevalier et al., 2020). To counter this last point, we decided only to keep modern and fossil samples with a sum (excluding *Pinus*) superior to or equal to 100 grains.

Regarding whether or not we should remove *Pinus* from the pollen records, we decided to conduct a test on marine site 2 (Fig. 2.1; Table 2.1 and references therein) with climatic reconstructions with and without *Pinus.* We then compared the results to an indicator of sea-surface conditions from the same core. The results led us to agree with previous authors (e.g., Sánchez Goñi et al., 2018 and references therein) about the necessity to remove *Pinus* from the fossil and modern pollen samples as the overrepresentation of this taxon seems to dilute the climatic signature of the overall assemblage (See Supplementary Information Section 2.8.3.1.). We thus made a second (marine) version of our modern pollen database, for which we removed *Pinus* and recalculated relative abundances of taxa (%). Since we had already removed samples with sums (excluding *Pinus*) under 100 grains, it comprises the same number of modern samples as in the "terrestrial" version. Validation tests with and without *Pinus* (87 or 88 taxa) yield comparable results, with slightly higher RMSEP without *Pinus* (see Table 2.S5). The results are consistent with those of non-pollen-based climate indicators. Nevertheless, we agree that pollen-based climatic reconstructions from marine sediments must always be viewed with caution since the climatic signature

of the initial pollen assemblages (fossil and modern) is not fully preserved (See Supplementary Information Section 2.8.3.1).

2.3.3.3 The atmospheric CO_2 effect

The atmospheric CO_2 concentration is another parameter that may affect the vegetation since it controls plant water-use efficiency (Prentice et al., 2017). Hence, it has been argued that accounting for CO_2 changes when reconstructing climatic parameters from vegetation proxies such as pollen assemblages is important, especially for periods with low CO_2 concentrations such as the last glacial (Bauska et al., 2021), during which climate estimates from pollen were possibly biased toward drier values (e.g., Prentice et al., 2022).

MAT, like most other paleoclimate proxies or reconstruction techniques, does not account for the atmospheric CO_2 effect, which may be a limitation. In a recent study, Davis et al. (2022) tried to assess the bias that might result from atmospheric CO_2 variations by reconstructing the paleoclimate of the LGM in Europe, North Africa and the Middle East using MAT and Inverse Modelling (see Guiot et al., 2000). The results show good agreement between the two methods, strengthening the reliability of MAT for climatic reconstructions of glacial times and suggesting that low CO_2 concentrations during the LGM had little impact on the pollen-based reconstructions of climate (Davis et al., 2022). Although the results of this last study (Davis et al., 2022) were encouraging, we cannot exclude a slight underestimation of the precipitation values, especially toward the end of MIS 3, since CO_2 concentrations were lower than today's (Bauska et al., 2021).

The consistency in the pacing of the pollen-based climatic reconstructions and the *G. bulloides* $\delta^{18}O$ record (Shackleton et al., 2000) of core MD95-2042 (Figure 2.S14), which also correlates to the oxygen stratigraphy of the Greenland Ice cores (e.g., Austin and Hibbert, 2012), is another argument in favour of an adequate paleoclimate signal from pollen data. Indeed, it has been demonstrated that vegetation during MIS 3 in Europe covaries with the climate signal in the Greenland Ice cores (Sanchez-Goñi et al., 2000).

Additionally, atmospheric CO_2 concentration during the last glacial period shows variations in phase with the Antarctic temperature record rather than with the Greenland temperature record (Bauska et al., 2021; Denton et al., 2022). Since both Antarctic and Greenland temperature records are apparently

out of phase, the changes in vegetation or the inferred climatic reconstructions in western Europe likely reflect regional climate dynamics, rather than variations in atmospheric CO_2.

2.3.3.4 Comparison to modern values

Paleoclimatic reconstructions were then compared to modern values for all terrestrial sites using the mean climatic values calculated from 1901 to 2022 with Climate Explorer (https://climexp.knmi.nl/start.cgi). The grid for the climatic compilation is 0.5° x 0.5°. Because pollen in marine cores may be advected from wider areas, we did not assess the modern climatic values at marine sites.

2.3.3.5 Multivariate analyses

Canonical Correspondence analyses (CCA) were performed on the modern database using the Canoco 5 software (Šmilauer and Lepš, 2014) to evaluate the relationship between pollen taxa and the environmental variables (Figure 2.S15). Square root transformation was applied to pollen assemblages to increase the weight of taxa occurring in low abundance. Figure 2.S15 shows the CCA ordination diagram of pollen taxa vs. environmental variables. The first axis explains 60.15% of the constrained variance and is negatively correlated with MTWA and, to a lesser extent with MTCO. Axis 2 explains 21,48% of the constrained variance and is positively correlated with Pann and Pdjf, and, to a lesser extent, positively and negatively correlated with Pjja and Seasonality, respectively. Overall, the first two CCA axes show different scores for the climatic parameters and a relatively large scatter of the 88 taxa, which confirms that the modern database can be used to reconstruct the climatic parameters selected (Figure 2.S15). Many taxa, including thermophilous taxa such as *Olea*, *Pistacia* or *Phillyrea* are grouped along with MTWA while we observe many taxa from temperate forests along the Pdjf and MTCO arrows, which illustrates their strong relationship with these climatic parameters (Figure 2.S15).

For each site, redundancy analysis (RDA) was performed with Canoco 5 (Šmilauer and Lepš, 2014) using the PFT and paleoclimatic estimates with two objectives: 1) to examine the primary variation patterns of the vegetation as illustrated from PFTs; 2) to identify which climatic parameter(s) influence(s) the primary variation patterns in the vegetation. Since square root transformations were applied to the initial pollen percentages for the PFT grouping, no additional transformation was made before running the RDAs.

Both PFTs and climate estimates are based on pollen assemblages and cannot be considered independent even if the PFTs result from grouped taxa (n = 23) and MAT is run with 88 taxa. In this respect, it is worth noting that the number of taxa retained for PFT grouping and MAT are different (Table 2.S4).

Hence, the RDA is used here not to examine the vegetation response to climate, which is implicit in the reconstruction, but rather to investigate the nature of the climate-vegetation linkages for the study regions during MIS 3.

2.4 Results and Discussion

The results of the redundancy analyses (RDA) performed on PFTs and pollen-based climatic estimates exhibit the same primary pattern for all sites (Figs. 2.S1b-2.S12b), with a cluster of arboreal PFTs including heath (H), opposed to a cluster of non-arboreal PFTs including *Juniperus* (ECPI). This is illustrated in the two examples of Figure 2.2, one from a western marine site (marine core MD95-2042; Site 2; Figs. 2.1 and 2.2a; Sanchez-Goñi et al., 2000, 2002, 2008, 2009; Sanchez-Goñi, 2006) and the other from an eastern terrestrial site (Megali Limni; Site 12; Figs. 2.1 and 2.2b; Margari et al., 2009). The vegetation variation pattern is characterized by the RDA-Axes 1, which explains 59% to 91% of the total variance depending on the site (Fig. 2.2; Figs 2.S1b-2.S12b).

Among the arboreal PFTs, Temperate Summergreen, Warm Temperate Broad-Leaved Evergreen, Pioneer, Boreal evergreen/cool-temperate conifer, and Boreal Evergreen Conifer display strong variability (See Table 2.2 for more details on the PFTs). The Eurythermic Conifer PFT is also an important component of the vegetation variability for terrestrial sites (Figs. 2.S5b-2.S12b). It does not appear in marine sites since *Pinus* was removed from the pollen records due to strong overrepresentation offshore (Figs. 2.S1b-2.S4b). Steppe forb/shrub, Desert forb/shrub and Grass are the most important non-arboreal PFTs (Figs. 2.S1b-2.S12b). Given the opposition of arboreal and non-arboreal-PFTs of the first principal component in our analysis, we refer to arboreal and non-arboreal vegetation phases even if non-arboreal vegetation proportion remained high throughout MIS 3.

2.4.1 Millennial-scale alternation of arboreal and non-arboreal PFTs

At marine sites (Fig. 2.3a; Figs. 2.S1c-2.4c), the primary pattern of PFT variations generally depicts important millennial-scale variability. It has been shown for the eastern North Atlantic region that proxies of sea-surface temperatures such as the $\delta^{18}O$ of planktonic foraminifera vary concomitantly with changes

in pollen assemblages (Sanchez-Goñi et al., 2000, 2002, 2008, 2009; Roucoux et al., 2005). The peaks of arboreal pollen indeed coincide with episodes of warm sea-surface conditions and the non-arboreal taxa are more abundant during cold phases (Fig. 2.3a and Figs. 2.S1c-2.4c). The arboreal/warm ocean phases and non-arboreal/cold ocean phases can thus be correlated to the GIs and GSs respectively (Austin and Hibbert, 2012) in our four marine sites (sites 1 to 4; Table 2.1 and references therein), which are also the westernmost sites of this compilation (Fig. 2.1). This is corroborated by the very well-dated $\delta^{13}C$ record of three stalagmites from Cueva Victoria, southeastern Iberia (Fig. 2.1), that relates to vegetation density above the cave and closely matches the $\delta^{18}O$ of NGRIP (Budsky et al., 2019).

Millennial-scale shifts from arboreal to non-arboreal vegetation are also recorded at most terrestrial sites (Fig. 2.3b and Figs. 2.S5c-2.S12c). However, the uncertainty of the age models renders the identification of GIs/GSs equivocal (Figs. 2.S1a-2.S12a; see Chapter 2.2.2 for details about chronology and temporal resolution). At Megali Limni (Margari et al., 2009), which is the easternmost site in our compilation (Fig. 2.1), there is evidence for a strong decline of the vegetation during HS4 and HS3 and development of arboreal vegetation during the GIs (Fig. 2.3b). Although the chronology of this site is not perfectly well-constrained (Fig. 2.S12a), a tephra layer (Y-5; Margari et al., 2009) dated at 39,280 cal. BP, thus compatible with HS4 (Sanchez-Goñi and Harrison, 2010), is recorded during a steppe phase, which would indicate a coherent response of the vegetation to climate millennial variability at a continental scale.

2.4.2 Winter forcing of millennial-scale vegetation shifts

Redundancy analyses performed on PFT data and climate reconstructions help to identify which climatic parameter(s) most influence(s) the primary patterns of PFT variation for each site. Positive relationships between arboreal PFTs and annual and winter precipitation characterize the overall dataset (Fig. 2.2; Figs 2.S1b-2.S12b). MTCO also appears positively correlated with arboreal PFTs at many sites. Conversely, non-arboreal PFTs are always positively related to seasonality (Fig. 2.2; Figs 2.S1b-2.S12b). MTWA and Pjja depict a more random behaviour, with MTWA being mostly correlated with seasonality in many sites, while Pjja is mostly correlated with arboreal vegetation (Fig. 2.2; Figs 2.S1b-2.S12b).

The growth of arboreal vegetation is thus associated with high MTCO and precipitation, notably in winter. Conversely, low precipitation, combined with colder winters, corresponds to the development of semi-desert vegetation (SF: Steppe forb/shrub, DF: Desert forb/shrub). The prominent role of moisture availability in this primary pattern of vegetation variation also explains why heaths (H; see Table 2.2) that

require humid conditions are always associated with arboreal PFTs (Figs. 2.S1b-2.S12b), whereas *Juniperus* (ECPI: Eurythermic conifer/Pioneer; see Table 2.2), which tolerates cold and dry conditions, is often associated with the non-arboreal cluster.

The predominant role of winter on vegetation dynamics is particularly obvious when looking at the climatic reconstructions over time (Fig. 2.3; Figs. 2.S1c-2.S12c). In the marine cores located on the Western Iberian margin (Figs. 2.1 and 2.3a; Fig. 2.S1c), millennial vegetation variations are associated with MTCO variations of large amplitude (up to 10 – 15 °C), with negative MTCO associated with steppe phases. In comparison, dinocyst-based winter SSTs inferred from proximal core U1385 (Fig. 2.1) show variations of about 5-6 °C (Datema et al., 2019). On the Southeastern Iberian margin, in the Mediterranean (Fig. 2.1; Figs. 2.S3c and 2.S4c), MTCO variations are smaller and remain mainly above 0°C, in line with previous pollen-based climatic estimates obtained from one of the cores (Prentice et al., 1992). Further north, in the Gulf of Lions, negative winter temperatures show variations from ~ -7.5 to -2°C (Sanchez-Goñi et al., 2008). Significant variations of winter and annual precipitation also characterize all four records (Fig. 2.3a; Figs. 2.S1c-2.S4c), with increased precipitation during arboreal phases. The Pann and Pdjf that are highly correlated in the RDA graphs (Figs. 2.S1b-2.S12b) depict similar behaviour through time although the amplitude of Pann is triple compared to that of Pdjf. On the Western Iberian margin, Pann values range from ~500 to 1200 mm and ~400 to 1000 mm for sites 1 and 2 respectively (Figs. 2.1 and 2.3a; Fig. 2.S1c; Table 2.1 and references therein). In the Alboran Sea, Pann values are slightly lower but still display important variations, with values from ~ 300 to 600 or 800 mm depending on the sites (Figs. 2.S3c-2.S4c). This is comparable to the annual precipitation reconstructions from the nearby terrestrial site Padul (Fig. 2.1), which shows values ranging from ~300 to 650 mm, highly correlated to winter precipitation (Camuera et al., 2022). Most terrestrial records also show important variations of MTCO, mostly negative values, with amplitudes up to ~10 to 20 °C, depending on the sites (Fig. 2.3; Figs. 2.S5c-2.S12c). Modern MTCO values are rarely reached or approached (less than 5 °C of difference), and only during the “greenest” phases of the sequences. Again, Pdjf and Pann correlate and thus depict comparable variations as in the marine cores (Figs. 2.2 and 2.3; Figs. 2.S1-2.S12). As for MTCO, modern Pann and Pdjf values are reached for some cores during the greenest phases of the sequences (Figs. 2.S5c, 2.S8c and 2.S10c). In rare cases, however (Fig. 2.3b; Figs. 2.S9c and 2.S11c), modern values are largely exceeded during some arboreal phases (with Pann values up to + 500 mm).

2.4.3 Warm summer climate stability despite large amplitude winter variations in southern Europe throughout MIS 3

Although the pronounced winter nature of DO cycles has already been shown in some studies (e.g., Sanchez-Goñi et al., 2000; Flückiger et al., 2008; Datema et al., 2019), little is known about the summer climate on the European continent during the DO cycles. There are no high-resolution quantitative reconstructions of summer precipitation in this region during MIS 3, and only very few recent temperature reconstructions of the warmest months (Zander et al., 2024 and reference therein). Except for these last studies (Zander et al., 2024), most recent studies using continental proxies focus on either winter (Sanchez-Goñi et al., 2021), mean annual temperature (Rodrigo-Gámiz et al., 2022), or show mean-summer precipitation but at a resolution not high enough to assess its behaviour during DO cycles (Camuera et al., 2022).

The pollen dataset, which includes several continuous high-resolution MTWA and summer precipitation records, provides strong evidence for relatively stable summer temperature and precipitation throughout MIS 3 in Southern Europe (Fig. 2.3; Figs. 2.S1c-2.S12c), but large amplitude winter variability. MTWA mostly depicts variations of less than half the amplitude of MTCO variations and shows relatively high values, close to modern ones, except for a few sites (Fig. 2.3b; Fig. 2.S11c). Although the capability of the modern pollen database EMPD2 (Davis et al., 2020) to infer accurately MTWA can be questioned, the CCA ordination diagram of pollen taxa vs. environmental variables (Fig. 2.S15) clearly shows the great sensitivity of many taxa to this environmental variable. The RDA graphs (Fig. 2.2; Figs. 2.S1b-2.S12b) also show that MTWA does not follow MTCO variations, implying that the “expected” DO signal is not imprinted evenly over both winter and summer temperature European records. The winter-summer temperature decoupling is further evidenced in Figure 2.4, which depicts differences between the averages of climatic values associated with arboreal (GIs) and non-arboreal (GSs) at each site. Winter temperatures (Fig. 2.4a) and precipitation (Fig. 2.4b) appear higher during GIs than GSs (full bars). Seasonality (Fig. 2.4e), which is winter-driven, appears stronger during GSs than during GIs (empty bars). More surprisingly, the average summer temperatures associated with GSs are slightly higher than the average summer temperatures associated with GIs for most sites (Fig. 2.4c). At first glance, the positive departure of GS temperatures might appear negligible, as the difference between climatic estimates lies within the margins of error (RMSEP; see Chapter 2.3.3.1), but they are still significant when considering that the averages are smoothed as they include GS-GI and GI-GS transition values. Conversely, for DO cycles at most sites, the maximum amplitude of each climatic parameter exceeds the error margins (Table

2.S5; Fig. 2.3; Figs. 2.S1c-2.S12c). Adding the consistency of the pattern from one site to another (except for the two easternmost sites) (Fig. 2.4a,c), we may consider the slight increase in summer temperatures during GSs as a real feature. Schenk et al. (2018) highlighted slightly warmer summers during the Younger Dryas stadial compared to the preceding interstadial (Bølling/Allerød). The authors proposed an atmospheric blocking of cold westerlies through a steady high-pressure ridge along the western European coast in response to the cold SSTs recorded in the North Atlantic Ocean, thus resulting in warm summer temperatures on the continent (Schenk et al., 2018). This warm summer atmospheric response to cold SSTs has also been observed in recent decades, with the coldest subpolar SST years being linked with major European heatwaves and droughts (e.g., Duchez et al. 2016; Ionita et al. 2017). Another possibility is that lower winter or annual precipitation may have resulted in less evaporative cooling during GS summers. Finally, increased summer temperatures may have been favoured by enhanced stratification of North Atlantic surface waters, fostering low thermal inertia and enhanced summer warming. Such stratification may have been even stronger further north, as demonstrated by dinocyst-based summer SSTs, south of the Faroe Islands, which depicted significant increases during GSs (Zumaque et al., 2012; Wary et al., 2015).

Summer precipitation shows relative steadiness at only half of the sites, in the westernmost and easternmost parts of the study region (Fig. 2.3; Figs. 2.S1c-2.S5c, 2.S12c). At the other sites (Figs. 2.S6c-2.S11c), Pjja shows comparable amplitude variations to Pdjf but do not depict the same behaviour. The decoupling between summer and winter precipitation may be explained by precipitation originating from different sources. Paleoclimate studies of the Last Glacial Maximum (LGM) in the Alps region have shown that winter precipitation was storm-related, whereas summer precipitation was mainly of regional convective origin (Del Gobbo et al., 2023).

2.4.4 Possible linkage with North Atlantic Oscillation-like atmospheric phenomenon and Subpolar Gyre (SPG) dynamics

Under present-day conditions, the vegetation growth in southern Europe depends upon winter precipitation (Gouveia et al., 2008), which is tightly linked to the winter North Atlantic Oscillation (NAO) circulation pattern. The NAO index commonly used is defined as the deviation from the normalized atmospheric pressure difference between the Icelandic Low and the Azores High from November to April (Hurrell, 1995). A negative mode of the NAO, corresponding to a weak pressure gradient, results in a mild and wet winter climate in southwestern Europe through the southward displacement of the westerlies. Conversely, a positive mode of the NAO, with a strong pressure gradient, causes a northward displacement

of the westerlies that brings moist air masses to northwest Europe, leading to cold and dry winters in the southernmost part of the continent.

The results of our analyses indicate that millennial-scale variations of the vegetation are tightly linked to winter precipitation and temperature (Fig. 2.2; Figs. 2.S1b-2.S12b), thus suggesting relationships with changes in the modes of atmospheric circulation pattern in phase with DO cycles. The NAO modes presently vary on annual to decadal timescales (Hurrell, 1995). Nevertheless, we hypothesized here that the arboreal phases in the MIS 3 records that are in phase with the GIs relate to a southward position of the westerlies, similar to the present NAO negative mode of circulation (see also Sanchez-Goñi et al., 2002, 2009). Conversely, GS/non-arboreal phases are associated with stronger/northward westerlies, resembling the NAO-like positive mode of circulation. Hence, since the DO cycles are mostly characterized by variations in winter climatic parameters in the Southern European records (Fig. 2.3; Figs. 2.S1c-2.S12c), we suggest that DO cycles are essentially the expression of winter atmospheric phenomenon resembling those of the present NAO mode of variability.

A salient feature of the present-day NAO is the dipole atmospheric pattern it generates over the European continent, with cold/warm and dry/wet climates over northern/southern Europe during NAO negative mode and vice versa (Hurrell, 1995). Unfortunately, the scarcity of terrestrial data in northern Europe for the last glacial period, notably because of the presence of the Fennoscandian Ice Sheet, precludes a full investigation of the dipole pattern. However, some authors have highlighted a “paradoxical response of the dinocysts” in the adjacent Norwegian Sea during MIS 3 (Eynaud et al., 2002; Wary et al., 2017), which indicated warmer surface conditions and reduced sea-ice cover duration in the southeastern Norwegian Sea during GSs compared to GIs, thus an opposite behaviour than in the North Atlantic Ocean.

Stables isotope data in speleothems from Southeastern Iberia also indicate increased winter precipitation during GIs (Budsky et al., 2019), and led to suggest that high SSTs over the North Atlantic and Mediterranean during GIs may have regulated the water vapour content of the atmosphere, thus precipitation. Conversely, cold SSTs during GSs might have diminished potential evaporation, the vapour content of the atmosphere and the amount of precipitation (Budsky et al., 2019). In the Nordic Seas, Wary et al. (2017) also suggested that relatively warm surface waters and reduced sea-ice cover during GSs had implications on atmospheric circulation and moisture sources. They notably evoked that the high deuterium excess recorded in the Greenland ice core during GSs (Masson-Delmotte et al., 2005) may

indicate moisture from the Nordic Seas rather than from the subtropical North Atlantic Ocean as it is the case during GIs (Wary et al., 2017 and references therein). The vapour content originating from the Nordic Seas during GSs could thus have contributed to the replenishment of the adjacent ice sheets and ensured the continued IRD signal recorded during stadials (Elliot et al., 1998; Menviel et al., 2014).

Both mechanisms, the modes of atmospheric circulation and the moisture availability through ocean surface conditions were probably related. During GSs, enhanced westerlies in winters with NAO^+-like conditions could have generated eastward expansion of the cold and low salinity surface waters in the Subpolar Gyre (SPG), overlying the warm but dense and salty North Atlantic Drift (NAD) (Fig. 2.1). Low salinity surface water well-stratified and isolating the underlying North Atlantic likely prevented heat release and evaporation from the NAD to the atmosphere, thus generating cold and dry winters over Southern Europe (Fig. 2.5a). As proposed by Wary et al. (2017), the NAD entering the Nordic Seas during GSs would be too warm and not dense enough to sink (see Figure 2.3 of Wary et al., 2017), resulting in a slowdown of the Atlantic meridional overturning circulation (AMOC; Gottschalk et al., 2015). During summer, in the North Atlantic, the stratified water characterized by low thermal inertia would have favoured energy uptake through solar insolation that was equal or even higher than at present (Laskar et al., 2004), thus leading to surface ocean warming (Fig. 2.5c) with consequently warm air temperatures over the adjacent continent (see Chapter 2.4.3).

During GIs, conversely, weakened westerlies under NAO^--like conditions would have favoured westward contracted SPG, enabling the NAD to flow and spread at the surface in the northeastern North Atlantic, allowing heat release and increased evaporation, thus mild and wet winters over Southern Europe (Fig. 2.5b). The NAD entering the Nordic Seas at the surface could then cool in winter and sink to contribute to the AMOC (Wary et al., 2017). Such a scenario is compatible with the freshwater hysteresis of the AMOC described by Hofmann and Rahmstorf (2009) although we hypothesize here that the switches from strong to slow AMOC might be related to the redistribution of the freshwater through winds and the resulting stratification rather than with the quantity of freshwater supply.

2.4.5 The key role of warm summer temperatures throughout MIS 3

In our compilation, the MTWA appears close to modern values throughout the MIS 3 (Fig. 2.3; Figs. 2.S1c-2.S12c), whereas the MTCO records large variations, with very low values during GSs. This is compatible with the hypothesis of Denton et al. (2005) stipulating that DO events were mainly a winter phenomenon

and that mild summer temperatures might have prevailed during the last glacial stage. Denton et al. (2022) also suggested that a global shift toward warmer summer temperatures at the end of GIs might have fostered the retreat of the Northern Hemisphere ice sheets, leading to enhanced freshwater input into the North Atlantic, thus weakening the AMOC and favouring freezing and sea-ice cover in winter, in turn hampering heat release from the ocean to the atmosphere and leading to winter climate cooling (Denton et al., 2022). Our mid-latitudes records showing warm but relatively stable summer temperatures partially support the Denton et al. hypotheses (Denton et al., 2005, 2022). The MTWA associated with non-arboreal phases (GSs) appear slightly higher than during GIs on average (Fig. 2.4c), but the time series do not show a clear increase from GSs to GIs (Fig. 2.3; Figs. 2.S1c-2.S12c), suggesting that the subtle changes may result from local/regional processes rather than global processes as suggested by Denton et al. (2022) (See also discussion in Chapter 2.4.3).

In the Norwegian Sea, Wary et al. (2017) reconstructed warmer summer SSTs during GSs than during GIs, which were interpreted as a consequence of meltwater lid in the North Atlantic (see Chapter 2.4.4) in contrary to what Denton et al. (2022) hypothesized. At these latitudes, high summer temperatures during GSs would imply a continuous supply of meltwater to the Nordic Seas and thus to the North Atlantic Ocean via the East Greenland Current. Considering the continuous presence of the surrounding continental ice sheets during MIS 3, we cannot attribute the switches to GI conditions to a potential meltwater supply shortage. Instead, we consider the distribution of the meltwater in the North Atlantic as key in the centennial to millennial scale climate variability recorded in the region. We further hypothesize that a weakening of the westerlies may result in a westward contraction of the fresh subpolar gyre, a warming and cooling of the North Atlantic and Nordic Seas respectively, and thus enhanced AMOC strength (See Chapter2.4.4).

2.5 Conclusion

Based on vegetation and climate information inferred from 12 pollen sequences from southern Europe, we highlighted a pronounced millennial-scale variability of the vegetation in the region, with alternation of arboreal and non-arboreal phases during Greenland interstadials (GIs) and stadials (GSs), respectively. Our results demonstrate that these variations were primarily driven by changes in winter precipitation and temperatures, with mild and wet winter conditions during GIs and cold and dry conditions during GSs. Conversely, summer conditions remained relatively warm and unchanged throughout MIS 3, with even slightly higher temperature values during GSs, supporting Denton et al.'s (2005, 2022) hypotheses.

The decoupling between winter and summer seasons and the relative flatness of summer records suggest that the Dansgaard-Oeschger cycles in southern Europe mainly express winter atmospheric oscillations, allowing analogy with the present North Atlantic Oscillation (NAO) modes of variability. We hypothesize that during GSs, strengthened westerlies (NAO+-like conditions) induced an eastward extension of the subpolar gyre (SPG), which constituted a freshwater lid that hampered heat release, diminished evaporation and favoured winter sea-ice formation, cooling and drying the southern European continent. Conversely, a weakening of the westerlies (NAO^--like conditions), with a westward contraction of the SPG, would have favoured flow of the NAD at the surface enabling heat release and evaporation and thus warmer and wetter conditions over southern Europe.

We therefore conclude that the oscillations of a winter atmospheric phenomenon resembling the present NAO modes of variability may have been instrumental in the millennial-scale climate variability of the North Atlantic sector, by modulating the distribution of the freshwater supply in the North Atlantic through the spreading/contraction of the SPG, thus impacting winter sea-ice expansion, air temperatures and moisture availability over southern Europe.

2.6 Acknowledgments

We acknowledge financial supports from the GEOTOP, funded by the *Fonds de Recherche du Québec – Nature et Technologies* (FRQNT) and the Hominin Dispersal Research Group (HDRG - http://www.hominindispersals.net/), funded by the Fonds de Recherche Québécois sur la Société et la Culture (FRQSC). This research also benefited from funding from the Natural Sciences and Engineering Research Council of Canada (NSERC) through a Discovery grant to AdV and through the international program "Processes and impacts of climate change in the North Atlantic Ocean and the Canadian Arctic (ArcTrain), which is a Collaborative Research and training Experience Program (CREATE). We also thank Dr. Basil Davis and Dr. Manuel Chevalier for their precious advice and for their help with the EMPD2.

2.7 References

Allen, J. R., & Huntley, B., Effects of tephra falls on vegetation: A Late-Quaternary record from southern Italy. *Journal of Ecology*, *106*(6), 2456-2472 (2018).

Allen, J. R., Watts, W. A., & Huntley, B., Weichselian palynostratigraphy, palaeovegetation and palaeoenvironment; the record from Lago Grande di Monticchio, southern Italy. *Quaternary International*, *73*, 91-110 (2000).

Austin, W. E., & Hibbert, F. D., Tracing time in the ocean: a brief review of chronological constraints (60–8 kyr) on North Atlantic marine event-based stratigraphies. *Quaternary Science Reviews*, *36*, 28-37 (2012).

Batchelor, C. L., et al., The configuration of Northern Hemisphere ice sheets through the Quaternary. *Nature communications*, *10*(1), 3713 (2019).

Bauska, T. K., Marcott, S. A., & Brook, E. J., Abrupt changes in the global carbon cycle during the last glacial period. *Nature Geoscience*, *14*(2), 91-96 (2021).

Birks, H. J. B., Heiri, O., Seppä, H., & Bjune, A. E. (2010). Strengths and weaknesses of quantitative climate reconstructions based on Late-Quaternary. *The Open Ecology Journal*, *3*(1).

Blaauw, M., Methods and code for 'classical'age-modelling of radiocarbon sequences. *quaternary geochronology*, *5*(5), 512-518 (2010).

Bottema, S., Pollen analytical investigations in Thessaly (Greece). *Palaeohistoria*, 19-40 (1979).

Brauer, A., *et al*., Evidence for last interglacial chronology and environmental change from Southern Europe. *Proceedings of the National Academy of Sciences*, *104*(2), 450-455 (2007).

Budsky, A., Western Mediterranean climate response to Dansgaard/Oeschger events: New insights from speleothem records. *Geophysical Research Letters*, *46*(15), 9042-9053 (2019).

Camuera, J., et al., Past 200 kyr hydroclimate variability in the western Mediterranean and its connection to the African Humid Periods. *Scientific Reports* 12.1 : 1-13 2022.

Carré, M., & Cheddadi, R., Seasonality in long-term climate change. *Quaternaire. Revue de l'Association française pour l'étude du Quaternaire*, *28*(2), 173-177 (2017).

Chevalier, M., Davis, B. A. S., Sommer, P. S., Zanon, M., Carter, V. A., Phelps, L. N., Mauri, A., and Finsinger, W. (2019): Eurasian Modern Pollen Database (former European Modern Pollen Database), Pangaea, https://doi.pangaea.de/10.1594/PANGAEA.909130.

Chevalier, M., *et al*., Pollen-based climate reconstruction techniques for late Quaternary studies. *Earth-Science Reviews*, *210*, 103384 (2020).

Combourieu Nebout, N., Enhanced aridity and atmospheric high-pressure stability over the western Mediterranean during the North Atlantic cold events of the past 50 ky. *Geology*, *30*(10), 863-866 (2002).

Dansgaard, W. *et al*., Evidence for general instability of past climate from a 250-kyr ice-core record. *nature*, *364*(6434), 218-220 (1993).

Datema, M., *et al.,* Millennial-scale climate variability and dinoflagellate-cyst-based seasonality changes over the last~ 150 kyrs at "Shackleton Site" U1385. *Paleoceanography and paleoclimatology*, *34*(7), 1139-1156 (2019).

Davis, B. A., Chevalier, M., Sommer, P., Carter, V. A., Finsinger, W., Mauri, A., ... & Zimny, M. (2020). "The Eurasian Modern Pollen Database (EMPD), version 2." Earth Syst. Sci. Data **12**(4): 2423-2445.

Davis, B. A. S., Fasel, M., Kaplan, J. O., Russo, E., & Burke, A. (2022). "The climate and vegetation of Europe, North Africa and the Middle East during the Last Glacial Maximum (21,000 years BP) based on pollen data." Clim. Past Discuss. **2022**: 1-66.

de Vernal, A. D., Eynaud, F., Henry, M., Hillaire-Marcel, C., Londeix, L., Mangin, S., ... & Turon, J. L., Reconstruction of sea-surface conditions at middle to high latitudes of the Northern Hemisphere during the Last Glacial Maximum (LGM) based on dinoflagellate cyst assemblages. *Quaternary Science Reviews*, *24*(7-9), 897-924 (2005).

Del Gobbo, C., Colucci, R. R., Monegato, G., Žebre, M., & Giorgi, F. (2023). Atmosphere–cryosphere interactions during the last phase of the Last Glacial Maximum (21 ka) in the European Alps. *Climate of the Past*, *19*(9), 1805-1823.

Denton, G. H., Alley, R. B., Comer, G. C., & Broecker, W. S., The role of seasonality in abrupt climate change. *Quaternary Science Reviews*, *24*(10-11), 1159-1182 (2005).

Denton, G. H., Toucanne, S., Putnam, A. E., Barrell, D. J., & Russell, J. L., Heinrich summers. *Quaternary Science Reviews*, *295*, 107750 (2022).

Duchez, A., Frajka-Williams, E., Josey, S. A., Evans, D. G., Grist, J. P., Marsh, R., ... & Hirschi, J. J. (2016). Drivers of exceptionally cold North Atlantic Ocean temperatures and their link to the 2015 European heat wave. *Environmental Research Letters*, *11*(7), 074004.

Ehlers, J., & Gibbard, P. L., *Quaternary glaciations-extent and chronology: part I: Europe*. Elsevier (2004).

Elliot, M., Labeyrie, L., Bond, G., Cortijo, E., Turon, J. L., Tisnerat, N., & Duplessy, J. C. (1998). Millennial-scale iceberg discharges in the Irminger Basin during the last glacial period: Relationship with the Heinrich events and environmental settings. *Paleoceanography*, *13*(5), 433-446.

Eynaud, F., Turon, J. L., Matthießen, J., Kissel, C., Peypouquet, J. P., De Vernal, A., & Henry, M. (2002). Norwegian sea-surface palaeoenvironments of marine oxygen-isotope stage 3: The paradoxical response of dinoflagellate cysts. *Journal of Quaternary Science: Published for the Quaternary Research Association*, *17*(4), 349-359.

Eynaud, F., et al., Position of the Polar Front along the western Iberian margin during key cold episodes of the last 45 ka. *Geochemistry, Geophysics, Geosystems*, *10*(7) (2009).

Fick, S. E., & Hijmans, R. J., WorldClim 2: new 1-km spatial resolution climate surfaces for global land areas. *International journal of climatology*, *37*(12), 4302-4315 (2017).

Fletcher, W. J., Goni, M. F. S., Allen, J. R., Cheddadi, R., Combourieu-Nebout, N., Huntley, B., ... & Tzedakis, P. C. (2010). Millennial-scale variability during the last glacial in vegetation records from Europe. *Quaternary Science Reviews*, *29*(21-22), 2839-2864.

Flückiger, J., Knutti, R., White, J. W., & Renssen, H., Modeled seasonality of glacial abrupt climate events. *Climate Dynamics*, *31*, 633-645 (2008).

Follieri, M., 250, 000-year pollen record from Valle di Castiglione. *Pollen et spores*, (3), 329-356 (1988).

Follieri, M., Magri, D., & Sadori, L., Pollen stratigraphical synthesis from Valle di Castiglione (Roma). *Quaternary International*, *3*, 81-84 (1989).

Follieri, M., Giardini, M., Magri, D., & Sadori, L., Palynostratigraphy of the last glacial period in the volcanic region of central Italy. *Quaternary International*, *47*, 3-20 (1998).

Genty, D. *et al.,* Isotopic characterization of rapid climatic events during OIS3 and OIS4 in Villars Cave stalagmites (SW-France) and correlation with Atlantic and Mediterranean pollen records. *Quaternary Science Reviews*, *29*(19-20), 2799-2820 (2010).

Giardini, M., Late quaternary vegetation history at Stracciacappa (Rome, central Italy). *Vegetation History and Archaeobotany*, *16*(4), 301-316 (2007).

Gottschalk, J. *et al.,* Abrupt changes in the southern extent of North Atlantic Deep Water during Dansgaard–Oeschger events. *Nature geoscience*, *8*(12), 950-954 (2015).

Gouveia, C., Trigo, R. M., DaCamara, C. C., Libonati, R., & Pereira, J. M., The North Atlantic oscillation and European vegetation dynamics. *International Journal of Climatology: A Journal of the Royal Meteorological Society*, *28*(14), 1835-1847 (2008).

Guiot, J., Methodology of the last climatic cycle reconstruction in France from pollen data. *Palaeogeography, Palaeoclimatology, Palaeoecology*, *80*(1), 49-69 (1990).

Guiot, J., *et al*., The climate in Western Europe during the last Glacial/Interglacial cycle derived from pollen and insect remains. *Palaeogeography, Palaeoclimatology, Palaeoecology*, *103*(1-2), 73-93 (1993).

Guiot, J., *et al*., Inverse vegetation modeling by Monte Carlo sampling to reconstruct palaeoclimates under changed precipitation seasonality and CO2 conditions: application to glacial climate in Mediterranean region. *Ecological modelling*, *127*(2-3), 119-140 (2000).

Guiot, J., & de Vernal, A., Chapter thirteen transfer functions: methods for quantitative paleoceanography based on microfossils. *Developments in marine geology*, *1*, 523-563 (2007).

Guiot, J., & De Vernal, A., Is spatial autocorrelation introducing biases in the apparent accuracy of paleoclimatic reconstructions? *Quaternary Science Reviews*, *30*(15-16), 1965-1972 (2011).

Hemming, S. R., Heinrich events: Massive late Pleistocene detritus layers of the North Atlantic and their global climate imprint. *Reviews of Geophysics*, *42*(1) (2004).

Hofmann, M., & Rahmstorf, S. (2009). On the stability of the Atlantic meridional overturning circulation. *Proceedings of the National Academy of Sciences*, *106*(49), 20584-20589.

Hurrell, J. W., Decadal trends in the North Atlantic Oscillation: Regional temperatures and precipitation. *Science*, *269*(5224), 676-679 (1995).

Ionita, M., Tallaksen, L. M., Kingston, D. G., Stagge, J. H., Laaha, G., Van Lanen, H. A., ... & Haslinger, K. (2017). The European 2015 drought from a climatological perspective. *Hydrology and Earth System Sciences*, *21*(3), 1397-1419.

Jackson, S. T., & Overpeck, J. T., Responses of plant populations and communities to environmental changes of the late Quaternary. *Paleobiology*, *26*(S4), 194-220 (2000).

Laskar, J., Robutel, P., Joutel, F., Gastineau, M., Correia, A. C., & Levrard, B. (2004). A long-term numerical solution for the insolation quantities of the Earth. *Astronomy & Astrophysics*, *428*(1), 261-285.

Magri, D., Late Quaternary vegetation history at Lagaccione near Lago di Bolsena (central Italy). *Review of Palaeobotany and Palynology*, *106*(3-4), 171-208 (1999).

Magri, D., & Tzedakis, P. C., Orbital signatures and long-term vegetation patterns in the Mediterranean. *Quaternary International*, *73*, 69-78 (2000).Magyari, E. K., *et al*., Late Pleniglacial vegetation in eastern-central Europe: are there modern analogues in Siberia?. *Quaternary Science Reviews*, *95*, 60-79 (2014).

Margari, V., Gibbard, P. L., Bryant, C. L., & Tzedakis, P. C., Character of vegetational and environmental changes in southern Europe during the last glacial period; evidence from Lesvos Island, Greece. *Quaternary Science Reviews*, *28*(13-14), 1317-1339 (2009).

Masson-Delmotte, V., Jouzel, J., Landais, A., Stievenard, M., Johnsen, S. J., White, J. W. C., ... & Fuhrer, K. (2005). GRIP deuterium excess reveals rapid and orbital-scale changes in Greenland moisture origin. *Science*, *309*(5731), 118-121.

Menviel, L., Timmermann, A., Friedrich, T., & England, M. H. (2014). Hindcasting the continuum of Dansgaard–Oeschger variability: mechanisms, patterns and timing. *Climate of the Past*, *10*(1), 63-77.

Morales-Molino, C., Devaux, L., Georget, M., Hanquiez, V., & Goñi, M. F. S. (2020). Modern pollen representation of the vegetation of the Tagus Basin (central Iberian Peninsula). *Review of palaeobotany and palynology*, *276*, 104193.

Moreno, A. *et al*., A compilation of Western European terrestrial records 60–8 ka BP: towards an understanding of latitudinal climatic gradients. *Quaternary Science Reviews*, *106*, 167-185 (2014).

North Greenland Ice Core Project members, High resolution record of Northern Hemisphere climate extending into the last interglacial period. *Nature*, *431*(7005), 147-151 (2004).

Olson, D. M., et al., Terrestrial Ecoregions of the World: A New Map of Life on Earth: A new global map of terrestrial ecoregions provides an innovative tool for conserving biodiversity. *BioScience*, *51*(11), 933-938 (2001).

Overpeck, J. T., Webb, T. I. I. I., & Prentice, I. C., Quantitative interpretation of fossil pollen spectra: dissimilarity coefficients and the method of modern analogs. *Quaternary Research*, *23*(1), 87-108 (1985).

Peyron, O. e*t al*., Climatic reconstruction in Europe for 18,000 yr BP from pollen data. *Quaternary research*, *49*(2), 183-196 (1998).

Prentice, I. C. *et al*., Special paper: a global biome model based on plant physiology and dominance, soil properties and climate. *Journal of biogeography*, 117-134 (1992).

Prentice, C., Guiot, J., Huntley, B., Jolly, D., & Cheddadi, R., Reconstructing biomes from palaeoecological data: a general method and its application to European pollen data at 0 and 6 ka. *Climate Dynamics*, *12*(3), 185-194 (1996).

Prentice, I. C., Cleator, S. F., Huang, Y. H., Harrison, S. P., & Roulstone, I., Reconstructing ice-age palaeoclimates: Quantifying low-CO2 effects on plants. *Global and Planetary Change*, *149*, 166-176 (2017).

Prentice, I. C., Villegas-Diaz, R., & Harrison, S. P., Accounting for atmospheric carbon dioxide variations in pollen-based reconstruction of past hydroclimates. *Global and Planetary Change*, *211*, 103790 (2022).

Rasmussen, T. L., Thomsen, E., & Moros, M. (2016). North Atlantic warming during Dansgaard-Oeschger events synchronous with Antarctic warming and out-of-phase with Greenland climate. *Scientific reports*, *6*(1), 20535.

Reimer, P. J., Bard, E., Bayliss, A., Beck, J. W., Blackwell, P. G., Ramsey, C. B., ... & Van Der Plicht, J. (2013). IntCal13 and Marine13 radiocarbon age calibration curves 0–50,000 years cal BP. *radiocarbon*, *55*(4), 1869-1887.

Rodrigo-Gámiz, M. *et al.,* Paleoclimate reconstruction of the last 36 kyr based on branched glycerol dialkyl glycerol tetraethers in the Padul palaeolake record (Sierra Nevada, southern Iberian Peninsula). *Quaternary Science Reviews*, *281*, 107434 (2022).

Roucoux, K. H., Shackleton, N. J., de Abreu, L., Schönfeld, J., & Tzedakis, P. C., Combined marine proxy and pollen analyses reveal rapid Iberian vegetation response to North Atlantic millennial-scale climate oscillations. *Quaternary Research*, *56*(1), 128-132 (2001).

Roucoux, K. H., De Abreu, L., Shackleton, N. J., & Tzedakis, P. C., The response of NW Iberian vegetation to North Atlantic climate oscillations during the last 65 kyr. *Quaternary Science Reviews*, *24*(14-15), 1637-1653 (2005).

Sanchez-Goñi, M. F., Turon, J. L., Eynaud, F., & Gendreau, S., European climatic response to millennial-scale changes in the atmosphere–ocean system during the Last Glacial period. *Quaternary Research*, *54*(3), 394-403 (2000).

Sánchez Goñi, M. F., et al., Synchroneity between marine and terrestrial responses to millennial scale climatic variability during the last glacial period in the Mediterranean region. *Climate dynamics*, *19*, 95-105 (2002).

Sánchez Goñi, M. F., Interactions végétation-climat au cours des derniers 425.000 ans en Europe occidentale. Le message du pollen des archives marines. *Quaternaire. Revue de l'Association française pour l'étude du Quaternaire*, *17*(1), 3-25 (2006).

Sanchez-Goñi, M. *et al*., Contrasting impacts of Dansgaard–Oeschger events over a western European latitudinal transect modulated by orbital parameters. *Quaternary Science Reviews*, *27*(11-12), 1136-1151 (2008).

Sanchez-Goñi, M. F., Landais, A., Cacho, I., Duprat, J., & Rossignol, L., Contrasting intrainterstadial climatic evolution between high and middle North Atlantic latitudes: A close-up of Greenland Interstadials 8 and 12. *Geochemistry, Geophysics, Geosystems*, *10*(4) (2009).

Sanchez-Goni, M. F., & Harrison, S. P. (2010). Millennial-scale climate variability and vegetation changes during the Last Glacial: Concepts and terminology. *Quaternary Science Reviews*, *29*(21-22), 2823-2827.

Sánchez Goñi, M. F. *et al.,* The ACER pollen and charcoal database: a global resource to document vegetation and fire response to abrupt climate changes during the last glacial period. *Earth System Science Data*, *9*(2), 679-695 (2017).

Sánchez Goñi, M. F., *et al*., Pollen from the deep-sea: A breakthrough in the mystery of the Ice Ages. *Frontiers in Plant Science*, *9*, 38 (2018).

Sanchez-Goñi, M-F. *et al*., Muted cooling and drying of NW Mediterranean in response to the strongest last glacial North American ice surges. *GSA Bulletin* 133.3-4: 451-460 (2021).

Schenk, F., Väliranta, M., Muschitiello, F., Tarasov, L., Heikkilä, M., Björck, S., ... & Wohlfarth, B. (2018). Warm summers during the Younger Dryas cold reversal. *Nature communications*, *9*(1), 1634.

Shackleton, N. J., Hall, M. A., & Vincent, E., Phase relationships between millennial-scale events 64,000–24,000 years ago. *Paleoceanography*, *15*(6), 565-569 (2000).

Šmilauer, P., & Lepš, J., *Multivariate analysis of ecological data using CANOCO 5*. Cambridge university press (2014).

Turon, J. L., Direct land/sea correlations in the last interglacial complex. *Nature*, *309*(5970), 673-676 (1984).

Tzedakis, P. C., *et al*., Buffered tree population changes in a Quaternary refugium: evolutionary implications. *science*, *297*(5589), 2044-2047 (2002).

Tzedakis, P. C., *et al*., Ecological thresholds and patterns of millennial-scale climate variability: the response of vegetation in Greece during the last glacial period. *Geology*, *32*(2), 109-112 (2004).

Wary, M., Eynaud, F., Sabine, M., Zaragosi, S., Rossignol, L., Malaize, B., ... & Charlier, K. (2015). Stratification of surface waters during the last glacial millennial climatic events: a key factor in subsurface and deep-water mass dynamics. *Climate of the Past*, *11*(11), 1507-1525.

Wary, M. *et al.,* Regional seesaw between the North Atlantic and Nordic Seas during the last glacial abrupt climate events. *Climate of the Past*, *13*(6), 729-739 (2017).

Watts, W. A., Allen, J. R. M., & Huntley, B., Vegetation history and palaeoclimate of the last glacial period at Lago Grande di Monticchio, southern Italy. *Quaternary Science Reviews*, *15*(2-3), 133-153 (1996).

Watts, W. A., Allen, J. R. M., & Huntley, B., Palaeoecology of three interstadial events during oxygen-isotope Stages 3 and 4: a lacustrine record from Lago Grande di Monticchio, southern Italy. *Palaeogeography, Palaeoclimatology, Palaeoecology*, *155*(1-2), 83-93 (2000).

Wulf, S., Kraml, M., Brauer, A., Keller, J., & Negendank, J. F. (2004). Tephrochronology of the 100 ka lacustrine sediment record of Lago Grande di Monticchio (southern Italy). *Quaternary International*, *122*(1), 7-30.

Zander, P. D., et al., Reconstruction of warm-season temperatures in central Europe during the past 60 000 years from lacustrine branched glycerol dialkyl glycerol tetraethers (brGDGTs). *Climate of the Past*, *20*(4), 841-864 (2024).

Zolitschka, B., & Negendank, J. F. (1996). Sedimentology, dating and palaeoclimatic interpretation of a 76.3 ka record from Lago Grande di Monticchio, southern Italy. *Quaternary Science Reviews*, *15*(2-3), 101-112.

Zumaque, J., Eynaud, F., Zaragosi, S., Marret, F., Matsuzaki, K. M., Kissel, C., ... & Palis, E. (2012). An ocean–ice coupled response during the last glacial: a view from a marine isotopic stage 3 record south of the Faeroe Shetland Gateway. *Climate of the Past*, *8*(6), 1997-2017.

Table 2.1 Terrestrial and marine pollen records used in this study *(Sánchez Goñi et al., 2017)

Site name	Code	Site type	Latitude (°N)	Longitude (°E)	Elevation (m)	References	Sources	Chronologies
MD95-2039	1	Marine	40.58	-10.35	-3381	Sánchez-Goñi et al. (2000); Roucoux et al. (2001, 2005)	ACER database*	ACER (file "dating_info_ACER)* (recalculated)
MD95-2042	2	Marine	37.8	-10.17	-3148	Sánchez-Goñi et al. (2000, 2002, 2008, 2009); Sánchez-Goñi (2006)	ACER database*	ACER (file "dating_info_ACER)* (recalculated)
ODP Site 976	3	Marine	36.2	-4.3	-1108	Combourieu-Nebout et al. (2002)	ACER database*	ACER (file "dating_info_ACER)*
MD95-2043	4	Marine	36.14	-2.62	-1841	Sánchez-Goñi et al. (2002, 2009); Sánchez-Goñi (2006)	ACER database*	ACER (file "dating_info_ACER)* (recalculated)
Lac du Bouchet	5	Terrestrial (lacustrine)	44.83	3.82	1200	Guiot et al. (1993)	ACER database*	ACER (file "dating_info_ACER)*
Lagaccione	6	Terrestrial (lacustrine)	42.57	11.8	355	Magri (1999)	ACER database*	ACER (file "dating_info_ACER)*
Stracciacappa	7	Terrestrial (lacustrine)	42.13	12.32	220	Follieri et al. (1998); Giardini (2007)	ACER database*	ACER (file "dating_info_ACER)*
Valle di Castiglione	8	Terrestrial (lacustrine)	41.9	12.76	44	Follieri (1988); Follieri et al. (1989); Magri and Tzedakis (2000)	ACER database*	ACER (file "dating_info_ACER)*
Lago Grande di Monticchio	9	Terrestrial (lacustrine)	40.94	15.61	656	Watts et al. (1996, 2000); Zolitschka and Negendank (1996); Allen et al. (2000); Wulf et al. (2004); Brauer	ACER database*	See references associated (file "dating_info"*)
Ioannina	10	Terrestrial (lacustrine)	39.75	20.85	470	Tzedakis et al. (2002, 2004)	ACER database*	ACER (file "dating_info_ACER)*
Lake Xinias	11	Terrestrial (lacustrine)	39.05	22.27	500	Bottema (1979)	ACER database*	ACER (file "dating_info_ACER)*
Megali Limni	12	Terrestrial (lacustrine)	39.1	26.32	323	Margari et al. (2009)	ACER database*	ACER (file "dating_info_ACER)*

Table 2.2 Assignments used for the PFTs. Codes in green represent arboreal PFTs while those in brown represent non-arboreal PFTs.

Codes	PFTs	Taxa included in PFTs
EC	Eurythermic conifer	*Pinus, Pinus* subgen. *Diploxylon*
ECPI	Eurythermic conifer/Pioneer	*Juniperus*
BS	Boreal summergreen	*Larix*
PI	Pioneer	*Betula*
BEC	Boreal evergreen conifer	*Picea, Pinus* subgen. *Haploxylon*
BCTC	Boreal evergreen/cool-temperate conifer	*Abies*
CTC1	Intermediate temperate conifer	*Cedrus, Taxus*
TSAA	Temperate/boreal summergreen/arctic-alpine	*Alnus, Salix*
TSBS	Temperate/boreal summergreen	*Populus*
TS	Temperate summergreen	*Acer, Fraxinus, Fraxinus excelsior, Quercus* (deciduous)
TS1	Cool-temperate summergreen	*Carpinus, Corylus, Fagus, Frangula, Tilia, Ulmus*
TS2	Warm-temperate summergreen	*Castanea, Fraxinus ornus, Juglans, Ostrya, Platanus,* Rhamnaceae, *Vitis*
WTE	Warm-temperate broad-leaved evergreen	*Quercus* (evergreen)
WTE1	Cool-temperate broad-leaved evergreen	*Buxus, Hedera, Ilex*
WTE2	Warm-temperate sclerophyll trees/shrub	*Acacia, Arbutus, Cistus, Mercuria,* Myrtaceae, *Olea, Phillyrea, Pistacia, Rhus*
AA	Arctic-alpine dwarf shrub	*Alnus fructicosa, Betula nana, Dryas, Empetrum, Rhododendron, Saxifraga, Vaccinium*
COGS	Cold grass shrub	*Hippophaë, Polygonum*
H	Heath	*Calluna,* Ericaceae
GR	Grass	Poaceae
WAGS	Warm grass shrub	Brassicaceae, *Ceratonia,* Crassulaceae, *Echium, Ephedra fragilis,* Fabaceae, *Galium,* Scrophulariaceae, *Zizyphus*
SF	Steppe forb/shrub	Apiaceae, *Armeria*, *Artemisia*, *Carduus*, Campanulaceae, Caryophyllaceae, *Centaurea*, Cyperaceae, Dipsacaceae, *Filipendula*, *Helianthemum*, *Plantago*, Plumbaginaceae, *Ranunculus*, Rosaceae, *Rosmarinus*, Rubiaceae, *Rumex*, *Sanguisorba*, *Thalictrum*, Urticaceae, *Viburnum*
SFDF	Steppe/desert forb/shrub	Boraginaceae, Compositae, Compositae *Tubuliflore,* Compositae *Liguliflore,* Zygophyllaceae
DF	Desert forb/shrub	Chenopodiaceae, *Ephedra, Ephedra distachya*

Figure 2.1 Map showing the location of the pollen data sites (numbered purple stars) used in this study (Table 2.1 and references therein) and of other sites referred to in the text (black dot). The main modern European biomes are defined by Olson et al. (2001). White areas represent the ice limits at the end of MIS 3 (around 30 ka) following Batchelor et al. (2019), except for the Alps and Pyrenees for which, in the absence of precise data for 30 ka, ice limits of the LGM are represented (Ehlers and Gibbard, 2004) (paleocoastlines not represented). The main modern surface currents and gyres are indicated as follows: Irminger Current (IC), North Atlantic Drift (NAD), East Greenland Current (EGC), Subpolar Gyre (SPG), Subtropical Gyre (STG).

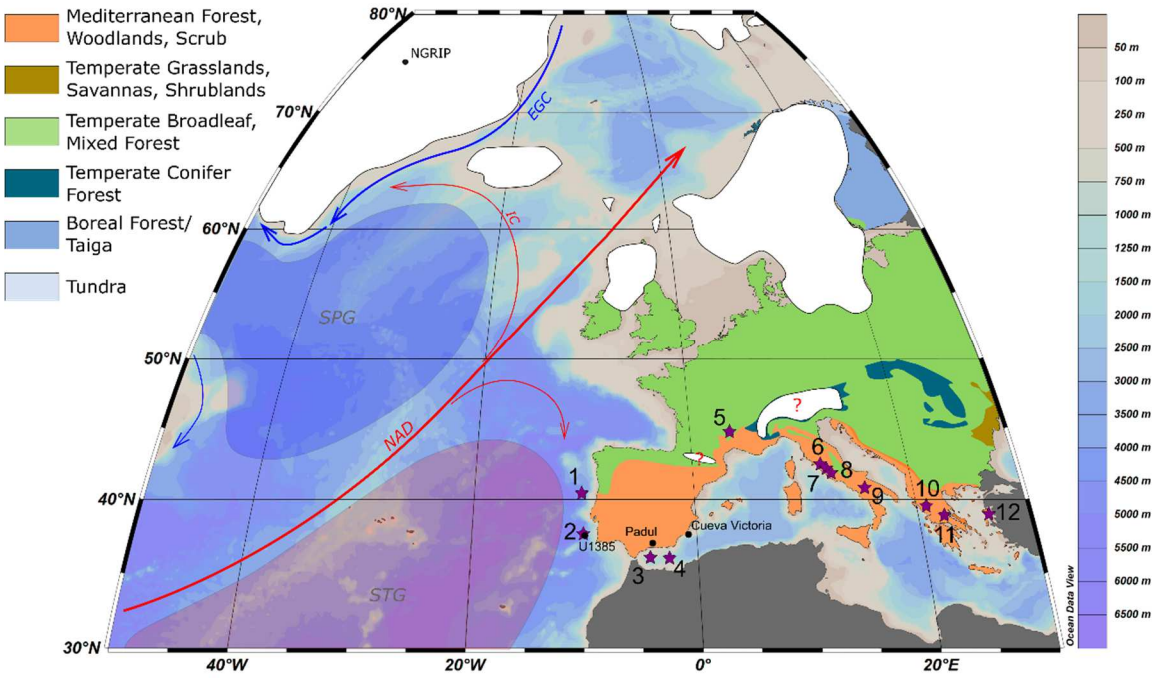

Figure 2.2 Results of the redundancy analysis (RDA) performed with MIS 3 data from a) marine core MD95-2042 (site 2 in Fig. 2.1), off Portugal (Sanchez-Goñi et al., 2000, 2002, 2008, 2009; Sanchez-Goñi, 2006) and b) terrestrial core Megali Limni (site 12 in Fig. 2.1), in Greece (Margari et al., 2009). Green and yellow arrows represent the arboreal and non-arboreal PFTs respectively (see Table 2.2 for further details on PFTs). Grey dashed arrows represent the climatic parameter discussed in this paper. Arrows pointing in the same/opposite direction indicate that they are positively/negatively correlated. The percentages along the axes indicate how much of the total variance they explain. Climatic parameters: Mean-temperature of the warmest (MTWA) and the coldest (MTCO) months; Summer (Pjja), Winter (Pdjf) Annual (Pann) precipitation; Seasonality (Season) = MTWA-MTCO.

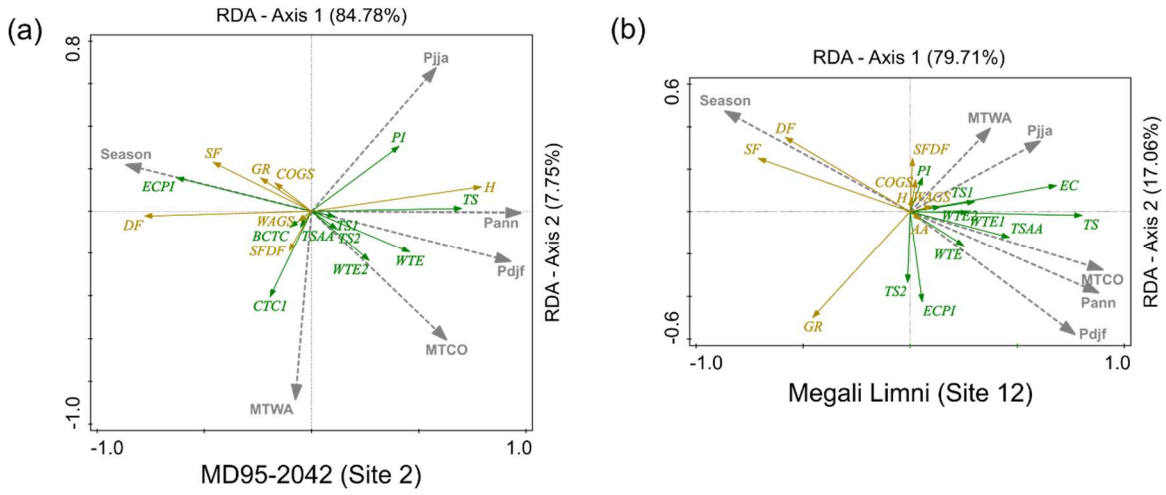

Figure 2.3 a) Time series encompassing MIS 3 showing the NGRIP oxygen isotopic data (NGRIP, 2004) and climate-related records from core MD2042 (site 2 in Fig. 2.1) : (from left to right) $\delta^{18}O$ of *Globigerina bulloides* (Gb) from Shackleton et al. (2000); MTCO (blue line) and MTWA (orange line); seasonality (difference between MTWA and MTCO); summer (orange line), winter (blue line) and annual precipitation (black line); square-chord distances of the 1st and 5th best analogues and analogue thresholds (see Material and Methods). Horizontal pink bars indicate the warm sea-surface phases defined after the $\delta^{18}O$ (Gb) record. b) Time series encompassing MIS 3 showing the NGRIP oxygen isotopic data (NGRIP, 2004) and climate-related records from Megali Limni (site 12 in Fig. 2.1): (from left to right) RDA axis-1 scores (with number of samples (n) for each side; MTCO (blue line) and MTWA (orange line); seasonality (difference between MTWA and MTCO); summer (orange line), winter (blue line) and annual precipitation (black line); square-chord distances of the 1st and 5th best analogues and analogue thresholds (see Chapter 2.3.3). Dashed vertical color lines in represent the mean 1901-2022 climate values (see Chapter 2.3.3.4). Horizontal green bars indicate the phases of arboreal increase defined after the RDA axis-1 scores.

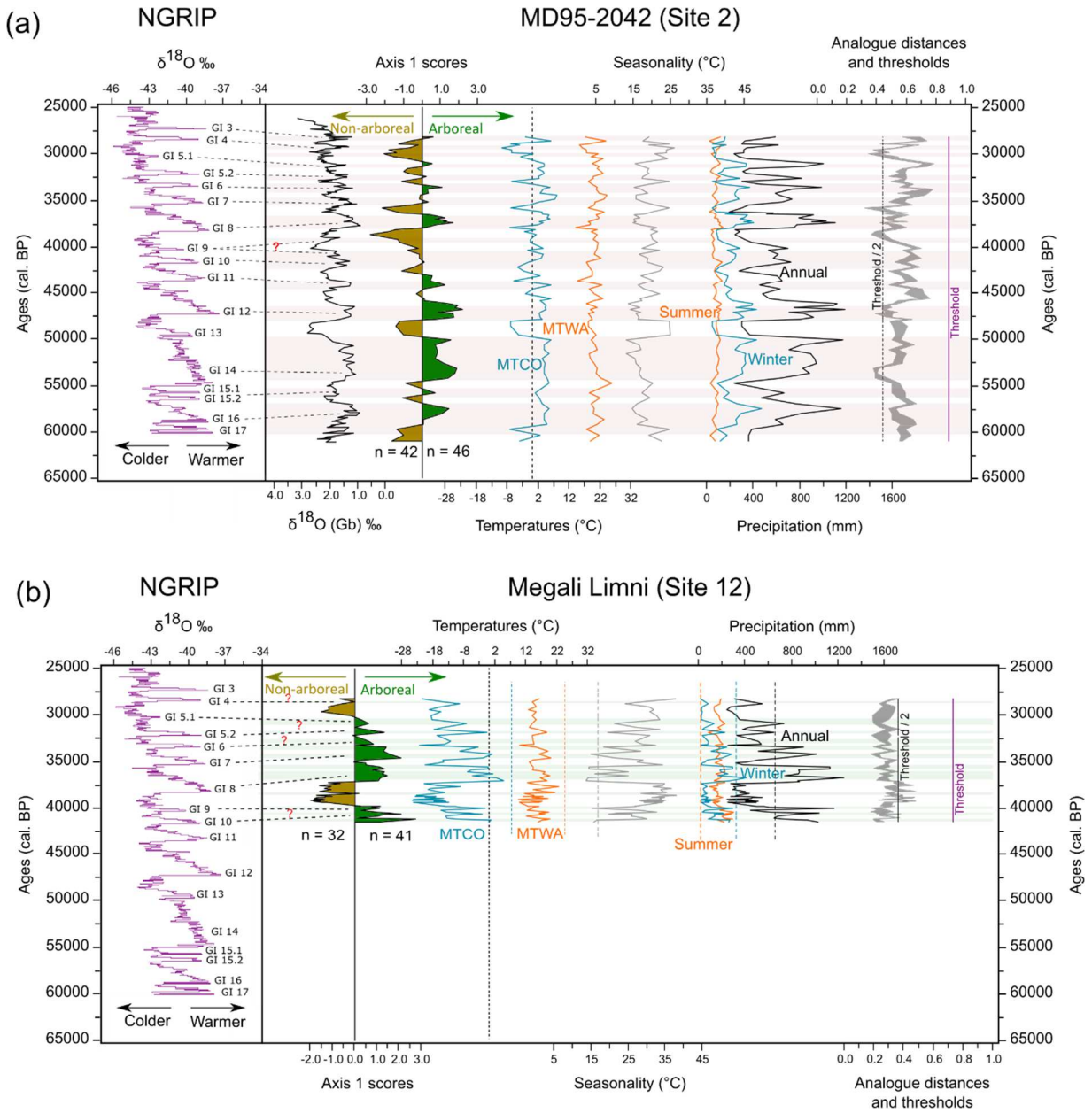

Figure 2.4 Difference between mean climatic values associated with arboreal (GIs) and non-arboreal (GSs) sides of the axis-1 scores for each marine (light blue) and terrestrial (light green) site (Figs. 2.1-2.3; Figs. 2.S1-2.S12). When the bars are full, GI values (upper limit of the bar) > GS values (lower limit of the bar). When the bars are empty, GS values (upper limit of the bar) > GI values (lower limit of the bar).

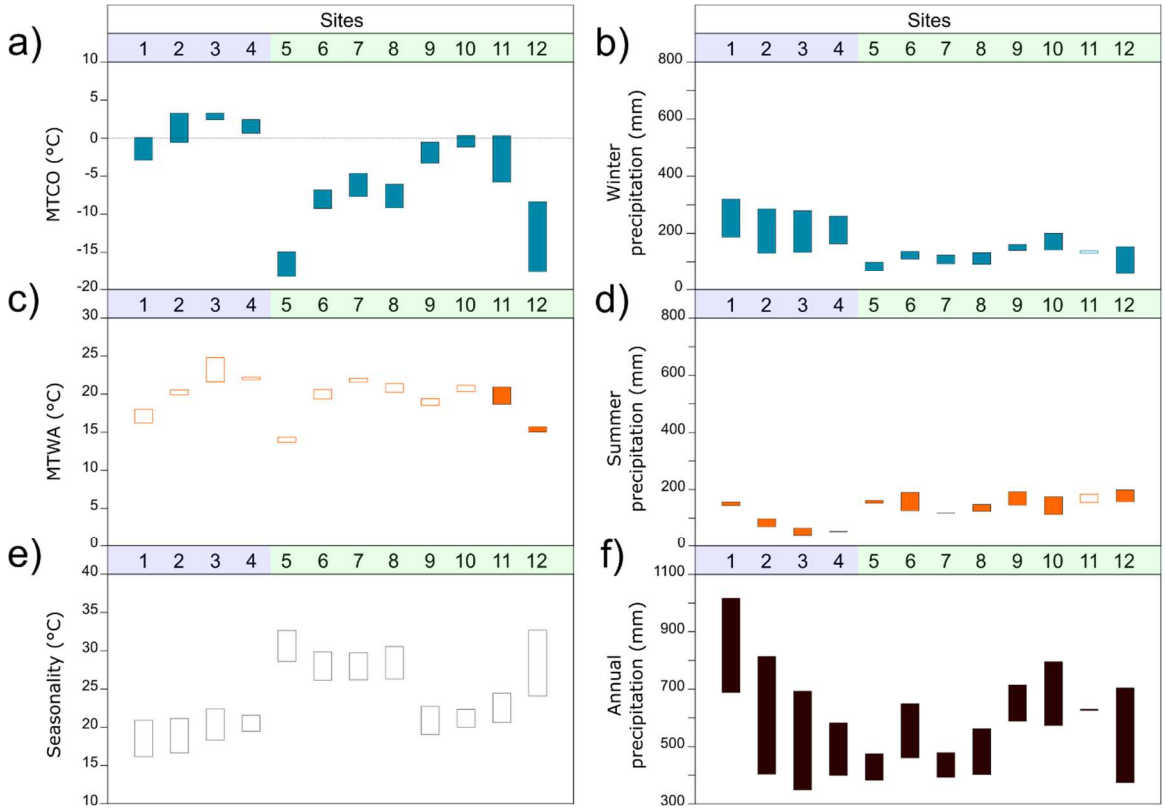

Figure 2.5 Conceptual scheme of seasonal climate and vegetation during GSs and GIs. Conifer-like tree symbols illustrate a majority of conifers or pioneers in the arboreal vegetation (whether it be from boreal forests or eurythermic conifer forests). The presence of deciduous (oak-like symbols) indicates a high proportion of temperate trees in the arboreal vegetation. Herb-like symbols indicate the presence of non-arboreal vegetation (green symbols for grass and yellow symbols for steppe forb/desert forb/shrub). NAD: North Atlantic Drift; NAO: North Atlantic Oscillation; SPG: Subpolar Gyre; SSTs: Sea-Surface Temperatures. White areas: ice limits at the end of MIS 3 (around 30 ka) following Batchelor et al. (2019), except for the Alps and Pyrenees for which, in the absence of precise data for 30 ka, ice limits of the LGM are represented (Elhers and Gibbard, 2004) (paleocoastlines not represented). Red solid arrow: the NAD flows at the surface; Red dashed arrow: the NAD flows under the freshwater lid (eastward extended SPG). The extent of the sea-ice cover is not illustrated, hence the question marks.

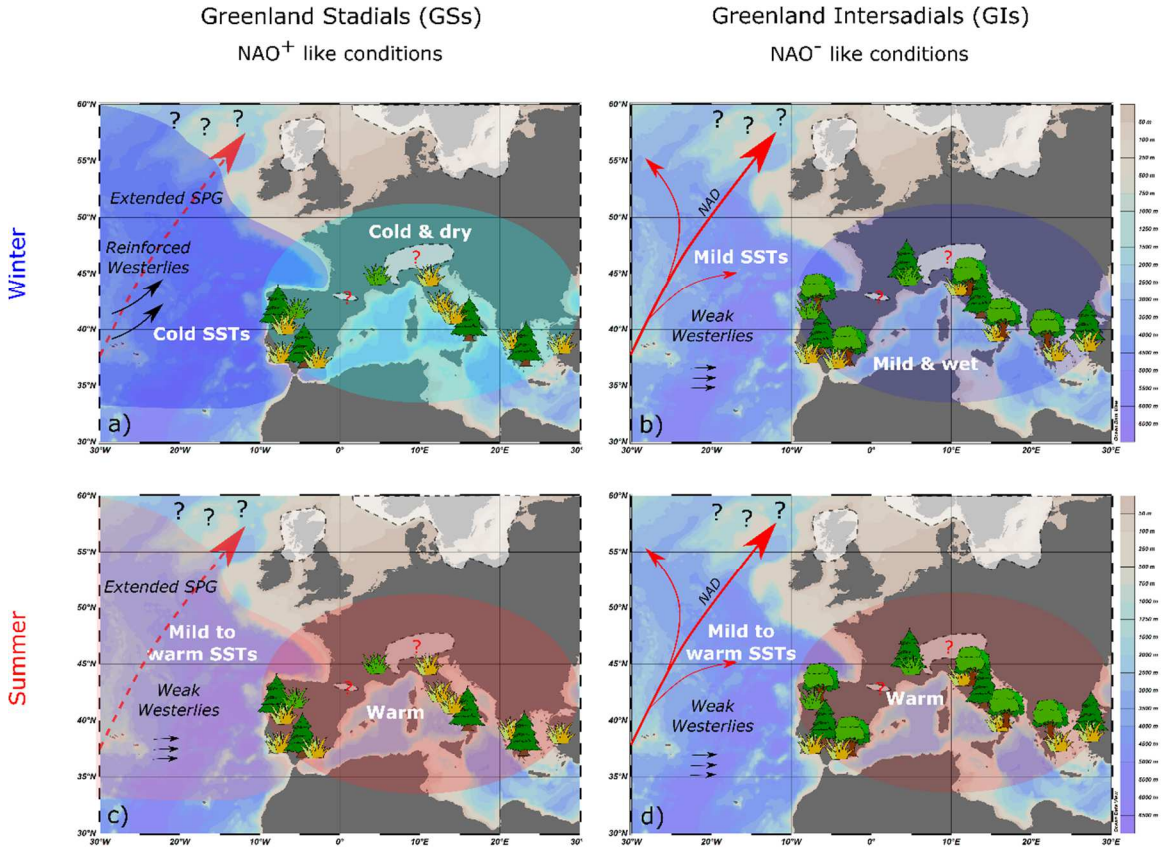

2.8 SUPPLEMENTARY INFORMATION

Detailed methodology

2.8.1 Modern Analogue Technique (MAT): Theory, limitations and relevance

Climate parameters were reconstructed from pollen data using the Modern Analogue Technique (MAT) (Overpeck et al. 1985; Guiot, 1990). MAT is based on the principle that the ecological affinities of the different species have not changed through time (Jackson and Overpeck, 2000), which is also named niche conservatism (Wiens et al., 2010) or uniformitarian principle (Chevalier et al., 2020). MAT principally compares a fossil pollen assemblage to all modern pollen assemblages within a given geographic area. This similarity assessment between fossil (*i*) and modern (*j*) pollen assemblages is based on the squared chord distance (SCD) (d^2) dissimilarity metric (Overpeck et al., 1985) which can be computed using the following formula:

$$d_{ij}^{2} = \sum_{k=1}^{m} (\sqrt{P_{ik}} - \sqrt{P_{jk}})^2 \qquad (1)$$

Where *m* is the number of taxa and *P* is the relative frequencies (percentage values) for each taxon (k = 1−m). The square-root transformation reduces the weight of ubiquitous taxa that are usually very abundant and increases the weight of underrepresented taxa. The equation (1) also shows the dependence between SCD and the number of pollen taxa (Sawada et al., 2004).

The SCD values vary between 0 and 2. Low values indicate a high degree of similarity between two samples, whereas high values indicate large dissimilarity. The modern samples presenting the lowest SCD are thus selected as the best analogues, and the weighted average of their climate parameter values is calculated to provide past climatic conditions. The number of analogues retained for interpolation of climate data is set usually from 5 to 10 depending on the studies and the software/script used (e.g., Sawada et al., 2004; Fréchette et al., 2008; Dugerdil et al., 2021).

There are situations, however, characterized by poor or no modern analogues (e.g., Ortu et al., 2006). Such situations can be due, for example, to anthropogenic disturbance of the ecosystems, different climatic configurations (low atmospheric CO_2 concentration, unique combination of seasonal irradiance, unprecedented speed of climate changes, lack of modern samples from some ecosystems, etc). To assess the "quality" of the analogues, an SCD threshold beyond which any analogue is rejected is calculated with a Monte-Carlo approach. Distance vectors are calculated between one modern spectrum randomly selected and each of the remaining modern spectra. The operation is repeated 1000 times and the final threshold is defined as the first quartile for these 1000 values (Guiot and de Vernal., 2007). In this work, we followed the approach adopted by de Vernal et al. (2005) who defined a reliability index with three categories: 1) Poor or no analogue situation when the SCD of the closest analogue is higher than the SCD threshold, 2) Acceptable analogue situation when the SCD is between half of the threshold value and the threshold, and 3) Good analogue situation when the SCD is between 0 and half of the threshold value.

Model performances are assessed mostly based on two indicators that are calculated from different cross-validation tests, with a subset of the modern dataset used for calibration and another for prediction (see Chevalier et al. (2020) for more details). One indicator is the coefficient of correlation (R^2) between estimated and observed climatic values. The other indicator is the root mean square error of prediction (RMSEP), which also corresponds to the deviation standard of the difference between observed and reconstructed values (Guiot and de Vernal., 2007). With MAT, a measure of the uncertainty can also be given from the climatic dispersion of the selected closest modern analogues for a target sample (Guiot, 1990).

A remaining issue debated in the community is spatial autocorrelation (Telford and Birks, 2005, 2009, 2011; Guiot and de Vernal, 2011a, 2011b; Birks et al., 2010; Chevalier et al., 2020), which relates to the fact that sites geographically close to each other tend to be more similar than randomly selected sites. Many authors, notably Telford and colleagues (Telford and Birks, 2005, 2009, 2011), argue that spatial autocorrelation biases the evaluation of MAT performance, making it look better than it is. They consider MAT to be oversensitive to spatial autocorrelation and to select analogues geographically close to the target sample, resulting in over-optimistic estimates of the errors. They also show that MAT performance decreases significantly when prevented from selecting geographically close analogues (Telford and Birks, 2011). Regardless of the issue of spatial autocorrelation, the important question is the ability of the approach to make sensible reconstructions. In other words, is MAT working or not? As mentioned before,

MAT like most models leading to climate reconstruction uses reference ecological data sets and is based on the principle that ecological affinities of species have not changed through time (Jackson and Overpeck, 2000). It also means that they do not change through space either providing the ecological properties are the same. Since climate is a large-scale phenomenon and vegetation intimately depends upon climate, one might expect that geographically close modern pollen samples, under very similar climatic conditions, present similar assemblages. The high values of R^2 for many climatic parameters that are often calculated on large modern pollen databases (e.g., Fréchette et al., 2008; Dugerdil et al., 2021; Davis et al., 2022) illustrate the spatial consistency of climate (Guiot and de Vernal, 2011a). Positive spatial autocorrelation is thus a property of most ecological data (Legendre, 1993) and a basis on which climate reconstruction models are built. However, it indeed can impact performance indicators. For example, in validation runs, if we have X analogues with a high distance to the target samples but with a small distance to each other, the "error" (RMSE or RMSEP) will be small (little spread between the analogues), but the results won't be accurate (Chevalier et al., 2020). On the other hand, if X analogues spatially close to the target sample are selected and the SCDs indicate good or acceptable analogue situations (cf. de Vernal et al., 2005), the estimate is correct and the approach performs at its best. Preventing selection of spatially close modern analogue would thus necessarily deteriorates the performances. This highlights the necessity of a modern database that covers the widest possible range of ecological configurations, hence the recent works to grow the reference modern pollen databases that should highly improve MAT results (e.g., Davis et al., 2020). But most importantly, it emphasizes the importance of always taking into account the SCDs of the selected analogues whenever a MAT reconstruction is made.

As an approach for paleoclimate reconstruction, MAT remains one of the most robust methods regarding paleoclimate reconstructions, as long as the following conditions are met: 1) a modern pollen database covering the widest possible range of ecological configurations, 2) high R^2(P) and low RMSEP, 3) good analogue situations with low SCD, 4) strong relationships between pollen assemblages and climatic parameters to estimate. This last point is particularly important and will be addressed in the next section. Lastly, although MAT is reliable for climatic reconstructions, confrontation with other paleoclimatic proxy records is always relevant (cf. Chevalier et al., 2020 and references therein).

2.8.2 Significance of pollen assemblages in terms of climate

MAT as any other model of climate reconstruction relies on the assumptions that the fossil assemblage is related to climate and that the ecological affinities of the taxa have remained unchanged through time, according to the uniformitarian principle (Juggins, 2013; Chevalier et al., 2020).

Pollen assemblages do not straightforwardly reflect the associations in the surrounding vegetation. The differences between the pollen representation of taxa in the source vegetation can be due to several factors. They include pollen productivity rates that differ from one taxon to another, the mechanisms of pollen transports (wind, rivers, animals) and the potential of wind transport depending upon the height of the inflorescence and pollen morphology, and differential pollen grain preservation, in addition to the depositional environment and related-processes, not to mention microclimates and anthropogenic activities (cf. Fréchette et al., 2018; Chevalier et al., 2020; Robles et al., 2022 and references therein). Among these factors, some bring more uncertainties than others.

Some studies about the variation in pollen productivity (e.g., Broström et al., 2008; Theuerkauf et al., 2015) concluded that a taxon like *Poaceae* can have pollen productivity differences depending upon the species. But a specific species can also present different pollen productivity depending on whether it is located in the middle (optimum climatic conditions) or at the edge of its geographical distribution (Broström et al., 2008). Very little is known about the link between pollen productivity of given species and climate. For example, lower concentrations of atmospheric CO_2 during glacial times impacted vegetation distribution and net primary production (Martin Calvo and Prentice, 2015) but did it also affect productivity rates of pollen species? Unfortunately, such information is not currently available.

Pollen preservation is also a source of uncertainties. Studies (Havinga, 1967; Li et al., 2005) have shown that differences in sporopollenin content or thickness and ornaments of the pollen walls play an important role in the potential of pollen preservation. The pH of soils, oxidation and degradation are also important and depend upon the nature of soils as well as climate. This is why a high proportion of pollen grains is lost from surface sediments to deeper buried levels (Li et al., 2005). Because the potential of pollen preservation is different from one species to another, we can question the representativeness of ancient pollen assemblages, and that is why comparison with non-pollen-based climatic reconstructions must always be encouraged.

Because human activities (e.g., deforestation, agriculture) have altered the natural vegetation distribution (Theuerkauf et al., 2015; Marchant et al., 2018; Robles et al., 2022) for a long time over Europe (e.g., Giesecke et al., 2019), concerns have also been raised about the relationship between climate and recent pollen assemblages (St. Jacques et al., 2015) and thus on the capability of pollen-based models to accurately reconstruct climate. Nevertheless, comparisons of pollen-based climatic reconstructions with other source of climate information support the reliability of pollen-based models (e.g., Mauri et al., 2015). Here again, multi-technique or multi-proxy climatic reconstructions to cope with the inherent uncertainties of pollen-based models appear highly relevant.

2.8.3 Climate reconstruction in marine cores

The deposition environment and processes are important parameters in the redistribution of pollen (Chevalier et al., 2020). Modern pollen samples in our final version of the EMPD2 are all terrestrial since we removed the marine ones, which could not have a climatic assignment (see Davis et al., 2020). Terrestrial modern samples are retrieved from various environments such as mosses and peatlands, lake sediment, soil, etc. Small lakes or small peatlands usually record a more local signal while larger lakes integrate local and regional vegetation. Marine sediments record regional vegetation of the adjacent continent since no pollen is locally produced (Turon, 1984; Naughton et al., 2007; Sánchez Goñi et al., 2018). Pollen in marine sediment principally results from long-distance transport by wind and rivers, the contribution from oceanic currents being negligible (Koreneva, 1966). However, we may question to what extent marine pollen assemblages can represent the adjacent continental vegetation.

Pollen grains are transported through different mechanisms (wind, rivers, animals) and preservation may vary from one taxon to another. In marine cores collected more than 300 km offshore, it has been shown that pollen transport is mainly aeolian and input from rivers is weak (e.g., Hooghiemstra et al., 2006), thus leading to potential biases due to differential wind transport of pollen taxa. However, the marine cores used in this study are all located less than 150 km offshore (Fig. 2.1; Table 2.1 and references therein). Some cores are situated on the Western Iberian margin where a well-developed hydrographic system results in large pollen inputs from fluvial transport (Naughton et al., 2007). The others are located off the Southeastern Iberian Margin, in the Alboran Sea, where there is no major river system. Nevertheless, local torrential rains may generate large riverine inputs to the Alboran Sea, whereas aeolian lithogenic particles only represent 12% of the total particle supply (Fabres et al., 2002). It thus implies that the main pollen contribution to these sites likely comes from the adjacent riverine system (Sánchez Goñi

et al., 2002). Furthermore, even if pollen of nearshore marine settings essentially comes from fluvial and/or riverine transport, pollen input related to wind contribution is not negligible. Hence selective pollen transport by wind results in the overrepresentation of some pollen taxa, notably *Pinus* (Connor et al., 2004), which can be transported over very long distances and is produced in large quantities (Li et al., 2005). *Pinus* can dominate pollen assemblages even when not present in the local environment (Campbell et al., 1999). This is especially the case in marine cores, in which *Pinus* is largely overrepresented (Heusser and Balsam, 1977; Turon, 1984). Finally, there are also concerns about the diversity of species, which is supposedly very low in marine sediment compared to terrestrial samples. Despite the impact of distal transport and overrepresentation of *Pinus*, several studies conducted in Western Europe and the Mediterranean region demonstrated that pollen assemblages in nearshore marine settings reflect the regional vegetation allowing comparisons with terrestrial pollen assemblages of the adjacent continent (Sánchez Goñi et al., 2018 and references therein).

The use of marine sedimentary sequences for inferring continental paleoclimate parameters is still highly debated (e.g., Sánchez Goñi et al., 2018; Chevalier et al., 2020; Davis et al., 2022). Detractors (e.g., Birks et al., 2010) stated that fossil and modern pollen samples should originate from comparable sedimentary environments to assume identical linkages between pollen and climate. Others on the other side have addressed this issue and demonstrated a strong concordance between marine and terrestrial pollen spectra of the adjacent landmasses (Sánchez Goñi et al., 2018 and references therein), acknowledging however an overrepresentation of *Pinus*.

To cope with the issue of *Pinus* overrepresentation, some authors (e.g., Sánchez Goñi et al., 2002; Combourieu-Nebout, 2009) have excluded *Pinus* from the fossil spectra and from the modern pollen database to apply MAT for quantitative reconstruction. However, it was argued that this removal might generate significant biases (e.g., Davis et al., 2022) because *Pinus* was the most abundant tree taxon in Southwestern Europe during the last glacial with important climatic significance (García-Amorena et al., 2007). Moreover, by removing *Pinus*, pollen sums lower than 100 are problematic in many samples, which do not meet quality criteria and are often removed from the datasets (see Material and Methods). Therefore, there are arguments in favour and against removing *Pinus* from the pollen sum.

2.8.3.1 Tests based on results from marine core MD95-2042

In this study, we feel confident with the representativeness of the pollen assemblages from the nearshore marine cores we are using. The counts are high enough (> 100 (excluding *Pinus*)), and the diversity of species, which is generally very low in marine sediment, is comparable with that of terrestrial sequences (Table 2.S6). For reconstructions, we decided to test the MAT approach with and without *Pinus* using the data from the marine core MD95-2042 (Sánchez Goñi et al., 2000, 2008, 2009), located near the southwestern margin of the Iberian Peninsula (Fig. 2.1; Table 2.1). The reconstructions are compared to sea-surface temperature estimates from the same core (Shackleton et al., 2000). Marine cores indeed provide the opportunity to make direct land-sea correlation (Roucoux et al., 2005; Sánchez Goñi et al., 2002, 2008, 2009), and to develop a chronology based on stable oxygen isotope records in foraminifera, which can be correlated with the Greenland Ice core stratigraphy (Kissel et al., 1999; Austin and Hibbert, 2012). The MIS 3 section in core MD95-2042 shows very high percentages of *Pinus* up to 94.7%, with a mean of 82.6 ± 7.1%. As mentioned above, the application of MAT after the exclusion of *Pinus* requires removing *Pinus* from the modern pollen database and recalculating percentages. Since modern samples with a pollen sum excluding *Pinus* <100 grains were already removed from the database, this version of the database with 87 taxa comprises the same number of modern samples (i.e., 7634 sites). Validation tests with and without *Pinus* (87 or 88 taxa) yield comparable results, with slightly higher RMSEP for the without *Pinus* version (see Table 2.S5).

Figure 2.S14 shows the MAT reconstructions from core MD95-2042, with and without *Pinus*, compared to the $\delta^{18}O$ of G. *bulloides* (Shackleton et al., 2000), which is interpreted as a proxy of sea-surface temperature (Malevich et al., 2019). The MAT curves are different, with much larger variations without *Pinus*. In both cases, however, winter temperatures depict larger variations than summer temperatures, with the cold winter phases corresponding to Greenland Stadials (GSs) identified from the $\delta^{18}O$ record (Austin and Hibbert, 2012). The cooling pulses are clear for every GSs in the reconstructions without *Pinus* and appear more subtle in the reconstructions with *Pinus*. Summer temperatures remained relatively unchanged throughout MIS 3 regardless of the approach and do not necessarily follow winter temperature variation. This is particularly visible for Heinrich Event 5 (HE5) (between GI 13 and GI 12; Fig. 2.S14) characterized by an important cooling of more than 10°C in winter temperatures whereas summer temperatures do not depict any change. As a consequence of summer temperature stability and high winter variability, seasonality shows more variability in the reconstruction without *Pinus*, with high values recorded during all GSs.

The largest differences in the reconstructions with and without *Pinus* are seen in the precipitation (Figs. 2.S14A and 2.S14B). In both cases, summer precipitation remains low with little changes throughout the record, contrary to the annual and winter precipitation. However, estimates without *Pinus* (Fig. 2.S14B) are characterized by much larger winter and annual precipitation with high values during all Greenland Interstadial phases (GIs) and significant drops during all GSs. In comparison, winter and annual precipitation reconstructed with *Pinus* (Fig. 2.S14A) depicts low amplitude variations of winter precipitation during most MIS 3.

To decipher which is the most correct reconstruction is an important question. The cross-validation test showed similar performance with both datasets (with and without *Pinus*), with slightly lower RMSEP with *Pinus* (Table 2.S5). The SCD values may, however, help us to discriminate which reference data to use (see Chapter 2.8.1) as the quality of analogues is much better with *Pinus* (Figs. 2.S14A and 2.S14B). Based on this criterion, we should opt for keeping *Pinus* in our MAT reconstructions from marine cores.

There are, however, some counterarguments. Given the very high percentages of *Pinus* in core MD95-2042, and thus low percentages of other taxa, low SCD values are expected as long as analogues have a very close percentage of *Pinus*. Taking into consideration the 88 fossil pollen samples of the MIS 3 section in core MD95-2042 and that 5 analogues are retained for each fossil sample, there is a maximum possibility of 440 analogues to be selected among the 7634 modern samples in the database. A total of 30 modern samples, belonging to three different biomes (temperate broadleaf and mixed forests; Mediterranean forests, woodlands and scrubs; Boreal forests / Taiga), were selected. These samples have high percentages of *Pinus* as well, comparable to those in core MD95-2042, which explains the low SCDs. It is also worth noting that without *Pinus*, among 440 possible analogues, 88 were retained, which is almost three times more analogues than when we keep *Pinus*. These 88 modern analogues belong to seven biomes, out of the 9 included in the EMPD2. This explains the larger dispersal of reconstructions when excluding *Pinus*.

Should we favour an approach that focuses on the relative abundance of a dominant and cosmopolitan taxon or an approach that excludes this overrepresented taxon to focus on the relative abundances of the rest of the assemblage, which might be more sensitive to climate? How to distinguish which part of these fossil pollen spectra bears the most representative climate signature? A closer look at

our MAT reconstructions and the literature might help us disentangle these issues. First, the comparison of MAT reconstructions (Fig. 2.S14) with the $\delta^{18}O$ record of *G. bulloides* (Shackleton et al., 2000) shows variations similar to winter temperatures and precipitation reconstructed without *Pinus*. Second, when *Pinus* is included (Fig. 2.S14A), annual precipitation remains high throughout MIS 3, with very few low values below 600 mm. Even HE4 (between GI9 and GI8), which is supposedly one of the most extreme events of MIS 3 in the North Atlantic and European continent (e.g., Hemming, 2004; Sepulchre et al., 2007; López-García et al., 2013), is only marked by slight decreases in annual precipitation and winter temperatures (Fig. 2.S14A). Such high precipitation values could not explain the ecological stress (cf. Tzedakis et al., 2004) necessary for the major changes recorded in the regional vegetation based on terrestrial pollen sequences (e.g., Guiot et al., 1993; Carrión and van Geel, 1999; Camuera et al., 2019), especially without important drops in temperatures (Fig. 2.S14A). High precipitation values do not echo either the pronounced episodes of dryness inferred from speleothems of Southwestern France (Genty et al., 2003, 2010). Conversely, the significant decrease in winter and annual precipitation during GSs in reconstructions without *Pinus* (Fig. 2.S14B), along with more pronounced winter cooling (Fig. 2.S14B) could have triggered the climate deteriorations recorded regionally (e.g., Guiot et al., 1993; Carrión and Van Geel, 1999; Genty et al., 2010; Budsky et al., 2019; Camuera et al., 2019).

We conclude that despite statistically better MAT results with *Pinus*, a deeper examination of the reconstructions and comparison with regional data suggest that removing *Pinus* from the dataset permits to better capture the climate changes. However, because of the weak analogue situation, results should be handled with caution.

Table 2.S1 Mean temporal resolution of the pollen records included in this study (Fig. 2.1; Table 2.1).

Site name	Code	Mean temporal resolution (yrs)	Standard deviation (yrs)
MD95-2039	1	289	150
MD95-2042	2	376	178
ODP Site 976	3	247	215
MD95-2043	4	291	220
Lac du Bouchet	5	129	21
Lagaccione	6	445	339
Stracciacappa	7	396	183
Valle di Castiglione	8	471	292
Lago Grande di Monticchio	9	193	156
Ioannina	10	273	69
Lake Xinias	11	420	104
Megali Limni	12	183	130

Table 2.S2 (also next page). List of the 88 pollen taxa retained in the data set with 7634 sites.

Taxa	Code	N (sites)	Range of %	Mean % ± SD	Median %
Trees+shrubs					
Acer	AACER	1064	0,02 - 30,58	0,80 ± 2,29	0,26
Anacardiaceae	ANACA	69	0,02 - 9,77	0,75 ± 1,72	0,22
Pistacia	APISTA	668	0,03 - 51,82	1,78 ± 4,14	0,45
Hedera	AHEDE	342	0,02 - 22,07	0,74 ± 1,81	0,30
Ilex	AILEX	231	0,01 - 51,13	2,57 ± 7,17	0,34
Alnus	BALBU	6362	0,02 - 96,44	6,62 ± 9,98	2,79
Betula	BBETU	5951	0,03 - 93,96	17,01 ± 17,44	10,54
Carpinus/Ostrya	BCARP	2661	0,03 - 70,36	2,99 ± 6,40	0,85
Corylus	BCORY	4159	0,03 - 69,71	2,08 ± 3,50	1,06
Buxus	BBUXU	243	0,03 - 20,45	0,63 ± 1,94	0,26
Caprifoliaceae	CAPRI	997	0,04 - 54,34	0,73 ± 2,37	0,29
Cistus	CCIST	621	0,03 - 40,56	2,00 ± 3,97	0,68
Helianthemum	CHELI	627	0,03 - 13,04	0,60 ± 0,93	0,33
Cornus	CCORN	146	0,02 - 3,31	0,35 ± 0,51	0,21
Cupressaceae	CUPRE	3166	0,01 - 98,12	2,79 ± 6,19	0,91
Hippophae	EHIPP	122	0,00 - 5,77	0,53 ± 0,85	0,29
Ephedra	EEPHE	623	0,01 - 70,90	1,17 ± 5,23	0,27
Ericaceae	ERICA	3991	0,01 - 74,29	3,58 ± 7,56	0,87
Calluna	ECALL	1623	0,01 - 73,27	4,10 ± 9,36	0,63
Ceratonia	FCERA	38	0,08 - 23,94	1,93 ± 4,87	0,35
Quercus deciduous	FQDEC	5057	0,02 - 92,24	7,07 ± 11,83	2,62
Quercus evergreen	FQEVE	1690	0,06 - 97,70	10,90 ± 17,81	3,03
Castanea	FCAST	1857	0,03 - 90,29	2,52 ± 8,07	0,63
Fagus	FFAGU	2777	0,03 - 77,55	5,19 ± 8,85	1,90
Juglans	JJUGL	1812	0,01 - 82,23	0,98 ± 4,28	0,30
Myricaceae	MYRIC	318	0,06 - 62,12	3,25 ± 7,77	0,73
Myrtaceae	MYRTA	258	0,02 - 40,84	1,22 ± 4,27	0,31
Oleaceae	OLEAC	406	0,01 - 68,18	0,77 ± 3,50	0,32
Olea	OOLEA	1986	0,03 - 83,88	4,72 ± 9,59	1,29
Phillyrea	OPHIL	636	0,05 - 62,62	1,59 ± 3,96	0,56
Fraxinus	OFRAX	2920	0,03 - 66,39	1,31 ± 3,25	0,49
Abies	PABIE	2599	0,00 - 74,17	2,51 ± 6,06	0,61
Picea	PPICE	4461	0,01 - 84,22	7,85 ± 11,77	2,81
Cedrus	PCEDR	358	0,04 - 89,40	11,95 ± 23,63	0,81
Larix	PLARI	1604	0,04 - 44,00	2,31 ± 4,08	0,92
*Pinus***	PPINU	7265	0,04 - 93,24	23,77 ± 20,37	18,25
Platanus	PPLAT	487	0,03 - 55,79	1,63 ± 4,99	0,33
Rhamnaceae	RHAMN	561	0,01 - 85,07	0,76 ± 3,88	0,23
Populus	SPOPU	845	0,02 - 19,44	0,66 ± 1,43	0,28
Salix	SSALI	4714	0,01 - 66,67	1,75 ± 4,46	0,57
Tamarix	TTAMA	100	0,06 - 39,18	2,47 ± 5,70	0,64
Taxus	TTAXU	184	0,00 - 95,34	3,88 ± 14,41	0,29
Daphne	TDAPH	173	0,03 - 11,85	0,92 ± 1,72	0,36
Tilia	TTILI	1731	0,02 - 47,97	0,74 ± 2,31	0,28
Celtis	UCELT	36	0,01 - 16,14	0,68 ± 2,62	0,18
Ulmus	UULMU	2539	0,01 - 54,19	0,79 ± 2,25	0,33
Vitis	VVITI	515	0,01 - 37,59	0,69 ± 2,97	0,24

Taxa	Code	N (sites)	Range of %	Mean % ± SD	Median %
Herbs					
Amaranthaceae	AMARA	5216	0,02 - 91,78	3,29 ± 9,51	0,62
Apiaceae	APIACE	3853	0,02 - 52,79	1,13 ± 2,69	0,42
Liguliflore	ALIGU	3890	0,02 - 61,01	2,34 ± 4,89	0,65
Tubuliflore	ATUBU	5604	0,03 - 63,93	1,97 ± 4,16	0,71
Artemisia	AARTE	5508	0,02 - 99,83	3,33 ± 8,31	0,81
Centaurea	ACENTA	1131	0,01 - 17,21	0,64 ± 1,24	0,29
Boraginaceae	BORAG	778	0,00 - 24,53	0,88 ± 1,87	0,36
Brassicaceae	BRASS	3619	0,03 - 56,25	1,04 ± 2,09	0,51
Campanulaceae	CAMPA	772	0,00 - 16,17	0,53 ± 1,23	0,26
Caryophyllaceae	CARYO	3559	0,01 - 43,28	0,92 ± 2,11	0,41
Convolvulaceae	CONVO	239	0,01 - 30,17	0,58 ± 2,23	0,24
Crassulaceae	CRASS	414	0,03 - 13,33	0,63 ± 1,32	0,30
Cyperaceae	CYPER	5801	0,01 - 82,38	5,12 ± 9,26	1,45
Dipsacaceae	DIPSA	469	0,01 - 13,64	0,46 ± 0,82	0,26
Euphorbiaceae	EUPHO	634	0,00 - 78,38	0,87 ± 3,58	0,28
Fabaceae	FABAC	3147	0,01 - 62,82	1,28 ± 3,13	0,47
Gentianaceae	GENTI	322	0,01 - 4,48	0,44 ± 0,57	0,26
Geraniaceae	GERAN	488	0,03 - 18,67	0,49 ± 1,31	0,24
Lamiaceae	LAMIA	1830	0,01 - 40,82	0,94 ± 2,00	0,37
Liliaceae	LILIA	1046	0,00 - 19,10	0,63 ± 1,20	0,34
Asphodelus	LASPH	228	0,03 - 15,48	0,88 ± 1,41	0,47
Onagraceae	ONAGR	444	0,00 - 75,77	0,87 ± 4,13	0,26
Papaveraceae	PAPAV	383	0,00 - 17,67	0,91 ± 1,72	0,29
Plantaginaceae	PLANT	4498	0,03 - 66,69	1,88 ± 3,98	0,80
Plumbaginaceae	PLUMB	226	0,03 - 11,89	0,92 ± 1,47	0,35
Poaceae	POACE	7347	0,04 - 92,86	12,74 ± 13,39	8,04
Polemoniaceae	POLEM	160	0,06 - 75,98	5,76 ± 12,03	0,67
Rumex/Oxyria	PRUME	4331	0,01 - 63,01	1,50 ± 3,77	0,67
Polygonum	PPOLY	1230	0,01 - 43,41	0,79 ± 2,19	0,30
Primulaceae	PRIMU	573	0,01 - 41,02	0,59 ± 1,85	0,25
Ranunculaceae	RANUN	4147	0,02 - 56,81	1,20 ± 2,57	0,55
Thalictrum	RTHAL	1224	0,01 - 21,88	0,70 ± 1,69	0,29
Rosaceae	ROSAC	4767	0,01 - 35,67	1,31 ± 2,43	0,60
Sanguisorba	RSANG	809	0,02 - 46,02	1,03 ± 3,71	0,29
Rubiaceae	RUBIA	2089	0,00 - 36,07	0,80 ± 2,13	0,29
Saxifragaceae	SAXIF	823	0,02 - 21,58	0,71 ± 1,56	0,32
Scrophulariaceae	SCROP	2284	0,01 - 13,93	0,67 ± 1,06	0,34
Solanaceae	SOLAN	243	0,01 - 33,04	0,62 ± 2,22	0,25
Cannabaceae/Urticace	CANURT	2795	0,02 - 88,91	1,29 ± 3,97	0,55
Valerianaceae	VALER	468	0,02 - 18,09	0,74 ± 1,52	0,30
Viola	VVIOL	168	0,03 - 9,45	0,49 ± 0,89	0,26

Table 2.S3 Accuracy of reconstructions (root mean square error of prediction (RMSEP) and coefficient of correlation (R^2)) for different numbers of analogues (from 5 to 10) with the 88 taxa database. The best results are highlighted in grey. Climatic variables: MTCO (mean-temperature of the coldest month), MTWA (mean-temperature of the warmest month), Pdjf (winter precipitation), Pjja (summer precipitation), Pann (annual precipitation), Seasonality (MTWA – MTCO).

	Number of analogues	Climatic parameters					
		MTCO (°C)	MTWA (°C)	Seasonality (°C)	Pdjf (mm)	Pjja (mm)	Pann (mm)
RMSEP	**5**	3.41	1.95	3.44	68.76	46.34	199.79
	6	3.43	1.95	3.46	68.72	46.27	199.79
	7	3.45	1.95	3.49	68.47	46.30	199.33
	8	3.49	1.95	3.53	69.97	46.84	202.79
	9	3.50	1.97	3.53	70.82	47.18	204.84
	10	3.51	1.99	3.54	71.55	47.08	205.98
		MTCO	MTWA	Seasonality	Pdjf	Pjja	Pann
R^2	**5**	0.91	0.83	0.88	0.76	0.79	0.76
	6	0.91	0.83	0.88	0.75	0.78	0.75
	7	0.91	0.83	0.88	0.75	0.78	0.75
	8	0.91	0.83	0.88	0.75	0.78	0.75
	9	0.90	0.83	0.87	0.74	0.78	0.75
	10	0.90	0.82	0.87	0.74	0.78	0.75

Table 2.S4 Taxonomical diversity of the fossil records included in this study (Fig. 2.1; Table 2.1). *N*: number. *All sequences cover partly or entirely MIS 3, but some of them also cover the previous and/or subsequent isotope stage (MIS 2 and 4). Marine and terrestrial sites are indicated in blue and green respectively.

Sites	Number of taxa initially identified*	Number of taxa kept for MAT		Number of taxa kept for PFT	
		N	%	*N*	%
MD95-2039	95	88	92,6	69	72,6
MD95-2042	131	118	90,1	98	74,8
MD95-2043	96	90	93,8	77	80,2
ODP 976	132	111	84,1	85	64,4
Lac du Bouchet	63	62	98,4	56	88,9
Lago Grande di Monticchio	138	126	91,3	100	72,5
Lagaccione	80	75	93,8	66	82,5
Stracciacappa	56	53	94,6	49	87,5
Valle du Castiglione	65	61	93,8	57	87,7
Ioannina	92	85	92,4	71	77,2
Megali Limni	75	70	93,3	56	74,7
Xinias	178	161	90,4	132	74,2

Table 2.S5 Accuracy of reconstructions as indicated from the root mean square error of prediction (RMSEP) and the coefficient of correlation (R^2) for the 88 and 87 (*Pinus* excluded) taxa databases (5 analogues). Climatic variables: MTCO (mean-temperature of the coldest month), MTWA (mean-temperature of the warmest month), Pdjf (winter precipitation), Pjja (summer precipitation), Pann (annual precipitation), Seasonality (MTWA – MTCO).

Climatic parameters	RMSEP		R^2	
	88 taxa	87 taxa (without *Pinus*)	88 taxa	87 taxa (without *Pinus*)
MTCO	3,4°C	3,5°C	0,91	0,91
MTWA	2°C	1,9°C	0,83	0,83
Seasonality	3,4°C	3,5°C	0,88	0,87
Pdjf	69mm	72mm	0,76	0,74
Pjja	46mm	47mm	0,79	0,79
Pann	200mm	205mm	0,76	0,75

Figure 2.S1 (a) Age model of core MD95-2039 (site 1), off southern Portugal (Fig. 2.1; Table 2.1 and references therein), obtained by using CLAM (Blaauw, 2010) (see Chapter 2.2.2.Chronologies, Table 2.1 and related files in Sanchez et al. (2017) for further details and data). The black line corresponds to the weighted average. Gray areas show the confidence intervals of the age-depth models calculated by defaults at 95% (2 sigma). The dates are indicated in blue and the correlated tie points are indicated in green. (b) RDA graph for site 1. Yellow arrows represent the non-arboreal PFTs while the green arrows represent the arboreal PFTs (see Table 2.2 for more details). Grey arrows represent the climatic parameters reconstructed. The percentages next to each axis indicate how much of the total constrained variance of PFTs they explain. (c) Comparison between NGRIP oxygen isotopic record (NGRIP, 2004) and records related to sea-surface conditions, vegetation and climate at site 1: (from bottom to top) $\delta^{18}O$ of *Globigerina bulloides* (Gb) (Eynaud et al., 2009) used as a proxy of sea-surface temperature (Malevich et al., 2019), the warm sea-surface phases are indicated by red bars; RDA axis-1 scores (with number of samples (n) for each side; MTCO (blue line) and MTWA (orange line); seasonality (difference between MTWA and MTCO); summer (orange line), winter (blue line) and annual precipitation (black line); square-chord distances of the 1st and 5th best analogues and analogue thresholds (see Material and Methods).

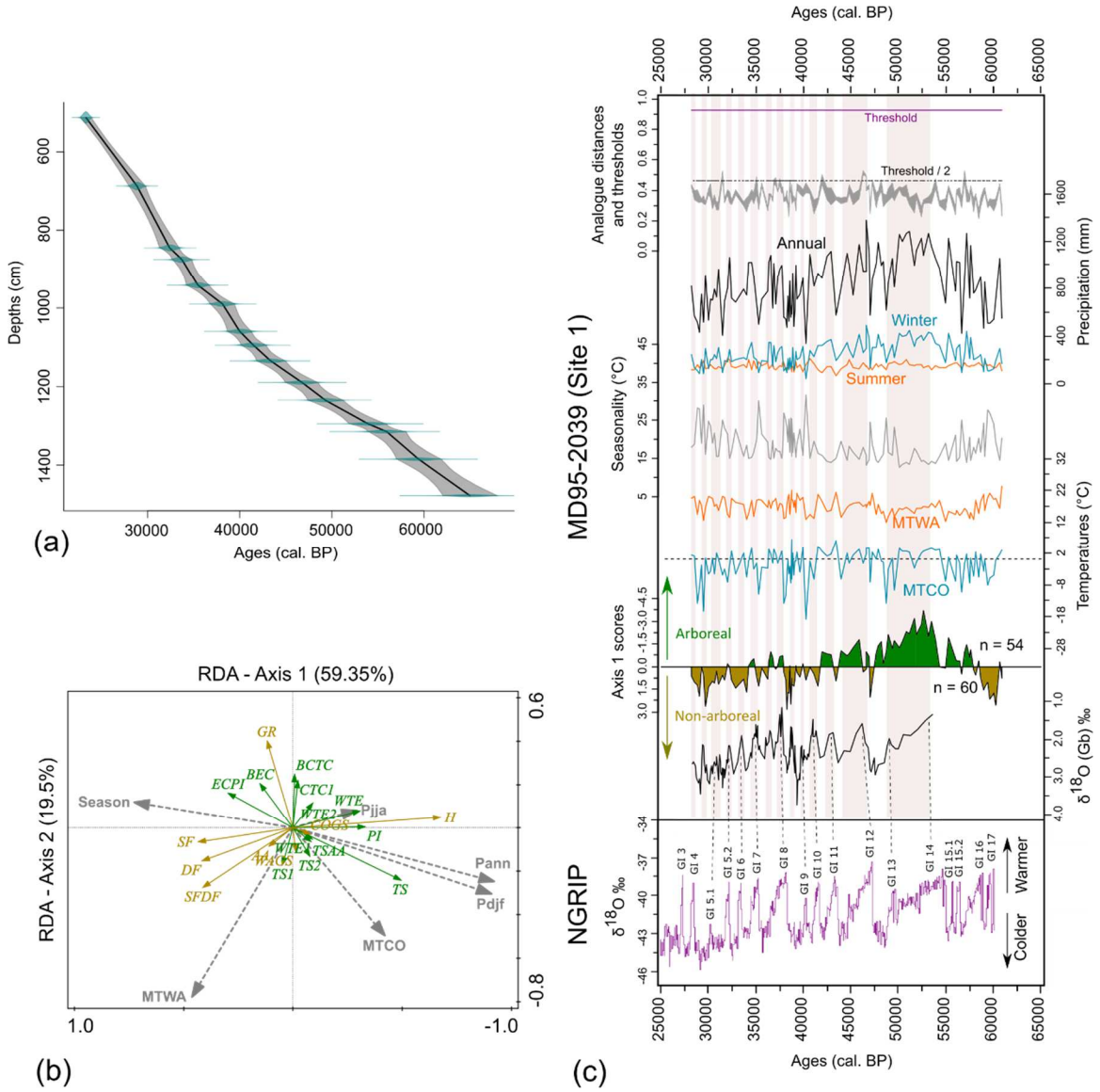

Figure 2.S2 (a) Age model of core MD95-2042 (site 2), off southern Portugal (Fig. 2.1; Table 2.1 and references therein), obtained by using CLAM (Blaauw, 2010) (see Chapter 2.2.2.Chronologies, Table 2.1 and related files in Sanchez et al. (2017) for further details and data). The black line corresponds to the weighted average. Gray areas show the confidence intervals of the age-depth models calculated by defaults at 95% (2 sigma). The dates are indicated in blue and the correlated tie points are indicated in green. (b) RDA graph for site 2. Yellow arrows represent the non-arboreal PFTs while the green arrows represent the arboreal PFTs (see Table 2.2 for more details). Grey arrows represent the climatic parameters reconstructed. The percentages next to each axis indicate how much of the total constrained variance of PFTs they explain. (c) Comparison between NGRIP oxygen isotopic record (NGRIP, 2004) and records related to sea-surface conditions, vegetation and climate at site 2: (from bottom to top) $\delta^{18}O$ of *Globigerina bulloides* (Gb) (Shackleton et al., 2000) used as a proxy of sea-surface temperature (Malevich et al., 2019), the warm sea-surface phases are indicated by red bars; RDA axis-1 scores (with number of samples (n) for each side; MTCO (blue line) and MTWA (orange line); seasonality (difference between MTWA and MTCO); summer (orange line), winter (blue line) and annual precipitation (black line); square-chord distances of the 1st and 5th best analogues and analogue thresholds (see Material and Methods).

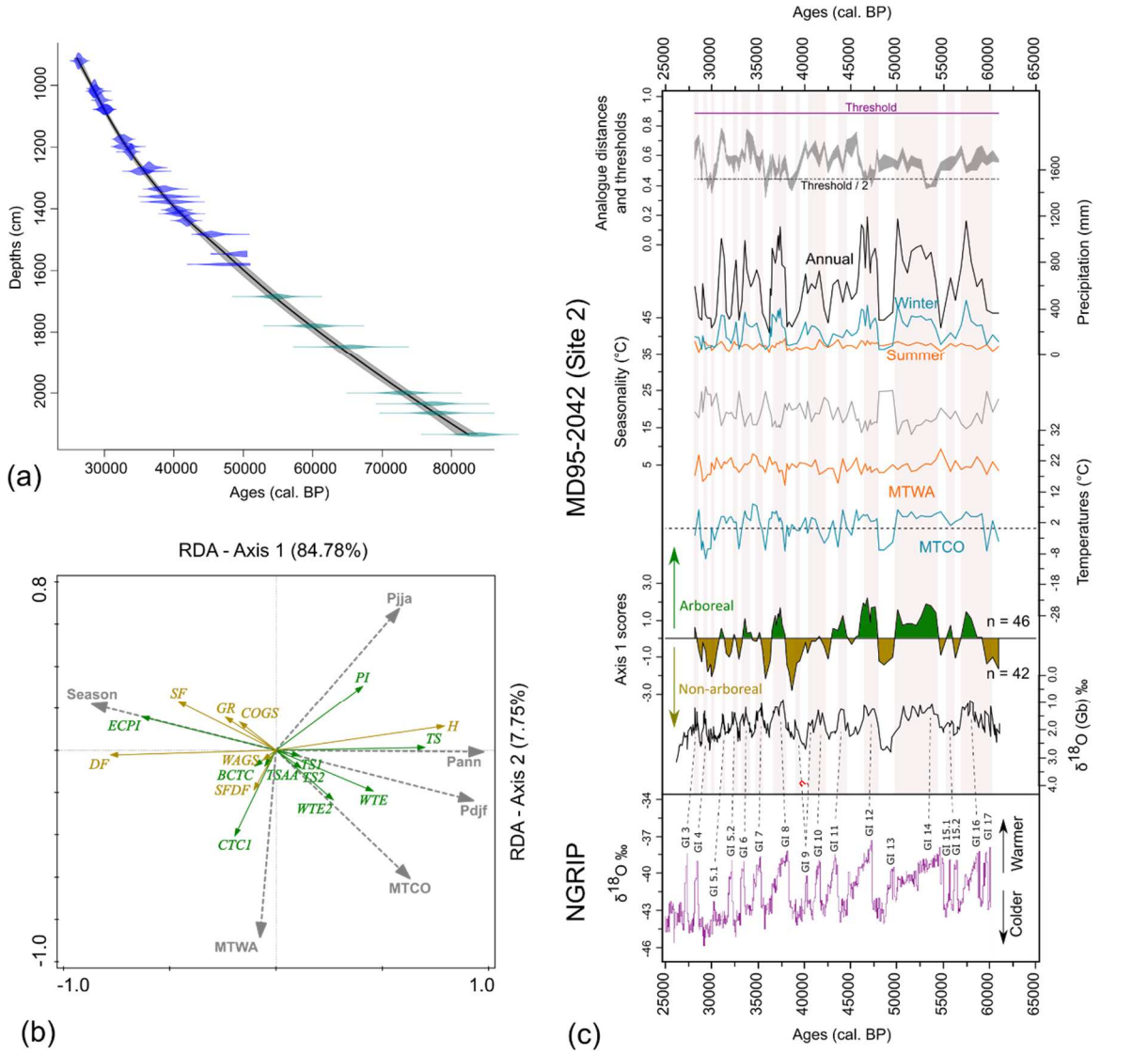

Figure 2.S3 (a) Age model of core ODP 976 (site 3), in the Alboran Sea (Fig. 2.1; Table 2.1 and references therein), obtained by using CLAM (Blaauw, 2010) (see Chapter 2.2.2.Chronologies, Table 2.1 and related files in Sanchez et al. (2017) for further details and data). The black line corresponds to the weighted average. Gray areas show the confidence intervals of the age-depth models calculated by defaults at 95% (2 sigma). The dates are indicated in blue and the correlated tie points are indicated in green. (b) RDA graph for site 3. Yellow arrows represent the non-arboreal PFTs while the green arrows represent the arboreal PFTs (see Table 2.2 for more details). Grey arrows represent the climatic parameters reconstructed. The percentages next to each axis indicate how much of the total constrained variance of PFTs they explain. (c) Comparison between NGRIP oxygen isotopic record (NGRIP, 2004) and records related to vegetation and climate at site 3: (from bottom to top) RDA axis-1 scores (with number of samples (n) for each side; MTCO (blue line) and MTWA (orange line); seasonality (difference between MTWA and MTCO); summer (orange line), winter (blue line) and annual precipitation (black line); square-chord distances of the 1st and 5th best analogues and analogue thresholds (see Material and Methods). Green bars indicate the phases of arboreal increase defined after the RDA axis-1 scores.

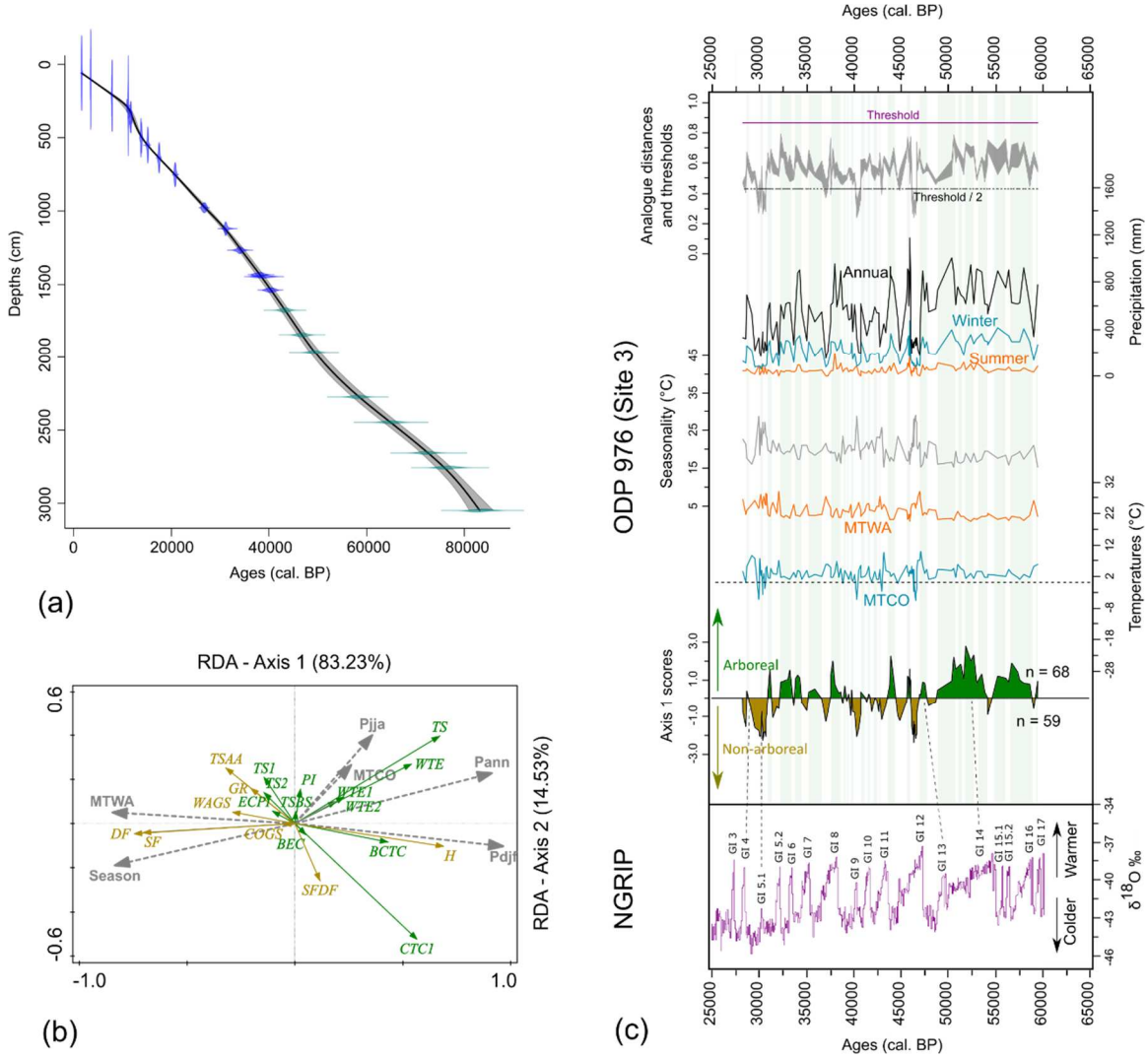

Figure 2.S4 (a) Age model of core MD95-2043 (site 4), in the Alboran Sea (Fig. 2.1; Table 2.1 and references therein), obtained by using CLAM (Blaauw, 2010) (see Chapter 2.2.2.Chronologies, Table 2.1 and related files in Sanchez et al. (2017) for further details and data). The black line corresponds to the weighted average. Gray areas show the confidence intervals of the age-depth models calculated by defaults at 95% (2 sigma). The dates are indicated in blue and the correlated tie points are indicated in green. (b) RDA graph for site 4. Yellow arrows represent the non-arboreal PFTs while the green arrows represent the arboreal PFTs (see Table 2.2 for more details). Grey arrows represent the climatic parameters reconstructed. The percentages next to each axis indicate how much of the total constrained variance of PFTs they explain. (c) Comparison between NGRIP oxygen isotopic record (NGRIP, 2004) and records related to sea-surface conditions, vegetation and climate at site 4: (from bottom to top) benthic $\delta^{18}O$ record based on *C. pachydermus* (Cp) (Cacho et al., 2006) which is indicative of global temperature, warm phases are indicated by red bars; RDA axis-1 scores (with number of samples (n) for each side; MTCO (blue line) and MTWA (orange line); seasonality (difference between MTWA and MTCO); summer (orange line), winter (blue line) and annual precipitation (black line); square-chord distances of the 1st and 5th best analogues and analogue thresholds (see Material and Methods).

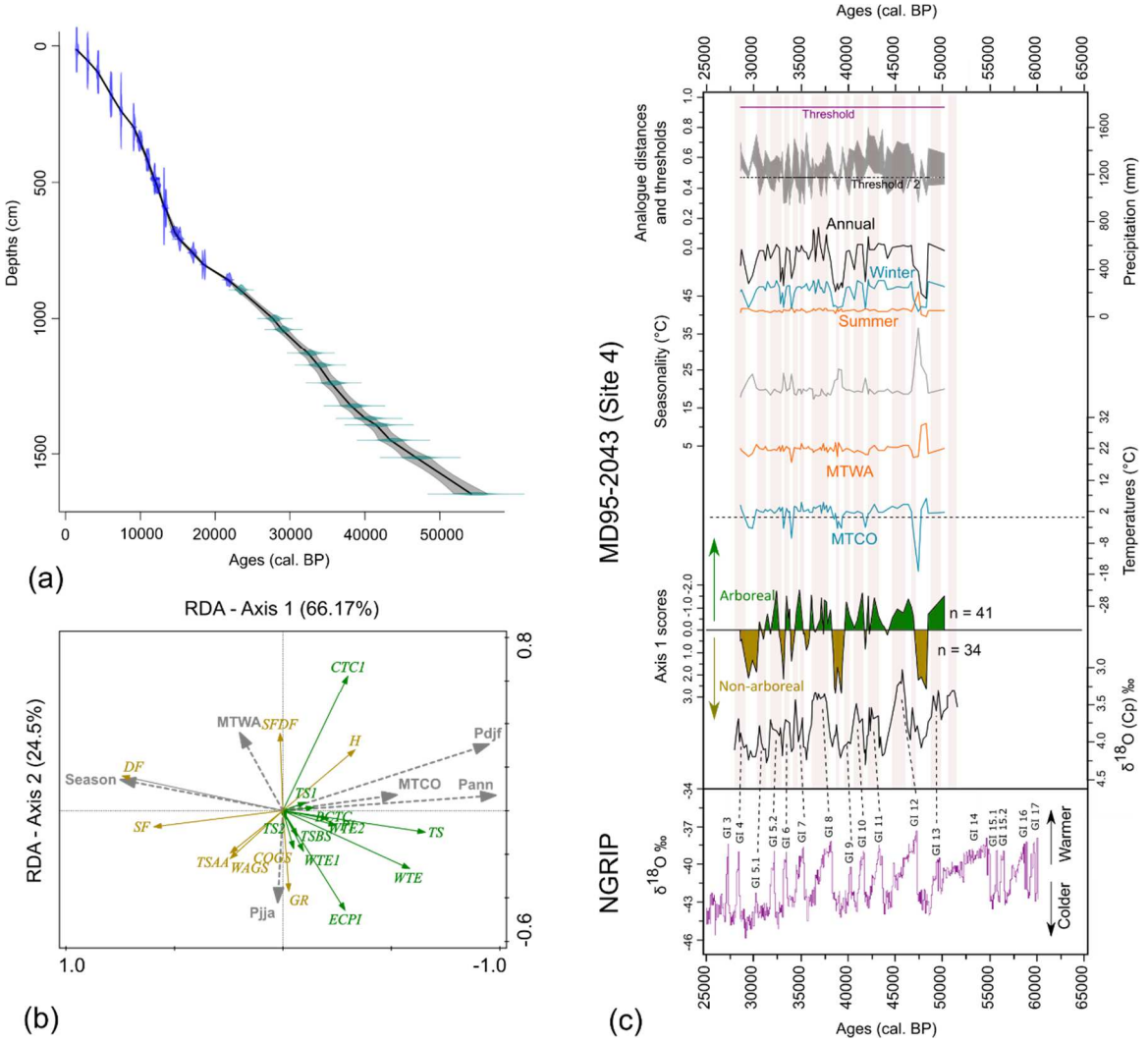

Figure 2.S5 (a) Age model of the Lac du Bouchet sequence (site 5), France (Fig. 2.1; Table 2.1 and references therein), obtained by using CLAM (Blaauw, 2010) (see Chapter 2.2.2.Chronologies, Table 2.1 and related files in Sanchez et al. (2017) for further details and data). The black line corresponds to the weighted average. Gray areas show the confidence intervals of the age-depth models calculated by defaults at 95% (2 sigma). The dates are indicated in blue and the correlated tie points are indicated in green. (a) RDA graph for site 5. Yellow arrows represent the non-arboreal PFTs while the green arrows represent the arboreal PFTs (see Table 2.2 for more details). Grey arrows represent the climatic parameters reconstructed. The percentages next to each axis indicate how much of the total constrained variance of PFTs they explain. (b) Comparison between NGRIP oxygen isotopic record (NGRIP, 2004) and records related to vegetation and climate at site 5: (from bottom to top) RDA axis-1 scores (with number of samples (n) for each side; MTCO (blue line) and MTWA (orange line); seasonality (difference between MTWA and MTCO); summer (orange line), winter (blue line) and annual precipitation (black line); square-chord distances of the 1st and 5th best analogues and analogue thresholds (see Material and Methods). Dashed colour lines represent the mean 1901-2022 climate values (see Material and Methods). Green bars indicate the phases of arboreal increase defined after the RDA axis-1 scores.

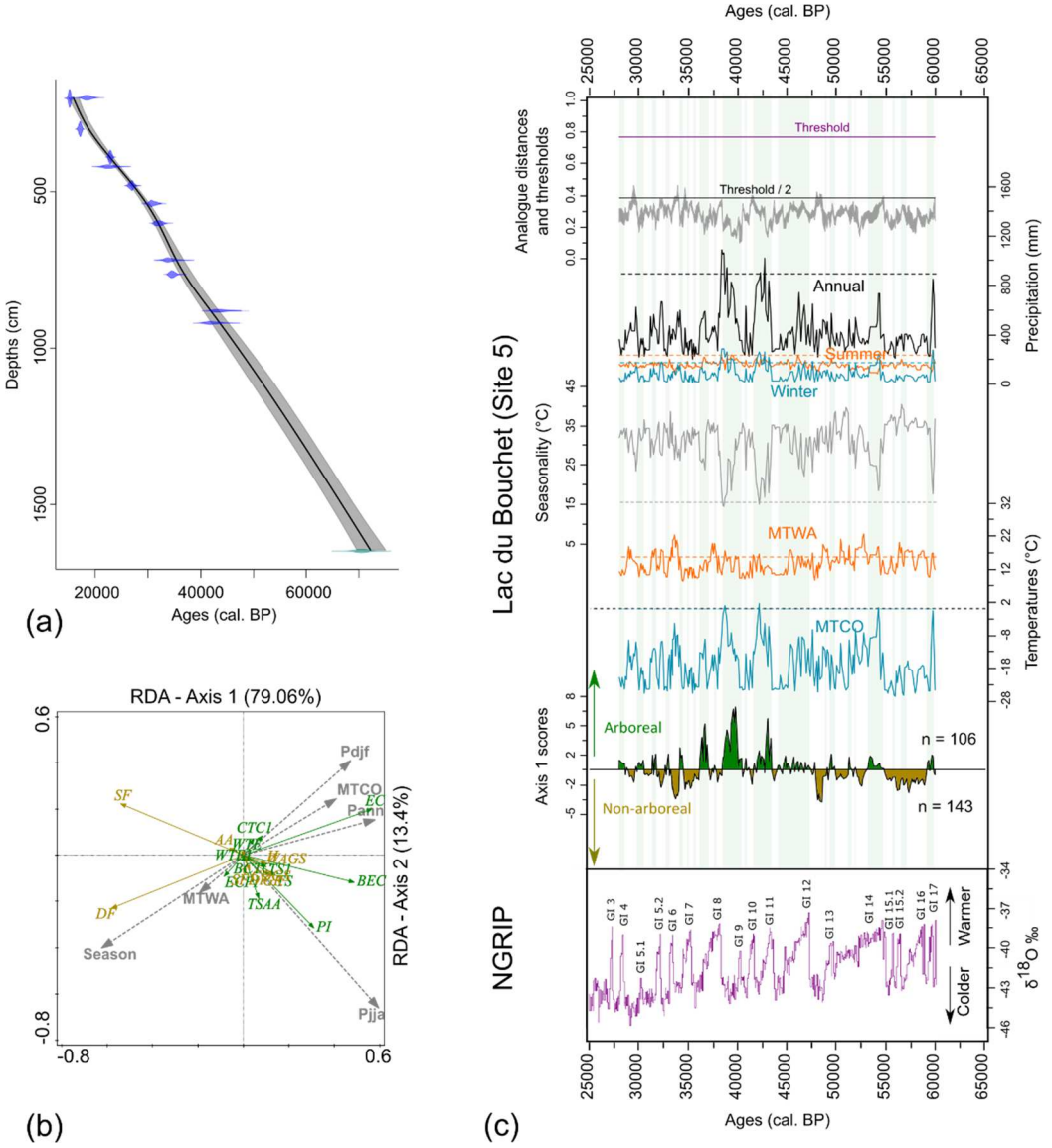

Figure 2.S6 (a) Age model of the Lagaccione sequence (site 6), Italy (Fig. 2.1; Table 2.1 and references therein), obtained by using CLAM (Blaauw, 2010) (see Chapter 2.2.2.Chronologies, Table 2.1 and related files in Sanchez et al. (2017) for further details and data). The black line corresponds to the weighted average. Gray areas show the confidence intervals of the age-depth models calculated by defaults at 95% (2 sigma). The dates are indicated in blue and the correlated tie points are indicated in green. (b) RDA graph for site 6. Yellow arrows represent the non-arboreal PFTs while the green arrows represent the arboreal PFTs (see Table 2.2 for more details). Grey arrows represent the climatic parameters reconstructed. The percentages next to each axis indicate how much of the total constrained variance of PFTs they explain. (c) Comparison between NGRIP oxygen isotopic record (NGRIP, 2004) and records related to vegetation and climate at site 6: (from bottom to top) RDA axis-1 scores (with number of samples (n) for each side; MTCO (blue line) and MTWA (orange line); seasonality (difference between MTWA and MTCO); summer (orange line), winter (blue line) and annual precipitation (black line); square-chord distances of the 1st and 5th best analogues and analogue thresholds (see Material and Methods). Dashed colour lines represent the mean 1901-2022 climate values (see Material and Methods). Green bars indicate the phases of arboreal increase defined after the RDA axis-1 scores.

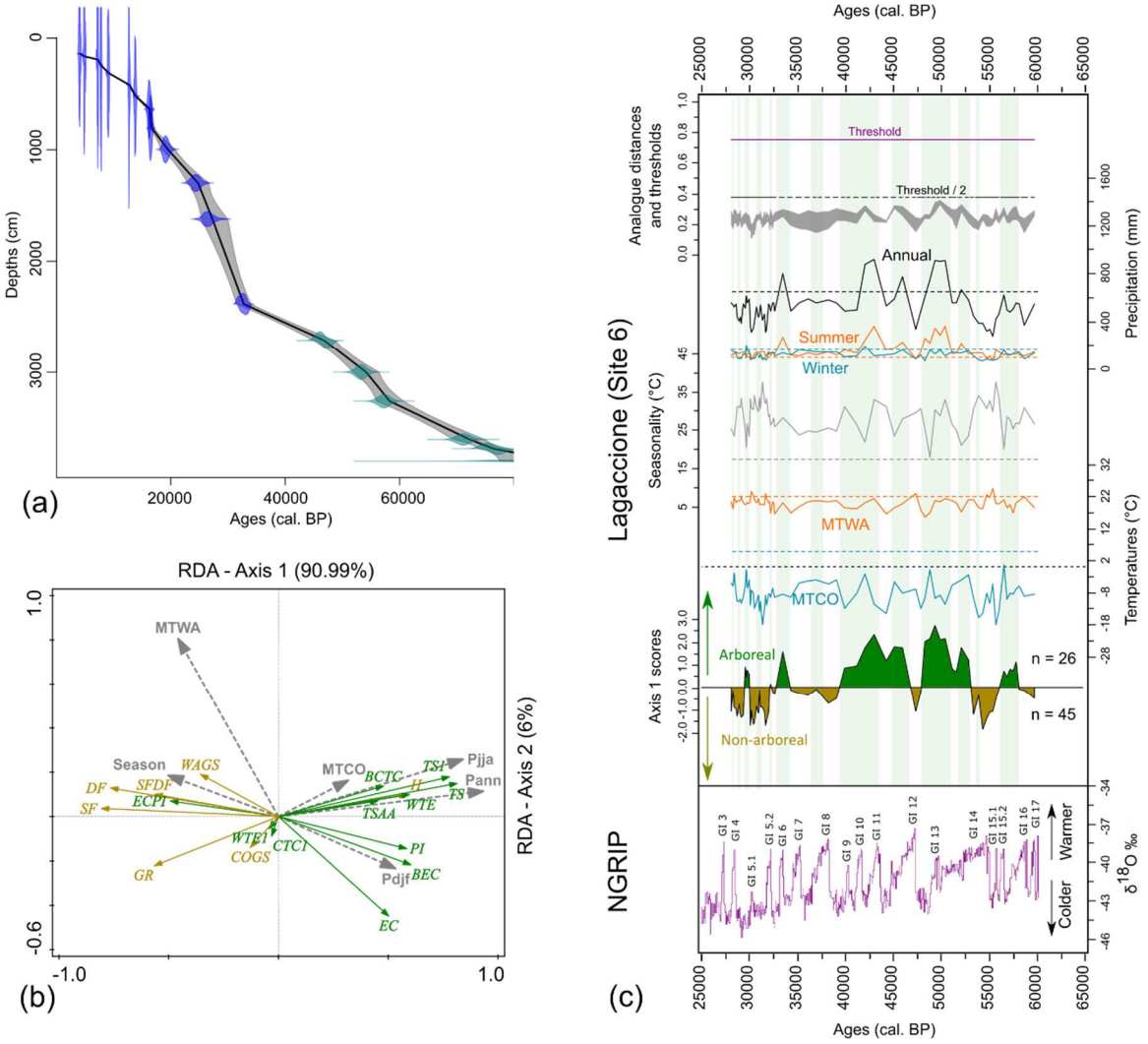

Figure 2.S7 (a) Age model of the Stracciacappa sequence (site 7), Italy (Fig. 2.1; Table 2.1 and references therein), obtained by using CLAM (Blaauw, 2010) (see Chapter 2.2.2.Chronologies, Table 2.1 and related files in Sanchez et al. (2017) for further details and data). The black line corresponds to the weighted average. Gray areas show the confidence intervals of the age-depth models calculated by defaults at 95% (2 sigma). The dates are indicated in blue and the correlated tie points are indicated in green. (b) RDA graph for site 7. Yellow arrows represent the non-arboreal PFTs while the green arrows represent the arboreal PFTs (see Table 2.2 for more details). Grey arrows represent the climatic parameters reconstructed. The percentages next to each axis indicate how much of the total constrained variance of PFTs they explain. (c) Comparison between NGRIP oxygen isotopic record (NGRIP, 2004) and records related to vegetation and climate at site 7: (from bottom to top) RDA axis-1 scores (with number of samples (n) for each side; MTCO (blue line) and MTWA (orange line); seasonality (difference between MTWA and MTCO); summer (orange line), winter (blue line) and annual precipitation (black line); square-chord distances of the 1st and 5th best analogues and analogue thresholds (see Material and Methods). Dashed colour lines represent the mean 1901-2022 climate values (see Material and Methods). Green bars indicate the phases of arboreal increase defined after the RDA axis-1 scores.

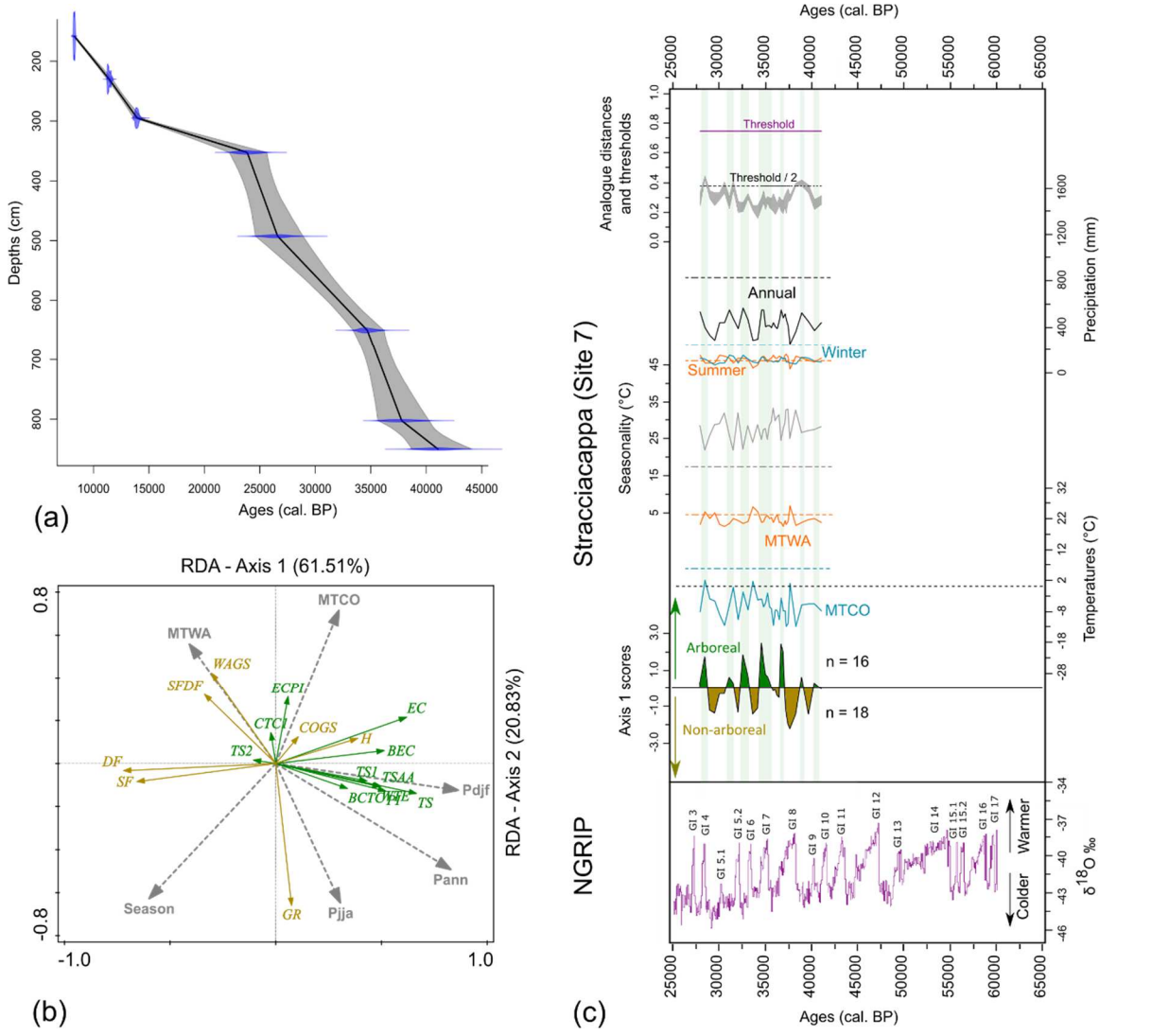

Figure 2.S8 (a) Age model of the Valle di Castiglione sequence (site 8), Italy (Fig. 2.1; Table 2.1 and references therein), obtained by using CLAM (Blaauw, 2010) (see Chapter 2.2.2.Chronologies, Table 2.1 and related files in Sanchez et al. (2017) for further details and data). The black line corresponds to the weighted average. Gray areas show the confidence intervals of the age-depth models calculated by defaults at 95% (2 sigma). The dates are indicated in blue and the correlated tie points and tephra layer are indicated in green and orange respectively. (b) RDA graph for site 8. Yellow arrows represent the non-arboreal PFTs while the green arrows represent the arboreal PFTs (see Table 2.2 for more details). Grey arrows represent the climatic parameters reconstructed. The percentages next to each axis indicate how much of the total constrained variance of PFTs they explain. (c) Comparison between NGRIP oxygen isotopic record (NGRIP, 2004) and records related to vegetation and climate at site: (from bottom to top) RDA axis-1 scores (with number of samples (n) for each side; MTCO (blue line) and MTWA (orange line); seasonality (difference between MTWA and MTCO); summer (orange line), winter (blue line) and annual precipitation (black line); square-chord distances of the 1st and 5th best analogues and analogue thresholds (see Material and Methods). Dashed colour lines represent the mean 1901-2022 climate values (see Material and Methods). Green bars indicate the phases of arboreal increase defined after the RDA axis-1 scores.

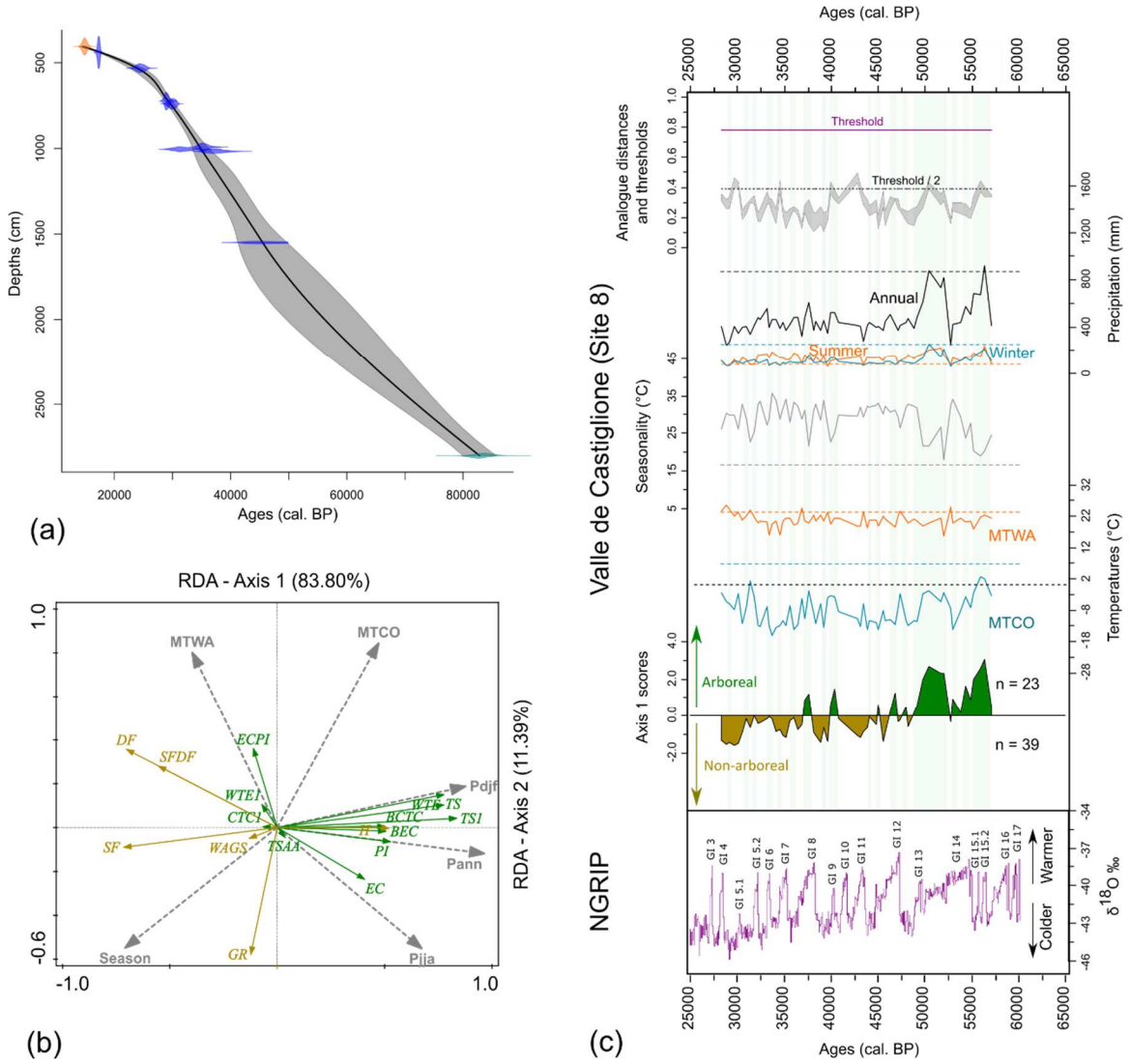

Figure 2.S9 (b) RDA graph for site 9 (Lago Grandi di Monticchio), Italy (Fig. 2.1; Table 2.1 and references therein). Yellow arrows represent the non-arboreal PFTs while the green arrows represent the arboreal PFTs (see Table 2.2 for more details). Grey arrows represent the climatic parameters reconstructed. The percentages next to each axis indicate how much of the total constrained variance of PFTs they explain. (c) Comparison between NGRIP oxygen isotopic record (NGRIP, 2004) and records related to vegetation and climate at site 9: (from bottom to top) RDA axis-1 scores (with number of samples (n) for each side; MTCO (blue line) and MTWA (orange line); seasonality (difference between MTWA and MTCO); summer (orange line), winter (blue line) and annual precipitation (black line); square-chord distances of the 1st and 5th best analogues and analogue thresholds (see Material and Methods). Dashed colour lines represent the mean 1901-2022 climate values (see Material and Methods). Green bars indicate the phases of arboreal increase defined after the RDA axis-1 scores. As mentioned in the main core of the paper, we used the initial chronology based on annual lamination ("varve") counts and sedimentological features in the non-varved intervals (Zolitschka and Negendank, 1996), hence the absence of an a) age model.

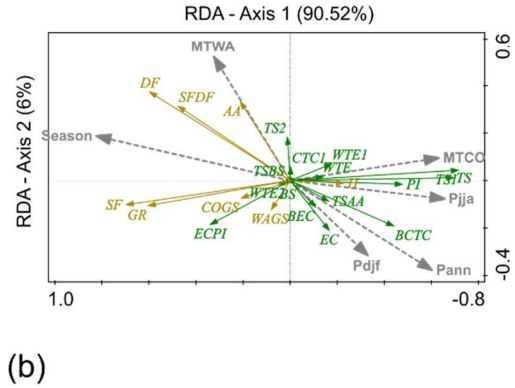

(b)

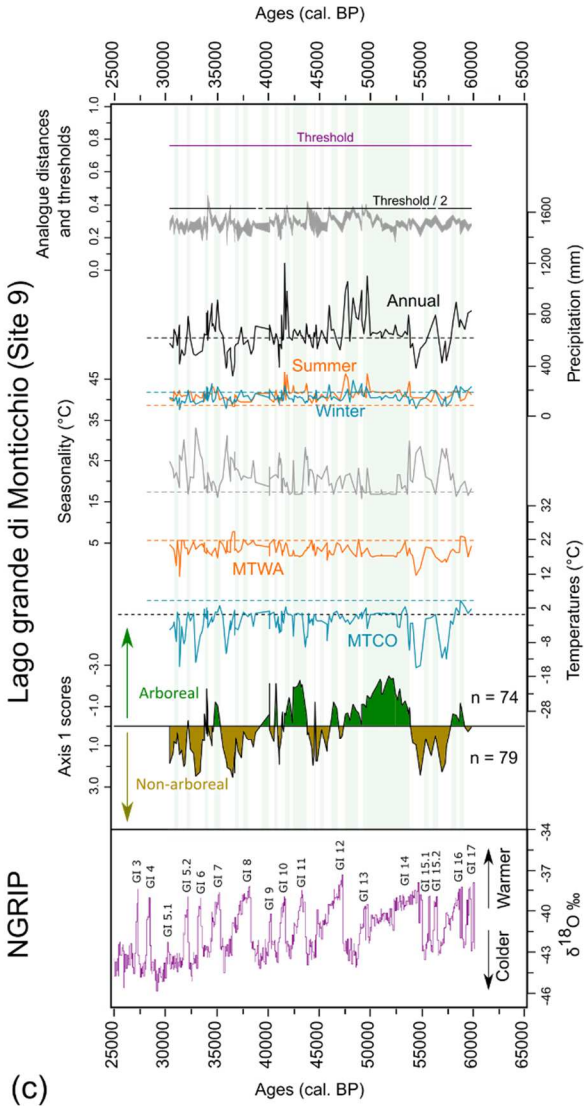

(c)

Figure 2.S10 (a) Age model of the Ioannina sequence (site 10), Greece (Fig. 2.1; Table 2.1 and references therein), obtained by using CLAM (Blaauw, 2010) (see Chapter 2.2.2.Chronologies, Table 2.1 and related files in Sanchez et al. (2017) for further details and data). The black line corresponds to the weighted average. Gray areas show the confidence intervals of the age-depth models calculated by defaults at 95% (2 sigma). The dates are indicated in blue and the correlated tie points are indicated in green. (b) RDA graph for site 10. Yellow arrows represent the non-arboreal PFTs while the green arrows represent the arboreal PFTs (see Table 2.2 for more details). Grey arrows represent the climatic parameters reconstructed. The percentages next to each axis indicate how much of the total constrained variance of PFTs they explain. (c) Comparison between NGRIP oxygen isotopic record (NGRIP, 2004) and records related to vegetation and climate at site 10: (from bottom to top) RDA axis-1 scores (with number of samples (n) for each side; MTCO (blue line) and MTWA (orange line); seasonality (difference between MTWA and MTCO); summer (orange line), winter (blue line) and annual precipitation (black line); square-chord distances of the 1st and 5th best analogues and analogue thresholds (see Material and Methods). Dashed colour lines represent the mean 1901-2022 climate values (see Material and Methods). Green bars indicate the phases of arboreal increase defined after the RDA axis-1 scores.

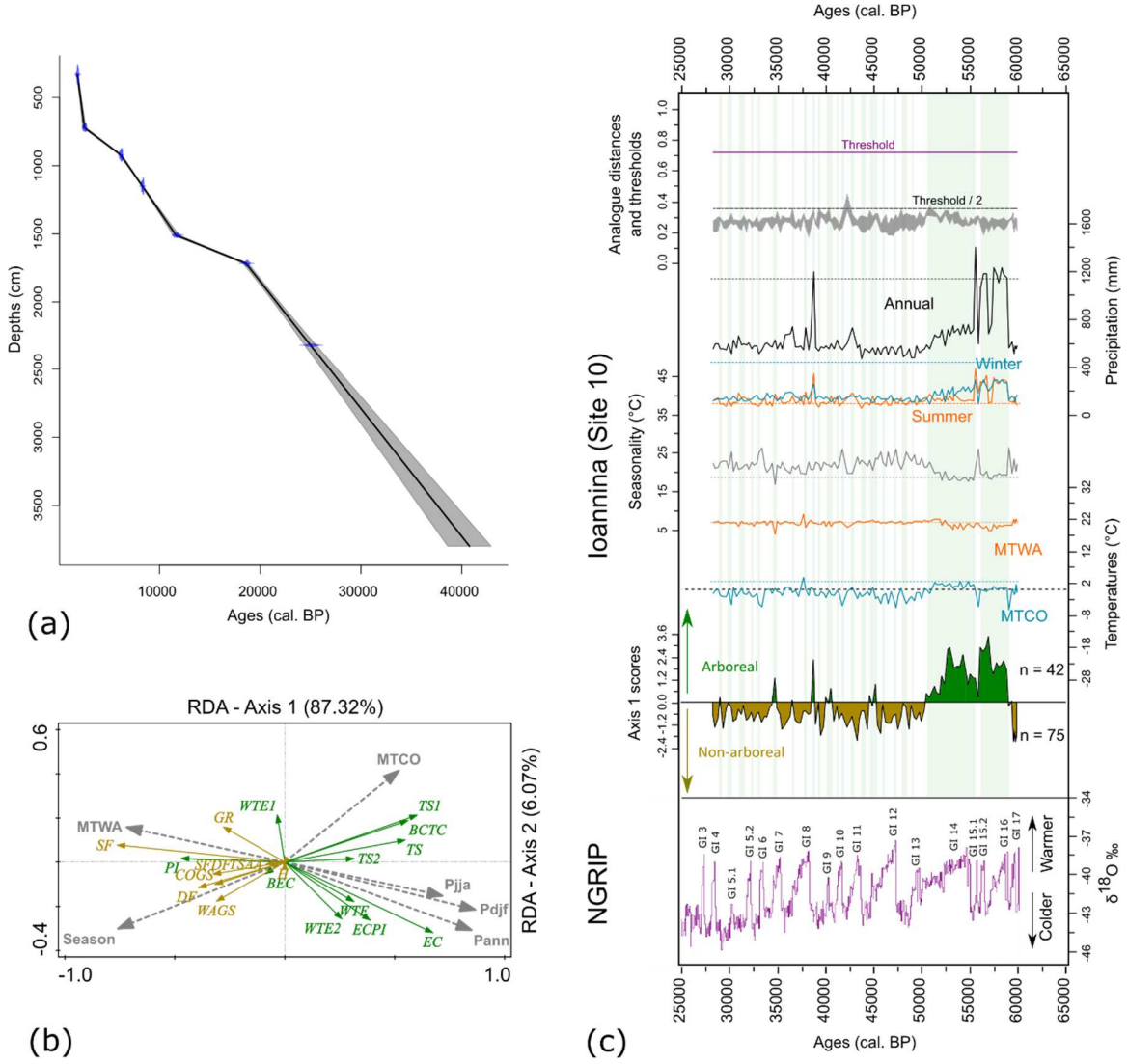

Figure 2.S11 (a) Age model of the Xinias sequence (site 11), Greece (Fig. 2.1; Table 2.1 and references therein), obtained by using CLAM (Blaauw, 2010) (see Chapter 2.2.2.Chronologies, Table 2.1 and related files in Sanchez et al. (2017) for further details and data). The black line corresponds to the weighted average. Gray areas show the confidence intervals of the age-depth models calculated by defaults at 95% (2 sigma). The dates are indicated in blue and the correlated tie points are indicated in green. (b) RDA graph for site 11. Yellow arrows represent the non-arboreal PFTs while the green arrows represent the arboreal PFTs (see Table 2.2 for more details). Grey arrows represent the climatic parameters reconstructed. The percentages next to each axis indicate how much of the total constrained variance of PFTs they explain. (c) Comparison between NGRIP oxygen isotopic record (NGRIP, 2004) and records related to vegetation and climate at site 11: (from bottom to top) RDA axis-1 scores (with number of samples (n) for each side; MTCO (blue line) and MTWA (orange line); seasonality (difference between MTWA and MTCO); summer (orange line), winter (blue line) and annual precipitation (black line); square-chord distances of the 1st and 5th best analogues and analogue thresholds (see Material and Methods). Dashed colour lines represent the mean 1901-2022 climate values (see Material and Methods). Green bars indicate the phases of arboreal increase defined after the RDA axis-1 scores.

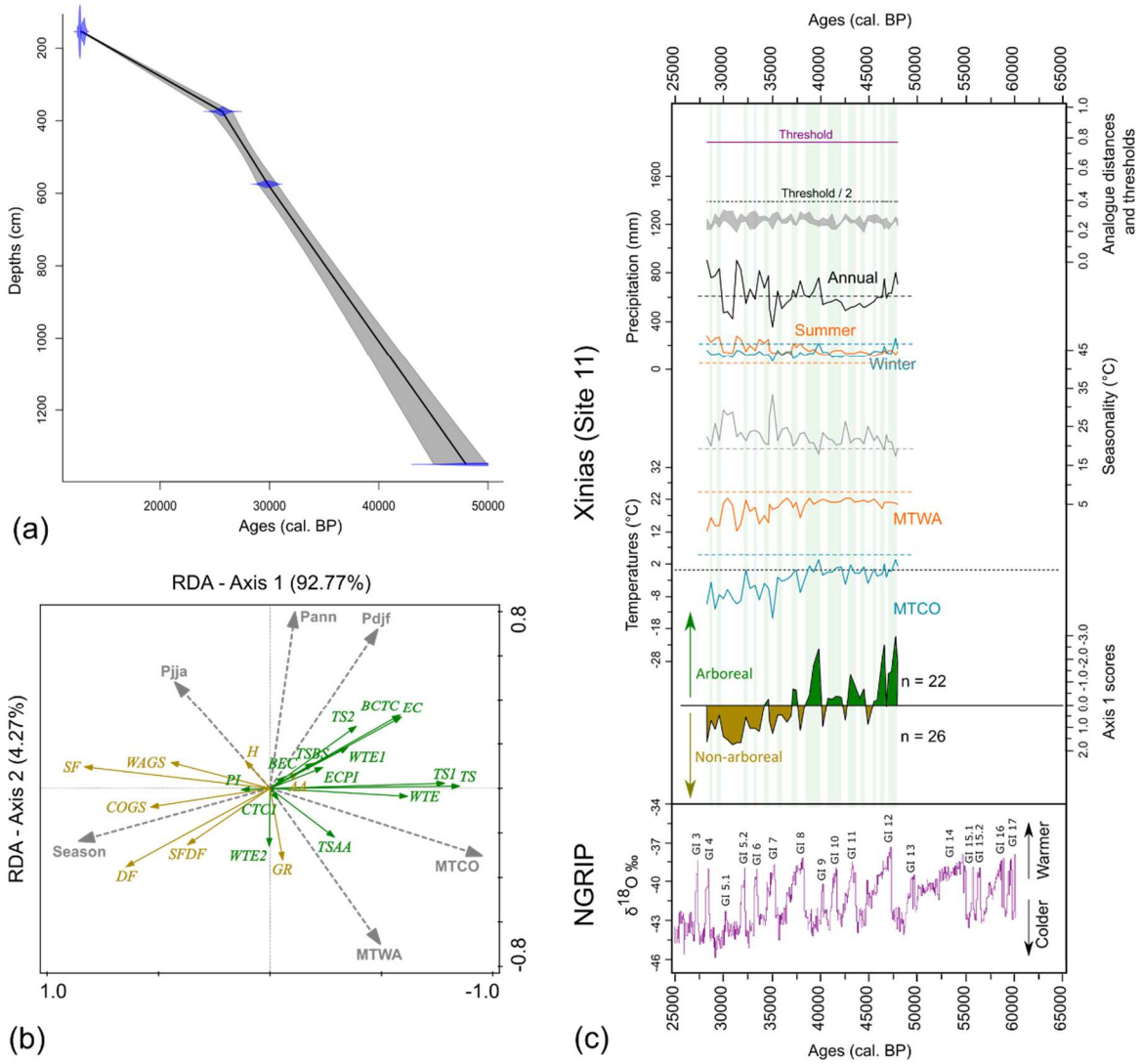

Figure 2.S12 (a) Age model of the Megali limni sequence (site 12), Greece (Fig. 2.1; Table 2.1 and references therein), obtained by using CLAM (Blaauw, 2010) (see Chapter 2.2.2.Chronologies, Table 2.1 and related files in Sanchez et al. (2017) for further details and data). The black line corresponds to the weighted average. Gray areas show the confidence intervals of the age-depth models calculated by defaults at 95% (2 sigma). The dates are indicated in blue and the correlated tie points and tephra layer are indicated in green and orange respectively. (b) RDA graph for site 12. Yellow arrows represent the non-arboreal PFTs while the green arrows represent the arboreal PFTs (see Table 2.2 for more details). Grey arrows represent the climatic parameters reconstructed. The percentages next to each axis indicate how much of the total constrained variance of PFTs they explain. (c) Comparison between NGRIP oxygen isotopic record (NGRIP, 2004) and records related to vegetation and climate at site 12: (from bottom to top) RDA axis-1 scores (with number of samples (n) for each side; MTCO (blue line) and MTWA (orange line); seasonality (difference between MTWA and MTCO); summer (orange line), winter (blue line) and annual precipitation (black line); square-chord distances of the 1st and 5th best analogues and analogue thresholds (see Material and Methods). Dashed colour lines represent the mean 1901-2022 climate values (see Material and Methods). Green bars indicate the phases of arboreal increase defined after the RDA axis-1 scores.

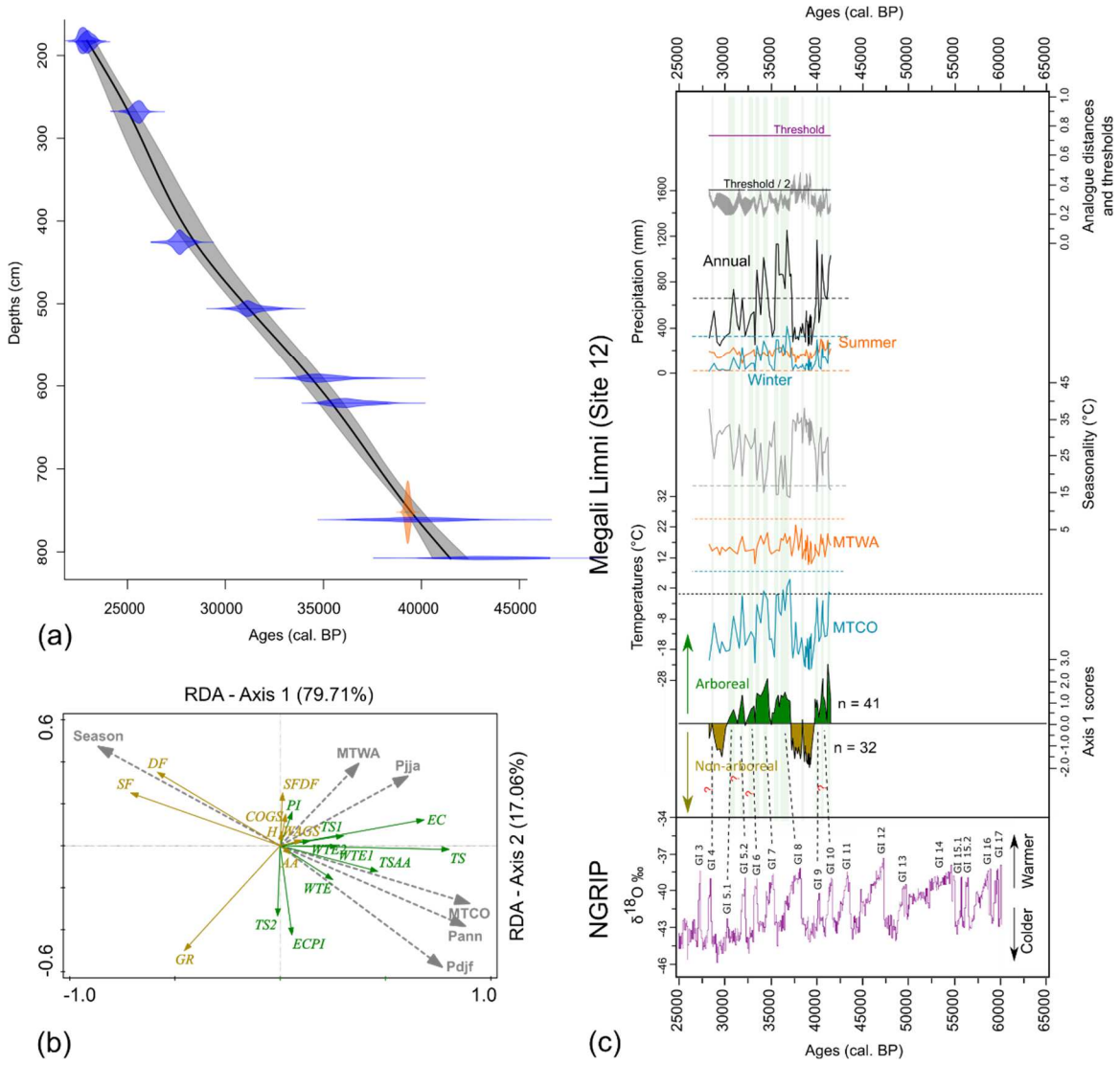

Figure 2.S13 Cross-validation results of the observed against estimated climatic parameters. The blue and red open circles correspond to the calibration and verification data sets, respectively. The Root Mean Square Error of Prediction (RMSEP) and the coefficient of correlation (R^2) indicate the degree of accuracy of estimates. MTCO: mean-temperature of the coldest month; MTWA: mean-temperature of the warmest month; Seasonality = MTWA – MTCO; Pann: annual precipitation; Pdjf: winter precipitation; Pjja: summer precipitation.

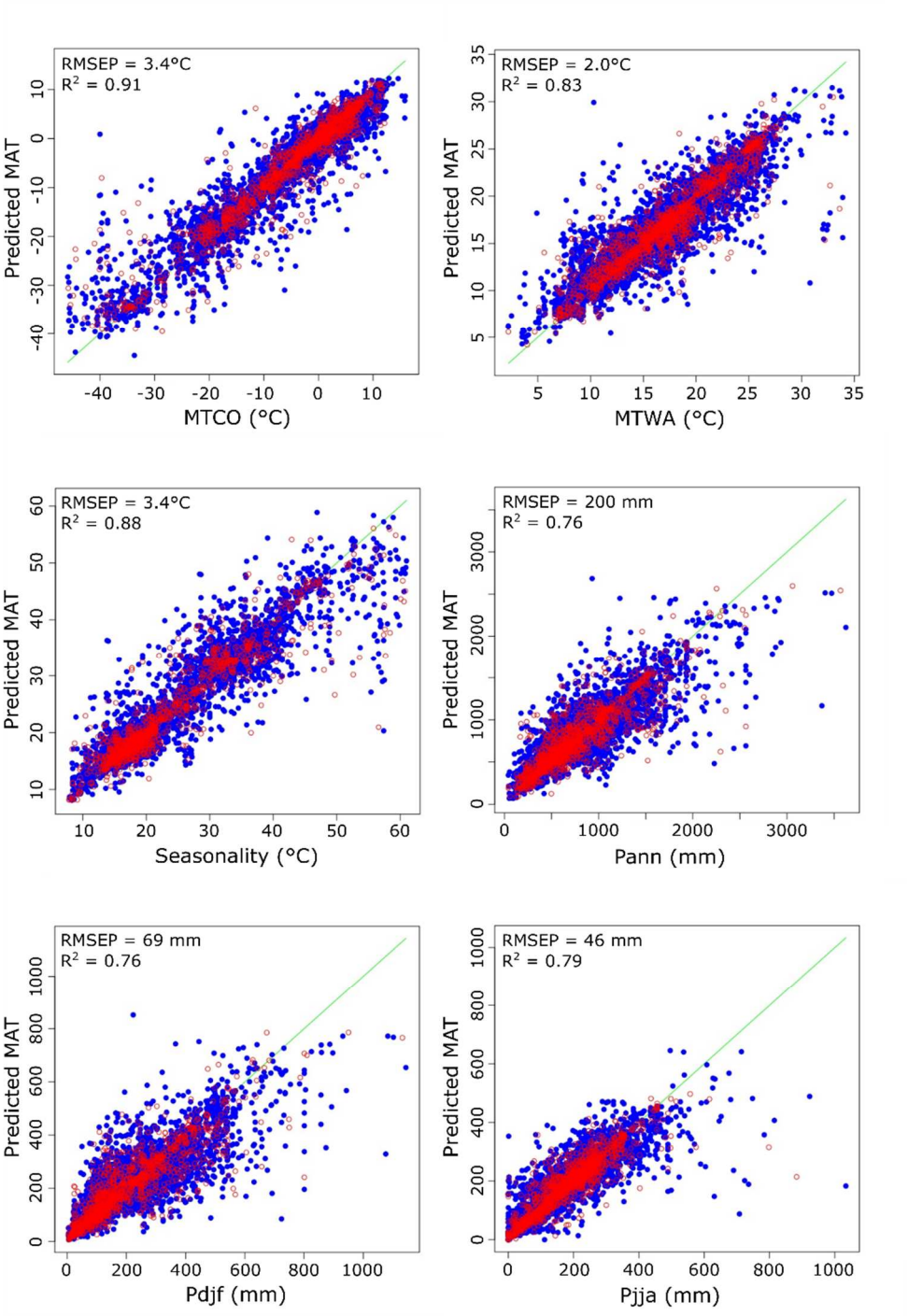

Figure 2.S14 Comparison between NGRIP oxygen isotopic record (NGRIP, 2004) and records related to sea-surface conditions and climate reconstructions with (A) and without *Pinus* (B) at site 2 (core MD95-2042), off southern Portugal (Fig. 2.1; Table 2.1 and references therein): (from left to right) $\delta^{18}O$ of *Globigerina bulloides* (Gb) (Shackleton et al., 2000) used as a proxy of sea-surface temperature (Malevich et al., 2019), the warm sea-surface phases are indicated by red bars; MTCO (blue line) and MTWA (red line); seasonality (difference between MTWA and MTCO); summer (red line), winter (blue line) and annual precipitation (black line); SCD of the 1st (green circles) and 5th (red circles) analogues for each sample and SCD threshold (red line) and half of this threshold (black dotted line).

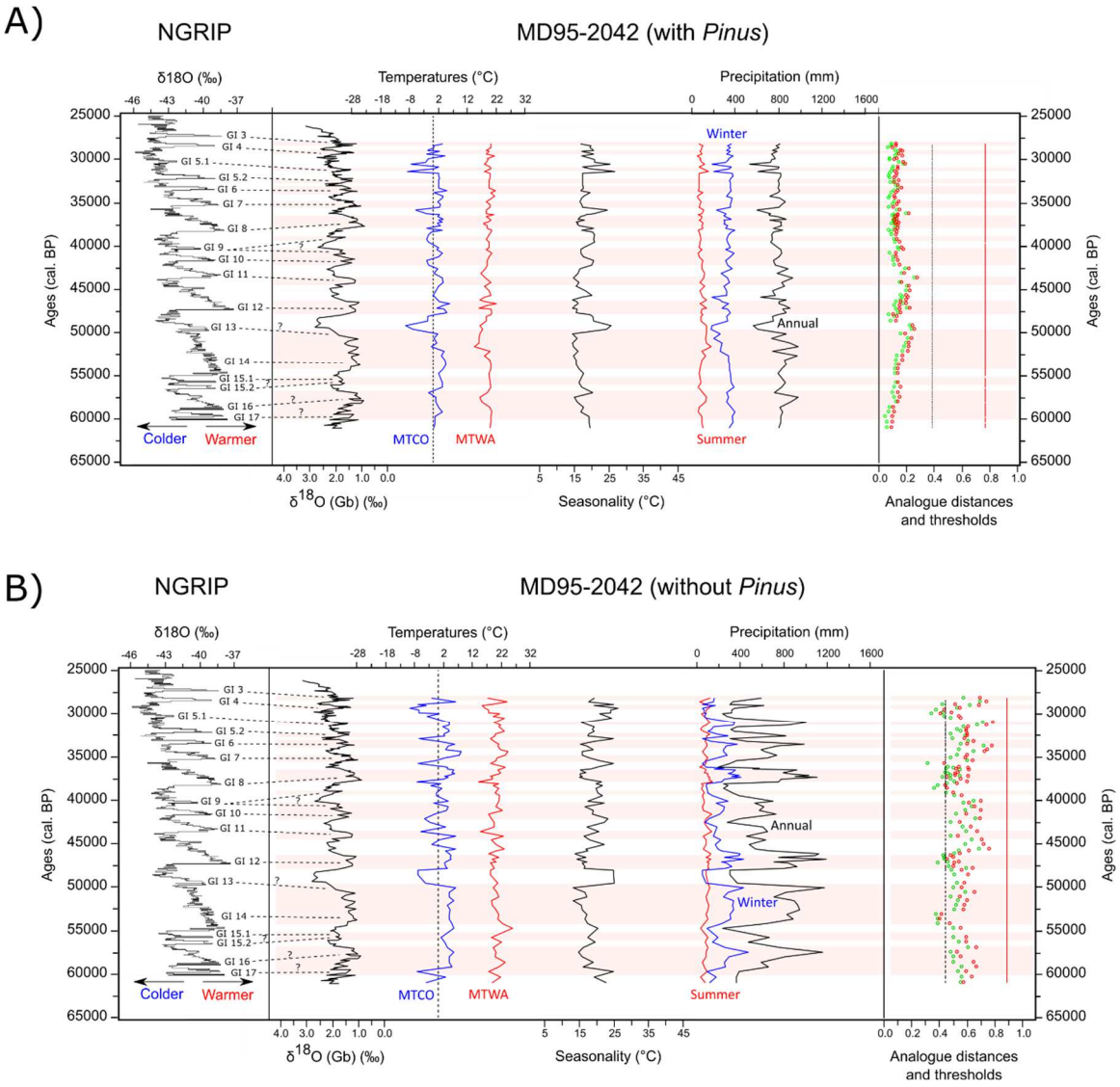

Figure 2.S15 CCA ordination diagram of pollen taxa (green (trees+shrubs) and orange (herbs) dots) (see Table 2.2 for codes) vs. environmental variables (blue arrows) of the European modern database. Analyses were performed on square root values of the relative frequency of pollen taxa (%) using the CANOCO software of (Šmilauer and Lepš, 2014).

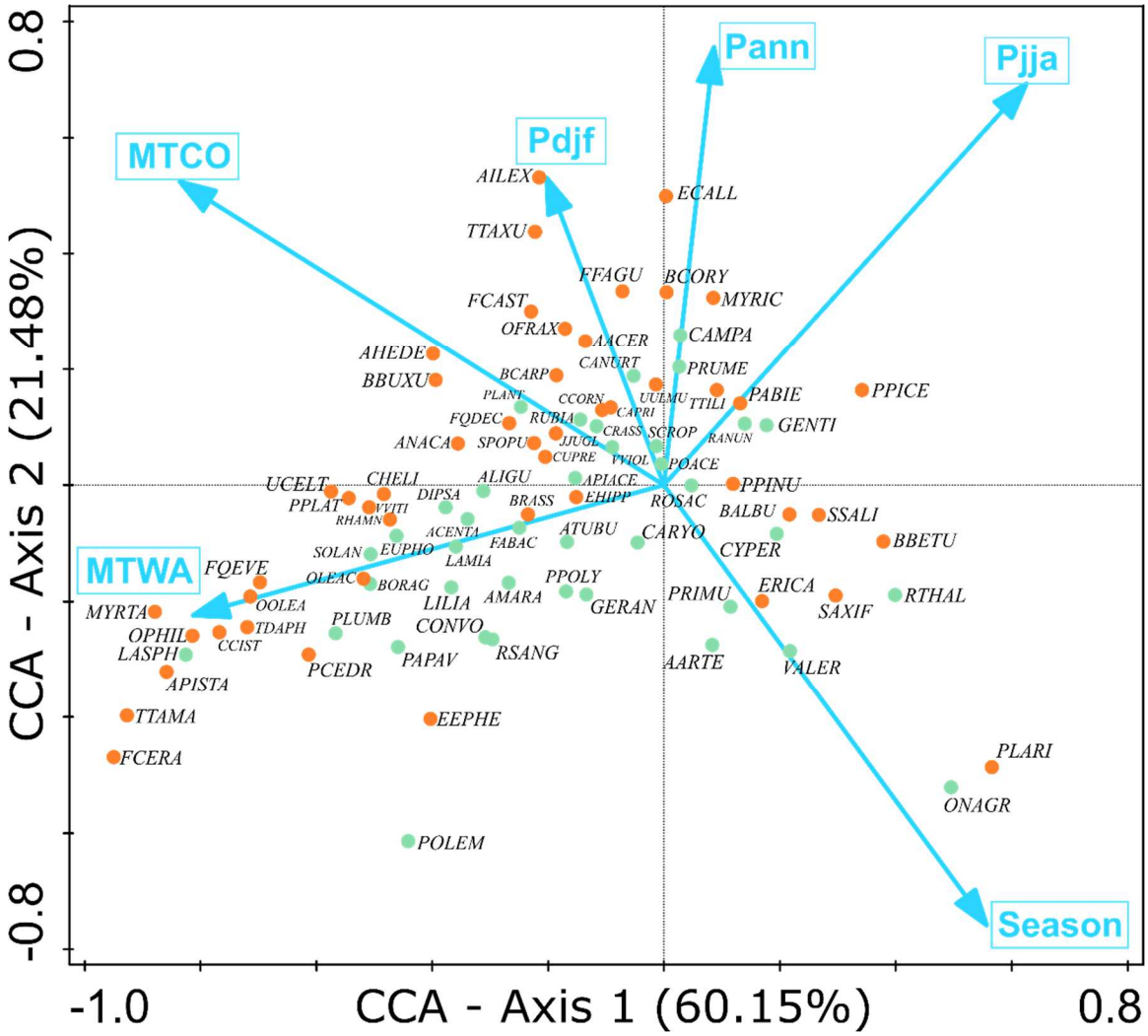

2.8.4 References

Austin, W. E., & Hibbert, F. D., Tracing time in the ocean: a brief review of chronological constraints (60–8 kyr) on North Atlantic marine event-based stratigraphies. *Quaternary Science Reviews*, *36*, 28-37 (2012).

Birks, H. J. B., Heiri, O., Seppä, H., & Bjune, A. E., Strengths and weaknesses of quantitative climate reconstructions based on Late-Quaternary. *The Open Ecology Journal*, *3*(1) (2010).

Broström, A., *et al.,* Pollen productivity estimates of key European plant taxa for quantitative reconstruction of past vegetation: a review. *Vegetation history and archaeobotany*, *17*, 461-478 (2008).

Budsky, A., Western Mediterranean climate response to Dansgaard/Oeschger events: New insights from speleothem records. *Geophysical Research Letters*, *46*(15), 9042-9053 (2019).

Cacho, I., Shackleton, N., Elderfield, H., Sierro, F. J., & Grimalt, J. O., Glacial rapid variability in deep-water temperature and δ18O from the Western Mediterranean Sea. *Quaternary Science Reviews*, *25*(23-24), 3294-3311 (2006).

Campbell, I. D., McDonald, K., Flannigan, M. D., & Kringayark, J., Long-distance transport of pollen into the Arctic. *Nature*, *399*(6731), 29-30 (1999).

Camuera, J., *et al*., Vegetation and climate changes during the last two glacial-interglacial cycles in the western Mediterranean: a new long pollen record from Padul (southern Iberian Peninsula). *Quaternary Science Reviews*, *205*, 86-105 (2019).

Carrión, J. S., & Van Geel, B., Fine-resolution Upper Weichselian and Holocene palynological record from Navarrés (Valencia, Spain) and a discussion about factors of Mediterranean forest succession. *Review of Palaeobotany and Palynology*, *106*(3-4), 209-236 (1999).

Chevalier, M., *et al*., Pollen-based climate reconstruction techniques for late Quaternary studies. *Earth-Science Reviews*, *210*, 103384 (2020).

Combourieu Nebout, N., *et al*., Rapid climatic variability in the west Mediterranean during the last 25 000 years from high resolution pollen data. *Climate of the Past*, *5*(3), 503-521 (2009).

Connor, S. E., *et al*., A survey of modern pollen and vegetation along an altitudinal transect in southern Georgia, Caucasus region. *Review of Palaeobotany and Palynology*, *129*(4), 229-250 (2004).

Davis, B. A., *et al*., The Eurasian Modern Pollen Database (EMPD), version 2. *Earth System Science Data Discussions*, *2020*, 1-41 (2020).

Davis, B. A. S., Fasel, M., Kaplan, J. O., Russo, E., & Burke, A., The climate and vegetation of Europe, North Africa and the Middle East during the Last Glacial Maximum (21,000 years BP) based on pollen data. *Climate of the Past Discussions*, *2022*, 1-66 (2022).

de Vernal, A. D., *et al*., Reconstruction of sea-surface conditions at middle to high latitudes of the Northern Hemisphere during the Last Glacial Maximum (LGM) based on dinoflagellate cyst assemblages. *Quaternary Science Reviews*, *24*(7-9), 897-924 (2005).

Dugerdil, L., *et al*., Late Holocene Mongolian climate and environment reconstructions from brGDGTs, NPPs and pollen transfer functions for Lake Ayrag: Paleoclimate implications for Arid Central Asia. *Quaternary Science Reviews*, *273*, 107235 (2021).

Eynaud, F., *et al*., Position of the Polar Front along the western Iberian margin during key cold episodes of the last 45 ka. *Geochemistry, Geophysics, Geosystems*, *10*(7) (2009).

Fabres, J., Calafat, A., Sanchez-Vidal, A., Canals, M., & Heussner, S., Composition and spatio-temporal variability of particle fluxes in the Western Alboran Gyre, Mediterranean Sea. *Journal of Marine Systems*, *33*, 431-456 (2002).

Frechette, B., *et al*., Methodological basis for quantitative reconstruction of air temperature and sunshine from pollen assemblages in Arctic Canada and Greenland. *Quaternary Science Reviews*, *27*(11-12), 1197-1216 (2008).

Fréchette, B., Richard, P. J., Grondin, P., Lavoie, M., & Larouche, A. C., *Histoire postglaciaire de la végétation et du climat des pessières et des sapinières de l'ouest du Québec*. Gouvernement du Québec, ministère des Forêts, de la Faune et des Parcs, Direction de la recherche forestière. Mémoire de recherche forestière n^{o} 179, 165 p. (2018).

García-Amorena, I., *et al*., The Late Quaternary coastal forests of western Iberia: A study of their macroremains. *Palaeogeography, Palaeoclimatology, Palaeoecology*, *254*(3-4), 448-461 (2007).

Genty, D., *et al*., Precise dating of Dansgaard–Oeschger climate oscillations in western Europe from stalagmite data. *Nature*, *421*(6925), 833-837 (2003).

Genty, D., *et al*., Isotopic characterization of rapid climatic events during OIS3 and OIS4 in Villars Cave stalagmites (SW-France) and correlation with Atlantic and Mediterranean pollen records. *Quaternary Science Reviews*, *29*(19-20), 2799-2820 (2010).

Giesecke, T., *et al*., Postglacial change of the floristic diversity gradient in Europe. *Nature communications*, *10*(1), 5422 (2019).

Guiot, J., Methodology of the last climatic cycle reconstruction in France from pollen data. *Palaeogeography, Palaeoclimatology, Palaeoecology*, *80*(1), 49-69 (1990).

Guiot, J., *et al*., The climate in Western Europe during the last Glacial/Interglacial cycle derived from pollen and insect remains. *Palaeogeography, Palaeoclimatology, Palaeoecology*, *103*(1-2), 73-93 (1993).

Guiot, J., & de Vernal, A., Chapter thirteen transfer functions: methods for quantitative paleoceanography based on microfossils. *Developments in marine geology*, *1*, 523-563 (2007).

Guiot, J., & De Vernal, A., Is spatial autocorrelation introducing biases in the apparent accuracy of paleoclimatic reconstructions? *Quaternary Science Reviews*, *30*(15-16), 1965-1972 (2011a).

Guiot, J., & De Vernal, A., QSR Correspondence “Is spatial autocorrelation introducing biases in the apparent accuracy of palaeoclimatic reconstructions?” Reply to Telford and Birks. *Quaternary Science Reviews*, *21*(30), 3214-3216 (2011b).

Havinga, A. J., Palynology and pollen preservation. *Review of Palaeobotany and Palynology*, *2*(1-4), 81-98 (1967).

Hemming, S. R., Heinrich events: Massive late Pleistocene detritus layers of the North Atlantic and their global climate imprint. *Reviews of Geophysics*, *42*(1) (2004).

Heusser, L., & Balsam, W. L., Pollen distribution in the northeast Pacific Ocean. *Quaternary Research*, *7*(1), 45-62 (1977).

Hooghiemstra, H., Lézine, A. M., Leroy, S. A., Dupont, L., & Marret, F., Late Quaternary palynology in marine sediments: a synthesis of the understanding of pollen distribution patterns in the NW African setting. *Quaternary International*, *148*(1), 29-44 (2006).

Jackson, S. T., & Overpeck, J. T., Responses of plant populations and communities to environmental changes of the late Quaternary. *Paleobiology*, *26*(S4), 194-220 (2000).

Juggins, S., Quantitative reconstructions in palaeolimnology: new paradigm or sick science?. *Quaternary Science Reviews*, *64*, 20-32 (2013).

Kissel, C., *et al*., Rapid climatic variations during marine isotopic stage 3: magnetic analysis of sediments from Nordic Seas and North Atlantic. *Earth and Planetary Science Letters*, *171*(3), 489-502 (1999).

Koreneva, E. V., Marine palynological researches in the USSR. *Marine Geology*, *4*(6), 565-574 (1966).

Legendre, P., Spatial autocorrelation: trouble or new paradigm?. *Ecology*, *74*(6), 1659-1673 (1993).

Li, Y. C., Xu, Q. H., Yang, X. L., Chen, H., & Lu, X. M., Pollen‐vegetation relationship and pollen preservation on the Northeastern Qinghai‐Tibetan Plateau. *Grana*, *44*(3), 160-171 (2005).

López-García, J. M., Blain, H. A., Bennàsar, M., Sanz, M., & Daura, J., Heinrich event 4 characterized by terrestrial proxies in southwestern Europe. *Climate of the Past*, *9*(3), 1053-1064 (2013).

Malevich, S. B., Vetter, L., & Tierney, J. E., Global core top calibration of δ 18O in planktic foraminifera to sea surface temperature. *Paleoceanography and Paleoclimatology*, *34*(8), 1292-1315 (2019).

Marchant, R., *et al*., Drivers and trajectories of land cover change in East Africa: Human and environmental interactions from 6000 years ago to present. *Earth-Science Reviews*, *178*, 322-378 (2018).

Martin Calvo, M., & Prentice, I. C., Effects of fire and CO 2 on biogeography and primary production in glacial and modern climates. *New Phytologist*, *208*(3), 987-994 (2015).

Mauri, A., Davis, B. A., Collins, P. M., & Kaplan, J. O., The climate of Europe during the Holocene: a gridded pollen-based reconstruction and its multi-proxy evaluation. *Quaternary Science Reviews*, *112*, 109-127 (2015).

Naughton, F., *et al*., Present-day and past (last 25 000 years) marine pollen signal off western Iberia. *Marine Micropaleontology*, *62*(2), 91-114 (2007).

North, G. R. I. P., Ice Core Project members. High-resolution record of northern hemisphere climate extending into the last interglacial period. *Nature*, *431*, 147-151 (2004).

Ortu, E., Brewer, S., & Peyron, O., Pollen‐inferred palaeoclimate reconstructions in mountain areas: problems and perspectives. *Journal of Quaternary Science: Published for the Quaternary Research Association*, *21*(6), 615-627 (2006).

Overpeck, J. T., Webb, T. I. I. I., & Prentice, I. C., Quantitative interpretation of fossil pollen spectra: dissimilarity coefficients and the method of modern analogs. *Quaternary Research*, *23*(1), 87-108 (1985).

Robles, M., *et al*., Impact of climate changes on vegetation and human societies during the Holocene in the South Caucasus (Vanevan, Armenia): A multiproxy approach including pollen, NPPs and brGDGTs. *Quaternary Science Reviews*, *277*, 107297 (2022).

Roucoux, K. H., De Abreu, L., Shackleton, N. J., & Tzedakis, P. C., The response of NW Iberian vegetation to North Atlantic climate oscillations during the last 65 kyr. *Quaternary Science Reviews*, *24*(14-15), 1637-1653 (2005).

Sánchez Goñi, M. F., Turon, J. L., Eynaud, F., & Gendreau, S., European climatic response to millennial-scale changes in the atmosphere–ocean system during the Last Glacial period. *Quaternary Research*, *54*(3), 394-403 (2000).

Sánchez Goñi, M. F., *et al*., Synchroneity between marine and terrestrial responses to millennial scale climatic variability during the last glacial period in the Mediterranean region. *Climate dynamics*, *19*, 95-105 (2002).

Sánchez Goñi, M. F., *et al*., Contrasting impacts of Dansgaard–Oeschger events over a western European latitudinal transect modulated by orbital parameters. *Quaternary Science Reviews*, *27*(11-12), 1136-1151 (2008).

Sánchez Goñi, M. F., Landais, A., Cacho, I., Duprat, J., & Rossignol, L., Contrasting intrainterstadial climatic evolution between high and middle North Atlantic latitudes: a close‐up of Greenland Interstadials 8 and 12. *Geochemistry, Geophysics, Geosystems*, *10*(4) (2009).

Sánchez Goñi, M. F., *et al*., The ACER pollen and charcoal database: a global resource to document vegetation and fire response to abrupt climate changes during the last glacial period. *Earth System Science Data Discussions*, *2017*, 1-33 (2017).

Sánchez Goñi, M. F., et al., Pollen from the deep-sea: A breakthrough in the mystery of the Ice Ages. *Frontiers in Plant Science*, *9*, 294622 (2018).

Sawada, M., Viau, A. E., Vettoretti, G., Peltier, W. R., & Gajewski, K., Comparison of North-American pollen-based temperature and global lake-status with CCCma AGCM2 output at 6 ka. *Quaternary Science Reviews*, *23*(3-4), 225-244 (2004).

Sepulchre, P., *et al*., H4 abrupt event and late Neanderthal presence in Iberia. *Earth and Planetary Science Letters*, *258*(1-2), 283-292 (2007).

Shackleton, N. J., Hall, M. A., & Vincent, E., Phase relationships between millennial‐scale events 64,000–24,000 years ago. *Paleoceanography*, *15*(6), 565-569 (2000).

Šmilauer, P., & Lepš, J., *Multivariate analysis of ecological data using CANOCO 5*. Cambridge university press (2014).

St. Jacques, J. M., Cumming, B. F., Sauchyn, D. J., & Smol, J. P., The bias and signal attenuation present in conventional pollen-based climate reconstructions as assessed by early climate data from Minnesota, USA. *PloS one*, *10*(1), e0113806 (2015).

Telford, R. J., & Birks, H. J. B., The secret assumption of transfer functions: problems with spatial autocorrelation in evaluating model performance. *Quaternary Science Reviews*, *24*(20-21), 2173-2179 (2005).

Telford, R. J., & Birks, H. J. B., Evaluation of transfer functions in spatially structured environments. *Quaternary Science Reviews*, *28*(13-14), 1309-1316 (2009).

Telford, R. J., & Birks, H. J. B., QSR Correspondence" Is spatial autocorrelation introducing biases in the apparent accuracy of palaeoclimatic reconstructions?". *Quaternary Science Reviews*, *30*(21), 3210-3213 (2011).

Theuerkauf, M., Dräger, N., Kienel, U., Kuparinen, A., & Brauer, A., Effects of changes in land management practices on pollen productivity of open vegetation during the last century derived from varved lake sediments. *The Holocene*, *25*(5), 733-744 (2015).

Turon, J. L., Direct land/sea correlations in the last interglacial complex. *Nature*, *309*(5970), 673-676 (1984).

Wiens, J. J., *et al.*, Niche conservatism as an emerging principle in ecology and conservation biology. *Ecology letters*, *13*(10), 1310-1324 (2010).

Zolitschka, B., & Negendank, J. F. (1996). Sedimentology, dating and palaeoclimatic interpretation of a 76.3 ka record from Lago Grande di Monticchio, southern Italy. *Quaternary Science Reviews*, *15*(2-3), 101-112.

CHAPITRE 3

HIGH WINTER PRECIPITATION INFERRED FROM POLLEN SEQUENCES IN SOUTHERN EUROPE DURING THE LAST GLACIAL MAXIMUM

Jena Zumaque*[a], Anne de Vernal[a], Frédérique Eynaud[b], Aurélie Penaud[c], Jon Camuera[d], Gonzalo Jiménez-Moreno[e]

[a] GEOTOP - Centre de recherche en géochimie et géodynamique, Université du Québec à Montréal, Canada

[b] EPOC (Environnements & Paléoenvironnements Océaniques et Continentaux) Laboratory, UMR 5805, Bordeaux University, France

[c] CNRS, Ifremer, Geo-Ocean UMR 6538, University Brest, France

[d] Unit of Botany, Faculty of Pharmacy, Complutense University of Madrid, Spain

[e] Department of Stratigraphy and Paleontology, University of Granada, Spain

Article en préparation pour soumission dans la revue *Quaternary Science Reviews*

Résumé en français

Le climat du Dernier Maximum Glaciaire (LGM – *Last Glacial Maximum*) dans le sud de l'Europe a largement été documenté. Pourtant, des divergences existent entre les informations climatiques fournies par les séquences polliniques, qui indiquent principalement une végétation steppique et donc des conditions arides, et les modèles qui simulent de grandes quantités de précipitations, notamment en hiver. Ici, nous explorons la végétation régionale et le climat saisonnier de 28 à 10 ka à l'aide de séquences polliniques déjà publiées provenant de cinq sites, incluant la carotte SU81-18 localisée sur la marge ouest ibérique, le site ODP 976 en Mer d'Alboran, Padul dans le sud-est de l'Espagne, Lago Grande di Monticchio (Monticchio) dans le sud de l'Italy et Xinias en Grèce. Les estimations saisonnières de températures et précipitations sont reconstituées à partir des pollens via la technique des analogues modernes, et ce, à l'aide de la dernière version de la base de données polliniques modernes eurasienne (EMPD2 - *Eurasian Modern Pollen Database*), qui comprend de nombreux échantillons en provenance d'environnements froids, et donc de potentiels analogues pour les conditions du LGM. Les résultats mettent en évidence un mode cohérent à échelle régionale de la dynamique de la végétation qui apparait étroitement liée aux températures et précipitations hivernales, lesquelles sont liées aux vents d'ouest. Plus important encore, nous reconstruisons de fortes précipitations hivernales et annuelles au cours du LGM dans les cinq séquences, notamment dans les trois enregistrements les plus à l'ouest où les estimations sont supérieures à celles du début de l'Holocène. Nos résultats suggèrent en outre qu'une importante variabilité des précipitations caractérise le LGM le long de la marge Atlantique alors que ces variations apparaissent plus faibles plus à l'est, et notamment en Mer d'Alboran, laissant supposer la présence d'un

front climatique entre les deux régions. Deux phases de fortes précipitations sont enregistrées, l'une de 24 à 22,5 ka et l'autre de 21,5 à 19,5 ka. Le timing de ces intervalles humides est en phase avec deux périodes d'avancée des glaciers des Alpes, suggérant une configuration atmosphérique cohérente à échelle régionale. L'augmentation des précipitations est attribuée à un déplacement vers le sud de l'Europe du courant jet, et donc des vents d'ouest, du fait de l'extension maximale des calottes de glace de l'hémisphère Nord, alors que la phase plus sèche pourrait correspondre à un affaiblissement ou à un mouvement latitudinal des vents d'ouest. Des indications de boisement au cours du LGM sont visibles aux sites ibériques, mais pas à Monticchio ou Xinias où un climat plus froid pourrait avoir empêché le développement d'une végétation plus arborée. Nous émettons l'hypothèse que ce gradient ouest-est de températures pourrait être relié à l'influence des calottes fennoscandienne et alpine du fait d'une cassure de l'onde de Rossby du courant jet à l'ouest des Alpes.

Abstract

The climate of the Last Glacial Maximum (LGM) in southern Europe has been thoroughly documented. Still, discrepancies exist between the climatic information provided by pollen sequences, which mainly indicate steppe vegetation and thus arid conditions, and models that simulate large amounts of precipitation, notably in winter. Here, we investigate the regional vegetation and seasonal climate from 28 ka to 10 ka using published pollen sequences from five sites, including core SU81-18 located on the western Iberian Margin, ODP Site 976 in the Alboran Sea, Padul in Southeastern Spain, Lago Grandi di Monticchio (Monticchio) in southern Italy and Xinias in Greece. Pollen-based seasonal estimates of temperatures and precipitation are reconstructed using the Modern Analogue Technique with the latest version of the Eurasian Modern Pollen Database (EMPD2), which comprises many samples from cold environments, providing potential analogues for LGM conditions. The results highlight a coherent regional pattern of vegetation dynamics that appear tightly linked to winter temperature and winter and annual precipitation, linked to the westerlies. Most importantly, we reconstruct high winter and annual precipitation during the LGM in the five study sequences, notably at the three western sites where estimates are even higher than for the early Holocene. Our results suggest high variability in precipitation characterized the LGM along the Atlantic margin sequence, and lower variations further east, notably in the Alboran Sea, pointing to a climatic front somewhere in between. Two phases of increased precipitation were shown in our records, one from 24 to 22.5 ka and the other from 21.5 to 19.5 ka. The timing of these humid intervals is in phase with two main glacier advance periods in the European Alps, suggesting a consistent regional atmospheric pattern. Increased precipitation is attributed to the southward displacement of the jet stream, and thus the westerlies, over the region due to maximum extension of the Northern Hemisphere ice sheets while the dry phase might correspond to a weakening or latitudinal movement of the westerlies. Indications of afforestation during the LGM are seen at the Iberian sites, not at Monticchio and Xinias where cold climate may have prevented forest vegetation. We hypothesize that the west-east temperature gradient is related to the influence of the Fennoscandian and Alpine ice sheets due to the Rossby wave breaking of the jet stream west of the Alps.

Keywords: Last Glacial Maximum, Southern Europe, Pollens, Modern Analogue Technique, Seasonality

3.1 Introduction

During Marine Isotope Stage 2 (MIS 2) (~29 – 14 ka; Lisiecki and Raymo, 2005) and the beginning of MIS 1 (until around 11.7 ka), the Earth climate underwent major changes that were particularly pronounced in the North Atlantic Region, notably the Southwestern European continent (e.g., Gonzalez-Samperiz et al., 2006; Combourieu-Nebout et al., 2009; Pascual et al., 2020; Argenio et al., 2021; Rodrigo-Gámiz et al., 2022). The cold episodes designed as Heinrich Stadials (HS) HS1 and HS2 (Sanchez-Goñi and Harrison, 2010), the Last Glacial Maximum (LGM), and the last phase of the deglaciation that includes the Bølling/Allerød (B/A) and the Younger Dryas (YD), have received special attention from paleoclimatologists and paleoceanographers (e.g., Zaragosi et al., 2001, 2006; Combourieu-Nebout et al., 2009; Penaud et al., 2011; Toucanne et al., 2015; Pascual et al., 2020; Argenio et al., 2021) because they illustrate abrupt, large amplitude climate and ocean variations, allowing to document the dynamics of the climate-ocean system.

The LGM (23 - 19 ka; Mix et al., 2001; MARGO, 2009) is defined as the most recent time of maximum global ice volume (Mix et al., 2001), when boundary conditions were drastically different from today, with the development of large ice-sheets in the Northern Hemisphere (e.g., Dyke et al., 2002; Svendsen et al., 2004; Lambeck et al., 2006; Tarasov et al., 2012), minimum global sea-level of ~ -120 m (Lambeck et al., 2014) and low concentration of greenhouse gas (375 ppb of CH_4, 190 ppm of CO_2) (e.g., Kageyama et al., 2017).

Paleoecological data indicate that during the LGM, cold and dry climatic conditions prevailed over most of Europe likely due to a southward displacement of the polar front and the westerlies (e.g., Eynaud et al., 2009; Lainé et al., 2009; Toucanne et al., 2015; Beghin et al., 2016), which resulted in open vegetation such as steppe and grasslands (e.g., Peyron et al., 1998; Elenga et al., 2000; Shao et al., 2018). However, discrepancies have been highlighted for the southwestern European region, and more specifically the Iberian Peninsula, where wet conditions, especially in winter, were estimated based on proxy data (e.g., Vegas et al., 2010; Moreno et al., 2012; Schafer et al., 2016) and model simulations (e.g., Lainé et al., 2009; Löfverström et al., 2014; Beghin et al., 2016; Löfverström and Lora, 2017; D'Agostino and Lionello, 2020; Kageyama et al., 2021) although many pollen sequences from the Pyrenean region indicated steppe vegetation and thus arid conditions (e.g., Andrieu et al., 1993; Reille and Andrieu 1995; Valero-Garces et al., 2004; Gonzalez-Sampériz et al. 2006). To explain such discrepancies, some authors have evoked the impact of low CO_2 atmospheric concentrations on the plant water-use efficiency (Ramstein et al., 2007), and the seasonality of precipitation as plants mainly depend on the amounts of precipitation falling during

the growing season (Prentice et al., 1992). However, the marine core SU81-18 (Turon et al., 2003) and ODP Site 976 (Combourieu-Nebout et al., 2009), located off the western and southeastern Iberian margins have recorded increased fluxes of Ericaceae pollen during the LGM, which suggests humid conditions. The pollen-based climatic reconstitutions from Site ODP 976 (Combourieu-Nebout et al., 2009), however, do not corroborate an increase in winter precipitation as inferred non-pollen proxies and some modelling experiments (e.g., Beghin et al., 2016).

Here, we address the issue of seasonality in temperatures and precipitation over southwestern Europe from 28 to 10 ka using the pollen data from the three southern Iberian records, that of cores SU81-18 (Turon et al., 2003), ODP Site 976 (Combourieu-Nebout et al., 2009) and Padul (Camuera et al., 2018, 2019) using the most recent Eurasian Modern Pollen Database (EMPD2; Davis et al., 2020). The EMPD2 database comprises more than 8000 samples, including many additional samples from cold environments, notably in Siberia, thus offering potential analogues for LGM conditions (Magyari et al., 2014a). Previous estimates of LGM sequences of core SU81-18 and ODP 976 were based on a modern pollen database of around 3500 (Bordon et al., 2009). Herein, we also reconstruct paleoclimate from the pollen sequences of Lago Grande di Monticchio (Allen et al., 2000; Wulf et al., 2004; Brauer et al., 2007) and Xinias (Bottema, 1979), located further east at the same latitudes, in the Central and Eastern Mediterranean basins respectively (Fig. 3.1). The dataset then comprised five mid-latitude sequences, allowing us to examine the regional coherency in the climatic pattern during MIS 2 and the beginning of MIS 1, and more specifically, during the LGM.

3.2 Environmental setting

3.2.1 Climate and Vegetation

The five studied pollen records, located in Southwestern and Southern Europe (Fig. 3.1; Table 3.1), belong to the Mediterranean region (MedR) (~36-40°N). In winter, the regional climate is mainly influenced by the North Atlantic Oscillation (NAO), a circulation pattern quantified as the atmospheric pressure difference between the Icelandic Low and the Azores High from November to April (Hurrell, 1995). The NAO modes of variability impact the strength and direction of the westerlies. An NAO positive mode, which corresponds to strong pressure gradients, causes cold and dry winters in Southern Europe due to a northward displacement of the westerlies that bring moisture-laden air masses to the northwest part of the continent. Conversely, a negative mode of the NAO (weak pressure gradients) results in a mild and wet winter climate in Southern Europe through the southward displacement of the storm track. In summer,

the influence of the westerlies weakens and strengthens anti-cyclonic cells over the sub-tropical eastern Atlantic Ocean generating the characteristic dry summers of the Mediterranean climate (Rodwell and Hoskins, 2001).

The above-mentioned climatic conditions favour the development of Mediterranean landscapes marked by altitudinal gradients according to the ecological affinities of plants (Combourieu-Nebout et al., 2009 and references therein). The lowlands are characterized by evergreen sclerophyllous woodland (evergreen *Quercus*, *Olea*, *Pistacia*, *Phillyrea*, *Cistus*) along with steppe and semi-desert taxa (*Artemisia*, Chenopodiaceae, *Ephedra*). The mid-altitude vegetation mainly comprises sclerophyllous and humid-temperate oak forests (notably deciduous *Quercus* and Ericaceae), while cold-temperate coniferous forest characterizes the highest altitudes.

3.2.2 Oceanography and sedimental processes at marine core locations

The site of deep-sea core SU81-18 (Fig. 3.1; Table 3.1) is located between 100 and 200 km off the coastline on the southwestern Iberian margin, where flows the equatorward southern branch of the North Atlantic Drift (Naughton et al., 2007). A well-developed hydrographic system accounts for pollen inputs from the Tagus River area through canyons and offshore filaments (Naughton et al., 2007). There is limited airborne pollen input because of the direction of the dominant North Atlantic westerlies but we cannot discard the possibility of pollen dispersal from northern Africa with Saharan winds (Rodriguez et al., 2001).

Site ODP 976 (Fig. 3.1; Table 3.1) is situated off the Southeastern Iberian Margin, in the Alboran Sea (1108 m deep), connected to the North Atlantic Ocean via the Strait of Gibraltar. The Atlantic water has lower salinity and density than the Mediterranean outflowing water occupying the upper part of the water column (La-Violette, 1986). There is no major river system in this region, but torrential rains from southeastern Iberia may generate large riverine inputs to the Alboran Sea. Aeolian lithogenic particles only represent 12% of the total particle supply (Fabrés et al., 2002). It thus implies that the main pollen contribution to this site comes essentially from the adjacent Iberian riverine system (Sánchez-Goñi et al., 2002). Nevertheless, as for site SU81-18, the occurrence of *Cedrus* pollen from the Atlas Mountains indicates that pollen can be advected through southerly Saharan winds from northern Africa.

3.3 Material and Methods

3.3.1 Pollen data and chronologies

The raw pollen data from core SU18-81, ODP Site 976, Lago Grande di Monticchio (named Monticchio hereafter) and Xinias were downloaded from the ACER (Abrupt Climate Changes and Environmental Responses) database (Sánchez-Goñi et al., 2017) (Fig. 3.1; Table 3.1). The raw pollen data from the Padul sequence were shared by authors of Camuera et al. (2018, 2019) (Fig. 3.1; Table 3.1). These sequences cover the entire MIS 2 and the beginning of MIS 1 until 10 ka and offer mean temporal resolutions from 95.3 to 492.9 years, for the section (Table 3.1).

The advantage of studying pollen from marine cores is the usually well-constrained chronology and the possibility of direct land-sea correlations by comparing pollen and proxy indicators of the ocean environment (Sánchez-Goñi et al., 2002, 2008, 2009; Roucoux et al., 2005). Furthermore, providing sufficiently high temporal resolution is achieved, the marine time series can be correlated to the reference Greenland interstadials (GI) and stadials (GS) succession (Austin and Hibbert, 2012). For core SU81-81 and ODP Site 976, we used the same dating points as in the ACER database (for more details, see file "dating_info_ACER" in Sánchez-Goñi et al., 2017) but we recalculated the ages using CLAM (Blaauw, 2010), implemented in R (R version 3.3.1) (R Development Core Team, 2016) for consistency in the age-model of the marine and continental records (Table 3.1). We used Marine13 (Reimer et al., 2013) to calibrate the marine sediment dates. A ΔR of 41 ± 70 yrs and -22 ± 35 yrs was used for cores SU81-81 and for ODP Site 976 respectively.

For the Xinias sequence, we used the updated chronology proposed in the ACER database (for more details, see Sanchez-Goñi et al., 2017). However, since the chronology of this sequence is very weak (only 5 radiocarbon dates for the period between 47 and 10 ka), the timing of the environmental changes inferred from this sequence needs to be interpreted with caution.

The age models of the three above-mentioned sequences are presented in Supplementary data (see also file "dating_info_ACER" in Sánchez-Goñi et al., 2017).

For the Monticchio sequence, we used the initial chronology based on annual lamination ("varves") counts and sedimentological features in the non-varved intervals (Zolitschka and Negendank, 1996) as was done by the ACER group (Sánchez-Goñi et al., 2017). However, although the chronology of the entire

Monticchio sequence, which covers at least the last 100,000 years, was overall corroborated by many dated tephra layers with a mean deviation of ~ 5% (Wulf et al., 2004), some sections appear problematic. The varve counting chronology of the lower half of the MIS 2 section may have underestimated the ages by up to 3000 years compared to the calibrated ages of the tephra layers (Wulf et al., 2004). Genty et al. (2010) have also highlighted possible offsets in the chronology of the Monticchio sequence. Hence, as for the Xinias sequence, we remain cautious regarding the interpretation of the timing of vegetation and climatic shifts from this sequence.

For the Padul sequence, we used the original chronology developed by Camuera et al. (2018) and presented in the associated paper.

3.3.2 Vegetation: Plant Functional Types (PFTs)

Since the pollen data is derived from different projects and investigators, the taxonomic can vary from one site to another. Grouping the taxa reduces the number of variables and facilitates the comparison between sites. We thus converted the pollen taxa into Plant Functional Types (PFTs) which are broad classes of plants defined by stature, leaf form, phenology and climatic thresholds, following the concept developed by Prentice et al. (1992). The three fossil records were consequently harmonized in 94 taxa to characterize 15 arboreal and 8 shrub/herbaceous PFTs (Table 3.2), each taxon being assigned to only one PFT according to the known biology of the species (Peyron et al., 1998). Virtual PFTs, which are a combination of the potential PFTs that a taxon could belong to, were initially created to handle ambiguous taxa and were then reassigned afterwards depending on the biome identified for the pollen sample (Peyron et al., 1998). Here, we do not interpret the assemblages as biomes and have made no reassignment. For each pollen sample, the relative abundances of the 94 pollen taxa included in this work were calculated (Table 3.2) and square-rooted to amplify the importance of the rare versus the more abundant taxa. We summed the square-rooted relative abundances of the taxa associated with their respective PFTs (Table 3.2) and calculated percentages from the scores obtained for each PFT. Unlike Prentice et al. (1996) and Peyron et al. (1998), we did not remove taxa with low abundances (< 0.5%).

3.3.3 Pollen-based climate reconstruction

We reconstructed climate parameters from pollen data using the Modern Analogue Technique (MAT) (Overpeck et al., 1985; Guiot, 1990). MAT is based on the principle that the ecological affinities of the different species have not changed through time (Jackson and Overpeck, 2000) and compares a fossil

pollen assemblage to all modern pollen assemblages in a reference database. The similarity assessment between fossil and modern pollen assemblages is based on the squared chord distance (SCD) dissimilarity metric (Overpeck et al., 1985), which varies between 0 and 2. Low values indicate a high degree of similarity, whereas high values indicate large dissimilarity between two samples. The closest modern pollen samples defined by the lowest SCDs), are best analogues, and the weighted average of their climate parameter values is calculated to provide information on past climatic conditions. An SCD threshold beyond which any analogue is rejected is also calculated based on the Monte Carlo method. In this work, we followed de Vernal et al. (2005) for a reliability index of analogues which defines three categories: 1) Poor or no analogue situation when the SCD of the closest analogue is higher than the SCD threshold, 2) Acceptable analogue situation when the SCD is between half of the threshold value and the threshold, and 3) Good analogue situation when the SCD is between 0 and half of the threshold value.

The paleoclimate reconstructions were made with the "bioindic" package (ftp://ftp.cerege.fr/R/Package_bioindic/), built on the R-platform (http://cran.r-project.org/), using a modern calibration dataset taken from the version 2 of the Eurasian Modern Pollen Database (EMPD2; Davis et al., 2020). This subset of data includes 7634 modern pollen samples from the Paleartic realm and a total of 88 pollen taxa. It covers a total of nine biomes (cf. Davis et al., 2020). It thus comprises a large number of potential modern analogues for different climates and vegetation types, which is particularly critical when considering the objective of climatic reconstructions of glacial times (Magyari et al., 2014; Davis et al., 2022). The climatic data in the initial EMPD2 were calculated using WordlClim2 (Fick and Hijmans, 2017) and include mean monthly, seasonal and annual temperatures and precipitation (Davis et al., 2020). We added the mean temperature of the warmest (MTWA) and the coldest months (MTCO), and the seasonality defined as the difference between MTWA and MTCO. MTWA, MTCO, seasonality, along with winter (Pdjf), summer (Pjja) and annual precipitation (Pann) were the climatic variables retained for this work. This ready-to-use version of the EMPD2 is presented in Zumaque et al. (*submitted to Data in Brief*).

Due to the overrepresentation of *Pinus* in marine sediments (Turon, 1984; Rochon and de Vernal, 1994), the modern calibration dataset was adapted for the data treatment of the two marine series of this study. We removed *Pinus* and recalculated the relative abundances of taxa (%). Since we had already removed samples with a sum (excluding *Pinus*) under 100 grains, the "marine version" of our adapted dataset comprises the same number of modern samples as the "terrestrial" version of the dataset. The

reasoning behind the decision to apply MAT to marine pollen sequences and remove Pinus from the modern and fossil assemblages is detailed in Zumaque et al. (*submitted to Quaternary Science Reviews*).

Validation tests were conducted to estimate the accuracy of quantitative reconstructions with the two final versions of our sub-dataset (with and without *Pinus*, i.e., with 87 or 88 taxa) and are presented in Table 3.3. We have used a set of 5 analogues, which seems to be the most adequate number of analogues for quantitative reconstructions, as shown by validation tests performed by Zumaque et al. (*submitted to Quaternary Science Reviews*).

Atmospheric CO_2 concentration impacts vegetation dynamics since it controls the plant water-use efficiency (Harrison and Prentice, 2003; Prentice et al., 2017). Therefore, atmospheric CO_2 variations through time likely impacted the relationships between pollen assemblages and climate, especially during glacial times when atmospheric CO_2 concentration values were low (Ahn and Brooks, 2008; Bauska et al., 2021). Many have argued that it was essential to account for CO_2 changes when reconstructing climate parameters from vegetation proxies, especially for periods with low CO_2 concentrations such as the LGM, during which climate estimates from pollen were possibly biased toward drier values (e.g., Cleator et al., 2020; Prentice et al., 2022). The fact that MAT, as many other paleoclimate proxies, does not account for atmospheric CO_2 effect is thus a limitation. In a recent study, Davis et al. (2022) compared MAT reconstructions with reconstructions from a method accounting for CO_2 changes (i.e., Inverse Modelling; Guiot et al., 2000) during the LGM in Europe and other regions. The results have shown good agreement between the two methods, strengthening the reliability of MAT for climatic reconstructions of glacial times and suggesting that low CO_2 concentrations during the LGM had little impact on the pollen-based reconstructions of climate (Davis et al., 20022).

MAT reconstructions are compared to modern values at the terrestrial sites using the mean climatic values calculated from 1901 to 2022 with Climate Explorer (https://climexp.knmi.nl/start.cgi). The grid for the climatic compilation is 0.5° x 0.5°. Because pollen in marine sediment cores may correspond to fluxes from wide areas, it is difficult to assess the modern climatic values at the two study marine sites.

3.3.4 Redundancy analysis (RDA)

A redundancy analysis (RDA) was performed for each site with PFT and paleoclimatic estimates using Canoco 5 software (Smilauer and Leps, 2014). It allows us to 1) examine the primary variation patterns of

the vegetation (PFTs) and 2) to better visualize which climatic parameters explain the primary variation patterns in the vegetation. As square root transformations were already applied to the initial pollen percentages for the PFT grouping, no additional transformation was made before running the RDAs. The goal here is not to show that vegetation responds to climate since it is one of the basic principles of climate reconstruction based on paleobotanical data, but rather to investigate the nature of the climate-vegetation linkages in the study region during MIS 2. It is also worth highlighting here that the paleoclimatic reconstructions are based on pollen taxa instead of grouped taxa, as is the case for the PFTs, and that the number of taxa retained for PFT grouping and MAT are different.

3.3.5 Paleohydrographic reconstructions at site SU81-18

Planktonic foraminifer analyses were previously carried out on core SU81-18 and the results were used to infer paleohydrographic reconstitutions (Penaud et al., 2011). Here, we present new paleohydrographic reconstitutions based on the latest version of the foraminifer modern database and using the MAT1007 transfer function developed at EPOC (see Eynaud et al, 2021). The modern reference database includes 1007 modern samples from the North Atlantic Ocean and its adjacent seas. Here, we show summer and winter SST reconstructions and mean annual sea-ice cover duration reconstructions.

3.4 Results

3.4.1 Primary patterns of PFT variations

The redundancy analysis (RDA) applied to the PFT and climatic reconstructions informs on the primary patterns of PFT variation at each site (Fig. 3.2). The RDA-Axis 1 explains 60.57, 73.5, 84,80 and 79.92% of the total PFT variance of the data in core SU81-18, at ODP Site 976, Padul and Monticchio, respectively. Hence, we consider axis 1 as reflecting the primary pattern of vegetation variation.

Axis 1 indicates an opposition between arboreal and non-arboreal PFTs (Fig. 3.2). At the marine locations of core SU81-18 and ODP Site 976 (Figs. 3.2a and 3.2b), Temperate Summergreen (TS), Warm Temperate Broad-Leaved Evergreen (WTE) and to a lesser degree Warm-temperate sclerophyll trees/shrub (WTE2) constitute the arboreal PFTs displaying the strongest variability. They are opposed to Steppe forb/shrub (SF), Desert forb/shrub (DF) and, to a lesser extent, *Juniperus* (ECPI; Table 3.2). The same PFTs are opposed at Padul with the addition of the Eurythermic conifer (EC), i.e., *Pinus*, which was removed from the marine sequences (see Material and Methods) and stands along the non-arboreal PFTs in the Padul RDA graph (Fig. 3.2c). At Monticchio, the arboreal PFTs TS, Cool-Temperate summergreen

(TS1) and Temperate/boreal summergreen/arctic-alpine (TSAA) are opposed to SF, Cold (COGS) and Warm grass shrubs (WAGS) and Grass (GR) (Fig. 3.2c).

At Xinias, RDA-Axis 1 also represents the primary pattern of vegetation variation with 73,52% of the total variance. However, at this site, the opposition between arboreal and non-arboreal PFTs is clearly reflected along Axis 2, which records 24.53% of the total variance (Fig. 3.2e). We will thus use this second RDA axis to compare with other sites in the discussion. Xinias RDA-Axis 1 scores through time are presented in Figure 3.S4 in Supplementary Data.

3.4.2 Vegetation and climate during the glacial episode

The primary (secondary for Xinias) patterns of PFT variations through time (Axis-1 scores) and the results of MAT reconstructions for SU81-18, ODP Site 976, Padul, Monticchio and Xinias are presented in Figures 3.3, 3.4, 3.5, 3.6 and 3.7 respectively, together with ocean proxy data from the same sites in the case of marine sequences and from adjacent sites in case of Monticchio.

3.4.2.1 Southwestern Iberian margin

The primary pattern of vegetation variations in core SU81-18 depicts important variations (Fig. 3.3b), with the lowest proportions of arboreal vegetation being recorded during HS2 and HS1, while the highest proportions of arboreal PFTs characterize the upper section (~15 to 10 ka) (Figs. 3.3a and 3.3b). Between HS2 and HS1, which encompasses the LGM, high variations around moderately high proportions of arboreal vegetation are recorded.

Arboreal PFTs are positively linked with MTCO (Figs. 3.2a and 3.3d) and, to a lesser degree, with Pann and Pdjf, both being highly correlated (Figs. 3.2a and 3.3g). However, there is no apparent relationship between the PFTs and Pjja (Figs. 3.2a and 3.3g) and MTWA (Figs. 3.2a and 3.3d). Hence, the MAT reconstructions suggest a predominant influence of the winter season on the vegetation.

MTCO displays important variations, with an amplitude of about 10°C and several incursions below 0°C (Fig. 3.3d) that might have constituted an ecological stress on the vegetation, favouring the decline of the arboreal vegetation. An IRD peak, which corresponds to the Heinrich layer (Sánchez-Goñi and Harrison, 2010), accompanies the low MTCO in the latest phase of each HS (Fig. 3.3e; Bard et al., 2000). Positive MTCO characterizes the B/A, the middle part of each HS and the intervals between HS, which encompasses

the LGM, despite a few incursions below 0°C around 22.5 and 19 ka (Fig. 3.3d). Overall, the 3-point running mean of MTCO is in good agreement with foraminifera-based SST curves (Fig. 3.3c), demonstrating close linkages between land and ocean conditions. The only noticeable exception is the MTCO peak recorded around 17 ka during HS1, which has no correspondence in the SST record nor in the relatively high percentages (50%) of *Neogloboquadrina pachyderma* (Fig. 3.3e; Eynaud et al., 2009), indicating almost polar conditions at this time. The close land-ocean linkage is further shown by the peaks of sea-ice cover duration inferred from planktonic foraminifer assemblages mirroring the biggest development of steppe vegetation that occurred during the HSs.

Throughout the entire section, pollen-based estimates of summer temperatures remain similar and seasonality mirrors the MTCO (Figs. 3.3d and 3.3f), with higher values during the cold HSs and during YD, while lower seasonality characterizes the LGM (Fig. 3.3f).

Annual and winter precipitation appear highly correlated (Figs. 3.2a and 3.3g), Pann mimicking Pdjf with a three times greater amplitude. The lowest values of Pann and Pdjf (around 300 and 100 mm respectively) are recorded during HS1 and the first half and the very end of HS2 (Fig. 3.3g), while moderately higher values characterize the MIS 1 section, with only a slight decrease during the cold YD. The most noticeable feature of the Pann and Pdjf records is, however, the significant millennial-scale variability that characterizes the period from 25.5 to 19.5 ka, and thus the LGM, with 5 peaks reaching the highest values of the entire sequence (Fig. 3.3g). Most of these peaks are concomitant with the MTCO peaks recorded during this same period (Fig. 3.3d).

3.4.2.2 Alboran Sea and Southeastern Spain

The primary patterns of PFT variations at ODP Site 976 (Fig. 3.4b) and Padul (Fig. 3.5b) show two highly distinguishable sections: the first one, until ~15 ka, is characterized by high proportions of non-arboreal vegetation. The other, after 15 ka, is marked by increased arboreal vegetation. The HS2 records the highest proportions of non-arboreal PFTs. It is followed by a progressive increase of the arboreal vegetation during the LGM until 19 ka, after which the proportions of treeless PFTs increase again, with high value during HS1 (Figs. 3.4a-b and 3.5a-b). After 15 ka, afforestation characterizes the B/A at both sites. However, a decrease of the arboreal PFTs during the following YD is only recorded at ODP Site 976. The beginning of the Holocene, around 11.7 ka, is then marked by the highest rates of arboreal vegetation in both sequences (Figs. 3.4a-b and 3.5a-b).

In the Alboran Sea, the RDA graph (Fig. 3.2b) shows a strong linkage between arboreal PFTs and the indicators of precipitation (Pann, Pjja and Pdjf) which seem highly correlated. Non-arboreal PFTs appear strongly correlated with seasonality, but also, although to a lesser extent, with MTWA. Conversely, MTCO does not seem to have a great influence on the primary pattern of PFT variations as it is strongly correlated with Axis 2 (Fig. 3.2b). Conversely, at Padul, in Southeastern Spain, arboreal PFTs appear more correlated with both winter and summer temperatures while winter and annual precipitation are strongly correlated with Axis 2 (Fig. 3.2c).

Pann and Pdjf show strong correlations and, similar behaviour at both southeastern Iberian sites ODP Site 976 and Padul (Figs. 3.4f and 3.5e). Overall, Pann and Pdjf record their lowest values during the HSs, although Padul records an increase of Pann and Pdjf during the middle part of HS1 and the highest values during the LGM. The important drop in annual precipitation recorded in the Padul sequence between 24.7 and 23 ka, which we attribute to HS2, could indicate an underestimation of the ages for the bottom section (Fig. 3.5). It is also worth mentioning that the period in between HSs, which encompasses the LGM, was marked by high amplitude variations of precipitation at ODP Site 976 with low values around 22 ka (Fig. 3.4f), while more stable conditions were recorded at Padul. The period after 15ka recorded relatively high and stable values at ODP Site 976 except for a slight decrease during the first part of the YD (Fig. 3.4f), while Pann at Padul mimics the NGRIP record with more pronounced decreased values during the YD (Figs. 3.5a and 3.5e).

The higher difference between both sequences is depicted by temperature estimates. ODP Site 976 shows small temperature variations, with an amplitude rarely exceeding 6 or 7 °C for both MTCO and MTWA (Fig. 3.4c). MTCO remains mostly positive throughout the sequence with only small decreases during the second halves of HS2 and HS1, at the end of the LGM, and during the YD. The SST estimated from alkenones (Fig. 3.4d; Martrat et al., 2014) depicted variations of similar amplitude (~ 5°C) mainly in the upper part of the study section (~ 18 to 10 ka). They, however, depict a general trend of increased temperature of almost 10°C from the LGM to the Holocene that is not apparent in our pollen-based temperature estimates. Conversely, MTCO at Padul exhibits large temperature drops (between 10 and 15°C) during HS1 and HS2 while the LGM and the beginning of MIS 1 are characterized by temperatures above 0°C. In Fig. 3.5c, those values of MTCO appear higher than the modern value (~ 0°C). However, these modern values have been inferred from a 0.5° x 0.5° grid, and Padul is located at the foothills of the Sierra Nevada which culminates at 3479 m a.s.l (Camuera et al., 2018, 2019). They may thus be overestimated,

as it is confirmed by authors in Camuera et al. (2018) who mention an average air temperature of 6.4 °C in January at present. On the other hand, MTWA remains relatively warm and stable until 15 ka, 5°C under the inferred modern values, which in that case are in adequation with the values reported for the present by Camuera et al. (2018). At 15 ka, an increase of about 5°C gets the MTWA close to the modern values.

3.4.2.3 Southern Italy

The PFT results at Monticchio (Fig. 3.6b) highlight relatively high proportions of non-arboreal PFTs during MIS 2, followed by afforestation. However, no afforestation is visible between the HSs (Figs. 3.6a and 3.6b), and a slight increase in arboreal PFTs is depicted from about 17 ka to 14.5 ka, after which the rapid shift toward dominant arboreal PFTs marked the beginning of the B/A. A slight decrease of arboreal PFTs around 12 ka probably corresponds to an opening of the forest canopy as the regional signature of the YD (Figs. 3.6a and 3.6b).

The redundancy analysis results at Monticchio (Fig. 3.2d) indicate a high correlation between arboreal PFTs and winter precipitation (Pdjf) and MTCO, while non-arboreal PFTs depict strong linkages with seasonality. As in core SU81-18, Pjja and MTWA do not seem related to this primary pattern of PFTs as both are strongly correlated with Axis 2.

Pollen-based estimates show variable but negative MTCO until about 17 ka (Fig. 3.6d). Relatively steady conditions from about 28 to 21 ka and a general decrease of MTCO toward minimum values are estimated from about 21 to 18 ka, while MTWA remained unchanged thus reflecting increased seasonal gradients of temperature. In an interval associated with the beginning of HS1, there is a trend from very negative to positive MTCO values, close to the modern values, which is surprisingly high given the stadial context. It should be viewed with caution, because of chronological uncertainties and also because the analogues display high SCDs (Fig. 3.6g). The selected modern analogues of this interval could correspond to warm steppes which are characterized by low precipitation but high temperatures (Tarasov et al., 1998). It is worth mentioning that the modern values calculated in this study are close to the ones presented in Watts et al. (1996b). Then, positive MTCO was recorded during arboreal vegetation phases (Figs. 3.6b and 3.6d), which probably correspond to the B/A and the Holocene, while slightly lower values (around 0°C) likely marked the YD.

The MTWA signal offers variations that are generally parallel with those of MTCO but of less amplitude, thus leading to significant changes in seasonality that globally mirror the MTCO curve (Fig. 3.6d). As for MTCO, the MTWA values get close to the modern values at the beginning of MIS 1 (Fig 3.6d).

According to the chronological frame used herein, high Pann and Pdjf characterize the HS2, the interval from 22 to 18.5 ka and MIS 1 (Fig. 3.6f), whereas the lowest values are recorded during the second half of HS1 and after HS2. These odd estimates might result from an underestimation of the ages, particularly in the first half of the MIS 2 section, where a shift of about 2000 - 3000 years, as evidenced by Wulf et al. (2004), would permit a better correspondence of dry conditions with HS2, and would suggest that the preceding Pann and Pdjf peaks belong to GI 3 and GI 4.

The mean annual SSTs recorded in two marine sediment cores located in the proximity of the Tyrrhenian Sea (Fig. 3.1; Cacho et al., 2001) show variations that are distinct from the pollen-based temperature reconstructions. The SSTs from both cores BS79-38 and BS79-33 (Figs. 3.1 and 3.6c; Cacho et al., 2001) show low amplitude variations but display a general warming trend, like the mean annual SST inferred at ODP Site 976 (Fig. 3.4d; Martrat et al., 2014). They do not illustrate significant cooling pulses during HS1 and HS2, and there is a low amplitude SST decrease corresponding to the YD. The comparison of the marine record and Monticchio data could illustrate a decoupling between ocean conditions and inland climate.

3.4.2.4 Greece

MIS 2 at Xinias was characterized by high proportions of non-arboreal PFTs with no apparent growth of the vegetation between HSs but a slightly increasing trend of arboreal vegetation from 28 to 17 ka (Figs. 3.7a and 3.7b). After 17 ka, the pollen data indicate afforestation, the precise age of which is difficult to assess due to poor dating control of the upper part of the sequence (see Material and Methods and Fig. 3.S3 in Supplementary data).

Increased arboreal vegetation was apparently related to increased winter precipitation and, to a lesser extent, temperatures, while non-arboreal PFTs correspond to high seasonality (Fig. 3.2e).

Annual precipitation (Pann) shows important variations throughout the sequence, with high values (between 800 and 900 mm) from 30 to 28 ka, 26 to 22 ka and from 17 to the top of the section, and low

values in between (Fig. 3.7e). The low values (~ 350 – 550 mm) observed between 28 and 26 ka could very likely correspond to HS2 and indicate an overestimation of the ages in the bottom half of the Xinias sequence as well (Fig. 3.7). The second period of low Pann seems to be divided into 2 phases, although the low temporal resolution might bias this interpretation: a first phase from 22 to 20 ka with relatively stable values around 400 mm and a second phase, more variable, with values ranging from 250 to 450 mm, that is recorded from 20 to 17 ka. Given that this last phase records the lowest values and directly precedes the significant afforestation that could be attributed to the B/A, we suggest that it corresponds to HS1 (Fig. 3.7). It is worth noting that conversely to MIS 1, during MIS 2, summer precipitation appears higher than winter precipitation. This must be regarded with caution considering that, at present, precipitation in the region is almost exclusively restricted to all seasons but summer (Bottema, 1979).

Overall, pollen-based temperature estimates show increasing values throughout the sequence, with negative MTCO values from 30 to 20 ka.

3.5 Discussion

3.5.1 Regionally coherent winter-annual precipitation pattern from 28 to 10 ka

The present-day vegetation in Southern Europe highly depends on winter precipitation (Gouveia et al., 2008), which is tightly linked to the North Atlantic Oscillation (NAO), a circulation pattern quantified as the atmospheric pressure difference between the Icelandic Low and the Azores High (Hurrell, 1995). The NAO index is calculated for the coldest months of the year, from November to April, when its variability is at its highest (Hurrell, 1995; Hurrell et al., 2003). A negative mode of the NAO, corresponding to weak pressure gradients, induces a southward displacement of the westerlies and results in mild and wet winters in Southwestern Europe. Conversely, a positive mode of the NAO, with strong pressure gradients, causes a northward displacement of the westerlies that brings moist air masses to northwest Europe and leads to cold and dry winters in southern Europe. In summary, the NAO is related to latitudinal displacements of the North Atlantic jet stream (Hurrel, 1995; Hurrell et al., 2003).

Vegetation variations at most sites (Fig. 3.2) show a strong dependency on winter precipitation and annual precipitation, both being correlated. Increased winter and annual precipitation favour afforestation, while dry conditions lead to the opening of the forest cover. Conversely, summer precipitation seems weakly correlated with winter and annual precipitation (Fig. 3.2). The decoupling between winter and summer precipitation may relate to different types of rainfall. Many LGM studies have

demonstrated that winter precipitation is related to storms from the westerlies, while summer precipitation is mainly of local convective origin (Lainé et al., 2009; Beghin et al., 2016; Del Gobbo et al., 2022). We may propose here that part of the autumn and spring precipitation embraces the processes for winter precipitation and also relates to the westerlies, thus explaining why annual precipitation offers the same behaviour as winter precipitation but with a tripled amplitude (Fig. 3.8). Camuera et al. (2022) who investigated pollen-based seasonal precipitation during the last 200 thousand years at Padul (Fig. 3.1), southeastern Spain, also demonstrated an anticorrelation between summer and winter-annual precipitation.

Despite chronological uncertainties and lags between the records, winter and annual precipitation (Fig. 3.8) seems to depict coherent regional patterns. Very low precipitation is recorded during HSs, although the marine core SU81-18 and ODP Site 976 record peaks of high amplitude within HS2 and the Padul site record high values within HS1. A general increase in both Pdjf and Pann is observed from HS1 to B/A. After the B/A transition, precipitation remains almost uniform at site ODP 976 with only a small decrease during the first half of the YD (Fig. 3.8), displaying a two-phases structure as already highlighted by previous authors (Combourieu-Nebout et al., 2009). Sites SU81-18 and Padul record a more pronounced decrease of precipitation during YD, mimicking the NGRIP record. In Italy, the Monticchio record is much noisier in this section, rendering it challenging to make an assessment, except for a decreasing trend towards the beginning of the Holocene, which should be viewed with caution due to the high SCDs of the analogues (Fig. 3.6g).

3.5.1.1 Regional increase of winter-annual precipitation during the LGM

One of the most striking features of the five studied sequences is the high values of Pdjf and Pann during the LGM (Fig. 3.8). The LGM section between HSs displays high variability with peaks up to ~ 375 mm and ~ 900 mm for Pdjf and Pann, respectively, in marine core SU81-18 and ODP Site 976 (Fig. 3.8). The highest precipitation values are also recorded in the LGM section at Padul, with annual precipitation values reaching ~ 900 mm, well above the modern values (Fig. 3.8; see also Camuera et al., 2018). While high precipitation values are recorded before HS2 and after HS1 at Monticchio and Xinias further east, the LGM is marked by similarly high annual precipitation, especially during its first part. It is also worth noting that despite the high SCDs of the analogues in the LGM at ODP Site 976, the winter-annual precipitation reconstructed is coherent with those of the other sites (Figs. 3.4g and 3.8).

In the context of extended Northern Hemisphere ice sheets, cold and dry climate in Southern Europe was often inferred for the LGM. Many continental pollen sequences from the Pyrenean region indicate dry conditions and dominant steppe vegetation (e.g., Andrieu et al., 1993; Reille and Andrieu, 1995; Valero-Garces et al., 2004; Gonzalez-Sampériz et al. 2006). García-Amorena et al. (2007) also reconstructed low annual precipitation on the Portuguese coast based on macrofossil remains, and Lécuyer et al. (2021) inferred drier and colder conditions from stable isotope measurements on tooth enamel carbonate of Cervidae, Equidae and Caprinae in southwest Europe. Steppic, semi-desertic and desertic vegetation also prevailed further east in the Mediterranean Basin (Langgut et al., 2011) where colder and drier than present-day conditions were also deduced from speleothem data (e.g., Bar-Matthews et al., 1997, 1999).

However, many proxies have also evidenced increased moisture in Southern Europe during the LGM, notably in the Iberian Peninsula on the basis of high lake levels (e.g., Harrison and Digerfeldt, 1993; Vegas et al., 2010; Moreno et al., 2012; Camuera et al., 2018). The analysis of leaf wax from palaeosols also suggested humid conditions because of the occurrence of drought-intolerant deciduous trees (Schafer et al., 2016). Increased moisture was also inferred from high river levels in northern Morocco (El Amrani et al., 2008). Although the evidence is not abundant further east, high lake levels have been reported in Italy (Giraudi et al., 2017) and Greece (Harrison and Digerfeldt, 1993), where annual precipitation similar to present-day during the LGM were also inferred from glacier modelling (Hughes et al., 2006).

The results of modelling experiments also suggest a wetter climate over southwestern Europe during the LGM, notably over the Iberian Peninsula (e.g., Laîné et al., 2009; Löfverström et al., 2014; Beghin et al., 2016; Löfverström and Lora, 2017; D'Agostino and Lionello, 2020; Kageyama et al., 2021). More importantly, they all evidence increased winter precipitation, some even simulating higher winter precipitation during the LGM than during the pre-industrial (e.g., Beghin et al., 2016). Although we cannot directly compare our climatic reconstructions from the marine sites with modern climate (see Chapter 3.3.3), Pdjf and Pann (Fig. 3.8) at both sites show higher values during the LGM than during the early Holocene, which is compatible with the model results (e.g., Beghin et al., 2016).

The high winter precipitation over Iberia during the LGM has been largely attributed to the southeastward shift of the North Atlantic storm-track because of the presence of the Laurentide and Fennoscandian ice sheets (e.g., Kageyama et al., 1999; Lainé et al., 2009; Luetscher et al., 2015; D'Agostino

and Lionello, 2020; Pinto and Ludwig, 2020). Enhanced precipitation from the westerlies was possibly favoured by relatively warm SSTs at middle latitudes during the LGM, while the HSs were marked by cold pulses (e.g., de Vernal et al., 2005; Eynaud et al., 2009; Penaud et al., 2011).

Further east, many studies of glacier advance in the Alps during the LGM led to suggest a southward shift of the North Atlantic Jet stream that would have increased moisture advection thus contributing to building up the glaciers to their maximum extent (e.g., Spötl and al., 2021; Ribolini et al., 2022; Roattino et al., 2022; Del Gobbo et al., 2022). There is however an ongoing debate on whether the precipitation was mainly from the North Atlantic via the westerlies or from the Mediterranean Sea due to pronounced Rossby-wave breaking west of the Alps (Fig. 3.1) (e.g., Luetcher et al., 2015; Löfverström, 2020; Spötl et al., 2021; Ribolini et al., 2022; Del Gobbo et al., 2022). Regardless of the origin of the precipitation, our results suggest that the increase in winter and annual precipitation recorded during the LGM was a regional feature of southern Europe.

3.5.2 Vegetation dynamics in southern Europe during the LGM and West-East gradient of winter temperatures

The five study sequences offer regionally consistent behaviour for the YD, B/A and HSs (Fig. 3.9). However, despite the high values of winter-annual precipitation recorded in southern Iberia, Italy and Greece between HSs, during the LGM, there is an apparent west-east gradient of the vegetation (Fig. 3.9). Indeed, there is no evidence of afforestation from 28 to 17 ka at Xinias and Monticchio, contrary to the records of Padul and ODP Site 976 in Southeastern Iberia. The afforestation appears more pronounced at the Atlantic record, with peaks of arboreal PFTs reaching values comparable to the B/A (Fig. 3.9). Nevertheless, the evidence for different afforestation rates between the southeastern and southwestern Iberian sites is weak, and the main point is that increased arboreal vegetation over the southern Iberian Peninsula occurred during the LGM. This aligns with the mean state LGM vegetation as reconstructed from pollen sequences by Davis et al. (2022), which show greater proportions of moisture-sensitive deciduous taxa and xerophytic woodlands in southern Iberia.

Further east, the reconstructed LGM PFTs at Monticchio and Xinias show a different behaviour, with no evidence of afforestation from 28 to 17 ka (Fig. 3.9). This concurs with the LGM vegetation reconstructions by Davis et al. (2022), with steppe vegetation occupying central and southern Italy and the development of steppe, semi-desertic or desertic vegetation reported further east in the Mediterranean Basin (Tzedakis et al., 2004; Langgut et al., 2011; Davis et al., 2022). Still, both Monticchio and Xinias sites

recorded high values of annual and winter precipitation during the LGM (Fig. 3.8). An increase in precipitation was also detected in the East Carpathian Mountains, where the proportions of wet-tundra vegetation also increased (Magyari et al., 2014b), thus supporting the hypothesis of a large regional coherent pattern regarding the winter-annual precipitation. However, contrary to the Iberian sites, negative MTCO were reconstructed for the whole section at Monticchio and Xinias, which could have hampered the growth of the dense forest vegetation (Figs. 3.9 and 3.10). Low MTCO, concomitant to the coldest MTWA (Figs. 3.6d and 3.7c), were possibly related to the influence of the Fennoscandian and Alpine ice sheets, due to the potential Rossby wave breaking of the jet stream west of the Alps (Fig. 3.1; Luetcher et al., 2015). According to Löfverstrom and Lora (2017), the significant change in the vegetation at Monticchio and Xinias after 15 ka, concomitant with warmer MTCO, could have been caused by a large-scale atmospheric reorganization caused by the splitting of the Laurentice Ice Sheet and the Cordilleran Ice Sheet, which would have generated a shift to more modern-like atmospheric circulation patterns. Under these modern-like conditions, the Rossby-wave over Central Europe would have decreased (Fig. 3.1; Luetcher et al., 2015) and, favoured by the shrinking of the Northern Hemisphere ice sheets, a northward displacement of the jet stream would have isolated the influence of glaciated areas to high latitudes.

3.5.3 Highly variable climate conditions in southwestern Europe during the LGM

Apart from the afforestation, the Atlantic Sector also shows high variability in the vegetation dynamics during the LGM, likely in relation to variations in winter temperature and winter-annual precipitation (Fig. 3.2a; Figs. 3.3b,3.3d and 3.3g). The MTCO reconstructed at site SU81-18 oscillates around 0°C, with values below the freezing point potentially constituting ecological stress for the vegetation. More importantly, the temperature variations are concomitant with large winter and annual precipitation variations, with amplitude of about 600 and 200 mm for Pann and Pdjf respectively (Figs. 3.3g and 3.10). The smoothed records highlight two phases of high precipitation, between 24 and 22.5 ka and from 21.5 to 19.5 ka. In the Alboran Sea (Fig. 3.10), the amplitude of variations is generally smaller than those estimated from core SU81-18, but there is a drop of the same magnitude around 21.5 - 22 ka in both records.

The precipitation drops are not evidenced eastward in the inland record at Padul, where annual precipitation oscillates between 650 and 900 mm, but the lowest values are recorded at 21.5 and 20.2 ka (Fig. 3.8). Due to chronological uncertainties, however, it is also difficult to assess if the oscillations of Pann and Pdjf at Monticchio around 20 ka correspond to this event. The same applies to Xinias, which offers

poor dating control and temporal resolution but suggests low annual precipitation between high values peak in the lower LGM section (Fig. 3.8).

Many studies have reported two main glacier advance phases during the LGM in the European Alps. A first phase between 24 and 22 ka and a second phase between 21 and 19 ka with a significant retreat in between (e.g., Ivy-Ochs, 2015; Ivy-Ochs et al., 2018; Kamleitner et al., 2022; Roattino et al., 2022). Since the increase in annual and winter precipitation recorded at the two Iberian sites are concomitant with these phases of glacier advance, we may hypothesize that they are both the result of enhanced regional advection of moisture through the westerlies, while the pronounced decline of precipitation around 22 ka could correspond to regional changes in the atmospheric circulation. However, due to the scarcity and the chronological uncertainties of the data further east, this assertion is made with caution.

Aside from this important drop of precipitation recorded around 22 ka, larger decreases in precipitation occurred on the western Iberian Margin facing the Atlantic (core SU81-18) than in any other records, notably the ODP Site 976 in the Alboran Sea (Fig. 3.8). Similarly, larger variations of MTCO (Fig. 3.10) with several incursions below 0°C are reconstructed from core SU81-18, whereas MTCO seems to have remained stable in the Alboran Sea during the LGM (Fig. 3.10). Penaud et al. (2011), who reconstructed seasonal SSTs based on dinocysts and foraminifera in core SU81-18 and two other cores located further south, in the Gulf of Cadiz and on northwestern Morroco margin, also highlighted a difference between the western and the southern Iberian margin during the LGM. The foraminifer data from site SU81-18 (Penaud et al., 2011), which are used for SST reconstructed based on the latest version of the foraminifer modern database (Fig. 3.3c), display SST variations of 10°C amplitude between cold (HSs and YD) and warm phases (LGM, B/A, Holocene) but only 5°C variations during LGM, the dinocyst-based SST reconstructions depict higher amplitude variations between HS2 and HS1, with SST peaks as high as during the B/A and SST drops as low as HS values (Figure 5 of Penaud et al., 2011). Dinocyst-based SSTs at the two other sites located further south suggest conditions during the LGM as warm as during the Holocene, with very small variations (Figure 5 of Penaud et al., 2011), which led to the conclusion that a hydrological front was located between 38 and 36°N on the Atlantic Iberian margins (Penaud et al., 2011) during the last glacial period, including the LGM. Such a conclusion was shared by other authors (Voelker et al., 2009).

According to model simulations, the NAO did not record pronounced latitudinal shift during the LGM as in its present-day configuration, as the jet stream was forced to a more stable and meridional position due to the Northern Hemisphere ice sheets (Rivière et al., 2010; Beghin et al., 2016). The LGM NAO would have rather corresponded to acceleration/deceleration or extension/retraction of the southward jet stream (Rivière et al., 2010). We may thus consider that the variations of precipitation we reconstructed represent variations of NAO strength, and thus westerlies strength, during the LGM.

Justino et al. (2005) have argued that despite the forced southern position of the jet stream, positive phases of the NAO were marked by more southerly winds during the LGM. The differences of pollen-based climate estimates from core SU81-18 and ODP Site 976 could thus reflect small-scale movements of the Atlantic jet stream above the region, which, following Luetcher et al. (2015), was in an odd configuration due to Rossby-Wave breaking west of the Alps (Fig. 3.1). Those small-latitudinal jet stream variations over the Atlantic Iberian margin would have acted in concert with variations of the hydrological front highlighted by Penaud et al. (2011) although this needs to be backed by direct comparison with dinocyst-based paleohydrographic reconstructions. Hence, following Justino et al. (2005), we can hypothesize that increased precipitation at all sites was related to the positive phase of NAO during the LGM, leading to a displacement of the jet stream over the southern Iberic peninsula (Fig. 3.1), while negative phases of NAO (Fig. 3.1) led to shifting the jet stream southeastward, drastically diminishing precipitation over the southwestern Iberian margin, but not the southeastern margin. Many more winter-annual precipitation reconstructions over the region would be needed to confirm if this hypothesis is correct.

Despite the scarcity of the data and many uncertainties on the atmospheric circulation pattern over the study region during the LGM, we may assess millennial-scale variations of the North Atlantic atmospheric circulation linked to variations in oceanic conditions, which are independently demonstrated from IRD concentrations in Northeastern Atlantic core DSDP 609 (Bond and Lotti, 1995).

3.6 Conclusion

The reconstruction of vegetation types and seasonal climate from 28 ka to 10 ka at five sites from southern Europe highlights a coherent regional pattern of vegetation dynamics with pronounced afforestation during the warm Bølling/Allerød and at the beginning of the Holocene and slight forest decline during the Younger Dryas, while steppe-like vegetation characterizes the cold Heinrich Stadials (HS) HS1 and HS2

(Sanchez-Goñi and Harrison, 2010). All these changes appear tightly linked to winter climate, particularly to winter and annual precipitation, which also depict coherent regional patterns. Since present-day vegetation in Southern Europe is mainly influenced by winter precipitation, which depends on latitudinal movements of the westerlies over Europe (Gouveia et al., 2008), we attribute the past regional vegetation and related winter precipitation changes to variations in strength and/or position of the westerlies over the region.

One of the most important findings is that our pollen-based climatic estimates provide evidence of high winter and annual precipitation during the LGM in all five sequences, notably over Southern Iberia, in agreement with many model simulation results (e.g., Lainé et al., 2009; Löfverström et al., 2014; Beghin et al., 2016; Löfverström and Lora, 2017; D'Agostino and Lionello, 2020; Kageyama et al., 2021) and some proxy-data (Vegas et al., 2010; Moreno et al., 2012; Schafer et al., 2016). Large amounts of winter-annual precipitation over the study area are attributed to a southward displacement of the jet stream, and thus the westerlies, due to maximum extension of the Northern Hemisphere ice sheets at the time (e.g., Lainé et al., 2009; Löfverström et al., 2014; Beghin et al., 2016; Löfverström and Lora, 2017; D'Agostino and Lionello, 2020; Kageyama et al., 2021).

Despite regional coherency of the winter-annual precipitation, larger afforestation on the Iberic Peninsula during the LGM is evidenced from data of the three westernmost sites, whereas the remaining steppe-like vegetation at Monticchio and Xinias probably resulted from too cold climate. We hypothesize that climate was marked by strong west-east temperature gradients related to the influence of the Fennoscandian and Alpine ice sheets, due to the Rossby wave breaking of the jet stream west of the Alps (Luetcher et al., 2015).

High precipitation variability characterizes the LGM in the Atlantic margin sequence, whereas lower variations are displayed by sequences further east, notably the ODP Site 976 located in the Alboran Sea, pointing to a climatic front somewhere in between the two geographic areas, as already suggested by Penaud et al. (2011). Two increased precipitation phases are, however, clearly distinguishable in both Iberian records, from 24 to 22.5 ka and from 21.5 to 19.5 ka, but not as much at Padul, while chronological uncertainties prevent association with Monticchio or Xinias for this interval. Nevertheless, these two high precipitation phases match the two main glacier advance phases recorded during the LGM in the European Alps (e.g., Ivy-Ochs, 2015; Ivy-Ochs et al., 2018; Kamleitner et al., 2022; Roattino et al., 2022), indicating

strong westerlies or southerlies over the entire region while the arid phase in between could indicate significant weakening or latitudinal movement of the jet stream at the time.

The use of the last version of the EMPD2 to infer seasonal climatic estimates from pollen sequences from Southern Europe was promising and helped to reconcile climatic information from pollen sequences with some model results and other regional proxy data. Further MAT reconstructions of pollen sequences from Northern Morocco and Northern Spain would help to better assess the latitudinal zonation of the westerlies during the LGM, while pollen sequences from the western, central and eastern Mediterranean region could help to confirm or infirm the hypothesis of the impact of the jet stream Rossby wave breaking west of the Alps on temperatures.

3.7 References

Ahn, J., & Brook, E. J. (2008). Atmospheric CO2 and climate on millennial time scales during the last glacial period. *Science*, *322*(5898), 83-85.

Allen, J. R., Watts, W. A., & Huntley, B. (2000). Weichselian palynostratigraphy, palaeovegetation and palaeoenvironment; the record from Lago Grande di Monticchio, southern Italy. *Quaternary International*, *73*, 91-110.

Allen, J. R., & Huntley, B. (2018). Effects of tephra falls on vegetation: A Late-Quaternary record from southern Italy. *Journal of Ecology*, *106*(6), 2456-2472.

Andrieu, V., Eicher, U., & Reille, M. (1993). La fin du dernier Pléniglaciaire dans les Pyrénées (France): données polliniques, isotopiques et radiométriques. *Comptes rendus de l'Académie des sciences. Série 2, Mécanique, Physique, Chimie, Sciences de l'univers, Sciences de la Terre*, *316*(2), 245-250.

Argenio, C., Flores, J. A., Balestra, B., & Amore, F. O. (2021). Reconstructing ocean surface dynamics over the last 25 kyr at "Shackleton Site" IODP-U1385. *Palaeogeography, Palaeoclimatology, Palaeoecology*, *579*, 110587.

Austin, W. E., & Hibbert, F. D. (2012). Tracing time in the ocean: a brief review of chronological constraints (60–8 kyr) on North Atlantic marine event-based stratigraphies. *Quaternary Science Reviews*, *36*, 28-37.

Bar-Matthews, M., Ayalon, A., & Kaufman, A. (1997). Late Quaternary paleoclimate in the eastern Mediterranean region from stable isotope analysis of speleothems at Soreq Cave, Israel. *Quaternary Research*, *47*(2), 155-168.

Bar-Matthews, M., Ayalon, A., Kaufman, A., & Wasserburg, G. J. (1999). The Eastern Mediterranean paleoclimate as a reflection of regional events: Soreq cave, Israel. *Earth and Planetary Science Letters*, *166*(1-2), 85-95.

Bard, E., Rostek, F., Turon, J. L., & Gendreau, S. (2000). Hydrological impact of Heinrich events in the subtropical northeast Atlantic. *Science*, *289*(5483), 1321-1324.

Bauska, T. K., Marcott, S. A., & Brook, E. J. (2021). Abrupt changes in the global carbon cycle during the last glacial period. *Nature Geoscience*, *14*(2), 91-96.

Beghin, P., Charbit, S., Kageyama, M., Combourieu-Nebout, N., Hatté, C., Dumas, C., & Peterschmitt, J. Y. (2016). What drives LGM precipitation over the western Mediterranean? A study focused on the Iberian Peninsula and northern Morocco. *Climate dynamics*, *46*, 2611-2631.

Blaauw, M. (2010). Methods and code for 'classical'age-modelling of radiocarbon sequences. *Quaternary geochronology*, *5*(5), 512-518.

Bond, G. C., & Lotti, R. (1995). Iceberg discharges into the North Atlantic on millennial time scales during the last glaciation. *science*, *267*(5200), 1005-1010.

Bottema, S. (1979). Pollen analytical investigations in Thessaly (Greece). *Palaeohistoria*, 19-40.

Brauer, A., Allen, J. R., Mingram, J., Dulski, P., Wulf, S., & Huntley, B. (2007). Evidence for last interglacial chronology and environmental change from Southern Europe. *Proceedings of the National Academy of Sciences*, *104*(2), 450-455.

Cacho, I., Grimalt, J. O., Canals, M., Sbaffi, L., Shackleton, N. J., Schönfeld, J., & Zahn, R. (2001). Variability of the western Mediterranean Sea surface temperature during the last 25,000 years and its connection with the Northern Hemisphere climatic changes. *Paleoceanography*, *16*(1), 40-52.

Camuera, J., Jiménez-Moreno, G., Ramos-Román, M. J., García-Alix, A., Toney, J. L., Anderson, R. S., ... & Martínez-Ruiz, F. (2018). Orbital-scale environmental and climatic changes recorded in a new~ 200,000-year-long multiproxy sedimentary record from Padul, southern Iberian Peninsula. *Quaternary Science Reviews*, *198*, 91-114.

Camuera, J., Jiménez-Moreno, G., Ramos-Román, M. J., García-Alix, A., Toney, J. L., Anderson, R. S., ... & Carrión, J. S. (2019). Vegetation and climate changes during the last two glacial-interglacial cycles in the western Mediterranean: a new long pollen record from Padul (southern Iberian Peninsula). *Quaternary Science Reviews*, *205*, 86-105.

Camuera, J., Ramos-Román, M. J., Jiménez-Moreno, G., García-Alix, A., Ilvonen, L., Ruha, L., ... & Seppä, H. (2022). Past 200 kyr hydroclimate variability in the western Mediterranean and its connection to the African Humid Periods. *Scientific Reports*, *12*(1), 9050.

Cleator, S. F., Harrison, S. P., Nichols, N. K., Prentice, I. C., & Roulstone, I. (2020). A new multivariable benchmark for Last Glacial Maximum climate simulations. *Climate of the Past*, *16*(2), 699-712.

Combourieu Nebout, N., Peyron, O., Dormoy, I., Desprat, S., Beaudouin, C., Kotthoff, U., & Marret, F. (2009). Rapid climatic variability in the west Mediterranean during the last 25 000 years from high resolution pollen data. *Climate of the Past*, *5*(3), 503-521.

D'Agostino, R., & Lionello, P. (2020). The atmospheric moisture budget in the Mediterranean: Mechanisms for seasonal changes in the Last Glacial Maximum and future warming scenario. *Quaternary Science Reviews*, *241*, 106392.

Davis, B. A., Chevalier, M., Sommer, P., Carter, V. A., Finsinger, W., Mauri, A., ... & Zimny, M. (2020). The Eurasian Modern Pollen Database (EMPD), version 2. *Earth System Science Data Discussions*, *2020*, 1-41.

Davis, B. A. S., Fasel, M., Kaplan, J. O., Russo, E., & Burke, A. (2022). The climate and vegetation of Europe, North Africa and the Middle East during the Last Glacial Maximum (21,000 years BP) based on pollen data. *Climate of the Past Discussions*, 1-66.

de Vernal, A. D., Eynaud, F., Henry, M., Hillaire-Marcel, C., Londeix, L., Mangin, S., ... & Turon, J. L. (2005). Reconstruction of sea-surface conditions at middle to high latitudes of the Northern Hemisphere during the Last Glacial Maximum (LGM) based on dinoflagellate cyst assemblages. *Quaternary Science Reviews*, *24*(7-9), 897-924.

Del Gobbo, C., Colucci, R. R., Monegato, G., Žebre, M., & Giorgi, F. (2022). Atmosphere-cryosphere interactions at 21 ka BP in the European Alps. *Climate of the Past Discussions*, 1-24.

Dyke, A. S., Andrews, J. T., Clark, P. U., England, J. H., Miller, G. H., Shaw, J., & Veillette, J. J. (2002). The Laurentide and Innuitian ice sheets during the last glacial maximum. *Quaternary Science Reviews*, *21*(1-3), 9-31.

Ehlers, J., & Gibbard, P. L. (2004). *Quaternary glaciations-extent and chronology: part I: Europe*. Elsevier.

El Amrani, M., Macaire, J. J., Zarki, H., Bréhéret, J. G., & Fontugne, M. (2008). Contrasted morphosedimentary activity of the lower Kert River (northeastern Morocco) during the Late Pleistocene and the Holocene. Possible impact of bioclimatic variations and human action. *Comptes Rendus Geoscience*, *340*(8), 533-542.

Elenga, H., Peyron, O., Bonnefille, R., Jolly, D., Cheddadi, R., Guiot, J., ... & Jonson, H. (2000). Pollen-based biome reconstruction for southern Europe and Africa 18,000 yr BP. *Journal of Biogeography*, *27*(3), 621-634.

Eynaud, F., De Abreu, L., Voelker, A., Schönfeld, J., Salgueiro, E., Turon, J. L., ... & Cacho, I. (2009). Position of the Polar Front along the western Iberian margin during key cold episodes of the last 45 ka. *Geochemistry, Geophysics, Geosystems*, *10*(7).

Eynaud, F., Zaragosi, S., Wary, M., Woussen, E., Rossignol, L., & Voisin, A. (2021). Are Past Sea-Ice Reconstructions Based on Planktonic Foraminifera Realistic? Study of the Last 50 ka as a Test to Validate Reconstructed Paleohydrography Derived from Transfer Functions Applied to Their Fossil Assemblages. *Geosciences*, *11*(10), 409.

Fabres, J., Calafat, A., Sanchez-Vidal, A., Canals, M., & Heussner, S. (2002). Composition and spatio-temporal variability of particle fluxes in the Western Alboran Gyre, Mediterranean Sea. *Journal of Marine Systems*, *33*, 431-456.

Fick, S. E., & Hijmans, R. J. (2017). WorldClim 2: new 1-km spatial resolution climate surfaces for global land areas. *International journal of climatology*, *37*(12), 4302-4315.

García-Amorena, I., Manzaneque, F. G., Rubiales, J. M., Granja, H. M., de Carvalho, G. S., & Morla, C. (2007). The Late Quaternary coastal forests of western Iberia: A study of their macroremains. *Palaeogeography, Palaeoclimatology, Palaeoecology*, *254*(3-4), 448-461.

Genty, D., Combourieu-Nebout, N., Peyron, O., Blamart, D., Wainer, K., Mansuri, F., ... & Brauer, A. (2010). Isotopic characterization of rapid climatic events during OIS3 and OIS4 in Villars Cave stalagmites (SW-France) and correlation with Atlantic and Mediterranean pollen records. *Quaternary Science Reviews*, *29*(19-20), 2799-2820.

Giraudi, C. (2017). Climate evolution and forcing during the last 40 ka from the oscillations in Apennine glaciers and high mountain lakes, Italy. *Journal of Quaternary Science*, *32*(8), 1085-1098.

González-Sampériz, P., Valero-Garcés, B. L., Moreno, A., Jalut, G., García-Ruiz, J. M., Martí-Bono, C., ... & Dedoubat, J. J. (2006). Climate variability in the Spanish Pyrenees during the last 30,000 yr revealed by the El Portalet sequence. *Quaternary Research*, *66*(1), 38-52.

Gouveia, C., Trigo, R. M., DaCamara, C. C., Libonati, R., & Pereira, J. M. (2008). The North Atlantic oscillation and European vegetation dynamics. *International Journal of Climatology: A Journal of the Royal Meteorological Society*, *28*(14), 1835-1847.

Grousset, F. E., Pujol, C., Labeyrie, L., Auffret, G., & Boelaert, A. (2000). Were the North Atlantic Heinrich events triggered by the behavior of the European ice sheets?. *Geology*, *28*(2), 123-126.

Guiot, J. (1990). Methodology of the last climatic cycle reconstruction in France from pollen data. *Palaeogeography, Palaeoclimatology, Palaeoecology*, *80*(1), 49-69.

Guiot, J., Torre, F., Jolly, D., Peyron, O., Boreux, J. J., & Cheddadi, R. (2000). Inverse vegetation modeling by Monte Carlo sampling to reconstruct palaeoclimates under changed precipitation seasonality and CO2 conditions: application to glacial climate in Mediterranean region. *Ecological modelling*, *127*(2-3), 119-140.

Harrison, S. P., & Digerfeldt, G. (1993). European lakes as palaeohydrological and palaeoclimatic indicators. *Quaternary Science Reviews*, *12*(4), 233-248.

Harrison, S. P., & Prentice, C. I. (2003). Climate and CO2 controls on global vegetation distribution at the last glacial maximum: analysis based on palaeovegetation data, biome modelling and palaeoclimate simulations. *Global Change Biology*, *9*(7), 983-1004.

Hughes, P. D., Woodward, J., & Gibbard, P. L. (2006). Late Pleistocene glaciers and climate in the Mediterranean. *Global and Planetary Change*, *50*(1-2), 83-98.

Hurrell, J. W. (1995). Decadal trends in the North Atlantic Oscillation: Regional temperatures and precipitation. *Science*, *269*(5224), 676-679.

Hurrell, J. W., Kushnir, Y., Ottersen, G., & Visbeck, M. (2003). An overview of the North Atlantic oscillation. *Geophysical Monograph-American Geophysical Union*, *134*, 1-36.

Ivy-Ochs, S. (2015). Glacier variations in the European Alps at the end of the last glaciation. *Cuadernos de investigación geográfica: Geographical Research Letters*, (41), 295-315.

Ivy-Ochs, S., Lucchesi, S., Baggio, P., Fioraso, G., Gianotti, F., Monegato, G., ... & Schlüchter, C. (2018). New geomorphological and chronological constraints for glacial deposits in the Rivoli-Avigliana end-moraine system and the lower Susa Valley (Western Alps, NW Italy). *Journal of Quaternary Science*, *33*(5), 550-562.

Jackson, S. T., & Overpeck, J. T. (2000). Responses of plant populations and communities to environmental changes of the late Quaternary. *Paleobiology*, *26*(S4), 194-220.

Jost, A., Lunt, D., Kageyama, M., Abe-Ouchi, A., Peyron, O., Valdes, P. J., & Ramstein, G. (2005). High-resolution simulations of the last glacial maximum climate over Europe: a solution to discrepancies with continental palaeoclimatic reconstructions?. *Climate Dynamics*, *24*, 577-590.

Justino, F., & Peltier, W. R. (2005). The glacial North Atlantic Oscillation. *Geophysical Research Letters*, *32*(21).

Kageyama, M., Valdes, P. J., Ramstein, G., Hewitt, C., & Wyputta, U. (1999). Northern Hemisphere storm tracks in present day and last glacial maximum climate simulations: A comparison of the European PMIP models. *Journal of Climate*, *12*(3), 742-760.

Kageyama, M., Albani, S., Braconnot, P., Harrison, S. P., Hopcroft, P. O., Ivanovic, R. F., ... & Zheng, W. (2017). The PMIP4 contribution to CMIP6–Part 4: Scientific objectives and experimental design of the PMIP4-CMIP6 Last Glacial Maximum experiments and PMIP4 sensitivity experiments. *Geoscientific Model Development*, *10*(11), 4035-4055.

Kageyama, M., Harrison, S. P., Kapsch, M. L., Lofverstrom, M., Lora, J. M., Mikolajewicz, U., ... & Zhu, J. (2021). The PMIP4 Last Glacial Maximum experiments: preliminary results and comparison with the PMIP3 simulations. *Climate of the Past*, *17*(3), 1065-1089.

Kamleitner, S., Ivy-Ochs, S., Monegato, G., Gianotti, F., Akçar, N., Vockenhuber, C., ... & Synal, H. A. (2022). The ticino-toce glacier system (Swiss-Italian Alps) in the framework of the alpine last glacial maximum. *Quaternary science reviews*, *279*, 107400.

La Violette, P. E. (1986). Short-term measurements of surface currents associated with the Alboran Sea Gyre during Donde Va?. *Journal of Physical Oceanography*, *16*(2), 262-279.

Laîné, A., Kageyama, M., Salas-Mélia, D., Voldoire, A., Rivière, G., Ramstein, G., ... & Peterschmitt, J. Y. (2009). Northern hemisphere storm tracks during the last glacial maximum in the PMIP2 ocean-atmosphere coupled models: energetic study, seasonal cycle, precipitation. *Climate Dynamics*, *32*(5), 593-614.

Lambeck, K., Purcell, A., Funder, S., Kjaer, K. H., Larsen, E., & Moller, P. E. R. (2006). Constraints on the Late Saalian to early Middle Weichselian ice sheet of Eurasia from field data and rebound modelling. *Boreas*, *35*(3), 539-575.

Lambeck, K., Rouby, H., Purcell, A., Sun, Y., & Sambridge, M. (2014). Sea level and global ice volumes from the Last Glacial Maximum to the Holocene. *Proceedings of the National Academy of Sciences*, *111*(43), 15296-15303.

Langgut, D., Almogi-Labin, A., Bar-Matthews, M., & Weinstein-Evron, M. (2011). Vegetation and climate changes in the South Eastern Mediterranean during the Last Glacial-Interglacial cycle (86 ka): new marine pollen record. *Quaternary Science Reviews*, *30*(27-28), 3960-3972.

Lécuyer, C., Hillaire-Marcel, C., Burke, A., Julien, M. A., & Hélie, J. F. (2021). Temperature and precipitation regime in LGM human refugia of southwestern Europe inferred from δ13C and δ18O of large mammal remains. *Quaternary Science Reviews*, *255*, 106796.

Löfverström, M., Caballero, R., Nilsson, J., & Kleman, J. (2014). Evolution of the large-scale atmospheric circulation in response to changing ice sheets over the last glacial cycle. *Climate of the Past*, *10*(4), 1453-1471.

Löfverström, M., & Lora, J. M. (2017). Abrupt regime shifts in the North Atlantic atmospheric circulation over the last deglaciation. *Geophysical Research Letters*, *44*(15), 8047-8055.

Lofverstrom, M. (2020). A dynamic link between high-intensity precipitation events in southwestern North America and Europe at the Last Glacial Maximum. *Earth and Planetary Science Letters*, *534*, 116081.

Luetscher, M., Boch, R., Sodemann, H., Spötl, C., Cheng, H., Edwards, R. L., ... & Müller, W. (2015). North Atlantic storm track changes during the Last Glacial Maximum recorded by Alpine speleothems. *Nature Communications*, *6*(1), 6344.

Magyari, E. K., Kuneš, P., Jakab, G., Sümegi, P., Pelánková, B., Schäbitz, F., ... & Chytrý, M. (2014a). Late Pleniglacial vegetation in eastern-central Europe: are there modern analogues in Siberia?. *Quaternary Science Reviews*, *95*, 60-79.

Magyari, E. K., Veres, D., Wennrich, V., Wagner, B., Braun, M., Jakab, G., ... & Schäbitz, F. (2014b). Vegetation and environmental responses to climate forcing during the Last Glacial Maximum and deglaciation in the East Carpathians: attenuated response to maximum cooling and increased biomass burning. *Quaternary Science Reviews*, *106*, 278-298.

MARGO Project Members (2009), Constraints on the magnitude and patterns of ocean cooling at the Last Glacial Maximum, Nat. Geosci.**,** 2**,** 127–132

Martrat, B., Jimenez-Amat, P., Zahn, R., & Grimalt, J. O. (2014). Similarities and dissimilarities between the last two deglaciations and interglaciations in the North Atlantic region. *Quaternary Science Reviews*, *99*, 122-134.

Mix, A. C., Bard, E., & Schneider, R. (2001). Environmental processes of the ice age: land, oceans, glaciers (EPILOG). *Quaternary Science Reviews*, *20*(4), 627-657.

Monnin, E., Indermühle, A., Dällenbach, A., Flückiger, J., Stauffer, B., Stocker, T. F., ... & Barnola, J. M. (2001). Atmospheric CO2 concentrations over the last glacial termination. *Science*, *291*(5501), 112-114.

Moreno, A., González-Sampériz, P., Morellón, M., Valero-Garcés, B. L., & Fletcher, W. J. (2012). Northern Iberian abrupt climate change dynamics during the last glacial cycle: a view from lacustrine sediments. *Quaternary Science Reviews*, *36*, 139-153.

Naughton, F., Goñi, M. S., Desprat, S., Turon, J. L., Duprat, J., Malaizé, B., ... & Freitas, M. C. (2007). Present-day and past (last 25 000 years) marine pollen signal off western Iberia. *Marine Micropaleontology*, *62*(2), 91-114.

North Greenland Ice Core Project members, High resolution record of Northern Hemisphere climate extending into the last interglacial period. Nature, 431(7005), 147-151 (2004).

Overpeck, J. T., Webb, T. I. I. I., & Prentice, I. C. (1985). Quantitative interpretation of fossil pollen spectra: dissimilarity coefficients and the method of modern analogs. *Quaternary Research*, *23*(1), 87-108.

Pascual, A., Rodríguez-Lázaro, J., Martínez-García, B., & Varela, Z. (2020). Palaeoceanographic and palaeoclimatic changes during the last 37,000 years detected in the SE Bay of Biscay based on benthic foraminifera. *Quaternary International*, *566*, 323-336.

Pénaud, A., Eynaud, F., Voelker, A., Marret, F., Turon, J. L., Rossignol, L., ... & Mulder, T. (2011). Hydrological processes affecting the subtropical NE Atlantic (34-38° N) over the last 30 ka: Evidence from phyto-and zooplankton assemblages. *Biogeosciences Discussions*, *8*(2), 2281-2327.

Peyron, O., Guiot, J., Cheddadi, R., Tarasov, P., Reille, M., de Beaulieu, J. L., ... & Andrieu, V. (1998). Climatic reconstruction in Europe for 18,000 yr BP from pollen data. *Quaternary research*, *49*(2), 183-196.

Pinto, J. G., & Ludwig, P. (2020). Extratropical cyclones over the North Atlantic and western Europe during the Last Glacial Maximum and implications for proxy interpretation. *Climate of the Past*, *16*(2), 611-626.

Prentice, I. C., Guiot, J., & Harrison, S. P. (1992). Mediterranean vegetation, lake levels and palaeoclimate at the Last Glacial Maximum. *Nature*, *360*(6405), 658-660.

Prentice, I. C., Cramer, W., Harrison, S. P., Leemans, R., Monserud, R. A., & Solomon, A. M. (1992). Special paper: a global biome model based on plant physiology and dominance, soil properties and climate. *Journal of biogeography*, 117-134.

Prentice, C., Guiot, J., Huntley, B., Jolly, D., & Cheddadi, R. (1996). Reconstructing biomes from palaeoecological data: a general method and its application to European pollen data at 0 and 6 ka. *Climate Dynamics*, *12*, 185-194.

Prentice, I. C., Cleator, S. F., Huang, Y. H., Harrison, S. P., & Roulstone, I. (2017). Reconstructing ice-age palaeoclimates: Quantifying low-CO2 effects on plants. *Global and Planetary Change*, *149*, 166-176.

Prentice, I. C., Villegas-Diaz, R., & Harrison, S. P. (2022). Accounting for atmospheric carbon dioxide variations in pollen-based reconstruction of past hydroclimates. *Global and Planetary Change*, *211*, 103790.

Ramstein, G., Kageyama, M., Guiot, J., Wu, H., Hély, C., Krinner, G., & Brewer, S. (2007). How cold was Europe at the Last Glacial Maximum? A synthesis of the progress achieved since the first PMIP model-data comparison. *Climate of the Past*, *3*(2), 331-339.

Rasmussen, S. O., Bigler, M., Blockley, S. P., Blunier, T., Buchardt, S. L., Clausen, H. B., ... & Winstrup, M. (2014). A stratigraphic framework for abrupt climatic changes during the Last Glacial period based on three synchronized Greenland ice-core records: refining and extending the INTIMATE event stratigraphy. *Quaternary science reviews*, *106*, 14-28.

Reille, M., & Andrieu, V. (1995). The late Pleistocene and Holocene in the Lourdes Basin, Western Pyrénées, France: new pollen analytical and chronological data. *Vegetation history and Archaeobotany*, *4*, 1-21.

Reimer, P. J., Bard, E., Bayliss, A., Beck, J. W., Blackwell, P. G., Ramsey, C. B., ... & Van Der Plicht, J. (2013). IntCal13 and Marine13 radiocarbon age calibration curves 0–50,000 years cal BP. *radiocarbon*, *55*(4), 1869-1887.

Ribolini, A., Spagnolo, M., Cyr, A. J., & Federici, P. R. (2022). Last glacial maximum and early deglaciation in the stura valley, southwestern European Alps. *Quaternary Science Reviews*, *295*, 107770.

Riviere, G., Laine, A., Lapeyre, G., Salas-Mélia, D., & Kageyama, M. (2010). Links between Rossby wave breaking and the North Atlantic Oscillation–Arctic Oscillation in present-day and Last Glacial Maximum climate simulations. *Journal of Climate*, *23*(11), 2987-3008.

Roattino, T., Crouzet, C., Vassallo, R., Buoncristiani, J. F., Carcaillet, J., Gribenski, N., & Valla, P. G. (2023). Paleogeographical reconstruction of the western French Alps foreland during the last glacial maximum using cosmogenic exposure dating. *Quaternary Research*, *111*, 68-83.

Rodrigo-Gámiz, M., García-Alix, A., Jiménez-Moreno, G., Ramos-Román, M. J., Camuera, J., Toney, J. L., ... & Damsté, J. S. S. (2022). Paleoclimate reconstruction of the last 36 kyr based on branched glycerol dialkyl glycerol tetraethers in the Padul palaeolake record (Sierra Nevada, southern Iberian Peninsula). *Quaternary Science Reviews*, *281*, 107434.

Rodrıguez, S., Querol, X., Alastuey, A., Kallos, G., & Kakaliagou, O. (2001). Saharan dust contributions to PM10 and TSP levels in Southern and Eastern Spain. *Atmospheric Environment*, *35*(14), 2433-2447.

Rodwell, M. J., & Hoskins, B. J. (2001). Subtropical anticyclones and summer monsoons. *Journal of Climate*, *14*(15), 3192-3211.

Roucoux, K. H., De Abreu, L., Shackleton, N. J., & Tzedakis, P. C. (2005). The response of NW Iberian vegetation to North Atlantic climate oscillations during the last 65 kyr. *Quaternary Science Reviews*, *24*(14-15), 1637-1653.

Sánchez Goñi, M. F., Cacho, I., Turon, J. L., Guiot, J., Sierro, F. J., Peypouquet, J. P., ... & Shackleton, N. J. (2002). Synchroneity between marine and terrestrial responses to millennial scale climatic variability during the last glacial period in the Mediterranean region. *Climate dynamics*, *19*, 95-105.

Sánchez Goñi, M. F., Landais, A., Fletcher, W. J., Naughton, F., Desprat, S., & Duprat, J. (2008). Contrasting impacts of Dansgaard–Oeschger events over a western European latitudinal transect modulated by orbital parameters. *Quaternary Science Reviews*, *27*(11-12), 1136-1151.

Sánchez Goñi, M. F., Landais, A., Cacho, I., Duprat, J., & Rossignol, L. (2009). Contrasting intrainterstadial climatic evolution between high and middle North Atlantic latitudes: a close-up of Greenland Interstadials 8 and 12. *Geochemistry, Geophysics, Geosystems*, *10*(4).

Sanchez-Goni, M. F., & Harrison, S. P. (2010). Millennial-scale climate variability and vegetation changes during the Last Glacial: Concepts and terminology. Quaternary Science Reviews, 29(21-22), 2823-2827.

Sánchez Goñi, M. F., Desprat, S., Daniau, A. L., Bassinot, F. C., Polanco-Martínez, J. M., Harrison, S. P., ... & Yamamoto, M. (2017). The ACER pollen and charcoal database: a global resource to document vegetation and fire response to abrupt climate changes during the last glacial period. *Earth System Science Data Discussions*, *2017*, 1-33.

Schäfer, I. K., Bliedtner, M., Wolf, D., Faust, D., & Zech, R. (2016). Evidence for humid conditions during the last glacial from leaf wax patterns in the loess–paleosol sequence El Paraíso, Central Spain. *Quaternary International*, *407*, 64-73.

Shao, Y., Anhäuser, A., Ludwig, P., Schlüter, P., & Williams, E. (2018). Statistical reconstruction of global vegetation for the last glacial maximum. *Global and Planetary Change*, *168*, 67-77.

Šmilauer, P., & Lepš, J. (2014). *Multivariate analysis of ecological data using CANOCO 5*. Cambridge university press.

Spötl, C., Koltai, G., Jarosch, A. H., & Cheng, H. (2021). Increased autumn and winter precipitation during the Last Glacial Maximum in the European Alps. *Nature Communications*, *12*(1), 1839.

Svendsen, J. I., Alexanderson, H., Astakhov, V. I., Demidov, I., Dowdeswell, J. A., Funder, S., ... & Stein, R. (2004). Late Quaternary ice sheet history of northern Eurasia. *Quaternary Science Reviews*, *23*(11-13), 1229-1271.

Tarasov, L., Dyke, A. S., Neal, R. M., & Peltier, W. R. (2012). A data-calibrated distribution of deglacial chronologies for the North American ice complex from glaciological modeling. *Earth and Planetary Science Letters*, *315*, 30-40.

Toucanne, S., Soulet, G., Freslon, N., Jacinto, R. S., Dennielou, B., Zaragosi, S., ... & Bayon, G. (2015). Millennial-scale fluctuations of the European Ice Sheet at the end of the last glacial, and their potential impact on global climate. *Quaternary Science Reviews*, *123*, 113-133.

Turon, J. L. (1984). Direct land/sea correlations in the last interglacial complex. *Nature*, *309*(5970), 673-676.

Turon, J. L., Lézine, A. M., & Denèfle, M. (2003). Land–sea correlations for the last glaciation inferred from a pollen and dinocyst record from the Portuguese margin. *Quaternary Research*, *59*(1), 88-96.

Tzedakis, P. C., Frogley, M. R., Lawson, I. T., Preece, R. C., Cacho, I., & De Abreu, L. (2004). Ecological thresholds and patterns of millennial-scale climate variability: the response of vegetation in Greece during the last glacial period. *Geology*, *32*(2), 109-112.

Valero-Garcés, B. L., González-Sampériz, P., Navas, A., Machín, J., Delgado-Huertas, A., Peña-Monné, J. L., ... & Davis, B. (2004). Paleohydrological fluctuations and steppe vegetation during the last glacial maximum in the central Ebro valley (NE Spain). *Quaternary International*, *122*(1), 43-55.

Vegas, J., Ruiz-Zapata, B., Ortiz, J. E., Galán, L., Torres, T., García-Cortés, Á., ... & Gallardo-Millán, J. L. (2010). Identification of arid phases during the last 50 cal. ka BP from the Fuentillejo maar-lacustrine record (Campo de Calatrava Volcanic Field, Spain). *Journal of Quaternary Science*, *25*(7), 1051-1062.

Voelker, A. H. L., De Abreu, L., Schönfeld, J., Erlenkeuser, H., & Abrantes, F. (2009). Hydrographic conditions along the western Iberian margin during marine isotope stage 2. *Geochemistry, Geophysics, Geosystems*, *10*(12).

Watts, W. A., Allen, J. R. M., & Huntley, B. (1996a). Vegetation history and palaeoclimate of the last glacial period at Lago Grande di Monticchio, southern Italy. *Quaternary Science Reviews*, *15*(2-3), 133-153.

Watts, W. A., Allen, J. R. M., Huntley, B., & Fritz, S. C. (1996b). Vegetation history and climate of the last 15,000 years at Laghi di Monticchio, southern Italy. *Quaternary Science Reviews*, *15*(2-3), 113-132.

Watts, W. A., Allen, J. R. M., & Huntley, B. (2000). Palaeoecology of three interstadial events during oxygen-isotope Stages 3 and 4: a lacustrine record from Lago Grande di Monticchio, southern Italy. *Palaeogeography, Palaeoclimatology, Palaeoecology*, *155*(1-2), 83-93.

Wulf, S., Kraml, M., Brauer, A., Keller, J., & Negendank, J. F. (2004). Tephrochronology of the 100 ka lacustrine sediment record of Lago Grande di Monticchio (southern Italy). *Quaternary International*, *122*(1), 7-30.

Zaragosi, S., Eynaud, F., Pujol, C., Auffret, G. A., Turon, J. L., & Garlan, T. (2001). Initiation of the European deglaciation as recorded in the northwestern Bay of Biscay slope environments (Meriadzek Terrace and Trevelyan Escarpment): a multi-proxy approach. *Earth and Planetary Science Letters*, *188*(3-4), 493-507.

Zaragosi, S., Bourillet, J. F., Eynaud, F., Toucanne, S., Denhard, B., Van Toer, A., & Lanfumey, V. (2006). The impact of the last European deglaciation on the deep-sea turbidite systems of the Celtic-Armorican margin (Bay of Biscay). *Geo-Marine Letters*, *26*, 317-329.

Zolitschka, B., & Negendank, J. F. (1996). Sedimentology, dating and palaeoclimatic interpretation of a 76.3 ka record from Lago Grande di Monticchio, southern Italy. *Quaternary Science Reviews*, *15*(2-3), 101-112.

Zumaque, J., de Vernal, A., Peros, M., Barhoumi, C., Peyron, O., Guiot, J., Sánchez-Goñi, M. F., Burke, A., Fréchette, B., Camuera, J., Jiménez-Moreno, G., Ramos-Roman, M., Decoupled winter and summer climate changes in southern Europe during Dansgaard-Oeschger cycles (submitted to *Quaternary Science Reviews*).

Table 3.1 Marine and terrestrial pollen records used in this study.

Site name	Site type	Latitude (°N)	Longitude (°E)	Elevation (m)	Mean temporal resolution for the studied period (30 - 10 ka) (yr/sample)	References
SU81-18	Marine	37.77	-10.18	-3135	370.5	Lézine and Denèfle (1997); Turon et al. (2003)
ODP Site 976	Marine	36.2	-4.3	-1108	192.3	Combourieu-Nebout et al. (2002; 2009)
Padul	Terrestrial (wetland)	37.01	-3,6	726	124.5	Camuera et al. (2018, 2019, 2022)
Lago Grande di Monticchio	Terrestrial (lacustrine)	40.94	15.61	656	95.3	Watts et al. (1996a, 2000); Allen et al. (2000); Wulf et al. (2004); Brauer et al. (2007) ; Allen and Huntley (2018)
Lake Xinias	Terrestrial (lacustrine)	39.05	22.27	500	492.9	Bottema (1979)

Table 3.2 Assignments used for the PFTs. Codes in green represent arboreal PFTs while those in brown represent non-arboreal PFTs.

Codes	PFTs	Taxa included in PFTs
EC	Eurythermic conifer	*Pinus, Pinus* subgen. *Diploxylon*
ECPI	Eurythermic conifer/Pioneer	*Juniperus*
BS	Boreal summergreen	*Larix*
PI	Pioneer	*Betula*
BEC	Boreal evergreen conifer	*Picea, Pinus* subgen. *Haploxylon*
BCTC	Boreal evergreen/cool-temperate conifer	*Abies*
CTC1	Intermediate temperate conifer	*Cedrus, Taxus*
TSAA	Temperate/boreal summergreen/arctic-alpine	*Alnus, Salix*
TSBS	Temperate/boreal summergreen	*Populus*
TS	Temperate summergreen	*Acer, Fraxinus, Fraxinus excelsior, Quercus (*deciduous*)*
TS1	Cool-temperate summergreen	*Carpinus, Corylus, Fagus, Frangula, Tilia, Ulmus*
TS2	Warm-temperate summergreen	*Castanea, Fraxinus ornus, Juglans, Ostrya, Platanus,* Rhamnaceae*, Vitis*
WTE	Warm-temperate broad-leaved evergreen	*Quercus (*evergreen*)*
WTE1	Cool-temperate broad-leaved evergreen	*Buxus, Hedera, Ilex*
WTE2	Warm-temperate sclerophyll trees/shrub	*Acacia, Arbutus, Cistus, Mercuria,* Myrtaceae*, Olea, Phillyrea, Pistacia, Rhus*
AA	Arctic-alpine dwarf shrub	*Alnus fructicosa, Betula nana, Dryas, Empetrum, Rhododendron, Saxifraga, Vaccinium*
COGS	Cold grass shrub	*Hippophaë, Polygonum*
H	Heath	*Calluna,* Ericaceae
GR	Grass	Poaceae
WAGS	Warm grass shrub	Brassicaceae*, Ceratonia,* Crassulaceae*, Echium, Ephedra fragilis,* Fabaceae*, Galium,* Scrophulariaceae*, Zizyphus*
SF	Steppe forb/shrub	Apiaceae, *Armeria*, *Artemisia*, *Carduus*, Campanulaceae, Caryophyllaceae, *Centaurea*, Cyperaceae, Dipsacaceae, *Filipendula*, *Helianthemum*, *Plantago*, Plumbaginaceae, *Ranunculus*, Rosaceae, *Rosmarinus*, Rubiaceae, *Rumex*, *Sanguisorba*, *Thalictrum*, Urticaceae, *Viburnum*
SFDF	Steppe/desert forb/shrub	Boraginaceae*,* Compositae*,* Compositae *tubuliflore,* Compositae *liguliflore,* Zygophyllaceae
DF	Desert forb/shrub	Chenopodiaceae*, Ephedra, Ephedra distachya*

Table 3.3 Accuracy of MAT reconstructions estimated from the root mean square error of prediction (RMSEP) and the coefficient of correlation (R^2) for the 88 and 87 (*Pinus* excluded) taxa databases. MTCO: mean-temperature of the coldest month in °C; MTWA: mean-temperature of the warmest month in °C; Pdjf: winter precipitation in mm; Pjja: summer precipitation in mm; Pann: annual precipitation in mm; Seasonality: MTWA – MTCO in °C.

Climatic parameters	RMSEP		R^2	
	88 taxa	87 taxa (without *Pinus*)	88 taxa	87 taxa (without *Pinus*)
MTCO	3.41	3.52	0.91	0.91
MTWA	1.95	1.94	0.83	0.83
Seasonality	3.44	3.51	0.88	0.87
Pdjf	68.76	71.65	0.76	0.74
Pjja	46.34	47.34	0.79	0.79
Pann	199.79	204.84	0.76	0.75

Figure 3.1 Map showing the location of the five pollen sequences (yellow stars) used in this study (Table 3.1 and references therein). Black dots show the location of records that are mentioned in the text: NGRIP (NGRIP, 2004), BS79-38 and BS79-33 (Cacho et al., 2001). The main surface currents and gyres are indicated as follows: Irminger Current (IC), North Atlantic Drift (NAD), East Greenland Current (EGC), Subpolar Gyre (SPG), Subtropical Gyre (STG). White areas represent LGM ice sheets. The transparent blue line defines the jet stream and notably the Rossby wave breaking west of the Alps as illustrated in Luetscher et al. (2015) and the schematic ice limits at LGM are defined after Ehlers et al. (2004).

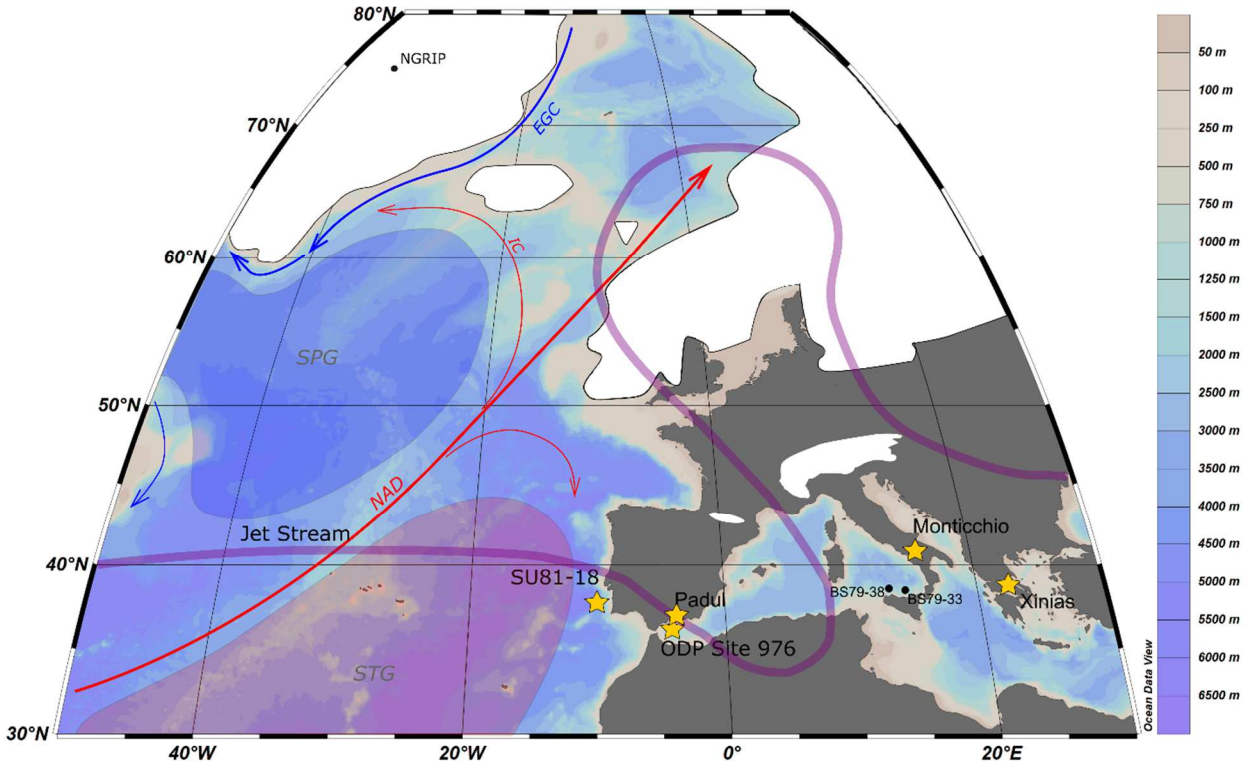

Figure 3.2 Results of the redundancy analysis (RDA) in the 4 study sequences. a) SU81-18 off South Portugal (Turon et al., 2003); b) ODP Site 976 in Alboran Sea (Combourieu-Nebout et al., 2009); c) Padul in Southeastern Spain (Camuera et al., 2018, 2019); d) Monticchio in Southern Italy (Allen et al., 2000) and e) Xinias in Greece (Bottema, 1979). Green and yellow arrows represent the arboreal and non-arboreal PFTs respectively (Table 3.2). Grey dashed arrows represent the climatic parameter discussed in this paper. Climatic parameters as in Table 3.3.

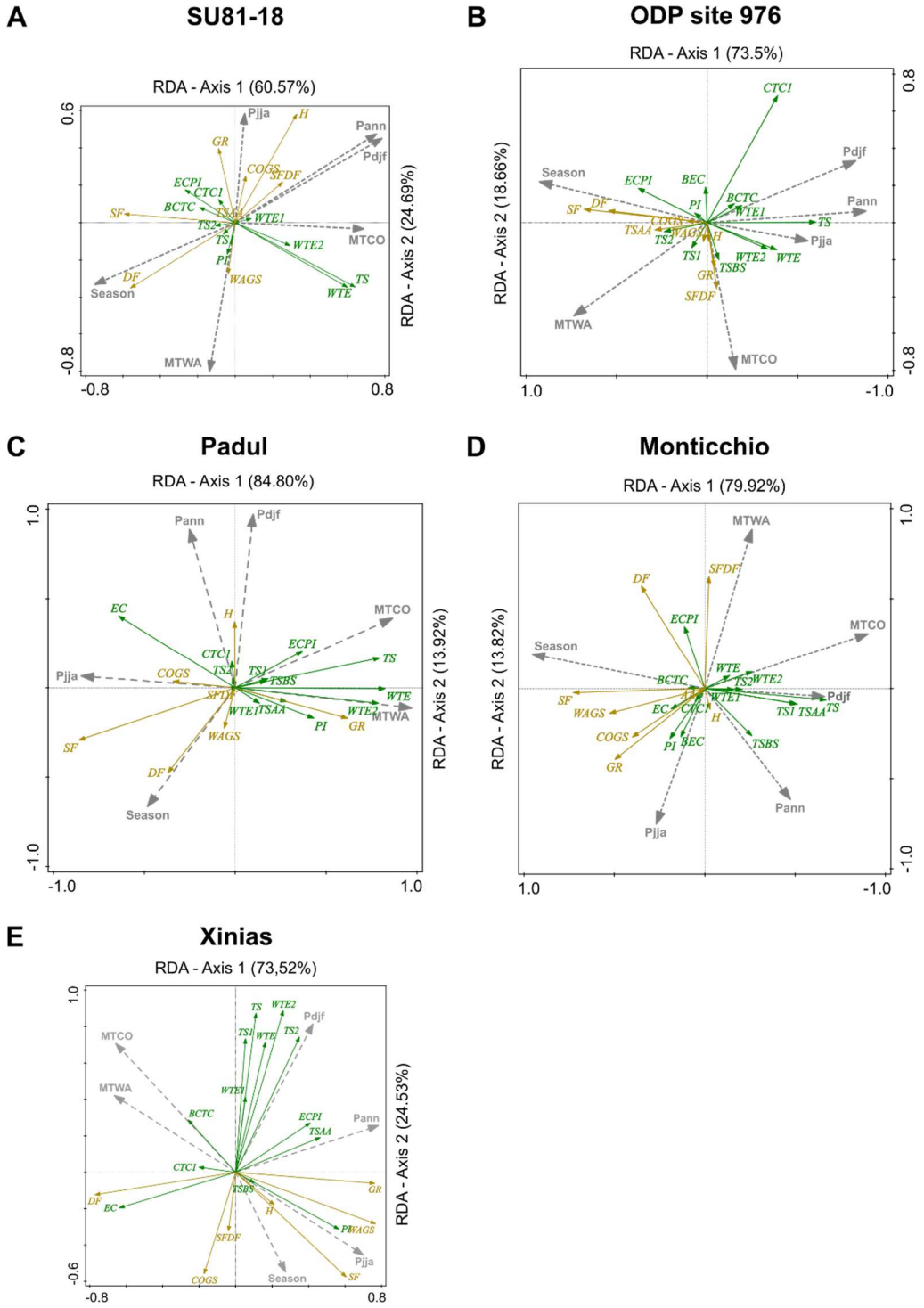

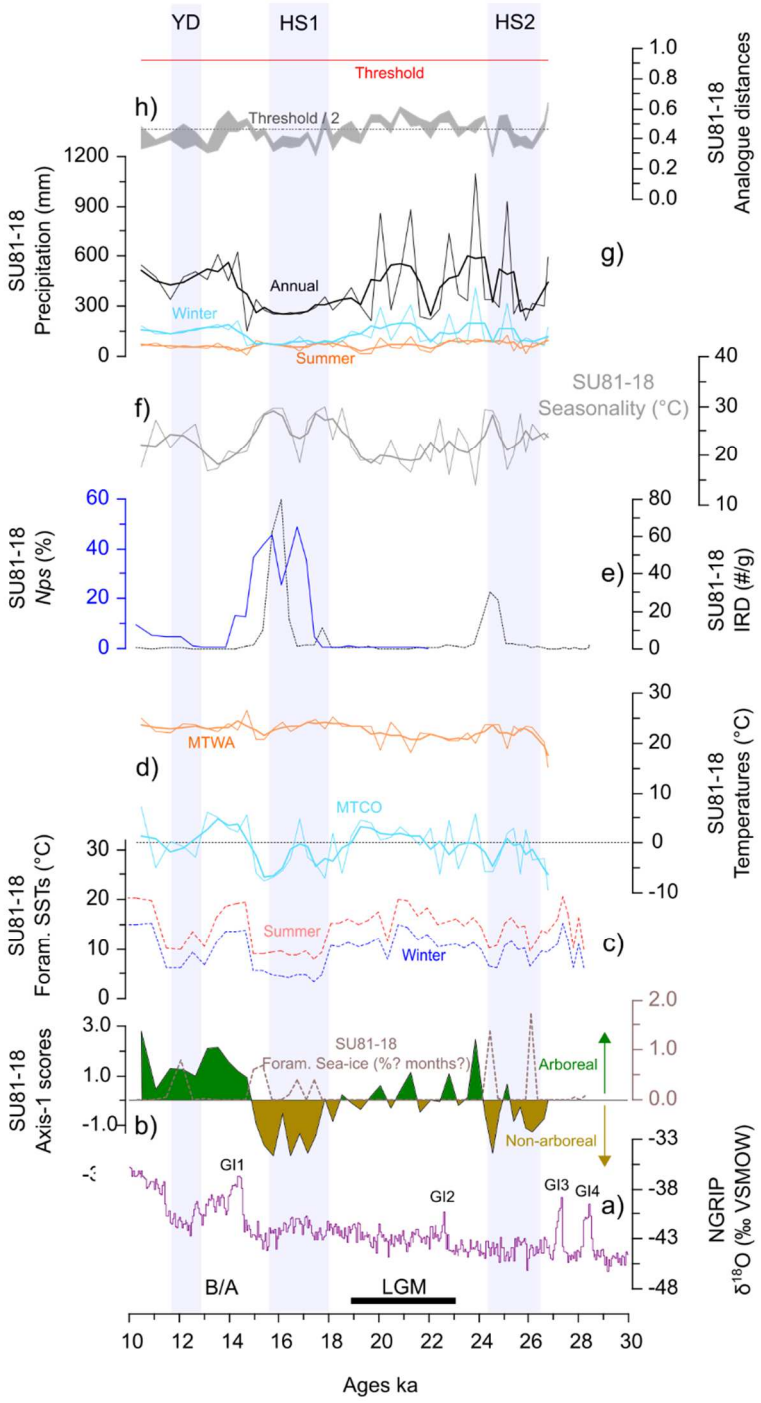

Figure 3.3 Records related to vegetation, sea-surface conditions, and pollen-based climate reconstructions at site SU81-18 (Figure 3.1; Table 3.1). a) NGRIP reference oxygen isotope record (NGRIP, 2004), b) RDA axis-1 scores (see Figure 3.2a) and foraminifera-based sea-ice cover duration reconstructions (this study, see Chapter 3.3.5.), c) foraminifera – based Sea-Surface Temperatures (SSTs) (this study, see Chapter 3.3.5.), d) Mean temperature of the coldest (MTCO) and the warmest months (MTWA), e) *Neogloboquadina pachyderma* (Nps) percentages in planktic foraminifer assemblages (Eynaud et al., 2009) and IRD (Bard et al., 2000), f) Seasonality (MTWA-MTCO), g) annual and seasonal precipitation, h) square-chord distances of the 1st and 5th best analogues and analogue thresholds (see text). Light curves: MAT values; Bold curves: 3-point running mean. The blue zones correspond to the Heinrich Stadials (HS) as defined in Sánchez-Goñi and Harrison (2010) and the Younger Dryas (YD) as defined in Rasmussen et al. (2014).

Figure 3.4 Records related to vegetation, sea-surface conditions, and pollen-based climatic reconstructions at ODP Site 976 (Figure 3.1; Table 3.1). a) reference NGRIP oxygen isotope record (NGRIP, 2004), b) RDA axis-1 scores (see Figure 3.2b), c) Mean temperature of the coldest (MTCO) and the warmest months (MTWA), d) Alkenone-based mean annual Sea-Surface Temperatures (SSTs) (Martrat et al., 2014), e) Seasonality (MTWA-MTCO), f) annual and seasonal precipitation and g) square-chord distances of the 1st and 5th best analogues and analogue threshold values (see text). Light curves: MAT values; Bold curves: 3-points running mean). The blue zones correspond to the Heinrich Stadials (HS) as defined in Sánchez-Goñi and Harrison (2010) and the Younger Dryas (YD) as defined in Rasmussen et al. (2014).

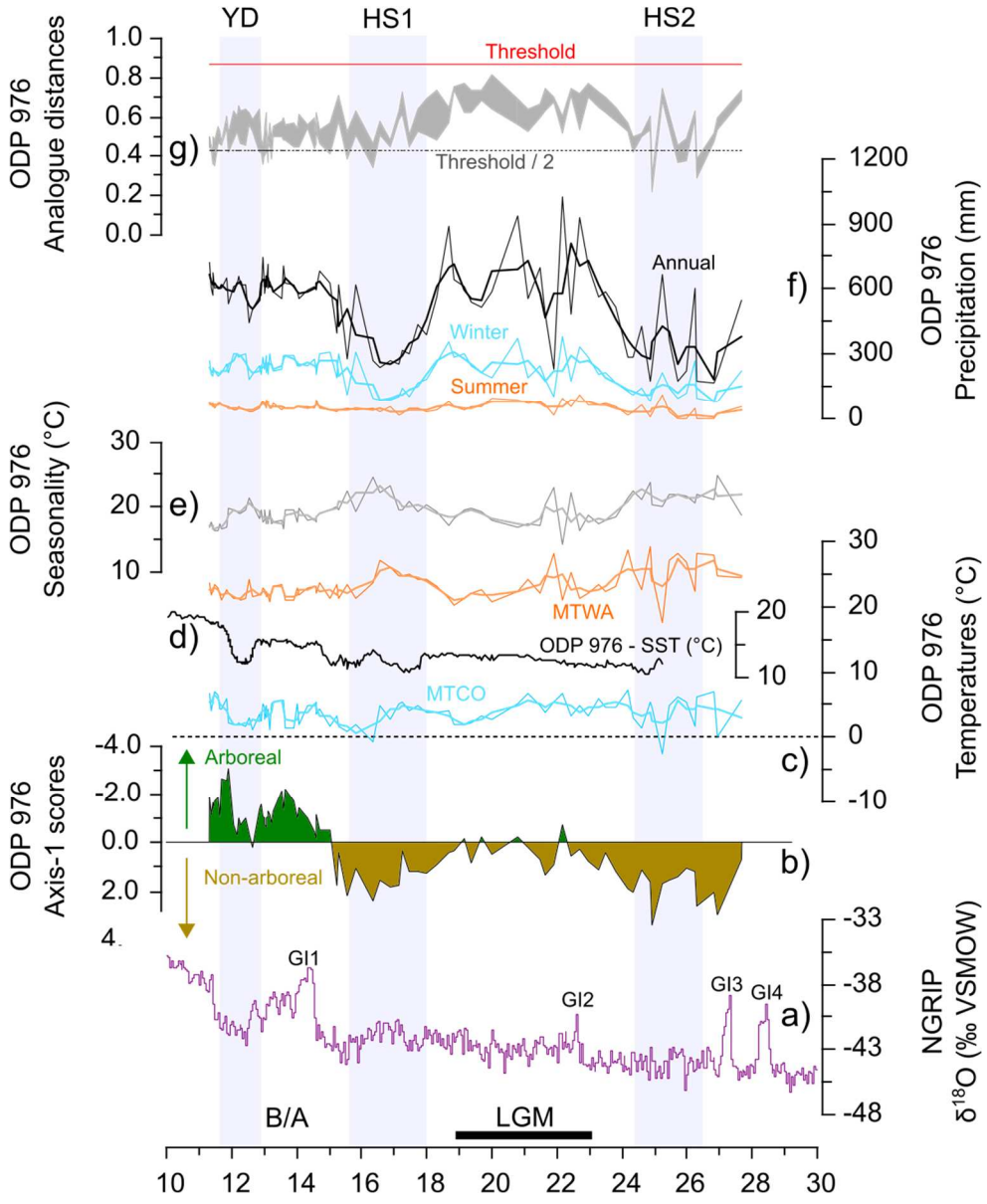

Figure 3.5 Records related to vegetation and pollen-based climatic reconstructions at Padul (Figure 3.1; Table 3.1). a) reference NGRIP oxygen isotope record (NGRIP, 2004), b) RDA axis-1 scores (see Figure 3.2c), c) Mean temperature of the coldest (MTCO) and the warmest months (MTWA), d) Seasonality (MTWA-MTCO), e) annual and seasonal precipitation and f) square-chord distances of the 1st and 5th best analogues and analogue threshold values (see text). Dashed color lines in c and e represent the mean 1901-2022 climate values (see Material and Methods). The blue zones correspond to the Heinrich Stadials (HS) as defined in Sánchez-Goñi and Harrison (2010) and the Younger Dryas (YD) as defined in Rasmussen et al. (2014). Dashed red lines indicate an alternative chronology.

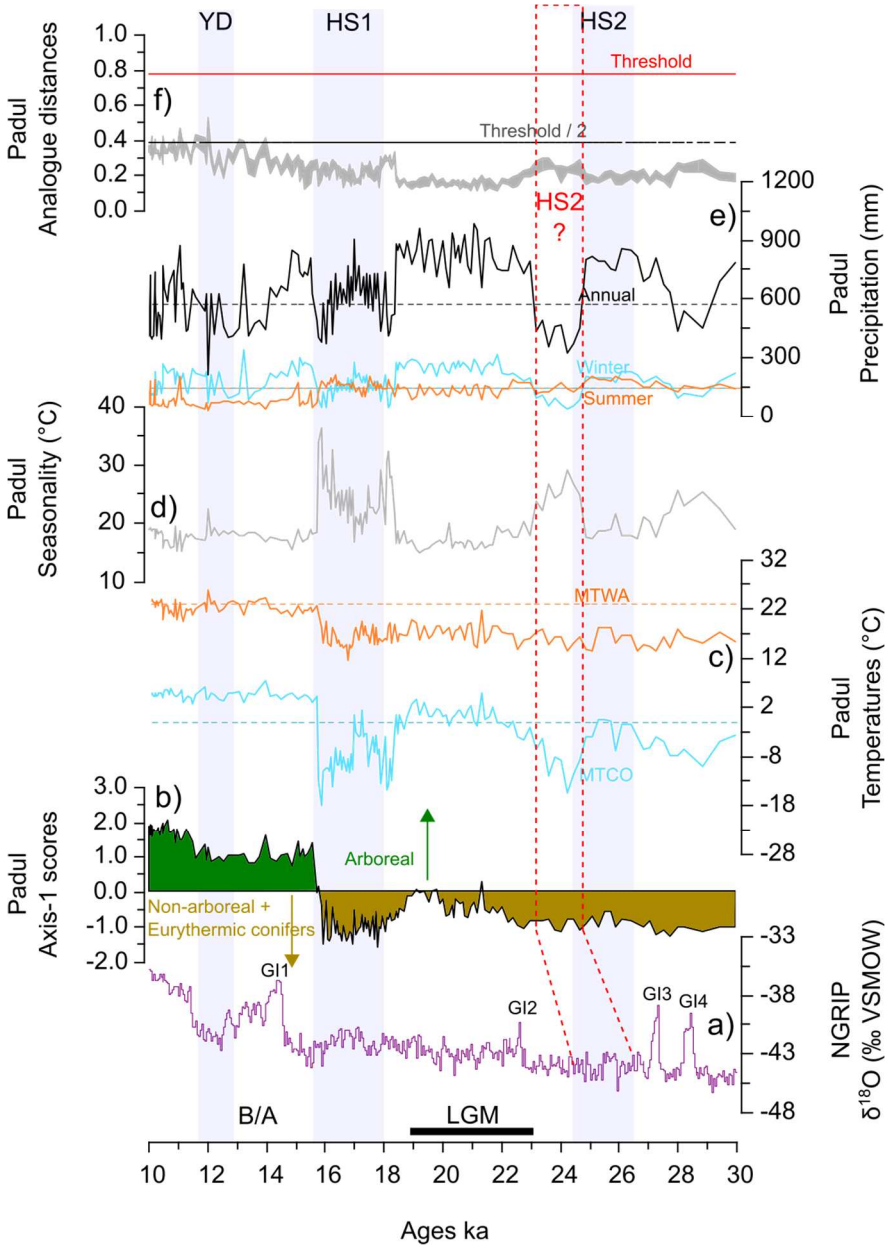

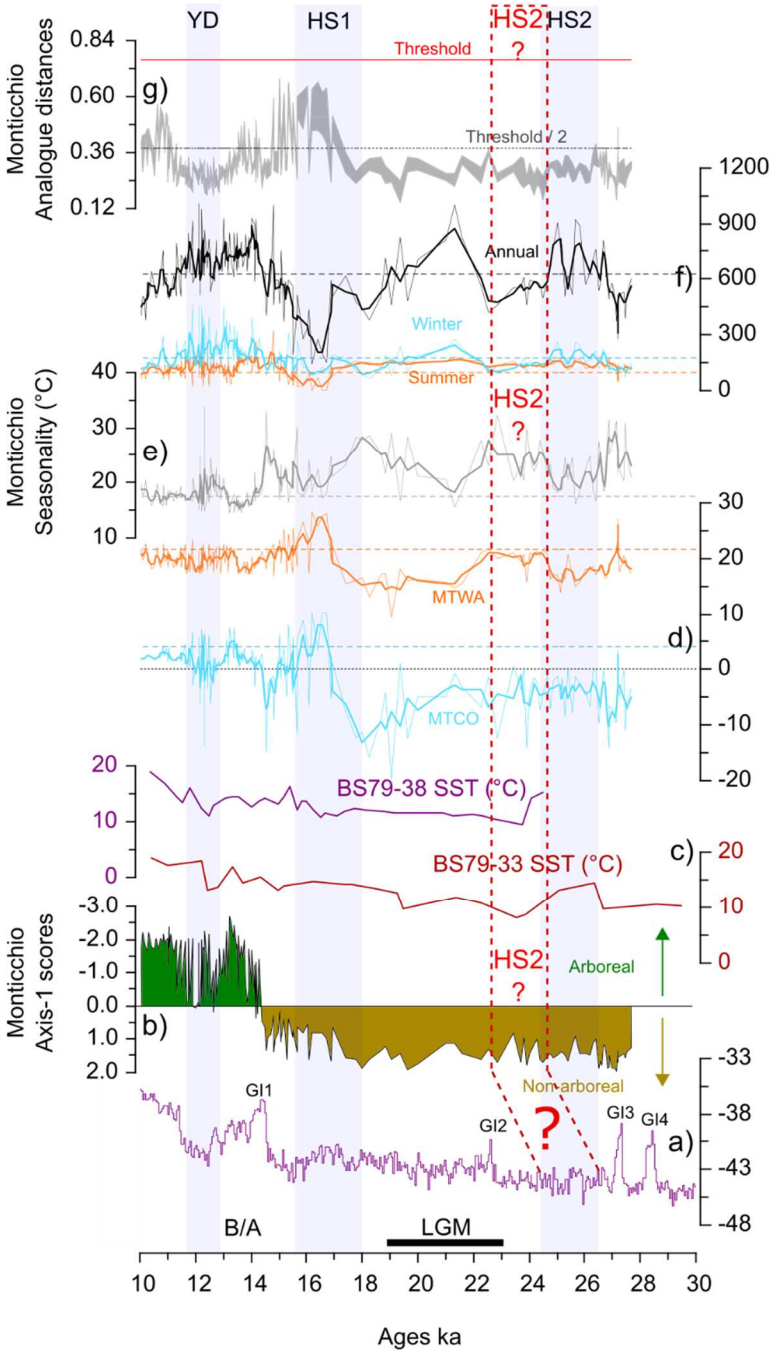

Figure 3.6 Records related to vegetation, and pollen-based climatic reconstructions at Monticchio (Figure 3.1; Table 3.1) and sea-surface conditions from proximal marine cores. a) reference NGRIP oxygen isotope record (GRIP, 2004), b) RDA axis-1 scores (see Figure 3.2d), c) Alkenone-based mean annual Sea-Surface Temperatures (SSTs) from cores BS79-33 and BS79-38 located in Tyrrhenian Sea (Cacho et al., 2001), d) Mean temperature of the coldest (MTCO) and the warmest months (MTWA) (MAT), e) Seasonality (MTWA-MTCO) (MAT), f) annual and seasonal precipitation (MAT) and g) square-chord distances of the 1st and 5th best analogues and threshold values for significant analogue (see text).

Light curves: MAT values; Bold curves: 3-points running mean. Dashed color lines in d, e and f represent the mean 1901-2022 climate values (see Material and Methods). The blue zones correspond to the Heinrich Stadials (HS) as defined in Sánchez-Goñi and Harrison (2010) and the Younger Dryas (YD) as defined in Rasmussen et al. (2014). Dashed red lines indicate an alternative chronology taking into consideration an underestimation of ages in the first half of MIS 2 encompassing HS2 as suggested by Wulf et al. (2004).

Figure 3.7 Records related to vegetation and pollen-based climatic reconstructions at Xinias (Figure 3.1; Table 3.1). a) reference NGRIP oxygen isotope record (NGRIP, 2004), b) RDA axis-2 scores (see Figure 3.2e), c) Mean temperature of the coldest (MTCO) and the warmest months (MTWA), d) Seasonality (MTWA-MTCO), e) annual and seasonal precipitation and f) square-chord distances of the 1st and 5th best analogues and analogue threshold values (see text). Dashed color lines in c and e represent the mean 1901-2022 climate values (see Material and Methods). The blue zones correspond to the Heinrich Stadials (HS) as defined in Sánchez-Goñi and Harrison (2010) and the Younger Dryas (YD) as defined in Rasmussen et al. (2014). Dashed red lines indicate an alternative chronology.

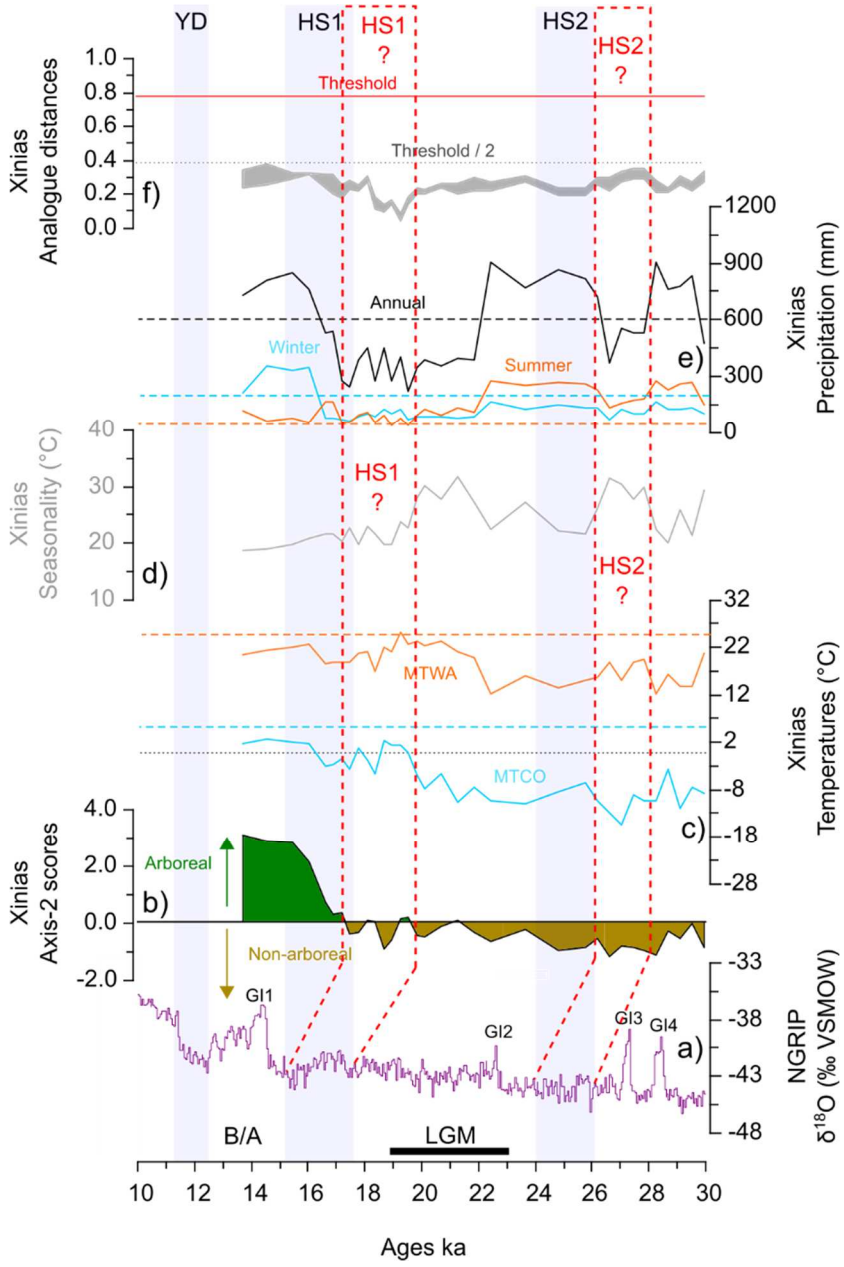

Figure 3.8 Pollen-based winter (Pdjf) and annual precipitation (Pann) estimates from the 5 studied sequences. Light curves: MAT values; Bold curves: 3-points running mean. The blue zones correspond to the Heinrich Stadials (HS) as defined in Sánchez-Goñi and Harrison (2010) and the Younger Dryas (YD) as defined in Rasmussen et al. (2014). Dashed blue and black lines represent the mean 1901-2022 climate values for winter and annual precipitation respectively (see Material and Methods). Dashed red lines indicate alternative chronologies for the Padul, Monticchio and Xinias sequences.

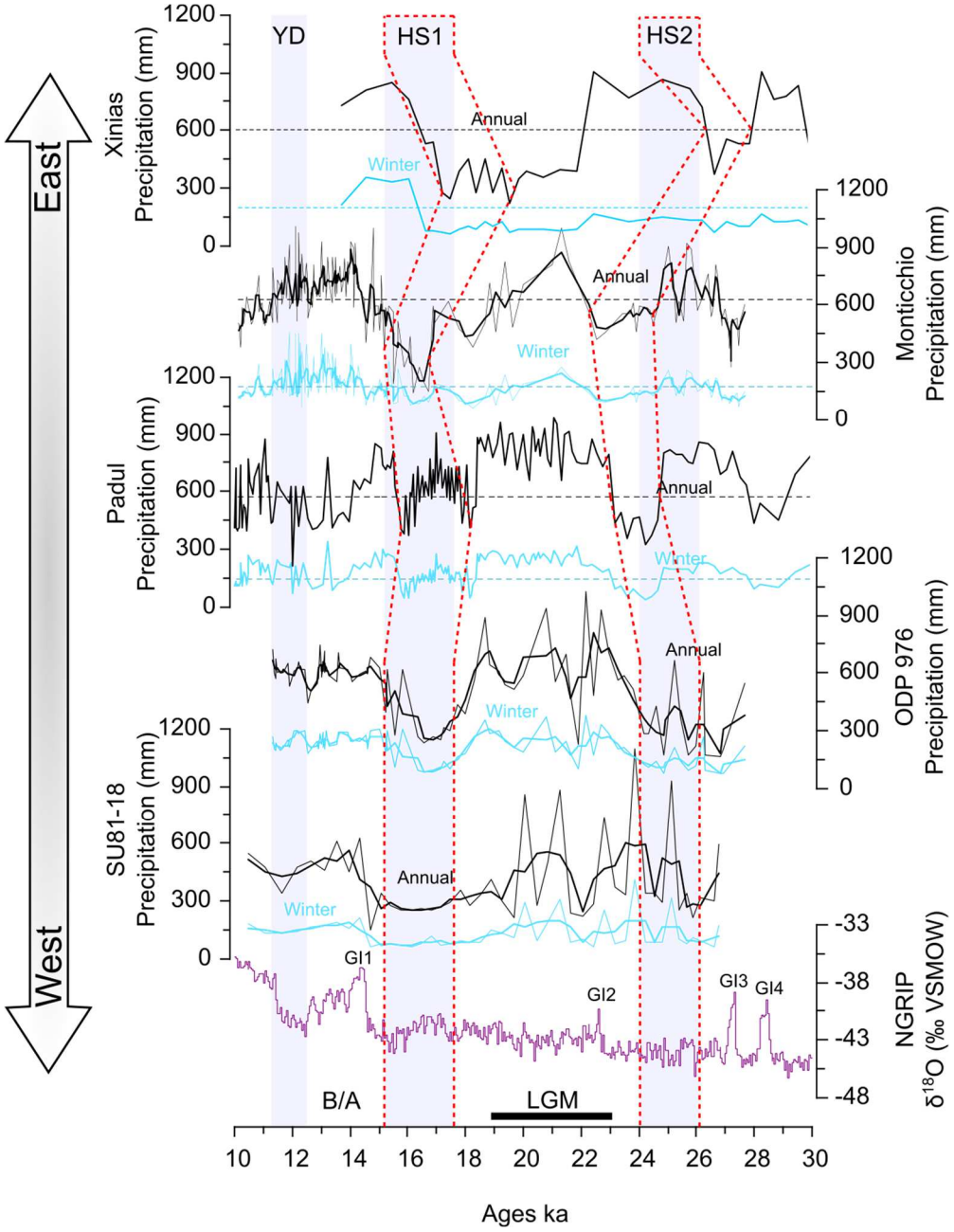

Figure 3.9 NGRIP oxygen isotope record (NGRIP, 2004) and RDA axis-1 scores (axis-2 scores for Xinias, see also Figure 3.2 and text) of the record from the five studied pollen sequences (Figure 3.1; Table 3.1). Dashed red lines indicate alternative chronologies for the Padul, Monticchio and Xinias sequences.

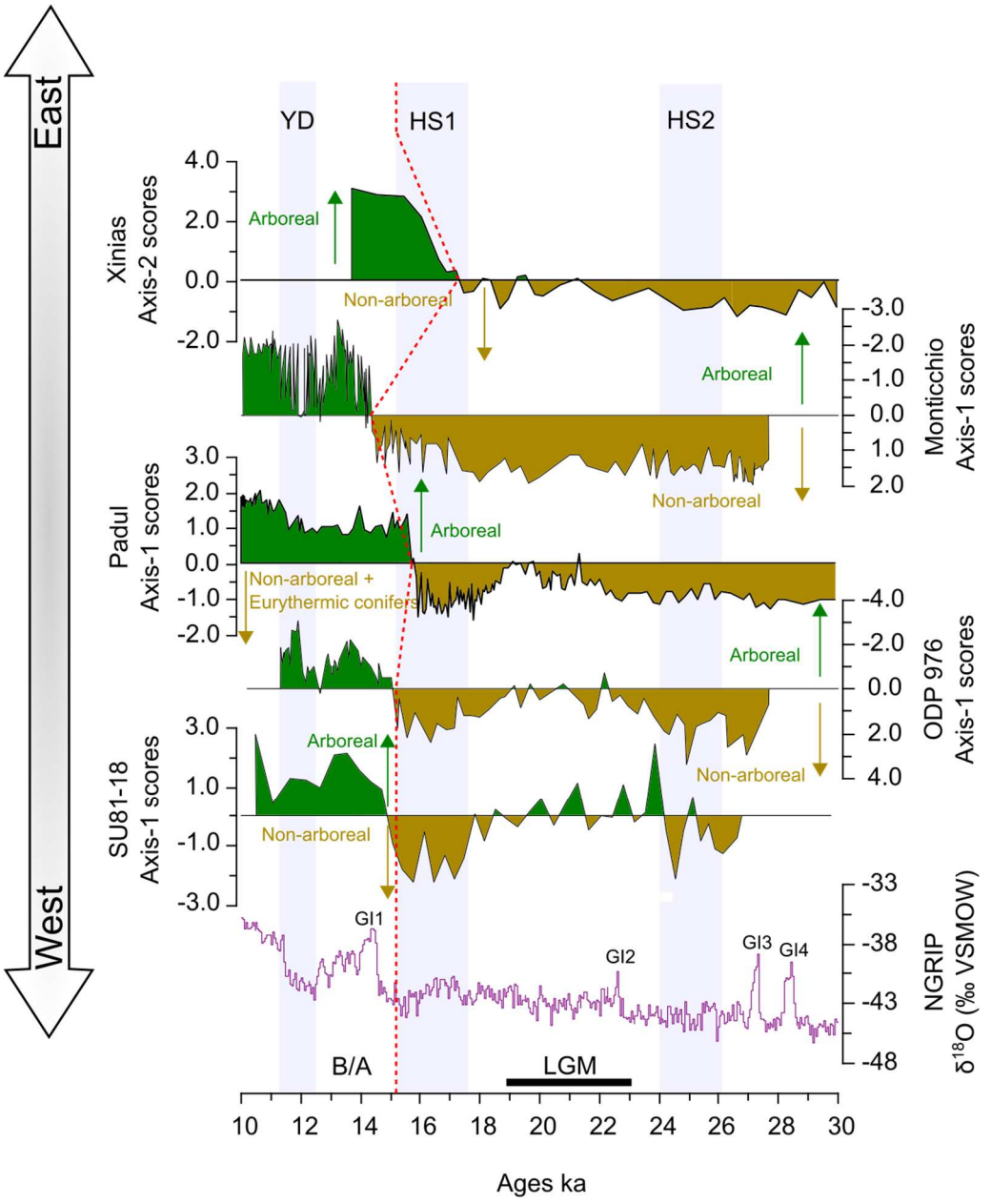

Figure 3.10 Pollen-based mean temperature of the coldest month (MTCO) estimates from the 5 studied sequences. Light curves: MAT values; Bold curves: 3-points running mean. The blue zones correspond to the Heinrich Stadials (HS) as defined in Sánchez-Goñi and Harrison (2010) and the Younger Dryas (YD) as defined in Rasmussen et al. (2014). Dashed blue lines represent the mean 1901-2022 climate values (see Material and Methods). Dashed red lines indicate alternative chronologies for the Padul, Monticchio and Xinias sequences.

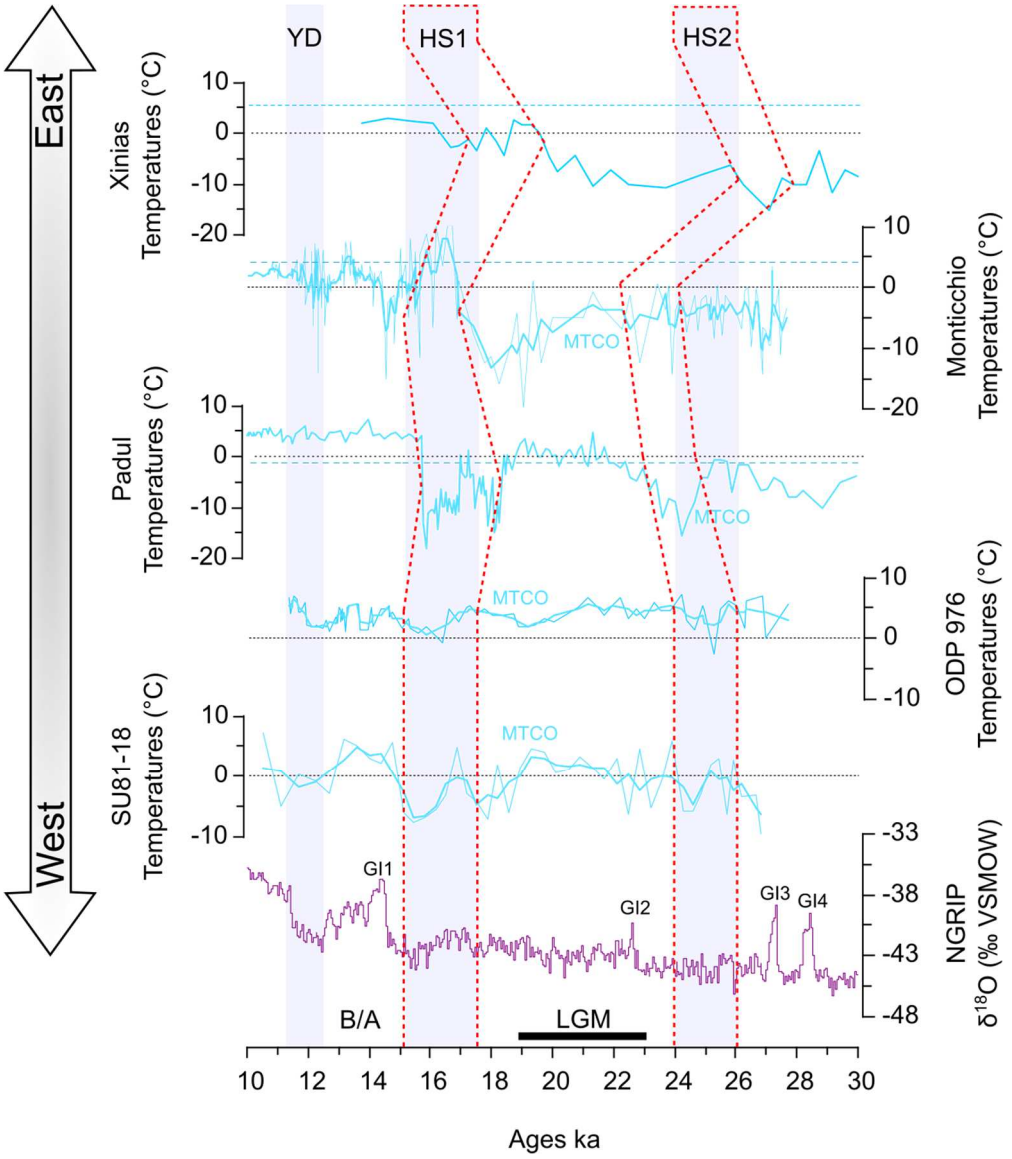

3.8 SUPPLEMENTARY DATA

Figure 3.S1 Age model of core SU81-18, off southern Portugal (Figure 3.1; Table 3.1 and references therein), obtained by using CLAM (Blaauw, 2010) (see Material and Methods and related files in Sanchez et al. (2017) for further details and data). The black line corresponds to the weighted average. Gray areas show the confidence intervals of the age-depth models calculated by defaults at 95% (2 sigma). The dates are indicated in blue.

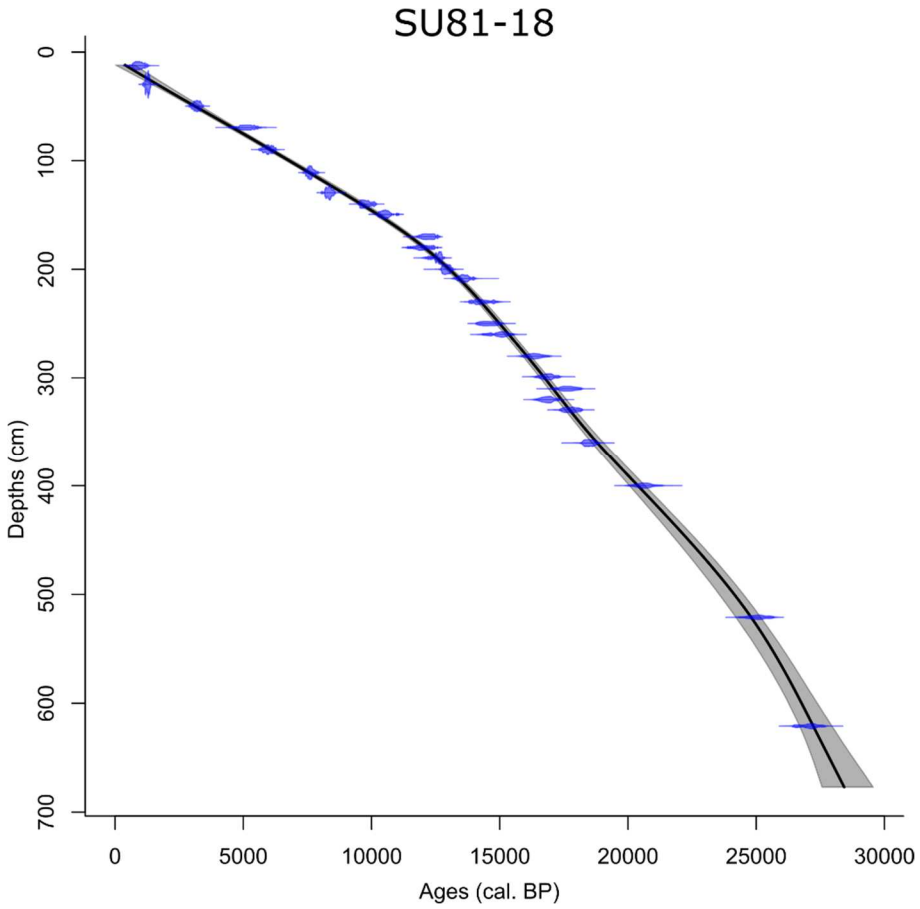

Figure 3.S2 Age model of core ODP Site 976, located in the Alboran Sea (Figure 3.1; Table 3.1 and references therein), obtained by using CLAM (Blaauw, 2010) (see Material and Methods and related files in Sanchez et al. (2017) for further details and data). The black line corresponds to the weighted average. Gray areas show the confidence intervals of the age-depth models calculated by defaults at 95% (2 sigma). The dates are indicated in blue and the correlated tie points are indicated in green.

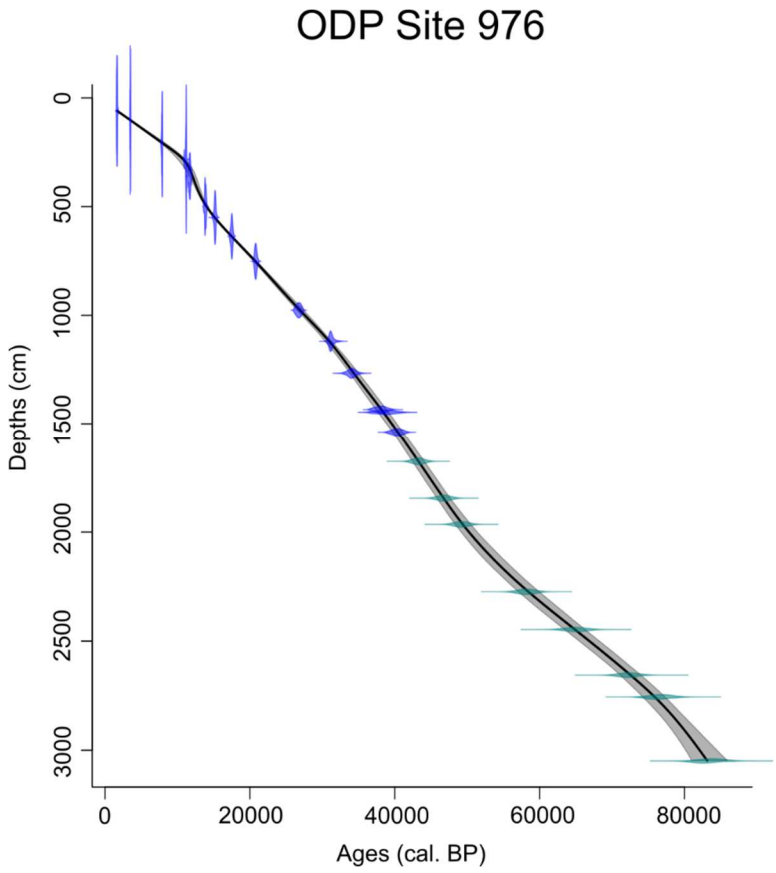

Figure 3.S3 Age model of the Xinias sequence, located in Greece (Figure 3.1; Table 3.1 and references therein), obtained by using CLAM (Blaauw, 2010) (see Material and Methods and related files in Sanchez et al. (2017) for further details and data). The black line corresponds to the weighted average. Gray areas show the confidence intervals of the age-depth models calculated by defaults at 95% (2 sigma). The dates are indicated in blue.

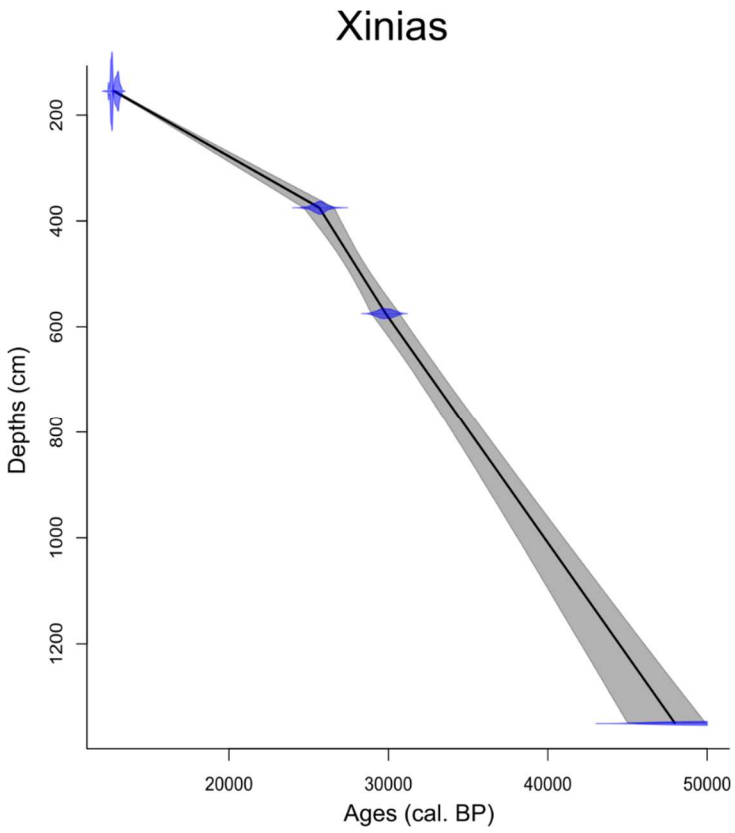

Figure 3.S4 Records related to vegetation and pollen-based climatic reconstructions at Xinias (Figure 3.1; Table 3.1) as it is presented in Figure 3.7. a) reference NGRIP oxygen isotope record (NGRIP, 2004), b) RDA axis-2 scores (see Figure 3.2e), c) Mean temperature of the coldest (MTCO) and the warmest months (MTWA), d) Seasonality (MTWA-MTCO), e) annual and seasonal precipitation and f) square-chord distances of the 1st and 5th best analogues and analogue threshold values (see text). Dashed color lines in c and e represent the mean 1901-2022 climate values (see Material and Methods). The blue zones correspond to the Heinrich Stadials (HS) as defined in Sánchez-Goñi and Harrison (2010) and the Younger Dryas (YD) as defined in Rasmussen et al. (2014). Dashed red lines indicate an alternative chronology.

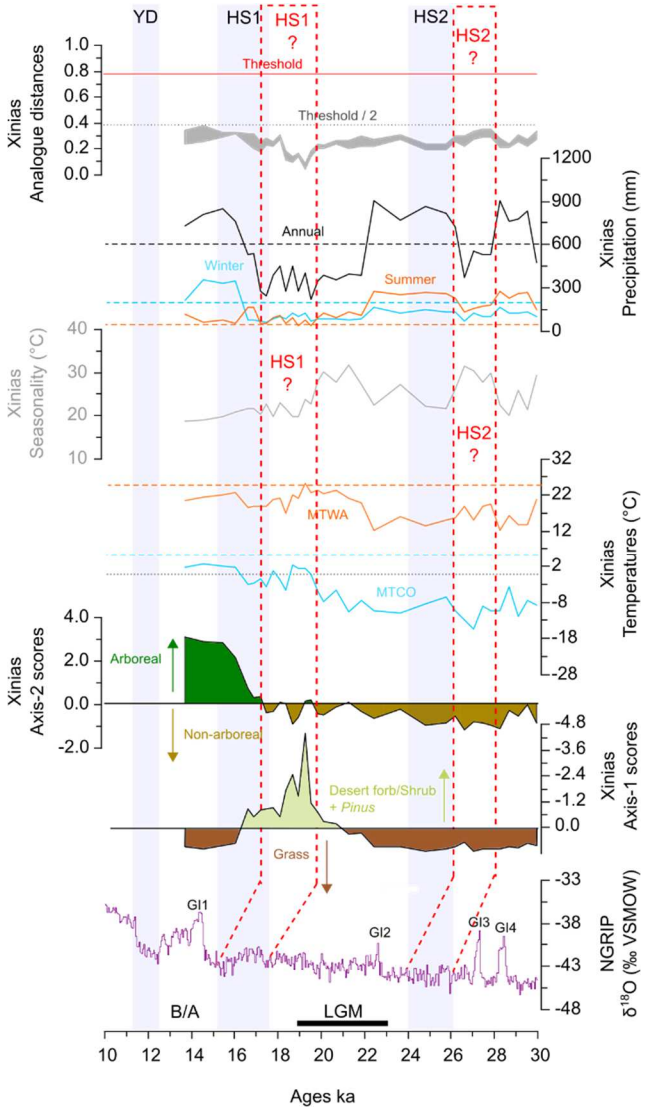

3.8.1 References

Blaauw, M. (2010). Methods and code for 'classical'age-modelling of radiocarbon sequences. *Quaternary geochronology*, *5*(5), 512-518.

North Greenland Ice Core Project members, High resolution record of Northern Hemisphere climate extending into the last interglacial period. Nature, 431(7005), 147-151 (2004).

Rasmussen, S. O., Bigler, M., Blockley, S. P., Blunier, T., Buchardt, S. L., Clausen, H. B., ... & Winstrup, M. (2014). A stratigraphic framework for abrupt climatic changes during the Last Glacial period based on three synchronized Greenland ice-core records: refining and extending the INTIMATE event stratigraphy. *Quaternary science reviews*, *106*, 14-28.

Sanchez-Goni, M. F., & Harrison, S. P. (2010). Millennial-scale climate variability and vegetation changes during the Last Glacial: Concepts and terminology. Quaternary Science Reviews, 29(21-22), 2823-2827.

Sánchez Goñi, M. F., Desprat, S., Daniau, A. L., Bassinot, F. C., Polanco-Martínez, J. M., Harrison, S. P., ... & Yamamoto, M. (2017). The ACER pollen and charcoal database: a global resource to document vegetation and fire response to abrupt climate changes during the last glacial period. *Earth System Science Data Discussions*, *2017*, 1-33.

CONCLUSION

Les reconstitutions de la végétation par l'examen des types de plantes fonctionnelles (PFT) à partir de 14 séquences polliniques du sud et sud-ouest de l'Europe et couvrant la période de 60 à 10 ka ont permis de mettre en lumière d'importantes variations de fréquence millénaire au cours de la dernière période glaciaire, avec une alternance de phases arborées et de phases plus steppiques. Parmi les séquences analysées, cinq proviennent de carottes sédimentaires marines et enregistrent un signal continental via les flux polliniques ainsi que les conditions océaniques de surface (flux pélagiques, $\delta^{18}O$ des foraminifères planctoniques, etc.), permettant de fixer un cadre chronologique sur la base de la stratigraphie isotopique marine et d'établir des corrélations avec les interstadiaires (GIs) et stadiaires (GSs) du Groenland. Ce travail a contribué à démontrer une correspondance entre les phases arborées aux GIs et les phases steppiques aux GSs, tel que cela avait déjà été suggéré par Sánchez-Goñi et al. (2000, 2002, 2008, 2009, 2021), Combourieu-Nebout et al. (2002, 2009), Roucoux et al. (2001, 2005), et Turon et al. (2003).

Outre les PFTs, les données polliniques nous ont servi à retracer les paramètres du climat à partir de la technique des analogues modernes (MAT – *Modern Analogue Technique*; Guiot, 1990) en utilisant une base de données polliniques modernes eurasienne, couvrant des biomes arctiques à tempérés chauds (Davis et al., 2020). Des analyses multivariées avec les données de PFT et les paramètres climatiques ont mis en évidence une prédominance de l'influence hivernale sur la dynamique de la végétation. En effet, les phases arborées des GIs sont marquées par une augmentation des précipitations et/ou températures hivernales. À l'inverse, un climat plus froid et plus sec en hiver caractérise les phases steppiques des GSs. Les cycles de Dansgaard-Oeschger (DO) ont donc une empreinte hivernale très prononcée, avec des hivers doux et humides sur le sud et le sud-ouest de l'Europe lors des GIs et inversement. En revanche, les reconstitutions paléoclimatiques de la plupart des enregistrements ont révélé des températures moyennes du mois le plus chaud (MTWA – *Mean Temperature of the Warmest Month*) élevées, proches des valeurs modernes en ce qui concerne les sites terrestres, et surtout relativement stables en comparaison des températures hivernales. La grande variabilité des températures hivernales et la stabilité relative des températures estivales viennent étayer la principale hypothèse défendue dans cette thèse selon laquelle les DOs ont avant tout un caractère hivernal et que des températures estivales élevées

auraient prévalu pendant la dernière période glaciaire, notamment au cours des GSs (cf. Denton et al., 2005).

Plusieurs études avaient permis de poser l'hypothèse de variations de température plus prononcées en hiver qu'en été au cours des DOs (e.g., Sánchez Goñi et al. 2000; Denton et al., 2005; Datema et al., 2019). Nos données apportent des éléments confirmant cette hypothèse et montrent de surcroît des comportements des températures estivales et hivernales pouvant même s'opposer. En effet, les phases arborées sont marquées par des températures estivales très légèrement supérieures en moyenne à celles des phases steppiques. Toutefois, les séries temporelles ne permettent pas d'illustrer une augmentation univoque des MTWA à chaque GSs, et indiquent que la variabilité climatique millénaire est un signal indépendant de celui des températures estivales au sud/sud-ouest de l'Europe.

Le signal prédominant des précipitations et températures hivernales sur les variations millénaires de la végétation, ainsi que le découplage du signal hiver/été, nous ont conduit à envisager des relations entre les oscillations climatiques pendant la dernière période glaciaire en Europe du sud et du sud-ouest et des changements de la circulation atmosphérique régionale. En effet, de nos jours, la végétation du sud de l'Europe dépend de la quantité de précipitations reçues en hiver, laquelle est fonction des modes de circulation associée à l'Oscillation Nord Atlantique (NAO – *North Atlantic Oscillation*) (Gouveia et al., 2008). L'indice de la NAO est défini comme la différence de pression atmosphérique entre la dépression islandaise et l'anticyclone des Açores et est calculé de novembre à avril, là où cette différence est la plus marquée. Un indice négatif de la NAO s'accompagne de faibles gradients de pression, causant un déplacement des vents d'ouest vers le sud et générant un climat doux et humide, propice au développement d'une dense végétation. À l'inverse, de forts gradients de pression, sous mode positif de la NAO, induisent un déplacement des vents d'ouest vers le nord du continent, causant des hivers secs et froids dans le sud de l'Europe (Hurrell, 1995). Les mesures de la NAO depuis plus d'un siècle dépeignent des variations interannuelles et décennales. Ici, nous émettons l'hypothèse de variations du mode dominant de la NAO à des échelles de temps séculaire à millénaire et que les DOs dans le sud/sud-ouest de l'Europe pourraient être le reflet de variations du mode dominant de la NAO, soit de la trajectoire des tempêtes et/ou de la force des vents d'ouest au-dessus du continent.

L'un des résultats les plus importants de cette étude est sans doute la mise en évidence de températures estivales élevées au cours du dernier épisode glaciaire, y compris pendant les phases les

plus froides (GSs). Denton et al. (2022) avaient estimé que les températures estivales pourraient avoir joué un rôle clé dans la variabilité climatique millénaire enregistrée dans la région Nord Atlantique, en modulant l'apport d'eaux de fonte dans le bassin Atlantique Nord. Ils avaient suggéré qu'une transition globale vers des températures estivales plus élevées à la fin des GIs aurait généré un grand apport d'eaux douces dans l'Atlantique Nord, impactant ainsi la circulation thermohaline, l'extension du couvert de glace de mer hivernal et donc le climat hivernal rigoureux (Denton et al., 2022). Bien que démontrant des valeurs élevées, proches des valeurs actuelles, nos reconstitutions ne montrent pas d'augmentation significative des températures estivales à la fin des GIs, mais présentent plutôt une certaine stabilité. Nous proposons donc que les températures estivales élevées pendant la dernière période glaciaire pourraient avoir joué un rôle clé sur le climat, en générant quantités d'eaux de fonte en Atlantique Nord, mais que ce sont des changements millénaires dans la force et/ou direction des vents d'ouest qui ont modulé l'impact des apports en eau de fonte en modifiant leur redistribution. Avec des vents d'ouest renforcés en hiver (GSs), les eaux douces issues de la fonte des glaces le long des marges groenlandaises et canadiennes se seraient dispersées de l'ouest de l'Atlantique Nord vers l'est, générant une couche d'eau froide et peu salée en surface du bassin Nord Atlantique. Cette couche d'eau douce favorable au développement de la glace de mer, aurait empêché la dérive nord atlantique, plus dense, de circuler en surface, limitant ainsi la diffusion de sa chaleur et l'évaporation à l'interface océan-atmosphère, générant ainsi un climat froid et sec sur la moitié sud du continent Européen. À son entrée dans les hautes latitudes, une dérive nord atlantique trop chaude, et donc moins dense, aurait ainsi contribué au ralentissement de la formation d'eaux profondes et de la circulation thermohaline, tel qu'observé pendant les GSs (e.g., Gottschalk et al., 2015). À l'inverse, au cours des GIs, des vents d'ouest plus faibles, auraient maintenu les eaux de fonte dans la partie ouest du bassin Nord Atlantique, permettant à la dérive nord atlantique de conserver ses propriétés thermiques et de circuler en surface vers l'est et le nord-est pour diffuser chaleur et humidité sur la moitié sud du continent européen, et de refroidir suffisamment pour assurer la convection.

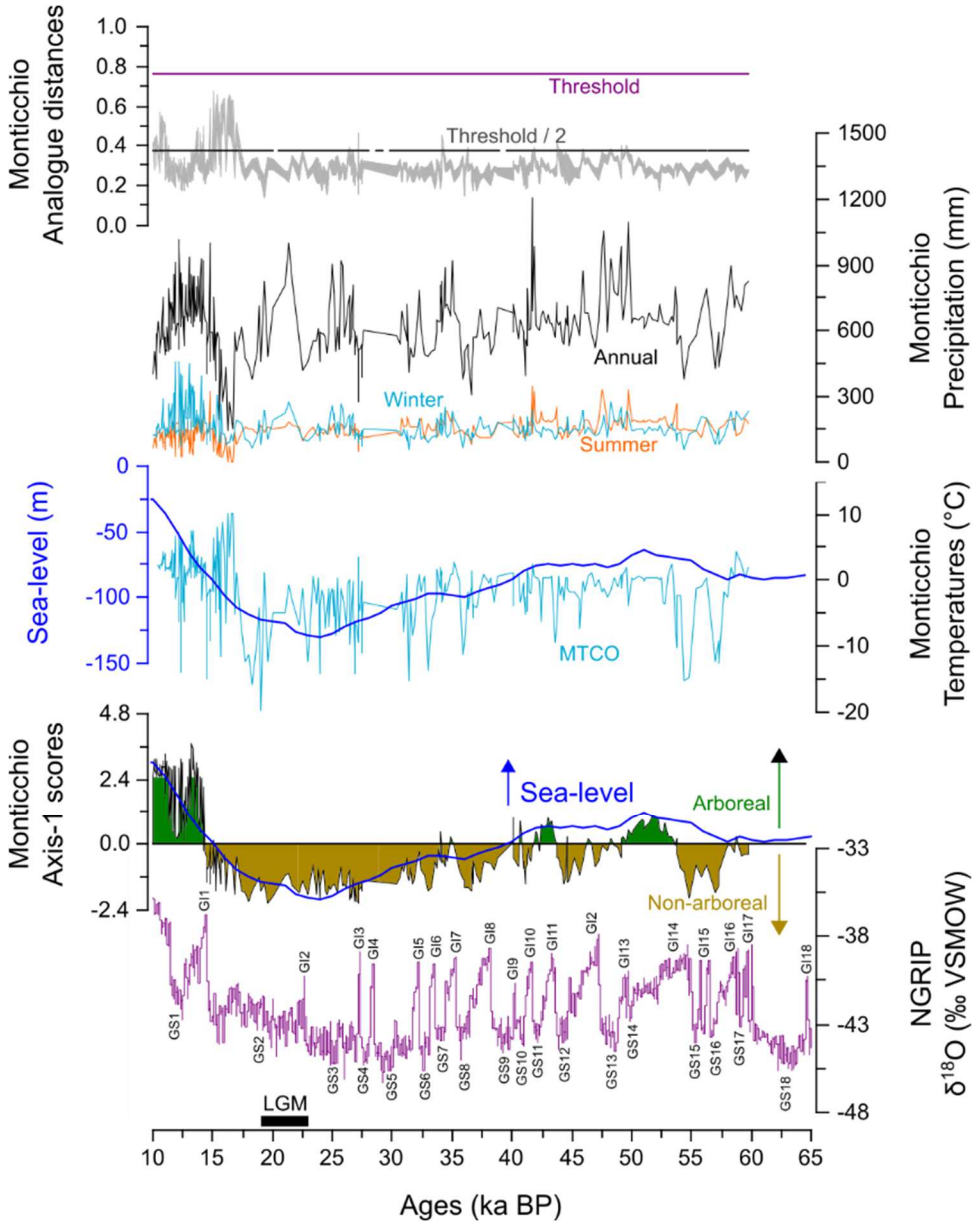

Figure 4.1 Enregistrements de signaux climatiques extra-régionaux et des variations de la végétation et de paramètres climatiques à partir des assemblages polliniques de Lago Grandi di Monticchio (Figure 3.1). De bas en haut : courbe de la composition isotopique de l'oxygène de carottes de glace du Groenland (*North Greenland Ice Core Project members*, 2004), évolution de la végétation à Monticchio telle que définie par une analyse multivariée des PFTs, , niveau marin (Spratt et Lisiecki, 2016), températures moyennes du mois le plus froid (MTCO - *Mean temperature of the coldest month*), précipitations annuelles et saisonnières et distances des premiers et cinquièmes meilleurs analogues, les distances inférieures au seuil/2 correspondant à de bons analogues, alors que celles comprises entre le seuil et le seuil/2 indiquent des analogues acceptables (de Vernal et al., 2005).

Des changements de la circulation atmosphérique hivernale en Atlantique Nord, à l'origine de la variabilité millénaire climatique et environnementale enregistrée dans la partie sud du continent européen, semblent avoir perduré au cours du Dernier Maximum Glaciaire (LGM – *Last Glacial Maximum*). En effet, nos reconstitutions climatiques affichent d'importantes variations des précipitations hivernales et annuelles, surtout aux sites SU81-18 et ODP 976 (Figure 3.1), avec des pics très élevés dont les valeurs égalent les valeurs de précipitations enregistrées lors des GIs les plus prononcés du stade isotopique marin (MIS – Marine Isotope Stage) 3 (Figures 4.2 et 4.3). C'est la première fois que des reconstitutions climatiques issues de séquences polliniques du sud-ouest européen illustrent de façon aussi évidente des précipitations hivernales et annuelles supérieures à celles du début de l'Holocène pendant le LGM. Nos reconstitutions sont compatibles avec les résultats de certains modèles climatiques (e.g., Beghin et al., 2016) et des indications fournies par les niveaux de lacs (e.g., Vegas et al., 2010; Moreno et al., 2012). En outre, deux phases de fortes précipitations pendant le LGM sont identifiables dans nos séquences marines et se corrèlent parfaitement à deux phases d'avancées glaciaires dans les Alpes (e.g., Ivy-Ochs, 2015; Ivy-Ochs et al., 2018; Kamleitner et al., 2022; Roattino et al., 2022), appuyant l'hypothèse de changements de la circulation atmosphérique à échelle régionale et de variations de la position et/ou de la vigueur des vents d'ouest et trajectoire des tempêtes.

La grande majorité des séquences polliniques du continent européen (Davis et al., 2022), et notamment celles du nord de la Péninsule Ibérique et du sud-ouest de la France (e.g., Andrieu et al., 1993; Reille et Andrieu 1995; Valero-Garces et al., 2004; Gonzalez-Sampériz et al. 2006), n'illustrent toutefois aucun développement d'un couvert végétal forestier au cours du LGM, traduisant plutôt un climat aride et froid. C'est également le cas des sites Lago Grande di Monticchio (Monticchio), situé dans le sud de l'Italie, et Xinias, en Grèce (Figures 3.1 et 3.9). Monticchio enregistre des variations millénaires importantes des précipitations et températures hivernales de 60 à 10 ka, avec des précipitations abondantes au LGM (Figure 4.1). Il enregistre également une tendance à long-terme vers une baisse des températures en lien avec le refroidissement global, la croissance des calottes glaciaires et la baisse du niveau marin au cours du stade isotopique 3 (Figure 4.1). Cela se traduit dans la végétation par un déclin des PFTs arborés du début du stade 3 au LGM, les températures hivernales plus faibles limitant le développement forestier de la végétation (Figure 4.1).

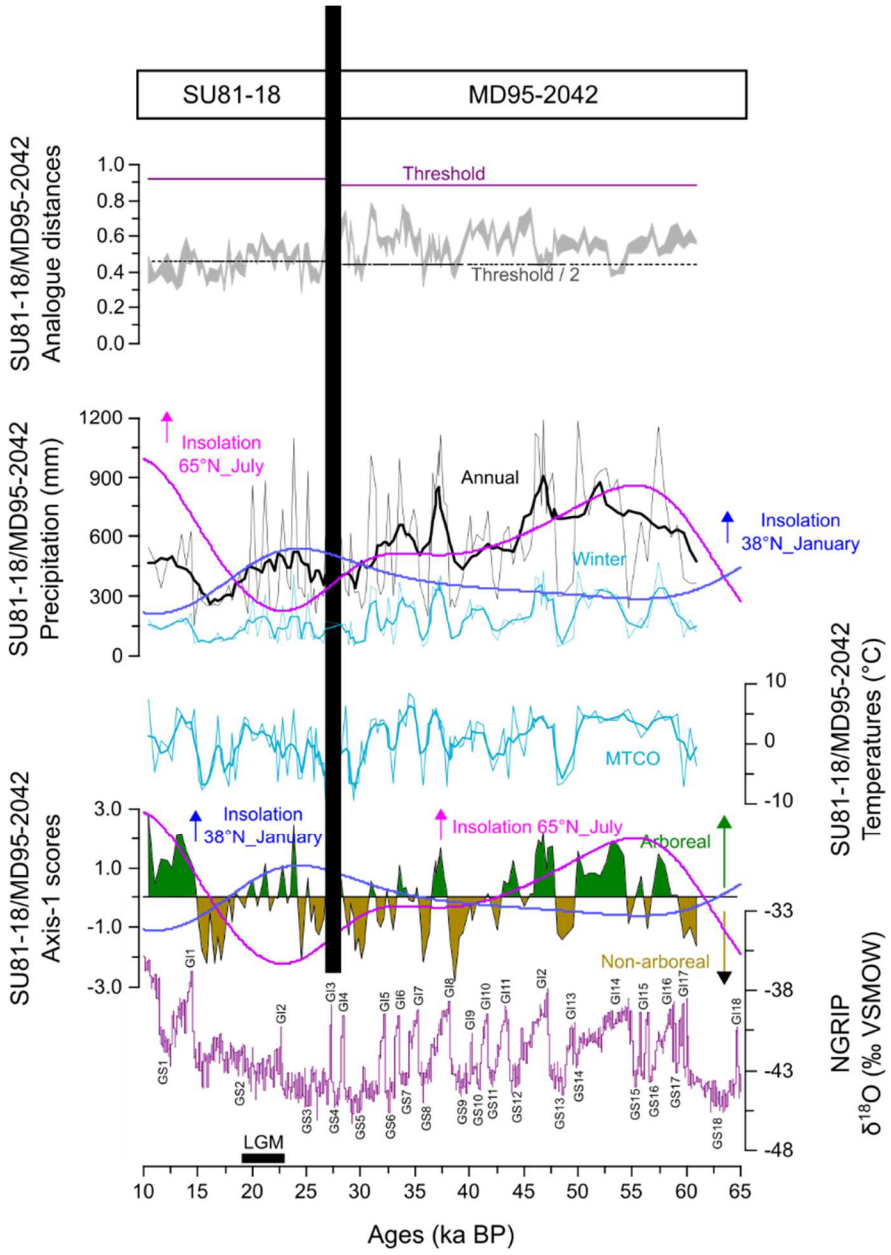

Figure 4.2 Enregistrements de signaux climatiques extra-régionaux et des variations de la végétation et de paramètres climatiques à partir des assemblages polliniques des carottes MD95-2042 et SU81-18 (Figure 1.1). De bas en haut : courbe de la composition isotopique de l'oxygène de carottes de glace du Groenland (North Greenland Ice *Core Project members*, 2004), évolution de la végétation telle que définie par une analyse multivariée des PFTs , courbes d'insolations estivale à 65°N et hivernale à 38°N (Laskar et al., 2004), températures moyennes du mois le plus froid (MTCO - *Mean temperature of the coldest month*) (lissage selon une fenêtre de 3 points en gras), précipitations annuelles (lissage selon une fenêtre de 9 valeurs en gras) et hivernales (lissage selon une fenêtre de 3 valeurs en gras), et distances des premiers et cinquièmes meilleurs analogues , les distances inférieures au seuil/2 correspondant à de bon analogues, alors que celles comprises entre le seuil et le seuil/2 indiquent des analogues acceptables (de Vernal et al., 2005).

Contrairement aux résultats obtenus au site de Monticchio, les MTCO des sites marins MD95-2042/SU81-18 et ODP 976 (Figures 4.2 et 4.3) ne mettent pas en évidence un refroidissement à long-terme. Toutefois, au site MD95-2042/SU81-18, sur la marge sud-ouest ibérique (Figures 1.1 et 4.2), les températures hivernales affichent de fortes variations de 60 à 10 ka, d'amplitude comparable à celles enregistrées à Monticchio (Figure 4.1), alors que les celles du Site ODP 976, situé en Mer d'Alboran (Figures 3.1 et 4.3), montrent peu de variations et des températures hivernales relativement clémentes, illustrant la possibilité d'un front climatique entre les deux sites, et plus particulièrement à proximité du site SU81-18, le long de la marge ouest ibérique, tel que déjà suggéré par Penaud et al. (2011). En revanche, les précipitations annuelles et hivernales aux deux sites marins présentent une décroissance à long-terme au cours du stade isotopique 3, avec une légère augmentation entre 37 et 32 ka, soit pendant un intervalle correspondant à un plateau dans la courbe de l'insolation estivale à 65°N (Figures 4.2 et 4.3 ; Laskar et al., 2004). Les données polliniques des deux sites marins représentant la végétation des territoires continentaux adjacents qui dépend des précipitations hivernales, évoquent une tendance long-terme de désertification vers la steppe avec une légère densification du couvert forestier entre 37 et 32 ka (Figures 4.2 et 4.3).

En dépit de relations qui paraissent lier les variations à long terme de la végétation et de l'insolation au cours du stade 3, un découplage entre le signal d'insolation estivale à 65°N et la dynamique de la végétation du sud-ouest de l'Europe semble caractériser le LGM (Figures 4.2 et 4.3). Malgré une insolation estivale minimale au stade isotopique 2, les précipitations estimées affichent de fortes valeurs, et on retrace un couvert forestier de la végétation semblable à celui du début du présent interglaciaire (Figure 4.2). Si nos reconstitutions sont exactes, de fortes précipitations au LGM seraient-elles le fruit d'une insolation hivernale élevée aux moyennes latitudes favorisant une forte évaporation? S'agirait-il de changements de la circulation atmosphérique avec une position très méridionale de la trajectoire des tempêtes forcée par un courant jet situé juste au-dessus du sud de la Péninsule Ibérique en raison de l'extension maximale des calottes glaciaires, (Figure 3.1; Luetscher et al., 2015) ? Il s'agit d'hypothèses qu'il serait intéressant d'explorer davantage.

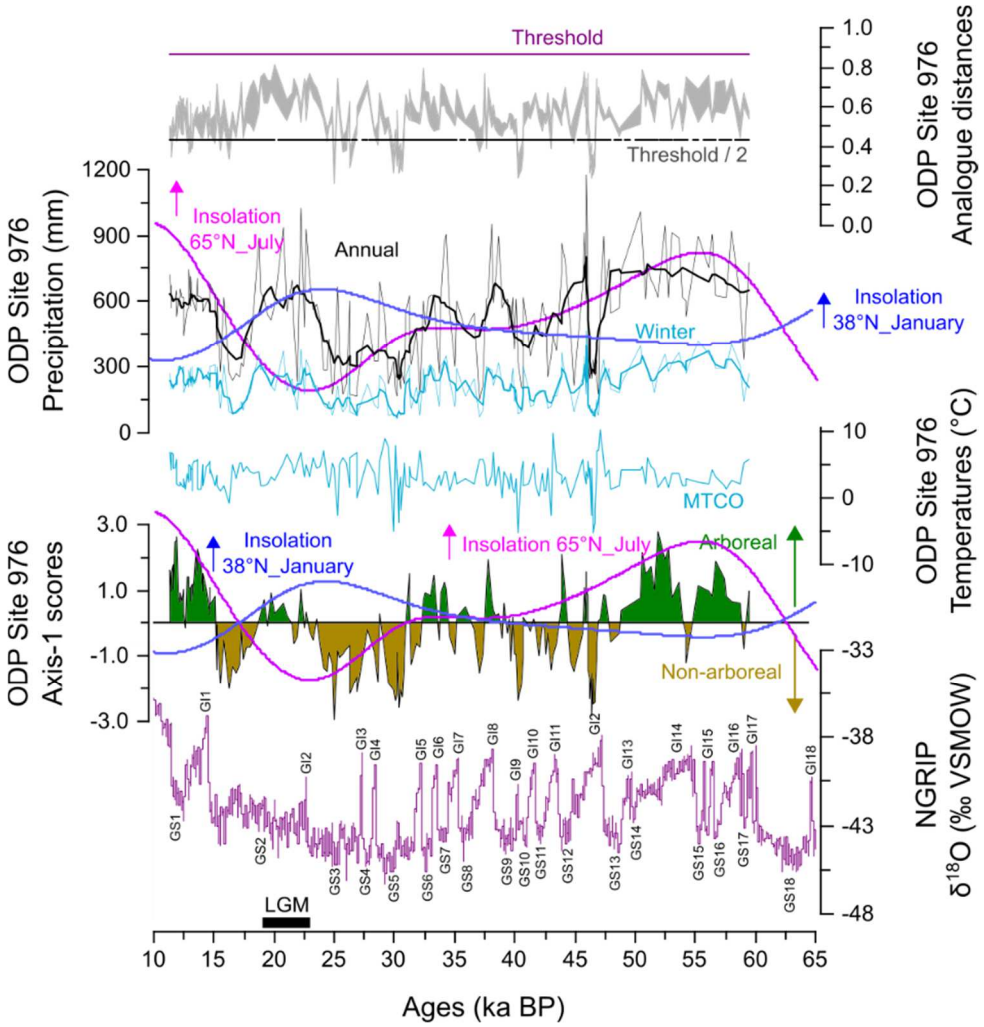

Figure 4.3 Enregistrements de signaux climatiques extra-régionaux et des variations de la végétation et de paramètres climatiques à partir des assemblages polliniques de la carotte ODP Site 976 (Figure 1.1). De bas en haut : courbe de la composition isotopique de l'oxygène de carottes de glace du Groenland (*North Greenland Ice Core Project members*, 2004), évolution de la végétation telle que définie par une analyse multivariée des PFTs , courbes d'insolations estivale à 65°N et hivernale à 38°N (Laskar et al., 2004), températures moyennes du mois le plus froid (MTCO - Mean temperature of the coldest month), précipitations annuelles (lissage selon une fenêtre de 9 valeurs en gras) et hivernales (lissage selon une fenêtre de 3 valeurs en gras), et distances des premiers et cinquièmes meilleurs analogues, les distances inférieures au seuil/2 correspondant à de bon analogues, alors que celles comprises entre le seuil et le seuil/2 indiquent des analogues acceptables (de Vernal et al., 2005).

Pour résumer, quelles que soient les incertitudes des reconstitutions que nous avons produites, nos résultats démontrent une variabilité millénaire de large amplitude au cours de la dernière période glaciaire dans le sud/sud-ouest de l'Europe, en particulier pendant la saison hivernale. Celle-ci pourrait être le reflet de variations de la circulation atmosphérique régionale en hiver, semblable aux variations du

mode dominant de l'actuelle NAO, laissant un signal à des échelles de temps séculaire à millénaire. De telles variations de force et/ou position des vents d'ouest se superposent aux tendances à long-terme, marquées par un refroidissement global au cours du stade isotopique 3 jusqu'au maximum glaciaire. La croissance progressive des calottes glaciaires a par ailleurs sans doute modifié la position du courant jet. Bien que rarement pris en compte dans les travaux de paléoclimatologie, des contrastes saisonniers de températures et de précipitations semblent constituer des paramètres très importants de la variabilité de climat de la dernière période glaciaire.

ANNEXE A

A ready-to-use version of the Eurasian Modern Pollen Database 2 (EMPD 2; Davis et al., 2020) for paleoclimatic reconstructions

Article soumis à la revue *Data in Brief* et qui présente la version « prête-à-l'emploi » de l'EMPD 2 (Davis et al., 2020) générée dans le cadre de cette thèse afin de procéder aux reconstitutions paléoclimatiques. Cette version est disponible sur PANGAEA (https://doi.pangaea.de/10.1594/PANGAEA.973997).

Jena Zumaque[a*], Anne de Vernal[a], Bianca Fréchette[a], Basil Davis[b], Manuel Chevalier[c]

[a] GEOTOP - Centre de recherche en géochimie et géodynamique, Université du Québec à Montréal, Montréal, Canada

[b] Institute of Earth Surface Dynamics, University of Lausanne, Lausanne, Switzerland

[c] Meteorology Department, University of Bonn, Bonn, Germany

Keywords

Pollen-based paleoclimatic reconstruction techniques, Continental Modern Pollen Database, Eurasia, homogenization of taxonomic entities, ready-to-use database

Abstract

Pollen-based paleoclimatic reconstructions based on calibration or analogue techniques require large collections of modern pollen samples, which together contain a very high number of pollen taxa. For paleoclimate reconstructions, however, the number of taxa needs to be reduced so the taxonomical resolution of modern and fossil pollen samples can be compatible. Version 2 of the Eurasian modern pollen database (EMPD2) (Davis et al., 2020) is the largest compilation of modern pollen samples covering these regions and comprises 840 pollen taxa. However, it cannot be used easily without homogenizing the taxonomic entities by grouping at genus or family levels or discarding certain rare taxa. This task is essential but time-consuming. Here, we present a ready-to-use homogenized version of the EMPD2 that comprises 88 pollen taxa, and which is adapted for paleoclimatic reconstructions in the Eurasian region.

SPECIFICATIONS TABLE

Subject	Earth and Planetary Sciences
Specific subject area	Preparation of continental-scale modern pollen databases for pollen-based paleoclimatic reconstruction techniques
Type of data	Table (.xlsx format) Supporting material (Table (.docx format))
Data collection	Original database (EMPD2), which contains 840 pollen taxa, was downloaded on Pangaea. Pollen taxa were homogenized to the genus or family levels based on ecological affinities and identification criteria as reported in the literature. Very rare taxa (< 100 occurrences) were discarded. Modern samples with no climatic or geographic (coordinates) information or pollen sum excluding Pinus <100 grains, were also discarded.
Data source location	*[2]; https://doi.pangaea.de/10.1594/PANGAEA.909130, 2019.*
Data accessibility	Repository name: Pangaea Data identification number: *https://doi.pangaea.de/10.1594/PANGAEA.973997* Direct URL to data:
Related research article	

VALUE OF THE DATA

- The data (Appendix A; *https://doi.pangaea.de/10.1594/PANGAEA.973997*) provide a ready-to-use modern pollen dataset for applying various pollen-based climate reconstruction techniques to reconstruct seasonal and annual climate parameters in Eurasia.
- Since it contains a relatively small number of taxonomic entities (88 pollen taxa), it can be used straightforwardly for paleoclimate reconstructions, even by non-pollen specialists.
- Table S1 in Supporting material, which details the grouping of the original 840 taxa into the final 88 taxa, provides useful information for future work on grouping and classification of pollen taxa.

BACKGROUND

Modern pollen datasets can be used to help investigate many different (paleo-)environmental processes [1] and are routinely used for quantitative paleoclimate reconstructions. Pollen-based paleoclimatic reconstructions require large collections of modern pollen samples to assess the relationship between vegetation and climate prior to applying calibration or analogue techniques, assuming that this relationship has remained unchanged through time. Modern pollen datasets have been developed over

the last four decades, originally on a regional basis [3] using lower quality digitized data, but now reaching continental scales with higher quality data represented by raw pollen counts [1, 4].

However, such continental-scale modern pollen datasets contain hundreds of taxa and cannot be straightforwardly used for paleoclimatic reconstructions as the taxonomic resolution of modern and fossil pollen samples must match [5]. The number and diversity of pollen taxa from the modern datasets therefore needs to be harmonized beforehand, an essential but very time-consuming task.

Version 2 of the Eurasian modern pollen database (EMPD2) [1] is the most recent and the largest compilation of modern pollen samples covering the Eurasian region (Figure 1). The EMPD2 is therefore very useful for reconstructing paleoclimate from these regions. However, as previously mentioned, it contains a very high number of pollen taxa (840), which needs to be reduced by grouping at genus or family levels or discarding certain rare taxa.

DATA DESCRIPTION

The dataset presented here was developed from the second version of the Eurasian Modern Pollen Database (EMPD2) [1]. It comprises 7634 modern pollen samples from the Palearctic realm (Figure 1). It provides for each modern sample the following data and metadata: coordinates and elevation, raw pollen counts and percentages of 88 selected taxa (see selection process below), climatic information for 37 parameters, and ecological description, such as ecoregion, biome and, when originally provided by the EMPD data contributors, vegetation description at the sampling location. These data are reported in Appendix A as an Excel file (*https://doi.pangaea.de/10.1594/PANGAEA.973997*).

EXPERIMENTAL DESIGN, MATERIALS AND METHODS

The EMPD2 [1] originally comprises 8134 modern pollen samples from the Paleartic realm, which includes Europe and parts of Asia, from the Atlantic to Pacific margins (Figure 1). This wide dataset covers a total of nine biomes [6] (Figure 1), and thus comprises potential modern analogues for many different climates and vegetation types, which is particularly critical when considering climatic reconstructions for glacial times [7,8].

The climatic data were calculated using WordlClim2 [9]. They include mean monthly, seasonal and annual temperatures and precipitation [1]. We added the mean temperature of the warmest (MTWA) and the coldest months (MTCO), and the seasonality defined as the difference between MTWA and MTCO.

MTWA corresponds to July temperatures at 77% of the sites and MTCO represents January temperatures at 83% of the sites. At other sites, MTCO is mostly February, and MTWA August.

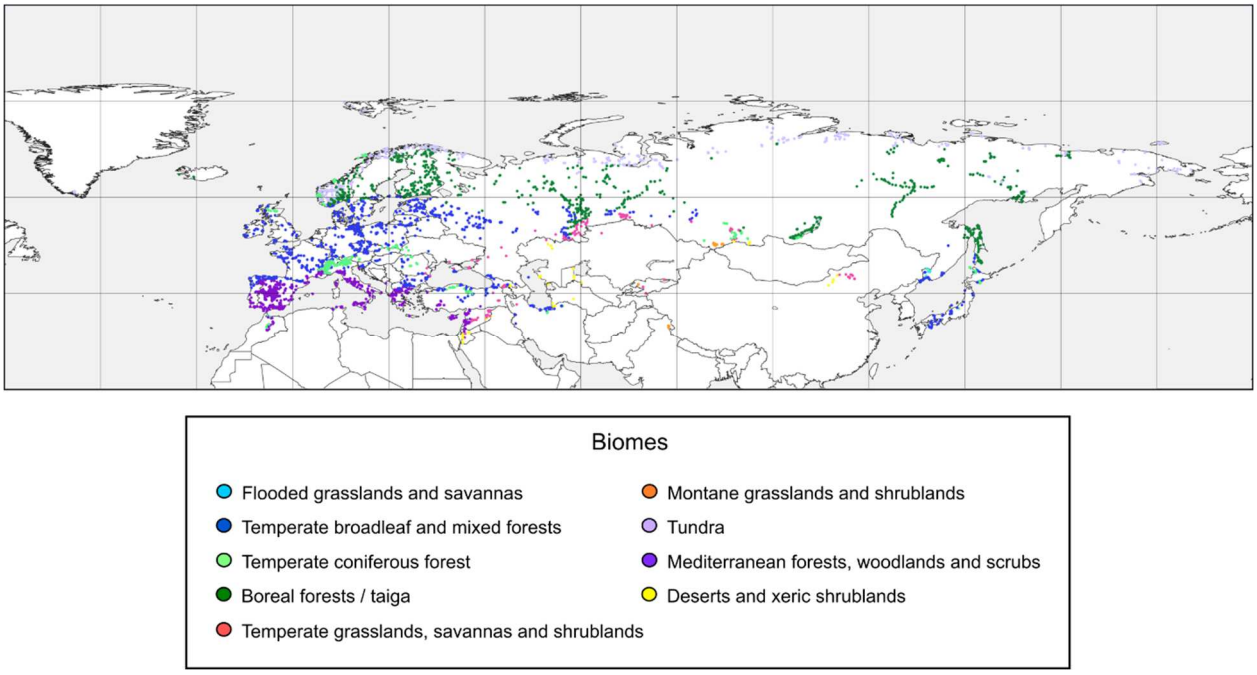

Figure 1. Biomes and locations of the modern pollen samples included in the ready-to-use version of the EMPD2 (modified from [1]).

The pollen analyses of modern samples were done in various laboratories, by different analysts, using different taxonomic levels (e.g., family, genus, species). Hence, the whole database includes a very high number of pollen taxa (n = 840). It also comprises many spore taxa belonging to pteridophyta and bryophyta that were excluded in this dataset because they are not always considered/identified by authors in pollen studies. Aquatic pollen taxa were also removed as they can be influenced by sets of environmental variables different from those influencing terrestrial pollen taxa [10].

To make the number of modern pollen taxa compatible with those of past pollen assemblages, we grouped the 840 different pollen categories into 184 taxa after harmonizing taxa to genus or family levels (see Table S1 in Supporting material). For most categories, taxonomic assignments to genera or families were made following Parent and Richard [11]. For the categories not referred to by Parent and Richard [11], the taxonomic classification was investigated in the literature on a case-by-case basis.

Because family names can differ depending upon the referred classification, a thorough review of original publications was needed to standardize the data set at the family level. Table S1 in Supporting material reports the information about the classification. We further reduced the number of taxa based on the number of occurrences, by discarding taxa with less than 100 occurrences in the EMPD2. Some exceptions were made for three taxa often identified in European fossil pollen records. These taxa are Anacardiaceae (mostly *Rhus,* now called *Searsia*), *Ceratonia*, and *Celtis* (Table 1). The final data set includes 88 taxa (Table 1; Table S1 in Supporting material).

We then removed all of the samples from this final dataset that had missing climatic information, primarily the marine samples [1]. We then filtered samples that had pollen sums (excluding *Pinus*) equal or higher than 100 pollen grains. The removal of *Pinus* from the pollen sums is based on the fact that pines have one of the highest pollen production rates and that their pollens can be wind-transported over very long distances, dominating pollen assemblages even when pines are not present in the local environment. Our final version of the EMPD2 thus includes 88 taxa and 7634 modern pollen samples (Appendix A, Tables 1 to 6). A list of the occurrence and relative abundance of the 88 taxa in the 7634 modern samples database is shown in Table 1. Table 7 of Appendix A contains 394 additional sites with pollen sums less than 100 pollen grains when excluding *Pinus* but higher or equal to 100 pollen grains when *Pinus* is included. Users can merge Tables 1 and 7 (8028 modern pollen samples) if they consider pollen sums (including *Pinus*) equal or higher than 100 pollen grains sufficient for accurate reconstructions.

It is worth noting that although the number of taxa retained for this work cannot be enlarged from this version of the EMPD2, it can be further reduced through grouping or removal of some taxa. In such a case, the percentages would need to be recalculated.

Table 1 (also next page). List of the 88 pollen taxa retained in the data set, which includes 7634 sites.

Taxa	Code	N (sites)	Range of %	Mean % ± SD	Median %
Trees+shrubs					
Acer	AACER	1064	0,02 - 30,58	0,80 ± 2,29	0,26
Anacardiaceae	ANACA	69	0,02 - 9,77	0,75 ± 1,72	0,22
Pistacia	APISTA	668	0,03 - 51,82	1,78 ± 4,14	0,45
Hedera	AHEDE	342	0,02 - 22,07	0,74 ± 1,81	0,30
Ilex	AILEX	231	0,01 - 51,13	2,57 ± 7,17	0,34
Alnus	BALBU	6362	0,02 - 96,44	6,62 ± 9,98	2,79
Betula	BBETU	5951	0,03 - 93,96	17,01 ± 17,44	10,54
Carpinus/Ostrya	BCARP	2661	0,03 - 70,36	2,99 ± 6,40	0,85
Corylus	BCORY	4159	0,03 - 69,71	2,08 ± 3,50	1,06
Buxus	BBUXU	243	0,03 - 20,45	0,63 ± 1,94	0,26
Caprifoliaceae	CAPRI	997	0,04 - 54,34	0,73 ± 2,37	0,29
Cistus	CCIST	621	0,03 - 40,56	2,00 ± 3,97	0,68
Helianthemum	CHELI	627	0,03 - 13,04	0,60 ± 0,93	0,33
Cornus	CCORN	146	0,02 - 3,31	0,35 ± 0,51	0,21
Cupressaceae	CUPRE	3166	0,01 - 98,12	2,79 ± 6,19	0,91
Hippophae	EHIPP	122	0,00 - 5,77	0,53 ± 0,85	0,29
Ephedra	EEPHE	623	0,01 - 70,90	1,17 ± 5,23	0,27
Ericaceae	ERICA	3991	0,01 - 74,29	3,58 ± 7,56	0,87
Calluna	ECALL	1623	0,01 - 73,27	4,10 ± 9,36	0,63
Ceratonia	FCERA	38	0,08 - 23,94	1,93 ± 4,87	0,35
Quercus deciduous	FQDEC	5057	0,02 - 92,24	7,07 ± 11,83	2,62
Quercus evergreen	FQEVE	1690	0,06 - 97,70	10,90 ± 17,81	3,03
Castanea	FCAST	1857	0,03 - 90,29	2,52 ± 8,07	0,63
Fagus	FFAGU	2777	0,03 - 77,55	5,19 ± 8,85	1,90
Juglans	JJUGL	1812	0,01 - 82,23	0,98 ± 4,28	0,30
Myricaceae	MYRIC	318	0,06 - 62,12	3,25 ± 7,77	0,73
Myrtaceae	MYRTA	258	0,02 - 40,84	1,22 ± 4,27	0,31
Oleaceae	OLEAC	406	0,01 - 68,18	0,77 ± 3,50	0,32
Olea	OOLEA	1986	0,03 - 83,88	4,72 ± 9,59	1,29
Phillyrea	OPHIL	636	0,05 - 62,62	1,59 ± 3,96	0,56
Fraxinus	OFRAX	2920	0,03 - 66,39	1,31 ± 3,25	0,49
Abies	PABIE	2599	0,00 - 74,17	2,51 ± 6,06	0,61
Picea	PPICE	4461	0,01 - 84,22	7,85 ± 11,77	2,81
Cedrus	PCEDR	358	0,04 - 89,40	11,95 ± 23,63	0,81
Larix	PLARI	1604	0,04 - 44,00	2,31 ± 4,08	0,92
Pinus	PPINU	7265	0,04 - 93,24	23,77 ± 20,37	18,25
Platanus	PPLAT	487	0,03 - 55,79	1,63 ± 4,99	0,33
Rhamnaceae	RHAMN	561	0,01 - 85,07	0,76 ± 3,88	0,23
Populus	SPOPU	845	0,02 - 19,44	0,66 ± 1,43	0,28
Salix	SSALI	4714	0,01 - 66,67	1,75 ± 4,46	0,57
Tamarix	TTAMA	100	0,06 - 39,18	2,47 ± 5,70	0,64
Taxus	TTAXU	184	0,00 - 95,34	3,88 ± 14,41	0,29
Daphne	TDAPH	173	0,03 - 11,85	0,92 ± 1,72	0,36
Tilia	TTILI	1731	0,02 - 47,97	0,74 ± 2,31	0,28
Celtis	UCELT	36	0,01 - 16,14	0,68 ± 2,62	0,18
Ulmus	UULMU	2539	0,01 - 54,19	0,79 ± 2,25	0,33
Vitis	VVITI	515	0,01 - 37,59	0,69 ± 2,97	0,24

Taxa	Code	N (sites)	Range of %	Mean % ± SD	Median %
Herbs					
Amaranthaceae	AMARA	5216	0,02 - 91,78	3,29 ± 9,51	0,62
Apiaceae	APIACE	3853	0,02 - 52,79	1,13 ± 2,69	0,42
Liguliflore	ALIGU	3890	0,02 - 61,01	2,34 ± 4,89	0,65
Tubuliflore	ATUBU	5604	0,03 - 63,93	1,97 ± 4,16	0,71
Artemisia	AARTE	5508	0,02 - 99,83	3,33 ± 8,31	0,81
Centaurea	ACENTA	1131	0,01 - 17,21	0,64 ± 1,24	0,29
Boraginaceae	BORAG	778	0,00 - 24,53	0,88 ± 1,87	0,36
Brassicaceae	BRASS	3619	0,03 - 56,25	1,04 ± 2,09	0,51
Campanulaceae	CAMPA	772	0,00 - 16,17	0,53 ± 1,23	0,26
Caryophyllaceae	CARYO	3559	0,01 - 43,28	0,92 ± 2,11	0,41
Convolvulaceae	CONVO	239	0,01 - 30,17	0,58 ± 2,23	0,24
Crassulaceae	CRASS	414	0,03 - 13,33	0,63 ± 1,32	0,30
Cyperaceae	CYPER	5801	0,01 - 82,38	5,12 ± 9,26	1,45
Dipsacaceae	DIPSA	469	0,01 - 13,64	0,46 ± 0,82	0,26
Euphorbiaceae	EUPHO	634	0,00 - 78,38	0,87 ± 3,58	0,28
Fabaceae	FABAC	3147	0,01 - 62,82	1,28 ± 3,13	0,47
Gentianaceae	GENTI	322	0,01 - 4,48	0,44 ± 0,57	0,26
Geraniaceae	GERAN	488	0,03 - 18,67	0,49 ± 1,31	0,24
Lamiaceae	LAMIA	1830	0,01 - 40,82	0,94 ± 2,00	0,37
Liliaceae	LILIA	1046	0,00 - 19,10	0,63 ± 1,20	0,34
Asphodelus	LASPH	228	0,03 - 15,48	0,88 ± 1,41	0,47
Onagraceae	ONAGR	444	0,00 - 75,77	0,87 ± 4,13	0,26
Papaveraceae	PAPAV	383	0,00 - 17,67	0,91 ± 1,72	0,29
Plantaginaceae	PLANT	4498	0,03 - 66,69	1,88 ± 3,98	0,80
Plumbaginaceae	PLUMB	226	0,03 - 11,89	0,92 ± 1,47	0,35
Poaceae	POACE	7347	0,04 - 92,86	12,74 ± 13,39	8,04
Polemoniaceae	POLEM	160	0,06 - 75,98	5,76 ± 12,03	0,67
Rumex/Oxyria	PRUME	4331	0,01 - 63,01	1,50 ± 3,77	0,67
Polygonum	PPOLY	1230	0,01 - 43,41	0,79 ± 2,19	0,30
Primulaceae	PRIMU	573	0,01 - 41,02	0,59 ± 1,85	0,25
Ranunculaceae	RANUN	4147	0,02 - 56,81	1,20 ± 2,57	0,55
Thalictrum	RTHAL	1224	0,01 - 21,88	0,70 ± 1,69	0,29
Rosaceae	ROSAC	4767	0,01 - 35,67	1,31 ± 2,43	0,60
Sanguisorba	RSANG	809	0,02 - 46,02	1,03 ± 3,71	0,29
Rubiaceae	RUBIA	2089	0,00 - 36,07	0,80 ± 2,13	0,29
Saxifragaceae	SAXIF	823	0,02 - 21,58	0,71 ± 1,56	0,32
Scrophulariaceae	SCROP	2284	0,01 - 13,93	0,67 ± 1,06	0,34
Solanaceae	SOLAN	243	0,01 - 33,04	0,62 ± 2,22	0,25
Cannabaceae/Urticace	CANURT	2795	0,02 - 88,91	1,29 ± 3,97	0,55
Valerianaceae	VALER	468	0,02 - 18,09	0,74 ± 1,52	0,30
Viola	VVIOL	168	0,03 - 9,45	0,49 ± 0,89	0,26

LIMITATIONS

There are some uncertainties inherent to the identification of pollen taxa and the handling of modern collections at continental scale [5]. One key assumption made when doing paleoclimate reconstructions is that all the entities assigned to the same taxon name occupy the same or similar environmental or ecological niche. Still, some pollen grains are only identifiable at the genus or family level. For example, a pollen identified in the original EMPD2 as Corylus might represent Corylus avellana, a widespread species in Europe, or Corylus chinensis, specific to western China, both species showing different ecological affinities/tolerance. Besides the location of the modern sample or the rest of the pollen assemblage, no additional information can help assess the species.

To homogenize and simplify the dataset, and thus lower the number of pollen taxa, we generated additional similar uncertainties by grouping pollen grains identified at the species or the genus level to the genus or the family level respectively. At the spatial scales of the Eurasian continent, we may have grouped species/genus that do not share the exact same environmental niche [5]. Depending on the purpose of their research project, users may choose to maintain homogenized taxonomy at the Eurasian scale or use some of the solutions that have been proposed to tackle this problem, including geographically constrained calibration datasets, or splitting of some pollen types into regional groups [5].

ETHICS STATEMENT

The authors have read and follow the ethical requirements for publication in Data in Brief and confirm that the current work does not involve human subjects, animal experiments, or any data collected from social media platforms.

CRediT AUTHOR STATEMENT

Jena Zumaque: Conceptualization, Methodology, Formal analysis, Writing - Original draft preparation. Anne de Vernal: Supervision, Reviewing and Editing. Bianca Fréchette: Supervision, Methodology, Reviewing and Editing. Basil Davis: Reviewing and Editing. Manuel Chevalier: Reviewing and Editing.

ACKNOWLEDGEMENTS

We acknowledge financial support from the Geotop, funded by the Fonds de Recherche du Québec – Nature et Technologies (FRQNT) and the Hominin Dispersal Research Group (HDRG - http://www.hominindispersals.net/), funded by the Fonds de Recherche Québécois sur la Société et la Culture (FRQSC). This research also benefited from funding from the Natural Sciences and Engineering

Research Council of Canada (NSERC) through a Discovery grant to AdV and the international program "Processes and impacts of climate change in the North Atlantic Ocean and the Canadian Arctic (ArcTrain), which is a Collaborative Research and training Experience Program (CREATE). MC is supported by the German Federal Ministry of Education and Research (BMBF) with the Research for Sustainability initiative (FONA) through the PalMod Phase III project (grant no. FKZ: 01LP2308B).

DECLARATION OF COMPETING INTERESTS

The authors declare that they have no known competing financial interests or personal relationships that could have appeared to influence the work reported in this paper.

REFERENCES

[1] Davis, B. A., Chevalier, M., Sommer, P., Carter, V. A., Finsinger, W., Mauri, A., ... & Zimny, M. (2020). "The Eurasian Modern Pollen Database (EMPD), version 2." Earth Syst. Sci. Data **12**(4): 2423-2445.

[2] Chevalier, M., Davis, B. A. S., Sommer, P. S., Zanon, M., Carter, V. A., Phelps, L. N., Mauri, A., and Finsinger, W. (2019): Eurasian Modern Pollen Database (former European Modern Pollen Database), Pangaea, https://doi.pangaea.de/10.1594/PANGAEA.909130.

[3] Avizinis, J., & Webb III, T. (1985). The computer file of modern pollen and climatic data at Brown University. *Unpublished. Brown University, Providence, RI*.

[4] Whitmore, J., Gajewski, K., Sawada, M., Williams, J. W., Shuman, B., Bartlein, P. J., ... & Brubaker, L. (2005). Modern pollen data from North America and Greenland for multi-scale paleoenvironmental applications. *Quaternary Science Reviews*, *24*(16-17), 1828-1848.

[5] Williams, J. W., & Shuman, B. (2008). Obtaining accurate and precise environmental reconstructions from the modern analog technique and North American surface pollen dataset. *Quaternary Science Reviews*, *27*(7-8), 669-687.

[6] Olson, D. M., Dinerstein, E., Wikramanayake, E. D., Burgess, N. D., Powell, G. V., Underwood, E. C., ... & Kassem, K. R. (2001). Terrestrial Ecoregions of the World: A New Map of Life on Earth: A new global map of terrestrial ecoregions provides an innovative tool for conserving biodiversity. *BioScience*, *51*(11), 933-938.

[7] Magyari, E. K., Kuneš, P., Jakab, G., Sümegi, P., Pelánková, B., Schäbitz, F., ... & Chytrý, M. (2014). Late Pleniglacial vegetation in eastern-central Europe: are there modern analogues in Siberia?. *Quaternary Science Reviews*, *95*, 60-79.

[8] Davis, B. A. S., Fasel, M., Kaplan, J. O., Russo, E., & Burke, A. (2022). "The climate and vegetation of Europe, North Africa and the Middle East during the Last Glacial Maximum (21,000 years BP) based on pollen data." Clim. Past Discuss. **2022**: 1-66.

[9] Fick, S. E., & Hijmans, R. J. (2017). WorldClim 2: new 1-km spatial resolution climate surfaces for global land areas. *International journal of climatology*, *37*(12), 4302-4315.

[10] Chevalier, M., Davis, B. A., Heiri, O., Seppä, H., Chase, B. M., Gajewski, K., ... & Kupriyanov, D. (2020). Pollen-based climate reconstruction techniques for late Quaternary studies. *Earth-Science Reviews*, *210*, 103384.

[11] Parent, J., & Richard, P. (1990). *Taxons sporo-polliniques du nord-est de l'Amérique du Nord*. Laboratorie de Paléobiogeographie et de Palynologie, Department de Géographie, Université de Montreal.

SUPPLEMENTARY MATERIAL: Detail of the grouping of the original 840 pollen taxa into the final 88 pollen taxa

Taxa of the Eurasian Modern Pollen Database (EMPD, version 2) (Davis et al., 2020)		
a) All taxa (n=840)	**b) First grouping (n=184)**	**c) 88 taxa retained**
Trees **(n=103)**	**(n=44)**	**(n=23)**
Acer campestre-type	*Acer* (Aceraceae)	*Acer* (Aceraceae)
Arecaceae *Chamaerops humilis* *Phoenix* *Trachycarpus*	Arecaceae	
Betula/Corylus *Betula/Corylus/Myrica* Betulaceae *Corylus/Myrica* *Ostryopsis*	Betulaceae	
Alnus *Alnus glutinosa*-type *Alnus viridis*	*Alnus* (Betulaceae)	*Alnus* (Betulaceae)
Betula *Betula glandulosa* *Betula pubescens*-type *Betula* sect. *Costatae* *Betula nana*-type	*Betula* (Betulaceae)	*Betula* (Betulaceae)
Carpinus betulus *Ostrya/Carpinus orientalis*	*Carpinus/Ostrya* (Betulaceae)	*Carpinus/Ostrya* (Betulaceae)
Casuarina	*Caduarina* (Casuarinaceae)	
Cupressaceae undiff. *Juniperus*-type *Juniperus communis*-type *Juniperus oxycedrus*-type *Juniperus sabina*	Cupressaceae	Cupressaceae
Diospyros	*Diospyros* (Ebenaceae)	
Ceratonia siliqua	*Ceratonia* (Fabaceae)	*Ceratonia* (Fabaceae)
Acacia	*Acacia* (Fabaceae)	
Fagaceae *Lithocarpus lepidocarpus*	Fagaceae	
Quercus (deciduous) *Quercus cerris*-type *Quercus robur*-type *Quercus* *Quercus ithaburensis*-type	*Quercus* deciduous (Fagaceae)	*Quercus* deciduous (Fagaceae)
Quercus ilex-type	*Quercus* evergreen (Fagaceae)	*Quercus* evergreen (Fagaceae)

Taxa of the Eurasian Modern Pollen Database (EMPD, version 2) (Davis et al., 2020)		
a) All taxa (n=840)	**b) First grouping (n=184)**	**c) 88 taxa retained**
Trees (continuation) **(n=103)**	**(n=44)**	**(n=23)**
Castanea sativa	*Castanea* (Fagaceae)	*Castanea* (Fagaceae)
Fagus	*Fagus* (Fagaceae)	*Fagus* (Fagaceae)
Aesculus *Aesculus hippocastanum*	*Aesculus* (Hippocastanaceae)	
Carya Juglandaceae *Pterocarya*	Juglandaceae	
Juglans *Juglans nigra* *Juglans regia*	*Juglans* (Juglandaceae)	*Juglans* (Juglandaceae)
Laurus	*Laurus* (Lauraceae)	
Meliaceae	Meliaceae	
Fraxinus *Fraxinus angustifolia* *Fraxinus sogdiana* *Fraxinus excelsior*-type *Fraxinus ornus*	*Fraxinus* (Oleaceae)	*Fraxinus* (Oleaceae)
Keteeleria Pinaceae *Pseudolarix amabilis* *Tsuga* *Tsuga diversifolia* *Tsuga sieboldii*	Pinaceae	
Abies *Abies marocana* *Abies pinsapo* *Abies sibirica*	*Abies* (Pinaceae)	*Abies* (Pinaceae)
Picea *Picea abies-type* *Picea omorika-type* *Picea schrenkiana*	*Picea* (Pinaceae)	*Picea* (Pinaceae)
Cedrus	*Cedrus* (Pinaceae)	*Cedrus* (Pinaceae)
Larix dahurica *Larix/Pseudo* *Larix/Pseudotsuga*	*Larix* (Pinaceae)	*Larix* (Pinaceae)
Pinus *Pinus cembra*-type *Pinus halepensis*-type *Pinus pinaster*	*Pinus* (Pinaceae)	*Pinus* (Pinaceae)

Taxa of the Eurasian Modern Pollen Database (EMPD, version 2) (Davis et al., 2020)		
a) All taxa (n=840)	**b) First grouping (n=184)**	**c) 88 taxa retained**
Trees (continuation) **(n=103)**	**(n=44)**	**(n=23)**
Pinus pumila *Pinus sylvestris*-type	*Pinus* (Pinaceae) (continuation)	*Pinus* (Pinaceae) (continuation)
Platanus	*Platanus* (Platanaceae)	*Platanus* (Platanaceae)
Podocarpus	*Podocarpus* (Podocarpaceae)	
Punica granatum	*Punica granatum* (Punicaceae)	
Citrus *Haplophyllum* *Phellodendron* *Ruta* Rutaceae *Zanthoxylum*	Rutaceae	
Chosenia	*Chosenia* (Salicaceae)	
Populus *Populus tremula*-type	*Populus* (Salicaceae)	*Populus* (Salicaceae)
Salix	*Salix* (Salicaceae)	*Salix* (Salicaceae)
Sapindaceae	Sapindaceae	
Sapotaceae	Sapotaceae	
Sciadopitys	*Sciadopitys* (Sciadopityaceae)	
Ailanthus	*Ailanthus* (Simaroubaceae)	
Taxaceae/Cephalotaxaceae/ Cupressaceae	Taxaceae/Cephalotaxaceae/ Cupressaceae	
Cryptomeria-type *Cryptomeria japonica*	*Cryptomeria* (Taxodiaceae)	
Tilia *Tilia cordata*-type *Tilia platyphyllos*-type	*Tilia* (Tiliaceae)	*Tilia* (Tiliaceae)
Celtis	*Celtis* (Ulmaceae)	*Celtis* (Ulmaceae)
Ulmus/Zelkova	*Ulmus* (Ulmaceae)	*Ulmus* (Ulmaceae)
Shrubs **(n=140)**	**(n=55)**	**(n=24)**
Actinidia deliciosa	*Actinidia deliciosa* (Actinidiaceae)	
Anacardiaceae *Cotinus* *Cotinus coggygria* *Rhus* *Rhus*-type *Rhus coriaria*-type	Anacardiaceae	Anacardiaceae
Pistacia	*Pistacia* (Anacardiaceae)	*Pistacia* (Anacardiaceae)

Taxa of the Eurasian Modern Pollen Database (EMPD, version 2) (Davis et al., 2020)		
a) All taxa (n=840)	**b) First grouping (n=184)**	**c) 88 taxa retained**
Shrubs (continuation) (n=140)	**(n=55)**	**(n=24)**
Nerium oleander *Vinca*	Apocynaceae	
Ilex	*Ilex* (Aquifoliaceae)	*Ilex* (Aquifoliaceae)
Araliaceae	Araliaceae	
Hedera	*Hedera* (Araliaceae)	*Hedera* (Araliaceae)
Impatiens	*Impatiens* (Balsaminaceae)	
Berberis *Leontice*	Berberidaceae	
Corylus	*Corylus* (Betulaceae)	*Corylus* (Betulaceae)
Buddleia	*Buddleia* (Buddlejaceae)	
Buxus	*Buxus* (Buxaceae)	*Buxus* (Buxaceae)
Capparaceae *Capparis*	Capparaceae	
Caprifoliaceae *Linnaea borealis* *Patrinia* *Weigela*	Caprifoliaceae	Caprifoliaceae
Lonicera *Lonicera periclymenum* *Lonicera periclymenum*-type *Lonicera xylosteum*-type	*Lonicera* (Caprifoliaceae)	
Sambucus *Sambucus ebulus* *Sambucus nigra* *Sambucus nigra/S. racemosa* *Sambucus racemosa* *Sambucus sibirica*	*Sambucus* (Caprifoliaceae)	
Viburnum *Viburnum lantana* *Viburnum opulus* *Viburnum opulus/V. tinus* *Viburnum/Euonymus* *Viburnum/Sambucus*	*Viburnum* (Caprifoliaceae)	
Celastraceae *Euonymus*	Celastraceae	
Cistaceae *Fumana* *Halimium/Tuberaria* *Tuberaria*	Cistaceae	

Taxa of the Eurasian Modern Pollen Database (EMPD, version 2) (Davis et al., 2020)		
a) All taxa (n=840)	**b) First grouping (n=184)**	**c) 88 taxa retained**
Shrubs (continuation) **(n=140)**	**(n=55)**	**(n=24)**
Cistus *Cistus albidus*-type *Cistus ladanifer*-type *Cistus monspeliensis*-type *Cistus salvifolius* *Cistus/Helianthemum*	*Cistus* (Cistaceae)	*Cistus* (Cistaceae)
Helianthemum *Helianthemum croceum*-type *Helianthemum nummularium-type*	*Helianthemum* (Cistaceae)	*Helianthemum* (Cistaceae)
Clethra	*Clethra* (Clethraceae)	
Coriaria myrtifolia	*Coriaria myrtifolia* (Coriariaceae)	
Cornus *Cornus mas* *Cornus mas*-type *Cornus sanguinea*-type *Cornus suecica*	*Cornus* (Cornaceae)	*Cornus* (Cornaceae)
Tamus communis	*Tamus communis* (Dioscoreaceae)	
Elaeagnaceae *Elaeagnus* *Elaeagnus* type	Elaeagnaceae	
Hippophae rhamnoides	*Hippophae* (Elaeagnaceae)	*Hippophae* (Elaeagnaceae)
Ephedra *Ephedra alata*-type *Ephedra distachya*-type *Ephedra fragilis*-type	*Ephedra* (Ephedraceae)	*Ephedra* (Ephedraceae)
Corema album *Erica* *Erica arborea*-type *Erica carnea* *Erica ciliaris*-type *Erica cinerea* *Ericales (tetrad)* *Loiseleuria procumbens* *Pyrola*-type *Rhododendron* *Vaccinium* *Vaccinium*-type	Ericaceae	Ericaceae
Arbutus	*Arbutus* (Ericaceae)	
Calluna vulgaris	*Calluna* (Ericaceae)	*Calluna* (Ericaceae)

Taxa of the Eurasian Modern Pollen Database (EMPD, version 2) (Davis et al., 2020)		
a) All taxa (n=840)	**b) First grouping (n=184)**	**c) 88 taxa retained**
Shrubs (continuation) **(n=140)**	**(n=55)**	**(n=24)**
Euptelea	*Euptelea* (Eupteleaceae)	
Corylopsis *Fothergilla major* *Liquidambar* *Parrotia* cf. *persica* *Parrotia persica*	Hamamelidaceae	
Hydrangea	*Hydrangea* (Hydrangeaceae)	
Loranthus europaeus *Arceuthobium oxycedri*	Loranthaceae	
Magnolia-type	type *Magnolia* (Magnoliaceae)	
Ficus *Ficus carica* Moraceae *Morus* *Morus alba* *Morus nigra*	Moraceae	
Myrica *Myricaria germanica*	Myricaceae	Myricaceae
Myrtaceae *Eucalyptus* *Myrtus communis*	Myrtaceae	Myrtaceae
Nitraria	*Nitraria* (Nitrariaceae)	
Fontanesia phillireoides *Forsythia* *Jasminum* *Jasminum fruticans* *Ligustrum* *Ligustrum*-type Oleaceae *Syringa*	Oleaceae	Oleaceae
Olea europaea	*Olea* (Oleaceae)	*Olea* (Oleaceae)
Phillyrea	*Phillyrea* (Oleaceae)	*Phillyrea* (Oleaceae)
Rhamnaceae *Rhamnus*-type *Frangula alnus* *Zizyphus*	Rhamnaceae	Rhamnaceae
Sabia limoniacea	*Sabia limoniacea* (Sabiaceae)	
Styrax	*Styrax* (Styracaceae)	
Tamarix	*Tamarix* (Tamaricaceae)	*Tamarix* (Tamaricaceae)

Taxa of the Eurasian Modern Pollen Database (EMPD, version 2) (Davis et al., 2020)		
a) All taxa (n=840)	**b) First grouping (n=184)**	**c) 88 taxa retained**
Shrubs (continuation) **(n=140)**	**(n=55)**	**(n=24)**
Taxus baccata	*Taxus* (Taxaceae)	*Taxus* (Taxaceae)
Camellia cf. *Camelia sinensis*	*Camelia* (Theaceae)	
Stellera Thymelaeaceae	Thymelaeaceae	
Daphne	*Daphne* (Thymelaeaceae)	*Daphne* (Thymelaeaceae)
Viscum *Viscum album*	*Viscum* (Viscaceae)	
Parthenocissus Vitaceae	Vitaceae	
Vitis	*Vitis* (Vitaceae)	*Vitis* (Vitaceae)
Tribulus terrestris Zygophyllaceae *Zygophyllum* *Peganum*	Zygophyllaceae	
Herbs **(n=597)**	**(n=85)**	**(n=41)**
Acanthus	*Acanthus* (Acanthaceae)	
Adoxa moschatellina Adoxaceae cf. *Adoxa moschatellina*	Adoxaceae	
Carpobrotus	*Carpobrotus* (Aizoaceae)	
Beta Chenopodiaceae/Amaranthaceae *Aellenia*-type *Salsola kali*	Amaranthaceae	Amaranthaceae
Aegopodium-type *Aegopodium podagraria* *Aethusa cynapium* *Anethum* *Anethum graveolens* *Anisosciadium* *Anthriscus sylvestris*-type Apiaceae *Apium* *Astrantia*-type *Athamanta cretensis*	Apiaceae	Apiaceae

Taxa of the Eurasian Modern Pollen Database (EMPD, version 2) (Davis et al., 2020)		
a) All taxa (n=840)	**b) First grouping (n=184)**	**c) 88 taxa retained**
Herbs (continuation) (n=597)	**(n=85)**	**(n=41)**
Bupleurum	Apiaceae (continuation)	Apiaceae (continuation)
Carum carvi		
Chaerophyllum hirsutum-type		
Cicuta virosa		
Conium maculatum		
Conopodium		
Conopodium majus		
Daucus		
Eryngium		
Falcaria-type		
Heracleum		
Heracleum sphondylium		
Laserpitium latifolium-type		
Laserpitium prutenicum		
Libanotis		
Ligusticum mutellina		
Malabaila		
Meum athamanticum		
Oenanthe		
Orlaya		
Pastinaca sativa		
Peucedanum-type		
Pimpinella anisum		
Pimpinella major-type		
Pleurospermum-type		
Sanicula europaea		
Scandix pecten-veneris/ Caucalis platycarpos		
Seseli-type		
Sium-type		
Torilis nodosa		
Trinia glauca		
Araceae	Araceae	
Aristolochia	*Aristolochia* (Aristolochiaceae)	

Taxa of the Eurasian Modern Pollen Database (EMPD, version 2) (Davis et al., 2020)		
a) All taxa (n=840)	**b) First grouping (n=184)**	**c) 88 taxa retained**
Herbs (continuation) (n=597)	**(n=85)**	**(n=41)**
Asteraceae subf. *Cichorioideae* *Crepis*-type *Lactuca*-type *Scorzonera humilis*-type *Scorzonera laciniata* *Sonchus*-type *Tragopogon*	Liguliflore (Asteraceae)	Liguliflore (Asteraceae)
Asteraceae *Calendula* *Carduncellus*-type *Carthamus*-type *Chardinia/Onopordon* *Cousinia* *Doronicum* *Echinops* *Homogyne*-type *Saussurea*-type *Saussurea alpina* Asteraceae subf. *Carduoideae* *Aster*-type *Ambrosia* *Ambrosia/Xanthium* *Antennaria-type* *Arctium* Asteraceae subf. *Asteroideae* *Bidens*-type *Carduus* *Carduus*-type *Carlina* *Cirsium* *Gnaphalium*-type *Helianthus* *Helianthus*-type *Inula* *Matricaria*-type *Petasites* *Senecio*-type *Tussilago*-type *Xanthium*	Tubuliflore (Asteraceae)	Tubuliflore (Asteraceae)

Taxa of the Eurasian Modern Pollen Database (EMPD, version 2) (Davis et al., 2020)		
a) All taxa (n=840)	**b) First grouping (n=184)**	**c) 88 taxa retained**
Herbs (continuation) (n=597)	**(n=85)**	**(n=41)**
Artemisia	*Artemisia* (Asteraceae)	*Artemisia* (Asteraceae)
Centaurea *Centaurea alpina*-type *Centaurea cyanus*-type *Centaurea montana*-type *Centaurea nigra*-type *Centaurea scabiosa*-type	*Centaurea* (Asteraceae)	*Centaurea* (Asteraceae)
Biebersteinia	Biebersteiniaceae	
Alkanna-type *Anchusa arvensis*-type *Anchusa/Pulmonaria* *Arnebia* Boraginaceae *Buglossoides arvensis* *Cerinthe* *Cynoglossum*-type *Cynoglossum creticum*-type *Heliotropium* *Lithospermum*-type *Lithospermum officinale* *Moltkia* *Myosotis-type* *Nonea* *Omphalodes*-type *Symphytum*	Boraginaceae	Boraginaceae
Echium *Echium/Onosma*	*Echium* (Boraginaceae)	
Brassicaceae *Cardamine*-type *Hornungia*-type *Matthiola* *Sinapis*-type	Brassicaceae	Brassicaceae

Taxa of the Eurasian Modern Pollen Database (EMPD, version 2) (Davis et al., 2020)		
a) All taxa (n=840)	**b) First grouping (n=184)**	**c) 88 taxa retained**
Herbs (continuation) (n=597)	**(n=85)**	**(n=41)**
Campanula giesekiana *Campanula medium* *Campanula trachelium*-type Campanulaceae *Jasione montana*-type *Legousia*-type *Phyteuma*-type	Campanulaceae	Campanulaceae
Agrostemma githago *Arenaria* Caryophyllaceae (peripor ate excl. Paronychioideae) *Cerastium*-type *Dianthus/Petrorhagia* *Gypsophila repens*-type *Herniaria* *Herniaria*-type *Herniaria glabra*-type *Illecebrum verticillatum* *Loeflingia* *Lychnis flos-cuculi* *Lychnis viscaria*-type *Minuartia rubra*-type/*Bufonia* *Moehringia*-type *Paronychia* *Sagina* *Sagina procumbens*-type *Scleranthus* *Scleranthus annuus* *Scleranthus perennis* *Silene*-type *Silene dioica*-type *Silene vulgaris*-type *Spergularia*-type *Stellaria holostea*	Caryophyllaceae	Caryophyllaceae
Calystegia Convolvulaceae Convolvulaceae undiff. *Convolvulus* *Convolvulus arvensis*-type	Convolvulaceae	Convolvulaceae

Taxa of the Eurasian Modern Pollen Database (EMPD, version 2) (Davis et al., 2020)		
a) All taxa (n=840)	**b) First grouping (n=184)**	**c) 88 taxa retained**
Herbs (continuation) (n=597)	**(n=85)**	**(n=41)**
Cuscuta	Convolvulaceae (continuation)	Convolvulaceae (continuation)
Cuscuta europaea-type		
Crassulaceae	Crassulaceae	Crassulaceae
Sedum-type		
Sempervivum		
Umbilicus-type		
Bryonia	Cucurbitaceae	
Citrullus		
Cucumis		
Cucurbitaceae		
Cyperaceae	Cyperaceae	Cyperaceae
Datisca cannabina	*Datisca cannabina* (Datiscaceae)	
Dipsacaceae	Dipsacaceae	Dipsacaceae
*Ebenus/He*dysarum		
Dipsacus fullonum-type		
Succisa-type		
Knautia		
Scabiosa		
Scabiosa argentea		
Scabiosa columbaria-type		
Scabiosa ochroleuca		
Drosera	*Drosera* (Droseraceae)	
Drosera rotundifolia-type		
Chrozophora	Euphorbiaceae	Euphorbiaceae
Euphorbia		
Euphorbia/Mercurialis		
Euphorbiaceae		
Flueggea		
Mallotus		
Ricinus communis		
Mercurialis	*Merculiaris* (Euphorbiaceae)	
Mercurialis annua		
Mercurialis perennis-type		
Cytisus-type	Fabaceae	Fabaceae
Amorpha fruticosa		
Anthyllis		
Astragalus-type		

Taxa of the Eurasian Modern Pollen Database (EMPD, version 2) (Davis et al., 2020)		
a) All taxa (n=840)	**b) First grouping (n=184)**	**c) 88 taxa retained**
Herbs (continuation) (n=597)	**(n=85)**	**(n=41)**
Caragana	Fabaceae (continuation)	Fabaceae (continuation)
Cercis siliquastrum		
Colutea		
Colutea arborescens		
Coronilla-type		
Coronilla varia		
Fabaceae		
Fabaceae undiff.		
Galega-type		
Genista-group		
Genista-type		
Hedysarum		
Laburnum-type		
Laburnum anagyroides		
Lathyrus-type		
Lathyrus/Vicia-type		
Lotus-type		
Medicago littoralis-type		
Medicago sativa-type		
Onobrychis		
Onobrychis-type		
Ononis		
Ornithopus		
Phaseolus		
Pisum sativum		
Prosopis		
Psoralea bituminosa		
Robinia pseudacacia		
Spartium junceum		
Trifolium-type		
Trifolium alpinum-type		
Trifolium badium-type		
Trifolium dubium type		
Trifolium montanum		
Trifolium pratense-type		
Trifolium repens-type		
Trigonella		
Vicia-type		
Vicia faba		
Leguminosae		

Taxa of the Eurasian Modern Pollen Database (EMPD, version 2) (Davis et al., 2020)		
a) All taxa (n=840)	**b) First grouping (n=184)**	**c) 88 taxa retained**
Herbs (continuation) (n=597)	**(n=85)**	**(n=41)**
Frankenia	Frankeniaceae	
Centaurium *Gentiana* *Gentiana lutea/G. pneumonanthe* *Gentiana nivalis* *Gentiana pneumonanthe*-type *Gentiana purpurea* *Gentiana verna* Gentianaceae *Gentianella campestris*-type *Gentianella tenella*-type *Lomatogonium* *Lomatogonium rotatum* *Ophelia*-type *Swertia perennis*	Gentianaceae	Gentianaceae
Geraniaceae *Geranium* *Geranium pratense-type* Gerianiaceae	Geraniaceae	Geraniaceae
Erodium	*Erodium* (Geraniaceae)	
Globularia	*Globularia* (Globulariaceae)	
Herbs	Herbs	
Phacelia	*Phacelia* (Hydrophyllaceae)	
Hypericum *Hypericum perforatum*-type	*Hypericum* (Hypericaceae)	
Juncaceae	Juncaceae	
Ballota-type *Galeopsis*-type *Galeopsis/Ballota*-type *Labiatae (6)* Lamiaceae Lamiaceae (hexacolpate) *Lamium album*-type *Lavandula* *Marrubium* *Origanum*-type *Origanum vulgare*	Lamiaceae	Lamiaceae

Taxa of the Eurasian Modern Pollen Database (EMPD, version 2) (Davis et al., 2020)		
a) All taxa (n=840)	**b) First grouping (n=184)**	**c) 88 taxa retained**
Herbs (continuation) (n=597)	**(n=85)**	**(n=41)**
Phlomis *Prunella*-type *Salvia*-type *Salvia officinalis*-type *Salvia verticillata* *Scutellaria*-type *Sideritis* *Teucrium*	Lamiaceae (continuation)	Lamiaceae (continuation)
Mentha-type	*Mentha*-type *(Lamiaceae)*	
Pinguicula *Utricularia*	Lentibulariaceae	
Leucojum-type *Crocus* *Gladiolus/Romulea* *Iris* *Iris humilis* *Iris pseudacorus*-type *Muscari* *Muscari/Veratrum* *Ruscus* *Asphodeline* *Merendera filifolia*-type *Allium-type* *Allium ursinum*-type *Anthericum* *Asparagus* *Colchicum*-type *Convallaria*-type *Eremurus* *Fritillaria* Liliaceae-type *Lilium* *Lloydia serotina* *Maianthemum bifolium* *Maianthemum/Paris* *Narthecium* *Ornithogalum*-type *Polygonatum*-type	Liliaceae	Liliaceae

Taxa of the Eurasian Modern Pollen Database (EMPD, version 2) (Davis et al., 2020)		
a) All taxa (n=840)	**b) First grouping (n=184)**	**c) 88 taxa retained**
Herbs (continuation) (n=597)	**(n=85)**	**(n=41)**
Smilax *Tofieldia* *Veratrum*	Liliaceae (continuation)	Liliaceae (continuation)
Asphodelus/Asphodeline *Asphodelus* *Asphodelus albus*-type	*Asphodelus (Liliaceae)*	*Asphodelus (Liliaceae)*
Linaceae *Linum* *Linum austriacum*-type *Linum catharticum* *Linum catharticum*-type *Linum usitatissimum/L. bienne*	*Linum* (Linaceae)	
Lobelia *Lobelia dortmanna*	*Lobelia* (Lobeliaceae)	
Lythrum *Lythrum portula*-type *Lythrum salicaria*-type	*Lythrum* (Lythraceae)	
Hibiscus *Malva sylvestris*-type Malvaceae	Malvaceae	
Circaea *Epilobium* *Epilobium angustifolium*-type *Oenothera* Onagraceae	Onagraceae	Onagraceae
Epipactis Orchidaceae	Orchidaceae	
Oxalis *Oxalis acetosella* *Oxalis stricta*	Oxalidaceae	
Paeonia	*Paeonia* (Paeoniaceae)	
Chelidonium majus *Corydalis* *Corydalis bracteata* *Fumaria* *Glaucium* *Hypecoum*	Papaveraceae	Papaveraceae

Taxa of the Eurasian Modern Pollen Database (EMPD, version 2) (Davis et al., 2020)		
a) All taxa (n=840)	**b) First grouping (n=184)**	**c) 88 taxa retained**
Herbs (continuation) (n=597)	**(n=85)**	**(n=41)**
Papaver *Papaver argemone* *Papaver rhoeas*-type Papaveraceae *Roemeria*-type	Papaveraceae (continuation)	Papaveraceae (continuation)
Plantaginaceae *Plantago lanceolata-type* *Plantago* *Plantago albicans* *Plantago atrata*-type *Plantago coronopus*-type *Plantago major* *Plantago major/P. media*-type *Plantago maritima*-type *Plantago maxima* *Plantago media* *Plantago tenuiflora*	Plantaginaceae	Plantaginaceae
Limonium Plumbaginaceae	Plumbaginaceae	Plumbaginaceae
Armeria-type	type *Armeria* (Plumbaginaceae)	
Avena-type *Avena/Triticum*-type *Hordeum*-type *Hystrix* *Lygeum spartum* *Phragmites australis*-type Poaceae *Secale cereale* *Triticum*-type *Zea mays*	Poaceae	Poaceae
Cerealia-type	*Cerealia* (Poaceae)	
Phlox sibirica Polemoniaceae *Polemonium* *Polemonium acutiflorum*	Polemoniaceae	Polemoniaceae

Taxa of the Eurasian Modern Pollen Database (EMPD, version 2) (Davis et al., 2020)		
a) All taxa (n=840)	**b) First grouping (n=184)**	**c) 88 taxa retained**
Herbs (continuation) (n=597)	**(n=85)**	**(n=41)**
Polygonaceae *Atraphaxis* *Calligonum* *Calligonum*-type *Fagopyrum* *Fagopyrum esculentum* *Fagopyrum tataricum* *Fallopia* *Knorringia* *Koenigia islandica* *Persicaria* *Persicaria maculosa*-type *Reynoutria* *Rheum*	Polygonaceae	
Oxyria digyna *Emex spinosa* *Rumex acetosa*-type *Rumex acetosella* *Rumex alpestris* *Rumex alpinus*-type *Rumex aquaticus*-type *Rumex crispus*-type *Rumex scutatus*-type *Rumex/Oxyria*	*Rumex/Oxyria* (Polygonaceae)	*Rumex/Oxyria* (Polygonaceae)
Polygala *Polygala comosa*-type	*Polygala* (Polygalaceae)	
Polygonum-type (tricolporate) *Polygonum aviculare*-type *Polygonum alpinum* *Polygonum bistorta* *Polygonum bistorta*-type *Polygonum cognatum* *Polygonum oxyspermum*-type *Polygonum polycnemoides* *Polygonum viviparum*	*Polygonum* (Polygonaceae)	*Polygonum* (Polygonaceae)
Montia Portulacaceae *Claytonia*	Portulacaceae	

Taxa of the Eurasian Modern Pollen Database (EMPD, version 2) (Davis et al., 2020)		
a) All taxa (n=840)	**b) First grouping (n=184)**	**c) 88 taxa retained**
Herbs (continuation) (n=597)	**(n=85)**	**(n=41)**
Anagallis	Primulaceae	Primulaceae
Anagallis-type		
Anagallis arvensis-type		
Anagallis tenella-type		
Androsace		
Cyclamen		
Cyclamen hederifolium		
Glaux maritima		
Hottonia palustris		
Lysimachia nemorum		
Lysimachia vulgaris-type		
Primula		
Primula farinosa-type		
Primula hirsuta-type		
Primula veris-type		
Primula/Linaria-type		
Primulaceae		
Soldanella		
Trientalis europaea		
Chimaphila umbellata	Pyrolaceae	
Cytinus	*Cytinus* (Rafflesiaceae)	
Actaea	Ranunculaceae	Ranunculaceae
Adonis		
Adonis aestivalis-type		
Adonis vernalis		
Anemone hortensis-type		
Anemone nemorosa-type		
Aquilegia		
Caltha-type		
Caltha palustris		
cf. *Pulsatilla alpina*		
Clematis		
Consolida-type		
Helleborus		
Helleborus foetidus		
Helleborus niger		
Helleborus viridis-type		

Taxa of the Eurasian Modern Pollen Database (EMPD, version 2) (Davis et al., 2020)		
a) All taxa (n=840)	**b) First grouping (n=184)**	**c) 88 taxa retained**
Herbs (continuation) (n=597)	**(n=85)**	**(n=41)**
Hepatica *Nigella* *Pulsatilla* Ranunculaceae *Ranunculus*-type *Ranunculus acris*-type *Ranunculus aquatilis*-type *Ranunculus arvensis* *Ranunculus arvensis*-type *Ranunculus asiaticus* *Ranunculus ficaria* *Ranunculus flammula*-type *Ranunculus glacialis*-type *Ranunculus lingua* *Ranunculus macrophyllus* *Ranunculus sceleratus*-type *Ranunculus serbicus* *Trollius europaeus*	Ranunculaceae (continuation)	Ranunculaceae (continuation)
Aconitum	*Aconitum* (Ranunculaceae)	
Thalictrum *Thalictrum alpinum*-type *Thalictrum aquilegiifolium* *Thalictrum flavum*-type	*Thalictrum* (Ranunculaceae)	*Thalictrum* (Ranunculaceae)
Reseda Resedaceae	Resedaceae	
Agrimonia/Aremonia *Alchemilla* *Alchemilla/Aphanes* *Aphanes* *Aruncus/Spiraea* *Chamaerhodos*-type *Cotoneaster* *Crataegus* *Geum*-type *Padus avium* *Potentilla*-type *Potentilla palustris*	Rosaceae	Rosaceae

Taxa of the Eurasian Modern Pollen Database (EMPD, version 2) (Davis et al., 2020)		
a) All taxa (n=840)	**b) First grouping (n=184)**	**c) 88 taxa retained**
Herbs (continuation) (n=597)	**(n=85)**	**(n=41)**
Prunus-type *Prunus padus* *Rosa* Rosaceae Rosaceae (non-operculate) Rosaceae (operculate) *Rubus* *Rubus arcticus* *Rubus chamaemorus* *Sorbus*-type	Rosaceae (continuation)	Rosaceae (continuation)
Dryas octopetala	*Dryas* (Rosaceae)	
Filipendula	*Filipendula* (Rosaceae)	
Sanguisorba-type *Sanguisorba dodecandra* *Sanguisorba minor*-type *Sanguisorba officinalis*	*Sanguisorba* (Rosaceae)	*Sanguisorba* (Rosaceae)
Cephalanthus Rubiaceae *Theligonum cynocrambe* *Galium uliginosum*	Rubiaceae	Rubiaceae
Comandra elegans *Osyris alba* Santalaceae *Thesium*	Santalaceae	
Bergenia crassifolia *Chrysosplenium* *Parnassia palustris* *Ribes* *Saxifraga* *Saxifraga cespitosa* *Saxifraga granulata*-type *Saxifraga hieraciifolia* *Saxifraga hirsuta-type* *Saxifraga oppositifolia*-type *Saxifraga stellaris*-type Saxifragaceae	Saxifragaceae	Saxifragaceae

Taxa of the Eurasian Modern Pollen Database (EMPD, version 2) (Davis et al., 2020)		
a) All taxa (n=840)	**b) First grouping (n=184)**	**c) 88 taxa retained**
Herbs (continuation) (n=597)	**(n=85)**	**(n=41)**
Digitalis *Digitalis*-type *Euphrasia* *Gratiola officinalis* *Linaria*-type *Melampyrum* *Odontites*-type *Pedicularis* *Pedicularis palustris*-type *Pedicularis verticillata*-type *Rhinanthus*-type *Rhinanthus*-type/*Veronica*-type *Scrophularia*-type Scrophulariaceae Scrophulariaceae (colporate-reticulate) *Verbascum* *Veronica*-type *Paulownia*	Scrophulariaceae	Scrophulariaceae
Datura *Hyoscyamus* *Hyoscyamus*-type *Lycium* *Nicotiana tabacum* *Physochlaina* Solanaceae *Solanum* *Solanum dulcamara* *Solanum nigrum*-type *Solanum tuberosum*	Solanaceae	Solanaceae
Cannabaceae Cannabaceae/Urticaceae *Cannabis sativa*	Cannabaceae	Cannabaceae/Urticaceae
Humulus lupulus *Humulus/Cannabis* *Humulus/Cannabis sativa*	*Humulus* (Cannabaceae)	
Parietaria *Urtica* *Urtica dioica*	Urticaceae	

Taxa of the Eurasian Modern Pollen Database (EMPD, version 2) (Davis et al., 2020)		
a) All taxa (n=840)	**b) First grouping (n=184)**	**c) 88 taxa retained**
Herbs (continuation) (n=597)	**(n=85)**	**(n=41)**
Urtica dioica-type *Urtica dubia*-type *Urtica membranacea*-type *Urtica pilulifera* *Urtica urens* Urticaceae Urticaceae/Moraceae	Urticaceae (continuation)	Cannabaceae/Urticaceae
Centranthus *Valeriana* *Valeriana capitata* *Valeriana dioica* *Valeriana montana*-type *Valeriana officinalis*-type *Valeriana saxatilis*-type Valerianaceae *Valerianella*	Valerianaceae	Valerianaceae
Valerianaceae/Dipsacaceae	Valerianaceae/Dipsacaceae	
Verbena officinalis Verbenaceae *Vitex* *Vitex agnus-castus*	Verbenaceae	
Veronica/Lamium album-type	Veronica/Lamium album-type	
Viola *Viola odorata*-type *Viola tricolor*-type	*Viola* (Violaceae)	*Viola* (Violaceae)
Others (n=7)	**(n=7)**	
Indeterminable: unknown	Indeterminable: unknown	
Callitriche	Callitrichaceae	
Hydrocotyle	Apiaceae	
Haloragaceae	Haloragaceae	
Pediastrum boryanum var. *boryanum*	Hydrodictyaceae	
Karnataka	Karnataka	
Cynomorium	*Cynomorium* (Cynomoriaceae)	

RÉFÉRENCES

Andrieu, V., Eicher, U., & Reille, M. (1993). La fin du dernier Pléniglaciaire dans les Pyrénées (France): données polliniques, isotopiques et radiométriques. *Comptes rendus de l'Académie des sciences. Série 2, Mécanique, Physique, Chimie, Sciences de l'univers, Sciences de la Terre*, *316*(2), 245-250.

Austin, W. E., & Hibbert, F. D., Tracing time in the ocean: a brief review of chronological constraints (60–8 kyr) on North Atlantic marine event-based stratigraphies. *Quaternary Science Reviews*, *36*, 28-37 (2012).

Bahr, A., Kaboth, S., Jiménez-Espejo, F., Sierro, F., Voelker, A., Lourens, L., . . . Hernández-Molina, F. (2015). Persistent monsoonal forcing of Mediterranean Outflow Water dynamics during the late Pleistocene. Geology, 43(11), 951-954.

Bauska, T. K., Marcott, S. A., & Brook, E. J. (2021). Abrupt changes in the global carbon cycle during the last glacial period. *Nature Geoscience*, *14*(2), 91-96.

Beghin, P., Charbit, S., Kageyama, M., Combourieu-Nebout, N., Hatté, C., Dumas, C., & Peterschmitt, J. Y. (2016). What drives LGM precipitation over the western Mediterranean? A study focused on the Iberian Peninsula and northern Morocco. *Climate dynamics*, *46*, 2611-2631.

Birks, H. J. B., Heiri, O., Seppä, H., & Bjune, A. E. (2010). Strengths and weaknesses of quantitative climate reconstructions based on Late-Quaternary. *The Open Ecology Journal*, *3*(1).

Bond, G., Broecker, W., Johnsen, S., McManus, J., Labeyrie, L., Jouzel, J., & Bonani, G. (1993). Correlations between climate records from North Atlantic sediments and Greenland ice. Nature, 365(6442), 143.

Bond, G. C., & Lotti, R. (1995). Iceberg discharges into the North Atlantic on millennial time scales during the last glaciation. Science, 267(5200), 1005-1010.

Budsky, A., Western Mediterranean climate response to Dansgaard/Oeschger events: New insights from speleothem records. *Geophysical Research Letters*, *46*(15), 9042-9053 (2019).

Camuera, J., et al., Past 200 kyr hydroclimate variability in the western Mediterranean and its connection to the African Humid Periods. *Scientific Reports* 12.1 : 1-13 2022.

Carré, M., & Cheddadi, R., Seasonality in long-term climate change. *Quaternaire. Revue de l'Association française pour l'étude du Quaternaire*, *28*(2), 173-177 (2017).

Carton, J. A., & Hakkinen, S. (2011). Introduction to: atlantic meridional overturning circulation (AMOC). *Deep Sea Research Part II: Topical Studies in Oceanography*, *58*(17-18), 1741-1743.

Chevalier, M., *et al*., Pollen-based climate reconstruction techniques for late Quaternary studies. *Earth-Science Reviews*, *210*, 103384 (2020).

Cleator, S. F., Harrison, S. P., Nichols, N. K., Prentice, I. C., & Roulstone, I. (2020). A new multivariable benchmark for Last Glacial Maximum climate simulations. *Climate of the Past*, *16*(2), 699-712.

Combourieu-Nebout, N., Turon, J. L., Zahn, R., Capotondi, L., Londeix, L., & Pahnke, K. (2002). Enhanced aridity and atmospheric high-pressure stability over the western Mediterranean during the North Atlantic cold events of the past 50 ky. *Geology*, *30*(10), 863-866.

Combourieu Nebout, N., Peyron, O., Dormoy, I., Desprat, S., Beaudouin, C., Kotthoff, U., & Marret, F. (2009). Rapid climatic variability in the west Mediterranean during the last 25 000 years from high resolution pollen data. *Climate of the Past*, *5*(3), 503-521.

D'Agostino, R., & Lionello, P. (2020). The atmospheric moisture budget in the Mediterranean: Mechanisms for seasonal changes in the Last Glacial Maximum and future warming scenario. *Quaternary Science Reviews*, *241*, 106392.

Dansgaard, W., Clausen, H. B., Gundestrup, N., Hammer, C. U., Johnsen, S. F., Kristinsdottir, P. M., & Reeh, N. (1982). A new Greenland deep ice core. *Science*, *218*(4579), 1273-1277.

Dansgaard, W. *et al*., Evidence for general instability of past climate from a 250-kyr ice-core record. *nature*, *364*(6434), 218-220 (1993).

Datema, M., *et al.,* Millennial-scale climate variability and dinoflagellate-cyst-based seasonality changes over the last~ 150 kyrs at "Shackleton Site" U1385. *Paleoceanography and paleoclimatology*, *34*(7), 1139-1156 (2019).

Davis, B. A., Brewer, S., Stevenson, A. C., & Guiot, J. (2003). The temperature of Europe during the Holocene reconstructed from pollen data. *Quaternary science reviews*, *22*(15-17), 1701-1716.

Davis, B. A., Zanon, M., Collins, P., Mauri, A., Bakker, J., Barboni, D., ... & Kaplan, J. O. (2013). The European modern pollen database (EMPD) project. *Vegetation history and archaeobotany*, *22*(6), 521-530.

Davis, B. A., Chevalier, M., Sommer, P., Carter, V. A., Finsinger, W., Mauri, A., ... & Zimny, M. (2020). The Eurasian Modern Pollen Database (EMPD), version 2. *Earth System Science Data Discussions*, *2020*, 1-41.

Davis, B. A. S., Fasel, M., Kaplan, J. O., Russo, E., & Burke, A. (2022). The climate and vegetation of Europe, North Africa and the Middle East during the Last Glacial Maximum (21,000 years BP) based on pollen data. *Climate of the Past Discussions*, 1-66.

de Vernal, A. D., Eynaud, F., Henry, M., Hillaire-Marcel, C., Londeix, L., Mangin, S., ... & Turon, J. L., (2005). Reconstruction of sea-surface conditions at middle to high latitudes of the Northern Hemisphere during the Last Glacial Maximum (LGM) based on dinoflagellate cyst assemblages. *Quaternary Science Reviews*, *24*(7-9), 897-924.

de Vernal, A., Radi, T., Zaragosi, S., Van Nieuwenhove, N., Rochon, A., Allan, E., ... & Richerol, T. (2020). Distribution of common modern dinoflagellate cyst taxa in surface sediments of the Northern Hemisphere in relation to environmental parameters: The new n= 1968 database. *Marine Micropaleontology*, *159*, 101796.

Denton, G. H., Alley, R. B., Comer, G. C., & Broecker, W. S., The role of seasonality in abrupt climate change. *Quaternary Science Reviews*, *24*(10-11), 1159-1182 (2005).

Denton, G. H., Toucanne, S., Putnam, A. E., Barrell, D. J., & Russell, J. L., Heinrich summers. *Quaternary Science Reviews*, *295*, 107750 (2022).

Elliot, M., Labeyrie, L., Bond, G., Cortijo, E., Turon, J. L., Tisnerat, N., & Duplessy, J. C. (1998). Millennial-scale iceberg discharges in the Irminger Basin during the last glacial period: Relationship with the Heinrich events and environmental settings. Paleoceanography and Paleoclimatology, 13(5), 433-446.

Elliot, M., Labeyrie, L., Dokken, T., & Manthé, S. (2001). Coherent patterns of ice-rafted debris deposits in the Nordic regions during the last glacial (10–60 ka). Earth and Planetary Science Letters, 194(1-2), 151-163.

Elliot, M., Labeyrie, L., & Duplessy, J.-C. (2002). Changes in North Atlantic deep-water formation associated with the Dansgaard–Oeschger temperature oscillations (60–10 ka). Quaternary Science Reviews, 21(10), 1153-1165.

Eynaud, F., Turon, J., Matthießen, J., Kissel, C., Peypouquet, J., De Vernal, A., & Henry, M. (2002). Norwegian sea-surface palaeoenvironments of marine oxygen-isotope stage 3: the paradoxical response of dinoflagellate cysts. Journal of Quaternary Science: Published for the Quaternary Research Association, 17(4), 349-359.

Flückiger, J., Knutti, R., White, J. W., & Renssen, H., Modeled seasonality of glacial abrupt climate events. *Climate Dynamics*, *31*, 633-645 (2008).

Genty, D. *et al.,* Isotopic characterization of rapid climatic events during OIS3 and OIS4 in Villars Cave stalagmites (SW-France) and correlation with Atlantic and Mediterranean pollen records. *Quaternary Science Reviews*, *29*(19-20), 2799-2820 (2010).

González-Sampériz, P., Valero-Garcés, B. L., Moreno, A., Jalut, G., García-Ruiz, J. M., Martí-Bono, C., ... & Dedoubat, J. J. (2006). Climate variability in the Spanish Pyrenees during the last 30,000 yr revealed by the El Portalet sequence. *Quaternary Research*, *66*(1), 38-52.

Gottschalk, J., Skinner, L. C., Misra, S., Waelbroeck, C., Menviel, L., & Timmermann, A. (2015). Abrupt changes in the southern extent of North Atlantic Deep Water during Dansgaard–Oeschger events. Nature geoscience, 8(12), 950.

Gouveia, C., Trigo, R. M., DaCamara, C. C., Libonati, R., & Pereira, J. M., The North Atlantic oscillation and European vegetation dynamics. *International Journal of Climatology: A Journal of the Royal Meteorological Society*, *28*(14), 1835-1847 (2008).

Guiot, J., Methodology of the last climatic cycle reconstruction in France from pollen data. *Palaeogeography, Palaeoclimatology, Palaeoecology*, *80*(1), 49-69 (1990).

Guiot, J., & De Vernal, A. (2011a). Is spatial autocorrelation introducing biases in the apparent accuracy of paleoclimatic reconstructions?. *Quaternary Science Reviews*, *30*(15-16), 1965-1972.

Guiot, J., & De Vernal, A. (2011b). QSR Correspondence "Is spatial autocorrelation introducing biases in the apparent accuracy of palaeoclimatic reconstructions?" Reply to Telford and Birks. *Quaternary Science Reviews*, *21*(30), 3214-3216.

Hall, I. R., Colmenero-Hidalgo, E., Zahn, R., Peck, V. L., & Hemming, S. (2011). Centennial-to millennial-scale ice-ocean interactions in the subpolar northeast Atlantic 18–41 kyr ago. Paleoceanography and Paleoclimatology, 26(2).

Hurrell, J. W., Decadal trends in the North Atlantic Oscillation: Regional temperatures and precipitation. *Science*, *269*(5224), 676-679 (1995).

Ivy-Ochs, S. (2015). Glacier variations in the European Alps at the end of the last glaciation. *Cuadernos de investigación geográfica: Geographical Research Letters*, (41), 295-315.

Ivy-Ochs, S., Lucchesi, S., Baggio, P., Fioraso, G., Gianotti, F., Monegato, G., ... & Schlüchter, C. (2018). New geomorphological and chronological constraints for glacial deposits in the Rivoli-Avigliana end-moraine system and the lower Susa Valley (Western Alps, NW Italy). *Journal of Quaternary Science*, *33*(5), 550-562.

Jackson, S. T., & Overpeck, J. T., Responses of plant populations and communities to environmental changes of the late Quaternary. *Paleobiology*, *26*(S4), 194-220 (2000).

Jost, A., Lunt, D., Kageyama, M., Abe-Ouchi, A., Peyron, O., Valdes, P. J., & Ramstein, G. (2005). High-resolution simulations of the last glacial maximum climate over Europe: a solution to discrepancies with continental palaeoclimatic reconstructions?. *Climate Dynamics*, *24*, 577-590.

Kaboth-Bahr, S., Bahr, A., Zeeden, C., Toucanne, S., Eynaud, F., Jiménez-Espejo, F., . . . Löwemark, L. (2018). Monsoonal forcing of European ice-sheet dynamics during the Late Quaternary. Geophysical Research Letters, 45(14), 7066-7074.

Kageyama, M., Harrison, S. P., Kapsch, M. L., Lofverstrom, M., Lora, J. M., Mikolajewicz, U., ... & Zhu, J. (2021). The PMIP4 Last Glacial Maximum experiments: preliminary results and comparison with the PMIP3 simulations. *Climate of the Past*, *17*(3), 1065-1089.

Kamleitner, S., Ivy-Ochs, S., Monegato, G., Gianotti, F., Akçar, N., Vockenhuber, C., ... & Synal, H. A. (2022). The ticino-toce glacier system (Swiss-Italian Alps) in the framework of the alpine last glacial maximum. *Quaternary science reviews*, *279*, 107400.

Kindler, P., Guillevic, M., Baumgartner, M., Schwander, J., Landais, A., & Leuenberger, M. (2014). Temperature reconstruction from 10 to 120 kyr b2k from the NGRIP ice core. *Climate of the Past*, *10*(2), 887-902.

Kissel, C., Laj, C., Labeyrie, L., Dokken, T., Voelker, A., & Blamart, D. (1999). Rapid climatic variations during marine isotopic stage 3: magnetic analysis of sediments from Nordic Seas and North Atlantic. Earth and Planetary Science Letters, 171(3), 489-502.

Laîné, A., Kageyama, M., Salas-Mélia, D., Voldoire, A., Rivière, G., Ramstein, G., ... & Peterschmitt, J. Y. (2009). Northern hemisphere storm tracks during the last glacial maximum in the PMIP2 ocean-atmosphere coupled models: energetic study, seasonal cycle, precipitation. *Climate Dynamics*, *32*(5), 593-614.

Laskar, J., Robutel, P., Joutel, F., Gastineau, M., Correia, A. C., & Levrard, B. (2004). A long-term numerical solution for the insolation quantities of the Earth. *Astronomy & Astrophysics*, *428*(1), 261-285.

Leduc, G., Vidal, L., Tachikawa, K., Rostek, F., Sonzogni, C., Beaufort, L., & Bard, E. (2007). Moisture transport across Central America as a positive feedback on abrupt climatic changes. Nature, 445(7130), 908.

Leuschner, D. C., & Sirocko, F. (2000). The low-latitude monsoon climate during Dansgaard–Oeschger cycles and Heinrich events. Quaternary Science Reviews, 19(1-5), 243-254.

Lisiecki, L. E., & Raymo, M. E. (2005). A Pliocene-Pleistocene stack of 57 globally distributed benthic δ18O records. *Paleoceanography*, *20*(1).

Löfverström, M., Caballero, R., Nilsson, J., & Kleman, J. (2014). Evolution of the large-scale atmospheric circulation in response to changing ice sheets over the last glacial cycle. *Climate of the Past*, *10*(4), 1453-1471.

Löfverström, M., & Lora, J. M. (2017). Abrupt regime shifts in the North Atlantic atmospheric circulation over the last deglaciation. *Geophysical Research Letters*, *44*(15), 8047-8055.

Luetscher, M., Boch, R., Sodemann, H., Spötl, C., Cheng, H., Edwards, R. L., ... & Müller, W. (2015). North Atlantic storm track changes during the Last Glacial Maximum recorded by Alpine speleothems. *Nature Communications*, *6*(1), 6344.

Magyari, E. K., Kuneš, P., Jakab, G., Sümegi, P., Pelánková, B., Schäbitz, F., ... & Chytrý, M. (2014). Late Pleniglacial vegetation in eastern-central Europe: are there modern analogues in Siberia?. *Quaternary Science Reviews*, *95*, 60-79.

MARGO Project Members (2009), Constraints on the magnitude and patterns of ocean cooling at the Last Glacial Maximum, Nat. Geosci.**,** 2**,** 127–132

Mix, A. C., Bard, E., & Schneider, R. (2001). Environmental processes of the ice age: land, oceans, glaciers (EPILOG). *Quaternary Science Reviews*, *20*(4), 627-657.

Moreno, A., González-Sampériz, P., Morellón, M., Valero-Garcés, B. L., & Fletcher, W. J. (2012). Northern Iberian abrupt climate change dynamics during the last glacial cycle: a view from lacustrine sediments. *Quaternary Science Reviews*, *36*, 139-153.

North Greenland Ice Core Project members, High resolution record of Northern Hemisphere climate extending into the last interglacial period. *Nature*, *431*(7005), 147-151 (2004).

Pénaud, A., Eynaud, F., Sánchez-Goñi, M., Malaizé, B., Turon, J.-L., & Rossignol, L. (2011). Contrasting sea-surface responses between the western Mediterranean Sea and eastern subtropical latitudes of the North Atlantic during abrupt climatic events of MIS 3. Marine Micropaleontology, 80(1-2), 1-17.

Peters, C., Walden, J., & Austin, W. E. (2008). Magnetic signature of European margin sediments: Provenance of ice-rafted debris and the climatic response of the British ice sheet during Marine Isotope Stages 2 and 3. Journal of Geophysical Research: Earth Surface, 113(F3).

Peyron, O. e*t al*., Climatic reconstruction in Europe for 18,000 yr BP from pollen data. *Quaternary research*, *49*(2), 183-196 (1998).

Prentice, I. C. *et al*., Special paper: a global biome model based on plant physiology and dominance, soil properties and climate. *Journal of biogeography*, 117-134 (1992).

Prentice, C., Guiot, J., Huntley, B., Jolly, D., & Cheddadi, R., Reconstructing biomes from palaeoecological data: a general method and its application to European pollen data at 0 and 6 ka. *Climate Dynamics*, *12*(3), 185-194 (1996).

Prentice, I. C., Villegas-Diaz, R., & Harrison, S. P. (2022). Accounting for atmospheric carbon dioxide variations in pollen-based reconstruction of past hydroclimates. *Global and Planetary Change*, *211*, 103790.

Rasmussen, T. L., Thomsen, E., van Weering, T. C., & Labeyrie, L. (1996). Rapid changes in surface and deep water conditions at the Faeroe Margin during the last 58,000 years. Paleoceanography, 11(6), 757-771.

Rasmussen, T. L., Balbon, E., Thomsen, E., Labeyrie, L., & Van Weering, T. C. (1999). Climate records and changes in deep outflow from the Norwegian Sea∼ 150–55 ka. Terra Nova, 11(2-3), 61-66.

Rasmussen, T. L., Thomsen, E., Troelstra, S. R., Kuijpers, A., & Prins, M. A. (2003). Millennial-scale glacial variability versus Holocene stability: changes in planktic and benthic foraminifera faunas and ocean circulation in the North Atlantic during the last 60 000 years. Marine Micropaleontology, 47(1-2), 143-176.

Rasmussen, T. L., & Thomsen, E. (2004). The role of the North Atlantic Drift in the millennial timescale glacial climate fluctuations. Palaeogeography, Palaeoclimatology, Palaeoecology, 210(1), 101-116.

Rasmussen, S. O., Bigler, M., Blockley, S. P., Blunier, T., Buchardt, S. L., Clausen, H. B., ... & Winstrup, M. (2014). A stratigraphic framework for abrupt climatic changes during the Last Glacial period based on three synchronized Greenland ice-core records: refining and extending the INTIMATE event stratigraphy. *Quaternary science reviews*, *106*, 14-28.

Rasmussen, T. L., Thomsen, E., & Moros, M. (2016). North Atlantic warming during Dansgaard-Oeschger events synchronous with Antarctic warming and out-of-phase with Greenland climate. *Scientific reports*, *6*(1), 20535.

Reille, M., & Andrieu, V. (1995). The late Pleistocene and Holocene in the Lourdes Basin, Western Pyrénées, France: new pollen analytical and chronological data. *Vegetation history and Archaeobotany*, *4*, 1-21.

Roattino, T., Crouzet, C., Vassallo, R., Buoncristiani, J. F., Carcaillet, J., Gribenski, N., & Valla, P. G. (2023). Paleogeographical reconstruction of the western French Alps foreland during the last glacial maximum using cosmogenic exposure dating. *Quaternary Research*, *111*, 68-83.

Rochon, A., Vernal, A. D., Turon, J. L., Matthiessen, J., & Head, M. J. (1999). Distribution of recent dinoflagellate cysts in surface sediments from the North Atlantic Ocean and adjacent seas in relation to sea-surface parameters. *American Association of Stratigraphic Palynologists Contribution Series*, *35*, 1-146.

Rodrigo-Gámiz, M., García-Alix, A., Jiménez-Moreno, G., Ramos-Román, M. J., Camuera, J., Toney, J. L., ... & Damsté, J. S. S. (2022). Paleoclimate reconstruction of the last 36 kyr based on branched glycerol dialkyl glycerol tetraethers in the Padul palaeolake record (Sierra Nevada, southern Iberian Peninsula). *Quaternary Science Reviews*, *281*, 107434.

Rodwell, M. J., & Hoskins, B. J. (2001). Subtropical anticyclones and summer monsoons. *Journal of Climate*, *14*(15), 3192-3211.

Roucoux, K. H., Shackleton, N. J., de Abreu, L., Schönfeld, J., & Tzedakis, P. C. (2001). Combined marine proxy and pollen analyses reveal rapid Iberian vegetation response to North Atlantic millennial-scale climate oscillations. *Quaternary Research*, *56*(1), 128-132.

Roucoux, K. H., De Abreu, L., Shackleton, N. J., & Tzedakis, P. C., The response of NW Iberian vegetation to North Atlantic climate oscillations during the last 65 kyr. *Quaternary Science Reviews*, *24*(14-15), 1637-1653 (2005).

Sanchez-Goñi, M. F., Turon, J. L., Eynaud, F., & Gendreau, S., European climatic response to millennial-scale changes in the atmosphere–ocean system during the Last Glacial period. *Quaternary Research*, *54*(3), 394-403 (2000).

Sánchez Goñi, M. F., Cacho, I., Turon, J. L., Guiot, J., Sierro, F. J., Peypouquet, J. P., ... & Shackleton, N. J. (2002). Synchroneity between marine and terrestrial responses to millennial scale climatic variability during the last glacial period in the Mediterranean region. *Climate dynamics*, *19*, 95-105.

Sanchez-Goñi, M. *et al*., Contrasting impacts of Dansgaard–Oeschger events over a western European latitudinal transect modulated by orbital parameters. *Quaternary Science Reviews*, *27*(11-12), 1136-1151 (2008).

Sanchez-Goñi, M. F., Landais, A., Cacho, I., Duprat, J., & Rossignol, L., Contrasting intrainterstadial climatic evolution between high and middle North Atlantic latitudes: A close-up of Greenland Interstadials 8 and 12. *Geochemistry, Geophysics, Geosystems*, *10*(4) (2009).

Sánchez Goñi, M. F., Desprat, S., Fletcher, W. J., Morales-Molino, C., Naughton, F., Oliveira, D., ... & Zorzi, C. (2018). Pollen from the deep-sea: A breakthrough in the mystery of the Ice Ages. *Frontiers in Plant Science*, *9*, 38.

Sanchez-Goñi, M-F. *et al*., Muted cooling and drying of NW Mediterranean in response to the strongest last glacial North American ice surges. *GSA Bulletin* 133.3-4: 451-460 (2021).

Schmidt, G. A., Shindell, D. T., & Harder, S. (2004). A note on the relationship between ice core methane concentrations and insolation. Geophysical Research Letters, 31(23).

Schmittner, A., Galbraith, E. D., Hostetler, S. W., Pedersen, T. F., & Zhang, R. (2007). Large fluctuations of dissolved oxygen in the Indian and Pacific oceans during Dansgaard-Oeschger oscillations caused by variations of North Atlantic Deep Water subduction. *Paleoceanography*, *22*(3).

Sierro, F. J., Hodell, D. A., Curtis, J. H., Flores, J. A., Reguera, I., Colmenero-Hidalgo, E., . . . Frigola, J. (2005). Impact of iceberg melting on Mediterranean thermohaline circulation during Heinrich events. Paleoceanography, 20(2).

Spratt, R. M., & Lisiecki, L. E. (2016). A Late Pleistocene sea level stack. *Climate of the Past*, *12*(4), 1079-1092.

Stríkis, N. M., Cruz, F. W., Barreto, E. A., Naughton, F., Vuille, M., Cheng, H., . . . Edwards, R. L. (2018). South American monsoon response to iceberg discharge in the North Atlantic. Proceedings of the National Academy of Sciences, 201717784.

Telford, R. J., & Birks, H. J. B. (2005). The secret assumption of transfer functions: problems with spatial autocorrelation in evaluating model performance. *Quaternary Science Reviews*, *24*(20-21), 2173-2179.

Telford, R. J., & Birks, H. J. B. (2009). Evaluation of transfer functions in spatially structured environments. *Quaternary Science Reviews*, *28*(13-14), 1309-1316.

Telford, R. J., & Birks, H. J. B. (2011). QSR Correspondence" Is spatial autocorrelation introducing biases in the apparent accuracy of palaeoclimatic reconstructions?". *Quaternary Science Reviews*, *30*(21), 3210-3213.

Toucanne, S., Mulder, T., Schönfeld, J., Hanquiez, V., Gonthier, E., Duprat, J., . . . Zaragosi, S. (2007). Contourites of the Gulf of Cadiz: a high-resolution record of the paleocirculation of the Mediterranean outflow water during the last 50,000 years. Palaeogeography, Palaeoclimatology, Palaeoecology, 246(2-4), 354-366.

Turon, J. L., Lézine, A. M., & Denèfle, M. (2003). Land–sea correlations for the last glaciation inferred from a pollen and dinocyst record from the Portuguese margin. *Quaternary Research*, *59*(1), 88-96.

Valero-Garcés, B. L., González-Sampériz, P., Navas, A., Machín, J., Delgado-Huertas, A., Peña-Monné, J. L., ... & Davis, B. (2004). Paleohydrological fluctuations and steppe vegetation during the last glacial maximum in the central Ebro valley (NE Spain). *Quaternary International*, *122*(1), 43-55.

Vegas, J., Ruiz-Zapata, B., Ortiz, J. E., Galán, L., Torres, T., García-Cortés, Á., ... & Gallardo-Millán, J. L. (2010). Identification of arid phases during the last 50 cal. ka BP from the Fuentillejo maar-lacustrine record (Campo de Calatrava Volcanic Field, Spain). *Journal of Quaternary Science*, *25*(7), 1051-1062.

Wary, M., Eynaud, F., Sabine, M., Zaragosi, S., Rossignol, L., Malaize, B., . . . Penaud, A. (2015). Stratification of surface waters during the last glacial millennial climatic events: a key factor in subsurface and deep-water mass dynamics. Climate of the Past, 11(11), 1507-1525.

Wary, M., Eynaud, F., Swingedouw, D., Masson-Delmotte, V., Matthiessen, J., Kissel, C., . . . Jouzel, J. (2016). Regional seesaw between the North Atlantic and Nordic Seas during the last glacial abrupt climate events. Climate of the Past, 13(6), 729-739.

Wary, M., Eynaud, F., Rossignol, L., Zaragosi, S., Sabine, M., Castera, M. H., & Billy, I. (2017). The southern Norwegian Sea during the last 45 ka: hydrographical reorganizations under changing ice-sheet dynamics. Journal of Quaternary Science, 32(7), 908-922.

Zumaque, J., Eynaud, F., Zaragosi, S., Marret, F., Matsuzaki, K., Kissel, C., . . . Billy, I. (2012). An ocean–ice coupled response during the last glacial: a view from a marine isotopic stage 3 record south of the Faeroe Shetland Gateway.

Zumaque, J., de Vernal, A., Fréchette, B., Davis, B., Chevalier, M., A ready-to-use version of the Eurasian Modern Pollen Database 2 (EMPD 2; Davis et al., 2020) for paleoclimatic reconstructions (submitted to *Data in Brief*)